# METALLOCENOPHANES AND METALLOPOLYMERS WITH ALUMINUM, GALLIUM, SILICON, AND TIN IN BRIDGING POSITIONS

A Thesis Submitted to the College of

Graduate Studies and Research

in Partial Fulfillment of the Requirements

for the Degree of Doctor of Philosophy

in the Department of Chemistry

University of Saskatchewan

Saskatoon

By

Nora Caroline Breit

## Permission to Use

In presenting this thesis in partial fulfilment of the requirements for a postgraduate degree from the University of Saskatchewan, I agree that the libraries of this University may make it freely available for inspection. I further agree that permission for copying of this thesis in any manner, in whole or in part, for scholarly purposes may be granted by the professor or professors who supervised my thesis work or, in their absence, by the Head of the Department or the Dean of the College in which my thesis work was done. It is understood that any copying or publication or use of this thesis or parts thereof for financial gain shall not be allowed without my written permission. It is also understood that due recognition shall be given to me and to the University of Saskatchewan in any scholarly use which may be made of any material in my thesis.

Requests for permission to copy or to make other use of material in this thesis in whole or part should be addressed to:

Head of the Department of Chemistry

University of Saskatchewan

Saskatoon, Saskatchewan (S7N 5C9)

Canada

## ABSTRACT

Three new aluminum and gallium dichlorides equipped with the ligands Pytsi$^{-SiMe_2}$ [Pytsi$^{-SiMe_2}$ = -C(SiMe$_3$)$_2$(C$_6$H$_4$N-2)], Pytsi$^{-2SiMe_3}$ [Pytsi$^{-2SiMe_3}$ = -CH$_2$(SiMe$_2$C$_6$H$_4$N-2)], and Mx (Mx = 4,6-di-*t*Bu$_2$-2-Me$_2$N-C$_6$H$_3$) were synthesized and fully characterized. (Mx)GaBr$_x$Cl$_{2-x}$ was isolated after a chlorine-bromine exchange that can be triggered by LiBr. Moreover, the stereoselective formation of *rac*-(Pytsi$^{-2SiMe_2}$)$_2$AlMe and *rac*-(Pytsi$^{-2SiMe_2}$)$_2$AlCl [Pytsi$^{-2SiMe_2}$ = -C(SiMe$_3$)Me(C$_6$H$_4$N-2)] was found.

Salt-metathesis reactions between aluminum or gallium dihalides decorated with the Pytsi$^{-SiMe_2}$ ligand and 1,1'-dilithioferrocene gave rise to aluminum- and gallium-bridged [1]ferrocenophanes ([1]FCPs). However, these [1]FCPs were not isolated, because they underwent ring-opening polymerization to yield low-molecular-weight polymers. When the Mx ligand was employed in salt-metathesis reactions with 1,1'-dilithioferrocene or 1,1'-dilithioruthenocene, metallopolymers were obtained as major products and aluminum- and gallium-bridged [1.1]FCPs were obtained as minor products. The formation of gallium-bridged [1]metallocenophanes that were consumed by ring-opening polymerization was observed. In the case of the Pytsi$^{-2SiMe_3}$ ligand, salt-metathesis reactions yielded an inseparable mixture of aluminum- and gallium-bridged [1.1]FCPs and oligomers. (Pytsi$^{-2SiMe_3}$)AlCl$_2$ and (Pytsi$^{-2SiMe_3}$)GaCl$_2$ were then reacted with lithioferrocene to give bis(ferrocenyl) compounds. The bis(ferrocenyl)aluminum and gallium compounds were fully characterized and electrochemically studied. The different outcome of the salt-metathesis reactions can be rationalized by the different steric bulk of the employed ligands.

The first examples of [1.1]FCPs with different bridging elements and polyferrocenes with alternating bridging elements containing combinations of silicon-tin

and silicon-gallium were synthesized and characterized. When silicon and tin were used as bridging elements, [1.1]FCPs were only formed as minor products in a mixture with other linear and cyclic polyferrocenes. A [1.1.1.1]FCP with alternating tin and silicon bridges was isolated and fully characterized and showed an interesting redox behavior. The gallium- and silicon-bridged [1.1]FCP was obtained as the major product and fully characterized including single-crystal X-ray analysis and cyclic voltammetry.

The first aluminum- as well as gallium-bridged [1.1]ruthenocenophanes ([1.1]RCPs) were synthesized and fully characterized. The solid-state structure of the gallium-bridged [1.1]RCP was similar to the respective [1.1]FCP. Electrochemical study of both species revealed two electrochemically irreversible oxidation waves. These properties contrast those of the methylene-bridged [1.1]RCP, the only [1.1]RCPs that was studied previously by single-crystal X-ray analysis and electrochemistry.

ACKNOWLEDGMENTS

I would like to thank Prof. Jens Müller for taking me as a Ph.D. student as well as for his support and input over these five years. I would like to thank my advisory committee members, Prof. Steven Foley, Prof. Robert Scott, and Prof. Jonathan Dimmock for their advice and support.

I would like to thank the crystallographers Dr. Gabriele Schatte, Dr. Wilson Quail and Dr. Klaus Harms for their work on the crystal structures and Ken Thoms for measuring the mass spectra. I am thankful to Prof. Joe Gilroy for measuring the MALDI-TOF and GPC data and to Prof. Ian Manners for making these instruments available. I would like to thank Prof. Ian Burgess for his help during our electrochemical measurements and for giving us access to these instruments. I would like to acknowledge Prof. Ildiko Badea for making the DLS instrument available to our studies.

I would like to thank all past and present group members for helpful discussions and the nice atmosphere in the lab. Most of all I want to thank Bidraha Bagh for his encouragement, his suggestions, for sharing some projects with me, for his help with ten thousand little things and for his additional efforts to make sure that the lab works well.

I would like to thank the University of Saskatchewan and Department of Chemistry for funding.

I would like to thank my parents and close friends for their constant support.

TABLE OF CONTENTS

LIST OF SCHEMES

Scheme page

LIST OF FIGURES

LIST OF TABLES

LIST OF ABBREVIATIONS

Abbreviation

Ar´.....2-($Me_2NCH_2$)$C_6H_4$

$BArF_{24}$.....[B{$C_6H_3(CF_3)_2$}$_4$]$^-$

CAP.....chromarenophane

cod.....1,5-cyclooctadiene

Cp.....cyclopentadienyl

DLS.....dynamic light scattering

FCP.....ferrocenophane

fc.....($C_5H_4$)$_2$Fe

Fc.....($C_5H_4$)Fe($C_5H_5$)

GPC.....gel permeation chromatography

Mamx.....4,6-di-*t*Bu-2-($Me_2NCH_2$)$C_6H_3$

Mamx$^{-tBu}$.....4-*t*Bu-2-($Me_2NCH_2$)$C_6H_4$

MAP.....molybdarenophane

MCP.....metallocenophane

$Me_2$Ntsi.....-C($SiMe_3$)$_2$$SiMe_2NMe_2$

Mes.....2,4,6-trimethylphenyl

Mx.....4,6-di-*t*Bu-2-$Me_2$N-$C_6H_3$

PFS.....poly(ferrocenylsilane)

Pytsi.....-C($SiMe_3$)$_2$($SiMe_2C_6H_4$N-2)

Pytsi$^{-SiMe_2}$.....-C($SiMe_3$)$_2$($C_6H_4$N-2)

Pytsi$^{-2SiMe_2}$.....-C($SiMe_3$)Me($C_6H_4$N-2)

Pytsi$^{-2SiMe_3}$.....-$CH_2$($SiMe_2C_6H_4$N-2)

*p*-*t*BuAr'.....5-*t*Bu-2-($Me_2NCH_2$)$C_6H_3$

*p*-$SiMe_3$Ar'.....5-$SiMe_3$-2-($Me_2NCH_2$)$C_6H_3$

r.t.....room temperature

RCP.....ruthenocenophane

RFCP.....ruthenoferrocenophane

ROP.....ring-opening polymerization

SSSC.....Saskatchewan Structural Sciences Center

tmeda.....N,N,N',N'-tetramethylethylenediamine

VAP.....vanadarenophane

VT-NMR.....variable temperature nuclear magnetic resonance

# CHAPTER 1
# INTRODUCTION

## 1.1 [1]Metallocenophanes

### 1.1.1 Ferrocene and [1]Ferrocenophanes

The synthesis of ferrocene (**1**) was reported independently by Paulsen and Miller in 1951 and 1952 (Figure 1-1).[1] The major contribution of understanding the structure of ferrocene was attributed to Wilkinson and Fischer and was a part of their achievements rewarded with the Nobel Prize in 1973.[2] Ferrocene was the first compound in which the metal is sandwiched between two planar and aromatic ligands that are parallel to each other (Figure 1-1). An introduction of a bridge between the cyclopentadienyl (Cp) ligands can tilt these away from parallelism and introduce strain to the species. These ring-tilted species are termed [n]ferrocenophanes ([n]FCPs) with "n" referring to the number of atoms in the bridge. Rinehart Jr. *et al.* reported the first carbon-bridged [2]FCP (**2**) in 1960 (Figure 1-1).[3] It took more than a decade till the first silicon-bridged [1]FCP (**3**) was reported by Osborne *et al.* (Figure 1-1).[4]

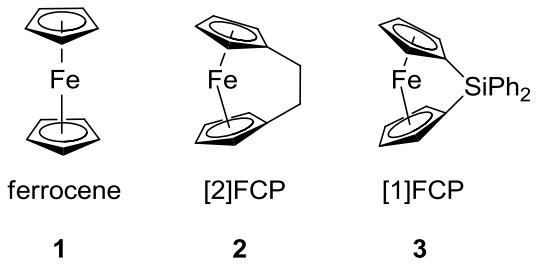


**Figure 1-1.** Ferrocene (**1**), the first carbon-bridged [2]FCP (**2**) and the first silicon-bridged [1]FCP (**3**).

The two most common routes applied for the synthesis of [1]FCPs are salt-metathesis reaction, in which 1,1'-dilithioferrocene·tmeda (tmeda = N,N,N',N'-tetramethylethylenediamine) is reacted with an element dihalide, and the flytrap route, in

which iron dichloride is reacted with an appropriately bridged dianionic linker (Scheme 1-1).[5] The interest in the field of [1]FCPs increased when high-molecular-weight metallopolymers were synthesized by ring-opening polymerization (ROP) of strained silicon-bridged [1]FCPs by Manners *et al.* in 1992.[6] In Chapter 1.3, the advances in the synthesis of metallopolymers by ROP of [1]FCPs and possible applications are discussed in more detail. The knowledge in this field was extended to a variety of bridging-elements (B, Al, Ga, Si, Ge, Sn, P, As, S, Se, Ti, Zr, Hf, Ni, Pd, Pt, U) and other bridged sandwich compounds termed [1]metallacyclophanes.[5, 7]

**Scheme 1-1.** The two major routes for the synthesis of [1]FCPs: a) salt-metathesis reaction and b) flytrap route.

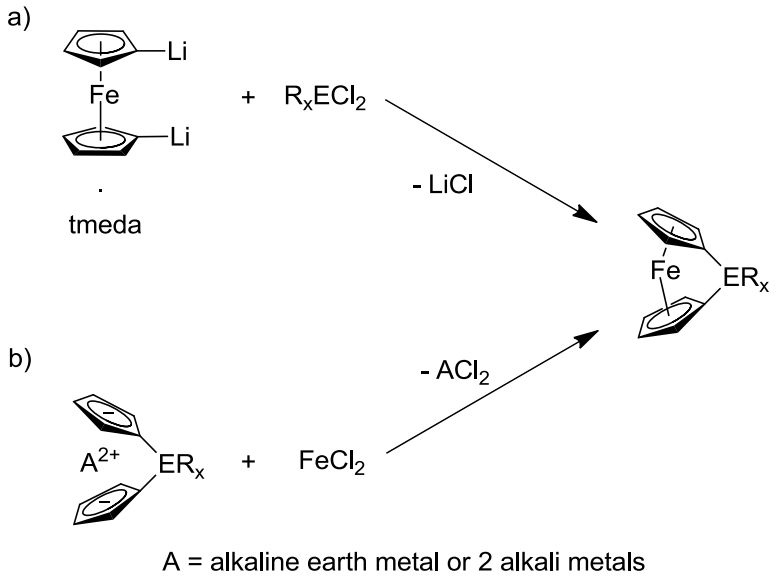


### 1.1.2 The Importance of Tilt Angle α

The tilt angle α is defined as the angle between the two tilted cyclopentadienyl rings (Figure 1-2).

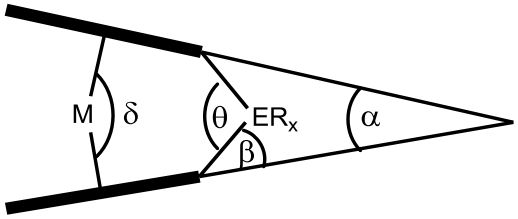


**Figure 1-2.** Depiction of tilt angle α.

The tilt angle α is the most commonly reported angle for [1]FCPs, because a major part of their strain is due to the tilt of the cyclopentadienyl rings. For example, an energy of more than 100 kJ mol$^{-1}$ was calculated to belong to the ring tilt of sulfur-bridged [1]FCP, while the strain energy of this species was determined to be 130(± 20) kJ mol$^{-1}$ by DSC.[8] Also an exponential increase in energy with increasing tilt angle of ferrocene was calculated.[9] The tilt angle α mainly depends on the size of the bridging element and the size of the metal; different ligands on the element have considerably less influence on the tilt angle α. With a decreasing size of the bridging element, the bond length between the element and the *ipso*-cyclopentadienyl carbon decreases. Hence, the *ipso*-carbon has to move further away from its original position to make this bond feasible and the tilt angle increases. If the size of the sandwiched metal increases, the distance of the aromatic ligands increases. Therefore, the *ipso*-carbon has to move further away from its original position to still keep the same bond length to the bridging-element. The tilt angle is used in arguments about the possibility of the formation of [1]metallacyclophanes with combinations of certain bridging elements and metals. The only known bridging element of the first period is boron with the highest tilt angle of 32°[10] and it is concluded that the strain due to the ring tilt is too high for other first period elements to form [1]metallacyclophanes. Similarly, [1]ruthenocenophanes ([1]RCPs) with a variety of bridging elements are reasoned not to be available, because the ring

strain would be too high. Table 1-1 shows an overview of measured tilt angles in [1]FCPs with different bridging elements.

**Table 1-1.**Tilt angles of [1]FCPs with different bridging elements.

| E | α [°] | E | α [°] | E | α [°] |
|---|---|---|---|---|---|
| B[10] | 32.4 | S[14] | 31.0 | Se[14] | 26.4 |
| Al[11] | 14.9 | Ga[15] | 15.8 | Sn[17] | 14.1 |
| Si[12] | 20.8 | Ge[16] | 19.0 | Zr[18] | 6.0 |
| P[13] | 26.9 | As[13] | 22.9 | Ni[7a)] | 28.4 |

A complete discussion of all known species and bridging moieties would go beyond the scope of this introduction. Only [1]metallacyclophanes with bridging elements relevant to this thesis will be elaborated on; group-13-bridged metallacyclophanes are the focus of Chapter 1.5, whereas silicon- and tin-bridged species are discussed in Chapters 1.1-1.4.

### 1.1.3 Silicon- and Tin-bridged [1]Ferrocenophanes

Silicon-bridged [1]FCPs are the most explored type of metallacyclophanes due to a variety of advantages in comparison with other bridging elements: minor air sensitivity, minor toxicity, comparably cheap, and some starting materials are commercially available. Moreover, the interest in their polymers obtained by ROP encouraged further research. The dimethylsilyl-bridged [1]FCP (**4**) is the most commonly utilized [1]FCP for ROPs of [1]metallacyclophanes (Figure 1-3). Many silicon-bridged [1]FCPs can be directly synthesized from salt-metathesis reactions of different dichlorodiorganosilanes with 1,1'-dilithioferrocene.[5] Other silicon-bridged [1]FCPs were obtained by replacing one or two chlorines on **5** with other groups (Figure 1-3).[19] Typically, silicon-bridged [1]FCPs have tilt angles between 19-22°.[5] Some less common species are five-

coordinated silicon-bridged [1]FCPs like **6** that exhibit significant structural changes compared to the four-coordinate silicon-bridged [1]FCPs like a weaker $C_{ispo}$–Si bond. This weaker bond can be cleaved by cationic initiators for ROP, while tetracoordinate silicon-bridged [1]FCPs are inert under these conditions (Figure 1-3).[20] Also the spirocyclic species **7** exhibits a different reactivity during polymerization as both rings open yielding cross-linked polymers (Figure 1-3).[21]

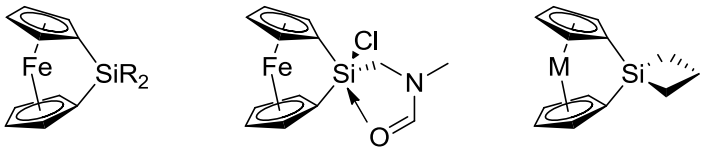


**4**: R = Me
**5**: R = Cl

**6** **7**

**Figure 1-3.** Selected silicon-bridged [1]FCPs: dimethylsilyl-bridged [1]FCP (**4**) dichlorosilyl-bridged [1]FCP (**5**) the hypercoordinated silicon-bridged [1]FCP **6**, and the spirocyclic silicon-bridged [1]FCP **7**.

A major difference between silicon-bridged [1]FCPs and tin-bridged [1]FCPs is the requirement of tin to have sterically bulky ligands like *tert*-butyl in **8**,[17] 2,4,6-trimethylphenyl (Mes) in **9**,[17] and 2,4,6-triisopropylphenyl in **10**.[22] Salt-metathesis reactions with dichlorostannanes equipped with less bulky ligands like methyl, ethyl, *n*-butyl or phenyl lead to the formation of oligomers and cyclic dimers. A similar reaction with dichlorodimethylsilane leads to the formation of a [1]FCP in a good yield. It is presumed that this is due to the larger tin atom being more exposed with smaller ligands.[23] As expected, the tilt angles of tin-bridged [1]FCPs are lower than for silicon-bridged [1]FCPs (Table 1-1). It was shown for both, silicon-bridged [1]FCPs and tin-bridged [1]FCPs, that they undergo reactions by cleaving the element-cyclopentadienyl bond in most of the ROPs.[24]

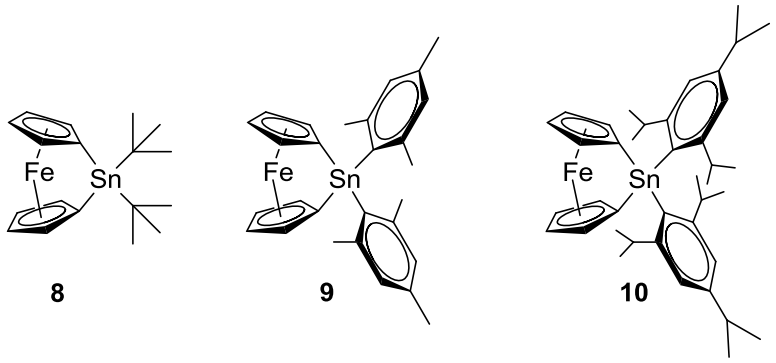


**Figure 1-4.** Tin-bridged [1]FCPs with sterically bulky ligands, **8**, **9**, and **10**.

### 1.1.4 [1]Ruthenocenophanes and other [1]Metallacyclophanes

[1]RCPs are comparably less studied than their iron homologues. Since the first report of the synthesis of a tin-bridged and a zirconium-bridged [1]RCP in 2004 (Figure 1-5),[25] the chemistry of [1]RCPs was only enriched by two aluminum- and two gallium-bridged species.[26] The aluminum- and gallium-bridged [1]RCPs are discussed in Chapter 1.5. Salt-metathesis reaction between the 1,1'-dilithioruthenocene tmeda adduct and $[ZrCl_2Cp'_2]$ ($Cp' = C_5H_4tBu$) gave the zirconium-bridged [1]RCP **11** in 35% yield (Figure 1-5). Reactions with $Mes_2SnCl_2$ afforded the tin-bridged [1]RCP **12** in 13% yield (Figure 1-5).

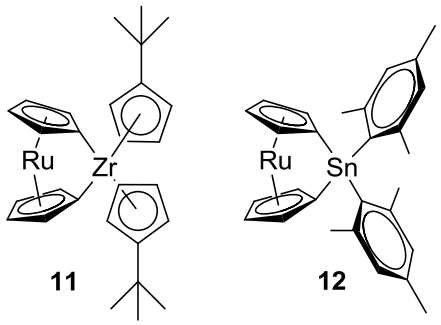


**Figure 1-5.** The tin- and zirconium-bridged [1]RCPs **11** and **12**.

The tilt angle increases expectedly by going from the tin-bridged [1]FCP equipped with the Mes ligand (**9**) to the tin-bridged [1]RCP **12** from an average of 15.2°

to an average of 20.6°. Thermal ROP of the tin-bridged [1]RCP **12** at 200 °C afforded high-molecular-weight polymers.

A variety of other metal compounds with bridged aromatic rings are known and described with the general term metallacyclophanes, which also includes FCPs and RCPs (Figure 1-6). However, for some species, for example $d^0$ *ansa* metallocenes, no ring strain evolves from the incorporation of the bridging element.[9] These species might have other applications, for example, as catalysts for olefin polymerization, but are not expected to undergo ROP to give metallopolymers. While RCPs are similar to FCPs, metallocenophanes (MCPs) incorporating other metals often prefer the presence of an additional ligand (L) attached to the metal center (Figure 1-6). Metallarenophanes consist of two benzene rings as aromatic ligands (Figure 1-6). Moreover, metallacyclophanes with two different aromatic ligands are known, for example, containing a benzene ring or a tropylium ligand in addition to the cyclopentadienyl ligand (Figure 1-6).[5]

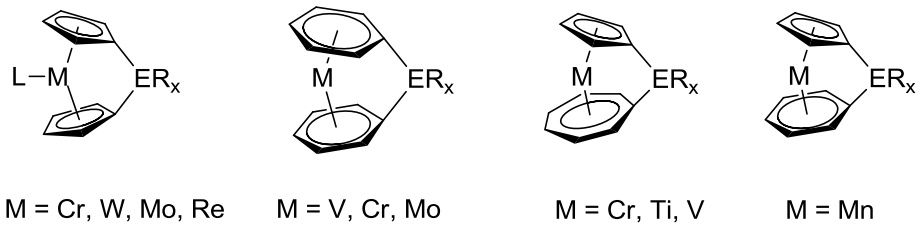


**Figure 1-6.** Examples for other known [1]metallacyclophanes.

## 1.2 [1.1]Metallocenophanes

[1.1]FCPs are formal dimers of [1]FCPs with two ferrocene moieties and two one-atom bridges (Figure 1-7). The cyclopentadienyl rings of [1.1]FCPs are nearly parallel in these species, thus [1.1]FCPs are lacking the ring-strain of [1]FCPs. Hence, [1.1]FCPs are not expected to undergo ROP. This might be the major reason, why [1.1]FCPs have been less investigated than [1]FCPs in spite of the fact that [1.1]FCPs were known nearly 20 years longer with the first carbon-bridged [1.1]FCP (**13**) being described in 1956 (Figure 1-7).[27]

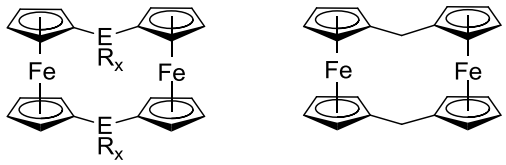


**13**

**Figure 1-7.** General formula for a [1.1]FCP and the first [1.1]FCP (**13**).

With respect to metallopolymers, [1.1]FCPs find their major importance as model compounds to probe the redox behavior of metallopolymers with similar constitution. Carbon-bridged [1.1]FCPs also found interest for their ability to produce hydrogen with strong acids (Scheme 1-2). First observations of a gas formation date back as far as 1973 (Scheme 1-2).[28] By 1988 the hydrogen formation from **13** was found to be a three-step process with two protonation reactions of the iron centers occurring fast and a rate determining step of dihydrogen elimination (Scheme 1-2).[29] The dicationic [1.1]FCP needs a reducing agent to be transferred back into its original state.

**Scheme 1-2.** Dihydrogen production from the carbon-bridged [1.1]FCP **13** in the presence of strong acids.

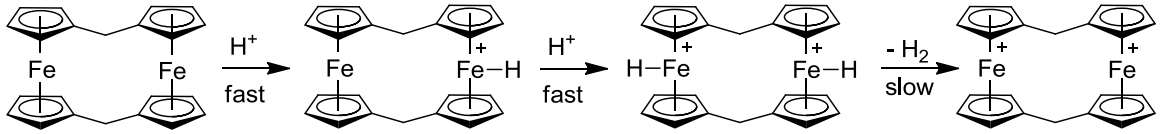


### 1.2.1 Geometric Parameters and Choices of Conformations

There are two major angles that need to be considered for [1.1]FCP, the tilt angle and the twist angle. Similar to [1]FCPs, the tilt angle α is the angle between cyclopentadienyl rings of the same ferrocene moiety, whereas the twist angle α' is defined as the angle between two bridged cyclopentadienyl groups (Figure 1-8). The tilt angle has commonly values below 5°, while the twist angle can have higher values.

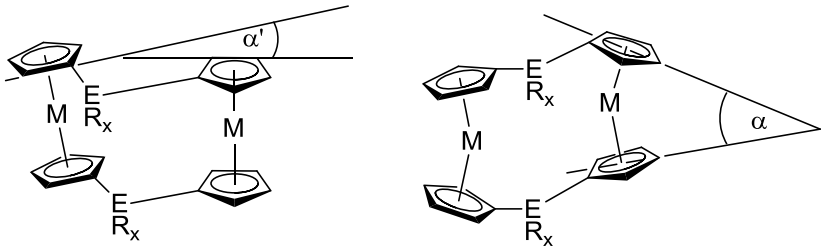


**Figure 1-8.** Twist angle α' and tilt angle α in [1.1]MCPs.

The bridges can have two possible orientations, *anti* and *syn*. In the *anti* conformation, the bridges are on opposite sides of each other, whereas in the *syn* conformation they are on top of each other (Figure 1-9).

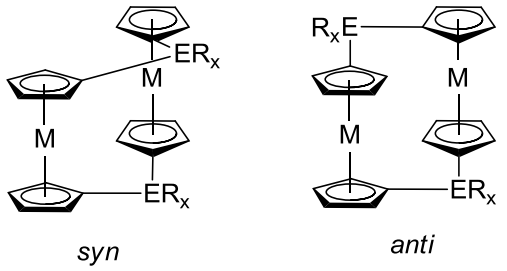


**Figure 1-9.** Depiction of the *syn* and *anti* conformation of [1.1]MCPs.

A major contributing factor to the formation of one isomer over the other is the size of the bridging element. A trend is observed, in which smaller bridging elements like boron and carbon prefer the *syn* conformation, but larger bridges favor the *anti* conformation. The metal-metal distance depends on the bridging element and increases or decreases with its size. If the metal···metal distance is shorter, then the α-protons are experiencing more repulsion from each other. Watts stated that if a carbon-bridged [1.1]FCP would have Cp-rings that are parallel to each other, then the distance between the α-protons would be only 0.8 Å, which would be an impossible severe steric interaction.[30] The steric repulsion can be reduced by twisting the Cp rings. However, the *anti* conformation is considerably more rigid than the *syn* conformation and would not allow for the same amount of the required twisting. Therefore, smaller bridging elements prefer the *syn* conformation. There is another steric repulsion that needs to be considered, namely, the repulsion between the ligands on the bridging elements. Naturally, this repulsion is larger for a *syn* conformation than for an *anti* conformation and increases with the size of the ligand.

Carbon-bridged [1.1]FCPs are usually in their *syn* conformation. However, the molecular structure for one example of a carbon-bridged [1.1]FCP in the *anti* conformation has been reported.[31] For phosphorus as a bridging element, the selectivity towards *syn* or *anti* conformation was studied. In a photolytical ROP of a phosphor-bridged [1]FCP, *syn* and *anti* conformers of the phosphor-bridged [1.1]FCP **14** were obtained (Scheme 1-3).[32] Thermal treatment of the *anti* conformer led to a nearly complete conversion to the *syn* isomer, thus, rendering the *anti* conformer less thermally stable (Scheme 1-3).

**Scheme 1-3.** Synthesis of *syn* and *anti* conformers of a phosphor-bridged [1.1]FCP (**14**) and the selective conversion to the *syn* isomer upon thermal treatment.

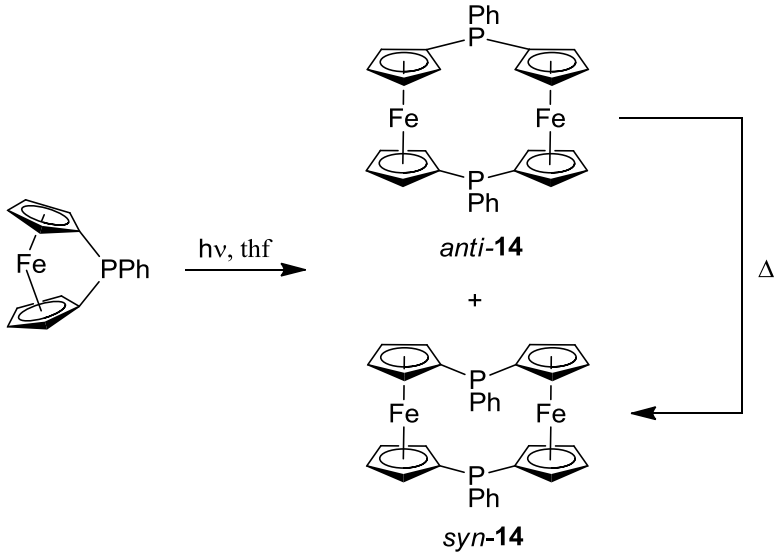


The steric repulsion between the inner α-hydrogen atoms was given as the major explanation of the higher thermal stability of the *syn* conformer. In this case, the contact of the inner hydrogen atoms was decreased by twisting the cyclopentadienyl rings about 24.8(1)°. Comparing the solid-state structure of two similar species, the authors found that the α-H···α-H distance was increased from 1.82 Å (*anti*) to 2.05 Å (*syn*).[32] Moreover, the requirement of prolonged elevated temperatures in comparison to methylene-bridged [1.1]FCPs, for which the *syn* and *anti* species are easily converted into each other even at room temperature, was attributed to the fact that an inversion of the trivalent phosphorus has higher energy barriers.[32] For another mixture of phosphor-bridged [1.1]FCP conformers, treatment with HCl at low temperatures yielded selectively *syn* conformers.[33]

There are two different orientations of substituents on the bridges. The substituents can either be in the same plane as the cyclopentadienyl rings called *endo* or perpendicular to the Cp rings named *exo* (Figure 1-10). These distinctions are particularly interesting, when it comes to bridging elements with different R groups. The

specifications *endo* and *exo* are used in the description of the *syn*-to-*syn* or *anti*-to-*anti* exchange.

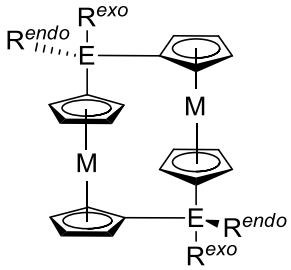


**Figure 1-10.** Depiction of the *endo* and *exo* positions in [1.1]MCPs.

*Exchanges between conformations*

An exchange of conformations was first described and thoroughly investigated for carbon-bridged [1.1]FCPs. This dynamic behavior of the carbon-bridged [1.1]FCPs is related to the exchange of conformations known for cyclohexane. In this comparison, the *anti*-[1.1]FCP can be seen as chair conformer, whereas the *syn*-[1.1]FCP would be the boat conformer (Scheme 1-4). Watts *et al.* suggested that the pathway would go through a twist conformer, in which the two ferrocenyl moieties are perpendicular to each other (Scheme 1-4),[34] whereas calculations on the MM2' level suggest that this transition state would be too high in energy.[35] As a result of their calculations, the authors suggested a different pathway that goes through an *anti* like, 60° twisted conformation.[35] However, the calculations for the 60° twisted conformation gave values that did not agree with low temperature NMR measurements.[36]

**Scheme 1-4.** *syn*-to-*syn* Isomerization via a twist conformation shown representatively for cyclohexane.

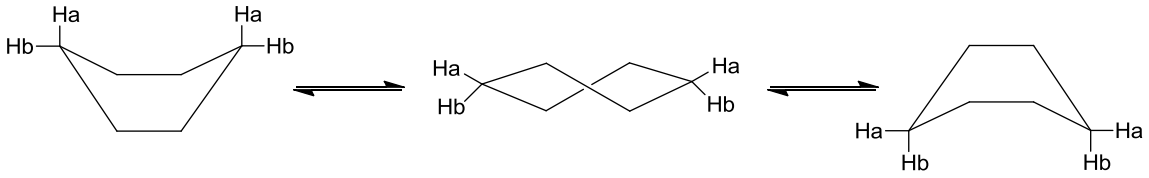


Scheme 1-5 shows how the *syn*-to-*syn* isomerization exchanges the protons in *endo* and *exo* position, $H_a$ and $H_b$, rendering them equivalent on the NMR timescale. At the same time, the inner α-cyclopentadienyl protons are taking the positions of the outer α-cyclopentadienyl protons. In this case a higher symmetry is observed on the NMR timescale and only two signals for the cyclopentadienyl protons, one for all α-protons and one for all β-protons are displayed. *anti*-to-*anti* isomerization is less common, but has been reported for a few silicon-, tin-, gallium-, and indium-bridged [1.1]FCPs (see below and Chapter 1.5).

**Scheme 1-5.** Exchange of the *exo* and *endo* protons and the outer and inner α- and β-protons during the *syn*-to-*syn* isomerization of **13**.

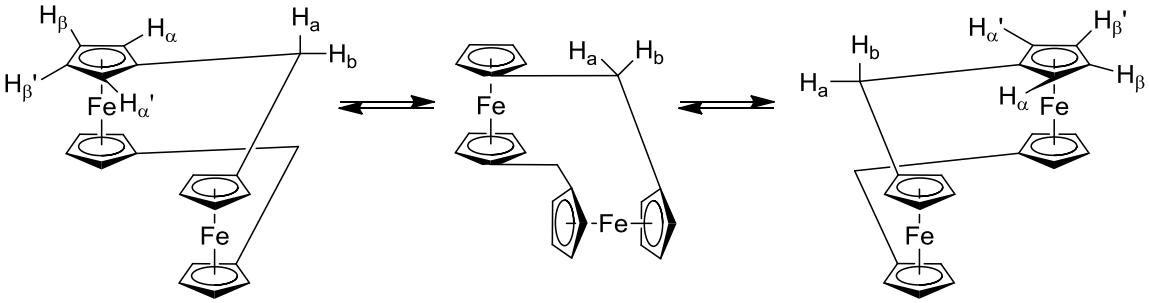


### 1.2.2 [1.1]Ferrocenophanes

*Overview of bridging elements of [1.1]FCPs*

[1.1]FCPs were known longer than [1]FCPs with the first carbon-bridged [1.1]FCP (**13**) being described in 1956 by Nesmeyanov.[27] Carbon-bridged [1.1]FCPs are

by far the most explored, but also the following bridging elements are known in literature: zinc,[37] mercury,[38] boron,[39] aluminum,[40] gallium,[41] indium,[42] silicon,[43] tin,[44] lead,[45] phosphorus,[46,32,33] arsenic,[47] and sulfur[48] are known. Table 1-2 gives an overview of known bridging units and their *syn* or *anti* conformation.

**Table 1-2.** Known bridging moieties $ER_x$ in [1.1]FCPs and their *syn* or *anti* conformations.

| Element | $R_x$ | *syn*/*anti* |
|---|---|---|
| Zn | tmeda[37] | *anti* |
| Hg | none[38] | *syn* |
| B | $Me_2$[-39] | *syn* |
| Al | Cl, tmeda;[40a] Ar′;[40b] Et, Py[40c] | *anti* |
| Ga | $CH(SiMe_3)_2$;[41a] Ar′;[41b] Me, donors[41c,d] | *anti* |
| In | Ar′;[41b] $Me_2$Ntsi[42] | *anti* |
| C | $H_2$; Ph, H; H, Me; O; S, O; S; $H_2$, O; $H_2$, S[49] | *syn (anti)*[a] |
| Si | $Me_2$;[43a,b] $Cl_2$;[43c] Me, CCPPh;[43d] Cl, $CH_2$NMeCMeO[43e] | *anti* |
| Sn | $Et_2$;[44a] *n*$Bu_2$;[44a] *n*Bu, I;[44b] *t*$Bu_2$;[44c] $Mes_2$[44c] | *anti* |
| Pb | Ph[45] | *anti* |
| P | (-)Men;[46] S, Ph;[32] Ph;[32] $NEt_2$;[33] Cl;[33] $CH_2SiMe_3$;[33] *p*-Tol[33] | *syn*, *anti* |
| As | Cl[47] | [b] |
| S | none[48] | *syn* |

a) Only once an exception of an *anti* isomer was structurally characterized. b) No comment was made by the authors about the formation of a *syn* or *anti* conformer, however, an *anti* isomer would be expected. Ar′ = 2-($NMe_2CH_2$)$C_6H_4$; $Me_2$Ntsi = –$C(SiMe_3)_2SiMe_2NMe_2$

Zinc-, mercury-, aluminum-, gallium-, indium-, lead-, phosphorus- and arsenic-bridged [1.1]FCPs were synthesized by the salt-metathesis reaction of the element dihalides with 1,1'-dilithioferrocene. Some of these elements require particular ligands to selectively form [1.1]FCPs (see the discussion in Chapter 1.5). However, for some species the salt-metathesis reaction leads to the selective formation of [1]FCPs (silicon)[43a,b] or to the formation of oligomeric material (tin).[44a] In these cases, a variety of multistep synthesis routes were explored. Recently, selective ring-opening reactions of

[1]FCPs were reported that gave [1.1]FCPs in good yields (phosphorous,[32] silicon,[49] tin[44c]).

*[1.1]FCPs with silicon and tin in bridging position*

Silicon-bridged [1.1]FCPs could not be obtained from salt-metathesis reactions, since they lead to the selective formation of silicon-bridged [1]FCPs. The first reported silicon-bridged [1.1]FCP (**15**) was synthesized separately by two groups in 1995. Chang *et al.* isolated **15** in 21% yield from the flytrap route (Scheme 1-1),[43b] whereas Manners *et al.* obtained **15** from a four step reaction in 14% overall yield (Scheme 1-6).[43a] The same product could later be isolated from transition-metal catalyzed ROP of **4** (30%),[50] through a dimerization of **4** with $[PdCl_2(PCy_3)_2]$ (90%)[49b] and through photo-controlled ring-opening of **4** in the presence of 4,4'-dimethylbipyridine (17% conversion).[49c]

**Scheme 1-6.** Synthesis of the silicon-bridged [1.1]FCP **15**.

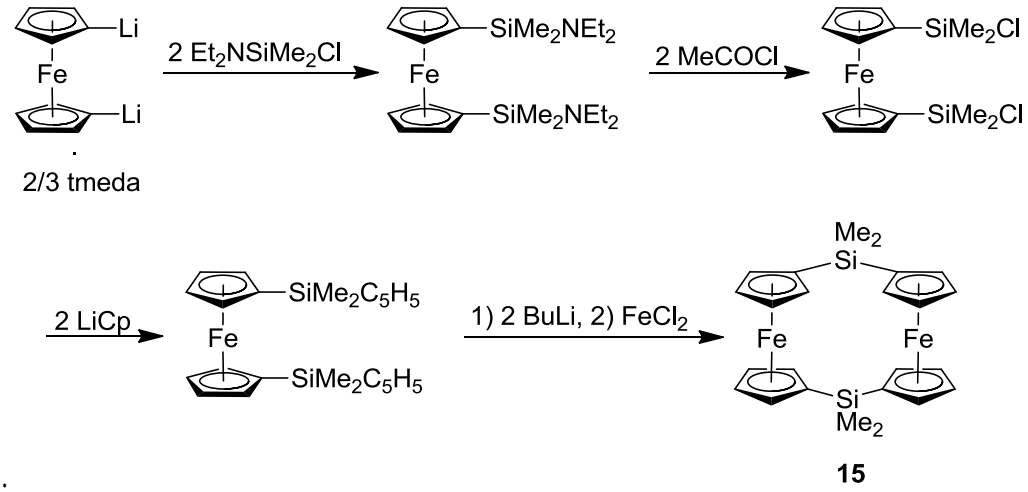


The silicon-bridged [1.1]FCP ($ER_x = SiCl_2$) **16** was obtained as a byproduct from thermal ROP of the respective [1]FCP (**5**) in 17% yield (Figure 1-11).[43c] Another silicon-bridged [1.1]FCP with $ER_x$ = SiMe(CCPh) (**17**) was obtained as a byproduct from transition-metal-catalyzed ROP of the respective [1]FCP in 22% yield (Figure 1-11).[43d]

An unsymmetrical tilting of the Cp rings with α = 10.3(3)° and 1.7(2)° in **17** was exhibited by its molecular structure in the solid state. An uncommon arrangement in which each ligand, Me and CCPh, occupies *endo* as well as *exo* positions was observed (Figure 1-11). A [1.1]FCP with a pentacoordinate silicon-bridge (**18**) was the only product formed by ring-opening of **6** with a Pd(II) catalyst and was isolated in 62% yield (Figure 1-11).[43e] In the solid state, **18** showed an unusual molecular structure with strongly tilted ferrocenyl moieties similar to a twist conformer (Scheme 1-3). Silicon-bridged [1.1]FCPs with small, symmetrical ligands exhibit only two signals in the proton NMR, thus suggesting an *anti*-to-*anti* isomerization.

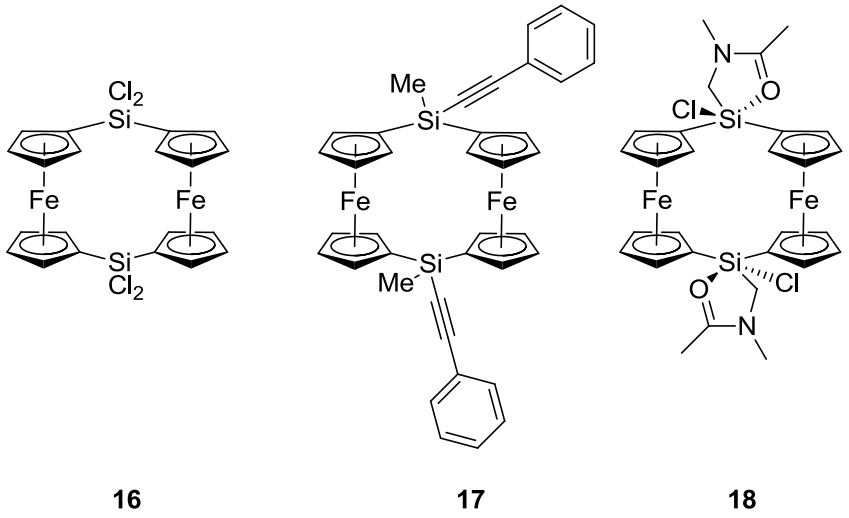


**16** **17** **18**

**Figure 1-11.** Selected silicon-bridged [1.1]ferrocenophanes (**16**, **17**, and **18**) known in the literature.

The first tin-bridged [1.1]FCPs with $ER_x$ = $SnEt_2$ (**19**) and $Sn(nBu)_2$ (**20**) were obtained in very low yields of 6 and 3% respectively from salt-metathesis reactions.[44a] The solid-state structure of **20** showed the expected *anti* conformation.[50] Reactions of **20** with iodine lead to the formation of the tin-bridged [1.1]FCP with $ER_x$ = Sn*I*n*Bu* (**21**).[44b] The butyl groups are occupying the *endo* positions, whereas the iodine atoms were in the

*exo* position. Similar to the silicon-bridged [1.1]FCPs discussed before, the $^{1}$H NMR spectrum shows only two peaks for the cyclopentadienyl groups, thus indicating that a fast *anti*-to-*anti* isomerization occurs. Nucleophilically-assisted or thermal ROP of tin-bridged [1]FCPs with $ER_x$ = Sn*t*Bu$_2$ or $SnMes_2$ (Mes = 2,4,6-trimethylphenyl) gave the respective [1.1]FCPs (**22** and **23**) in yields of 32% and 22%.[44c]

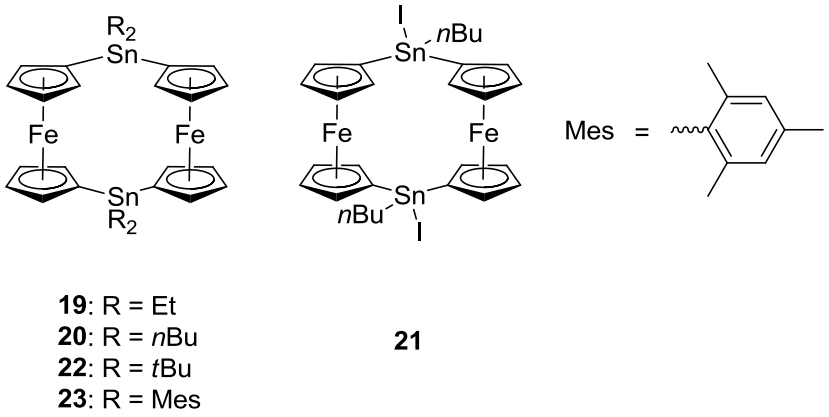


**19**: R = Et
**20**: R = *n*Bu
**22**: R = *t*Bu
**23**: R = Mes

**21**

**Figure 1-12.** Tin-bridged [1.1]FCPs (**19-23**) known in the literature.

### 1.2.3 [1.1]Ruthenocenophanes and Ruthenoferrocenophanes

[1.1]RCPs are scarcely studied species, especially in comparison with their lighter homologues, [1.1]FCPs. One possible reason for that is the difference in price between ruthenium and iron. In addition, little is known about poly(ruthenocenylsilane)s in comparison with their iron analogues which might have led to less interest in studying these model compounds. Therefore, only [1.1]RCPs with carbon and silicon as the bridging elements were reported before the research described in Chapter 5 extended the knowledge about these compounds to aluminum and gallium. In 1982, the first carbon-bridged [1.1]RCP (**24**) was reported by Mueller-Westerhoff *et al.* (Scheme 1-7).[51] It was

synthesized by a flytrap-based route and its electrochemical behavior was studied in addition to standard characterizations.[52]

**Scheme 1-7.** Synthesis of the first carbon-bridged [1.1]RCP (**24**).

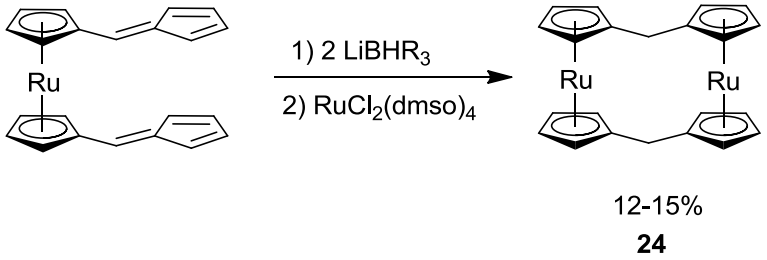


12-15%
**24**

Ten years later, the solid-state structure of **24** was reported, verifying the assumed *syn* configuration.[53] Moreover, an unexpectedly high twist angle of 33-34° was observed in **24** (Figure 1-8). The twist angles in the related [1.1]FCP **13** are significantly smaller with 13-14°. A different synthesis route for **24** as well as the synthesis of the carbonyl-bridged [1.1]RCP (**25**), the mixed carbonyl-methylene-bridged [1.1]RCP (**26**), and the carbon-bridged [1.1]RCP with $ER_x$ = CMe(OH) (**27**) was reported by Izumi *et al.* in 1988 (Scheme 1-8).[54]

**Scheme 1-8.** Synthesis of the carbon-bridged [1.1]RCPs **24-27**.

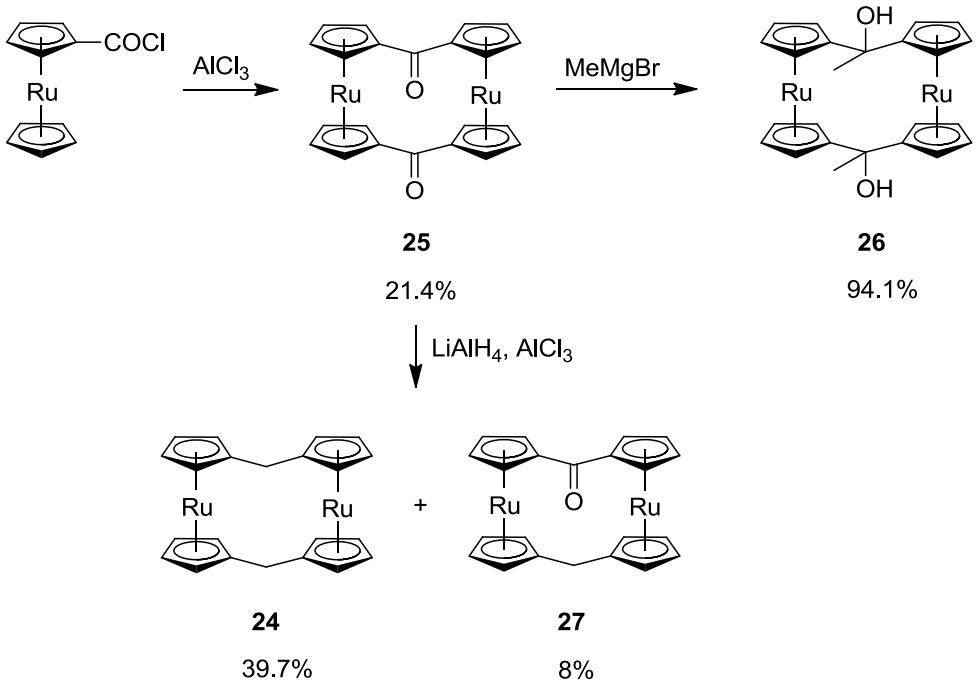


Sato *et al.* studied the [1.1]RCP **25** by variable temperature-NMR (VT-NMR) spectroscopy and found a large flexibility towards molecular twisting. The carbonyl-bridged *syn*-[1.1]FCP exhibited a similar behavior, which was not seen for the related *anti*-[1.1]FCP. On account of that, species **25** was assigned to be a *syn*-[1.1]RCP.[55] Neither the solid-state structures of **25**-**27** nor their redox properties were reported.

In 1995, Herberhold and Bärtl were able to isolate the silicon-bridged [1.1]RCP **28** from a reaction following the flytrap route (Scheme 1-9).[56] The compound was obtained in a low yield and no comment was made if **28** adopts a *syn* or an *anti* conformation. $^{1}$H NMR spectroscopy of **28** showed two signals for the Cp-protons and one signal for the dimethylsilyl group, which indicates a fast *anti*-to-*anti* or *syn*-to-*syn* isomerization.

**Scheme 1-9.** Synthesis of the silicon-bridged [1.1]RCP **28**.

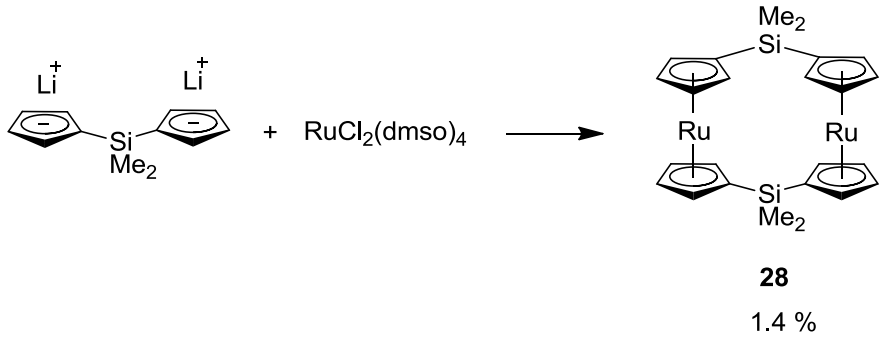


**28**

1.4 %

*[1.1]Ruthenoferrocenophanes*

[1.1]Ruthenoferrocenophanes (RFCPs) are only known with carbon as a bridging element. The first carbon-bridged [1.1]RFCP (**29**) was obtained by Mueller-Westerhoff *et al.* in yields of 15-25% (Figure 1-13).[51] Species **29** was obtained from reactions of 1,1'-bis(6-fulvenyl)ferrocene or 1,1'-bis(6-fulvenyl)ruthenocene follwing similar procedures as for the synthesis of the [1.1]RCP **24** (Scheme 1-7). The solid-state structure of this species revealed the expected *syn* conformation as well as a twisting of the metallocene units of 16.7 and 18.6°, which is larger than 12.7 and 13.8° reported for the [1.1]FCP **13**, but significantly smaller than 32.7 and 34.0° found for the [1.1]RCP **24**. The tilt angles α of **13**, **24**, and **29** all lie in the same range between 0.6-2.4°. The metal-metal distance in **13**, **24**, and **29** decreased with an increasing twist of the Cp rings and presence of ruthenium (metal-metal distance: in **13** 4.816(2) Å; in **29** 4.792(2) Å; in **24**: 4.701(1) Å).[53]

Thereafter, Watanabe *et al.* started to prepare [1.1]RFCPs. Their contribution to this area includes the synthesis of the carbonyl-bridged [1.1]RFCP (**30**) and the carbonyl-methylene-bridged [1.1]RFCP (**31**) (Figure 1-13). Species **31** was obtained by oxidation of **29** in a yield of 11.6%,[57] whereas **30** was obtained from a reaction of 1,1'-bis(chlorocarbonyl)ferrocene with ruthenocene in the presence of aluminum trichloride in

30% yield (Figure 1-13).[58] All these species were found to have *syn* conformations. However, in one of the oxidation reactions reported by Watanabe *et al.*, utilizing sulfuric acid and **29**, a monocationic species was obtained in 59.5% yield, exhibiting an *anti* conformation.[57]

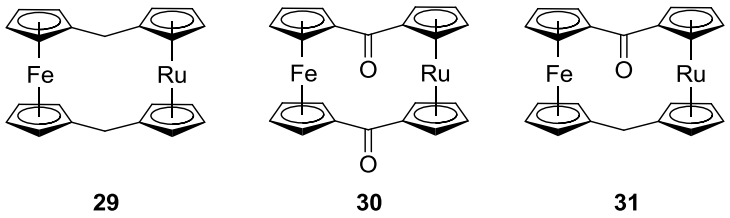


**29** **30** **31**

**Figure 1-13.** Carbon-bridged [1.1]RFCPs, **29**-**31** .

## 1.3 Ferrocenyl-based Polymers and Oligomers

Ferrocenyl-based polymers show unique properties based on the presence of the iron centers, for example redox properties. Some properties are directly linked to the molecular weight ($M_w$) of the polymers.

Generally, two different routes of polymerizations are possible: step-growth and chain-growth.[59] In a step-growth polymerization, monomers react with each other by eliminating another small molecule like LiCl or $H_2O$. Since reactions of all monomers and later formed oligomers can occur, only small oligomers are present in the beginning of step-growth polymerizations. At the end of the step-growth polymerization, the oligomers react more frequently with each other to give high-molecular-weight polymers only at conversions of >98%. In a chain-growth polymerization reaction an initiation occurs and the formed reactive species propagates, consuming monomers. The presence of high-molecular-weight polymers in relation to the conversion depends on whether or not chain determination occurs. In a non-terminating chain polymerization, the molecular weight increases proportionally to the conversion, while if chain termination occurs, the molecular weight of the polymers in the reaction mixture is independent from the conversion.[59]

For ferrocenyl-based polymers the step-growth polymerization is referred to as polycondensation reaction, while the chain-growth reaction is referred to as ROP. It is challenging to obtain high-molecular-weight organometallic polymers via condensation, because of the requirement of highly pure starting materials and exact stoichiometries. Already the possible starting material 1,1'-dilithioferrocene·tmeda is usually not obtained in a higher than 95% purity.[60]

Polycondensation reactions were utilized during the initial attempts to obtain organometallic polymers, but often only low-molecular-weight polymers could be synthesized. Seyferth *et al.* reported the synthesis of poly(ferrocenylphenylphosphine) (**32**) with a $M_w$ of 161 kDa by a condensation reaction (Scheme 1-10).[61] However, it is questionable that such a high-molecular-weight polymer can be formed by a polycondensation reaction and it was speculated that a phosphor-bridged [1]FCP formed *in situ* and underwent ROP to give **32**.[60]

**Scheme 1-10.** Synthesis of poly(ferrocenylphenylphosphine) **32** reported as a polycondensation reaction.

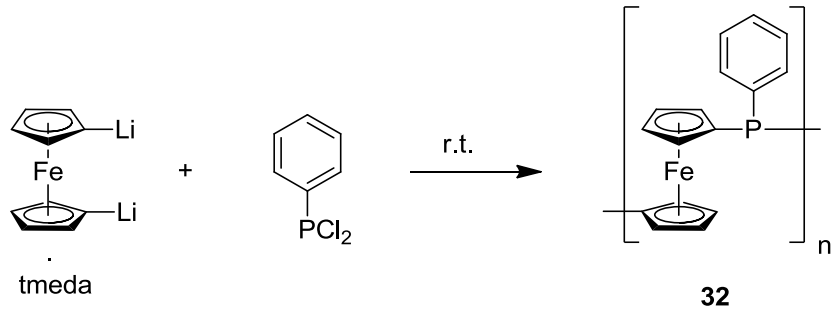


**32**

Even though ROPs have been attempted, often they led to oligomers or low-molecular-weight polymers. For example, the ring-opening of a phosphorus-bridged [1]FCP yielded only oligomers.[61] The research in this field intensified in 1992 when Manners *et al.* reported that the high-molecular-weight polymers **33** and **34** can be prepared through thermal ROP of the silicon-bridged [1]FCPs **3** and **4** (Scheme 1-11).[6]

**Scheme 1-11.** Thermal ROP of the silicon-bridged [1]FCPs **3** and **4** giving the high-molecular-weight polymers **33** and **34**.

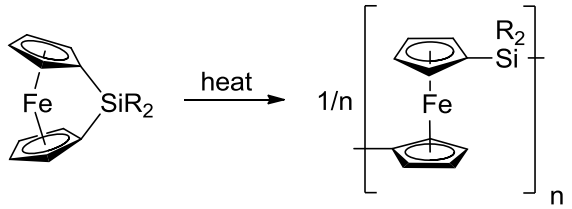


**3**: R = Ph
**4**: R = Me

**33**: R = Ph
**34**: R = Me

### 1.3.1 Ring-Opening Polymerization Methodologies

Since the discovery of thermal ROP, the ROP methodologies were extended from thermal to anionic, cationic, photo-controlled and transition-metal-catalyzed ROP. Many strained FCPs have been used as monomers for thermal ROP, because this method has a high tolerance toward functional groups and no need of highly pure starting materials. However, living polymerization cannot be achieved and the polymers exhibit a broad polydispersity. The mechanism of this reaction is unclear, but for a silicon-bridged [1]FCP the nonselective cleavage of the silicon-cyclopentadienyl bond was shown. Also an acceleration of this reaction was observed in the presence of nucleophiles like amines or pyridine.[62]

The first living carbanionic ROP initiated by lithioferrocene was reported in 1994 and yielded poly(ferrocenylsilane) (PFS) with $M_w$= 9.5 kDa.[63] The mechanism of this ROP includes silicon-cyclopentadiene bond cleavage. This methodology has the advantage that polymers with predictable molecular weight and narrow molecular weight distributions can be obtained. Manners *et al.* showed in 1994 that the copolymer **35** can be obtained from carbanionic ROP (Scheme 1-12).[64] However, the disadvantages of this method include the limitation to species that are inert to carbanions as well as the

requirement of extremely pure starting materials in order to avoid undesired chain-termination.[60]

**Scheme 1-12.** First example of the synthesis of ferrocenyl-based copolymers (**35**) via carbanionic ROP.

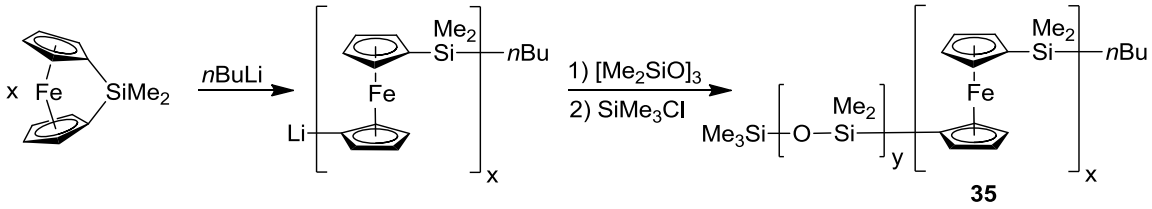


**35**

The first transition-metal-catalyzed ROPs date back to 1995.[65] Platinum [Pt(0), Pt(II)], palladium [Pd(0), Pd(II)], and rhodium [Rh(I)] complexes were found to catalyze ROPs. The mechanism is based on an insertion of the catalyst metal center into the silicon-cyclopentadienyl bond (Scheme 1-13).[24a] Moreover, the reaction was suggested to be at least partly heterogeneous, because of an observed retardation of the reaction in the presence of mercury, a known inhibitor for heterogeneous reactions (Scheme 1-13).[66] The transition-metal-catalyzed ROP methodology has the advantage that it does not require the extreme purities needed for the anionic ROP and that it can be done under mild conditions in comparison to the higher temperatures required for thermal ROP.[60]

**Scheme 1-13.** Suggested mechanism for a partly heterogeneous transition-metal-catalyzed ROP of the silicon-bridged [1]FCP **4** (cod = cyclooctadiene).

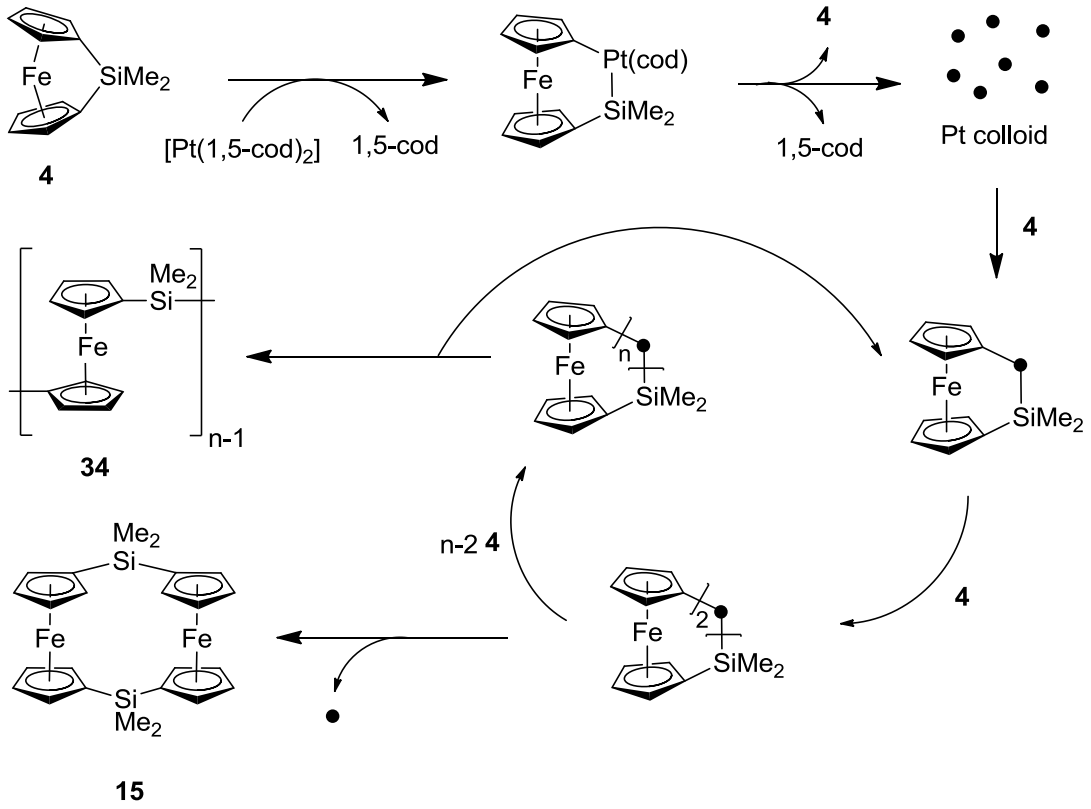


Poly(ferrocenylphosphane)s were the first species obtained through photo-controlled ROP.[67] Investigations suggest that the irradiation of the strained [1]FCP weakens the iron-cyclopentadienyl bond, which first reduces the hapticity from 5 to 1 and then leads to a bond breakage (Scheme 1-14).[68] The formed activated species with a reduced hapticity of the iron-cyclopentadienyl bond is assumed to initiate ROP of the other monomers. Scheme 1-14 shows the postulated mechanism for the example of the photolytical ROP of **36** yielding the polymers **37**. This methodology was extended to living photolytic carbanionic ROP.[69] In this case a weak carbanion like cyclopentadienyl sodium is used that can replace one of the cyclopentadienyl ligands to generate the propagating species when irradiation is active.[70]

**Scheme 1-14.** Proposed mechanism for the photolytic ROP of a phosphorous-bridged [1]FCP **36** to give the polymer **37**.

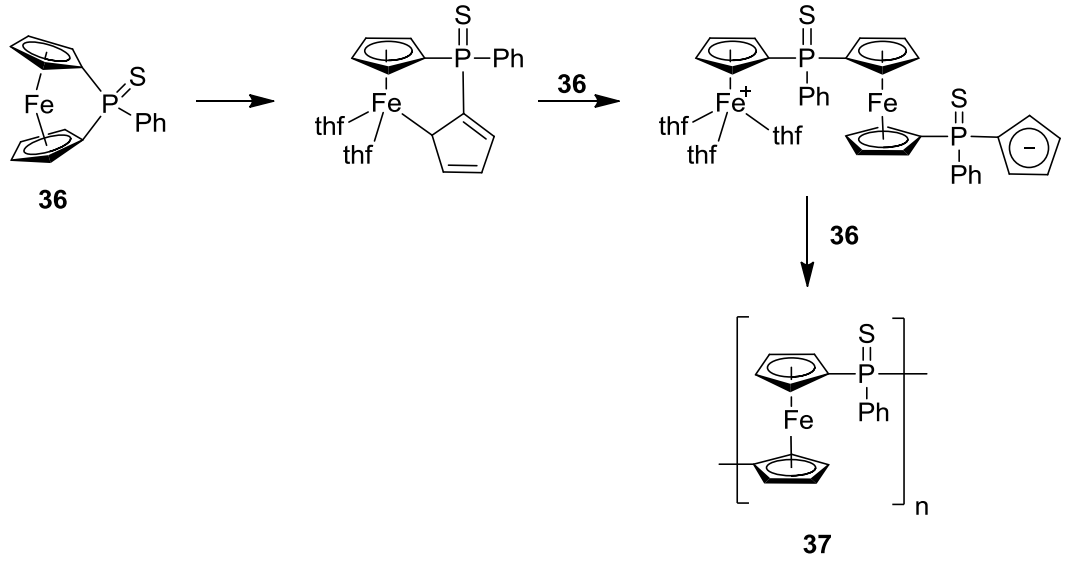


Since the first report in 1998, there are only few examples of cationic ROPs.[71]

### 1.3.2 Possible Applications of Ferrocenyl-based Polymers

PFSs are the most studied metallopolymers and many interesting results were obtained for possible applications. However, a comprehensive review of all these results would go beyond the scope of this thesis. Additionally there are several mini reviews published recently that focus on some parts of the newer developments.[72] Therefore, only a few selected fields and papers shall be introduced here to give an impression of this field and its possible developments.

Iron-, silicon-, and carbon-containing ceramics might find applications for data storage or electromagnetic shielding.[72a] These ceramics can be obtained by heating PFSs.[73] The ceramic yield is highly depending on the degree of cross-linking in the PFSs.[73] While the ceramic yields for **33** or **34** ranged from 17 to 45% (depending on the temperature), heating of **38** and **39**, respectively, afforded ceramic yields between 44 and

66% (Figure 1-14).[73] When PFS **40**, which was obtained by ROP of the spirocyclic silicon-bridged [1]FCP **7**, with a high degree of cross-linking was utilized, ceramic yields of 90% at 600 °C were achieved (Figure 1-14).[74] Moreover, the magnetic properties could be tuned between a superparamagnetic and a ferromagnetic state by applying different pyrolysis conditions.[74]

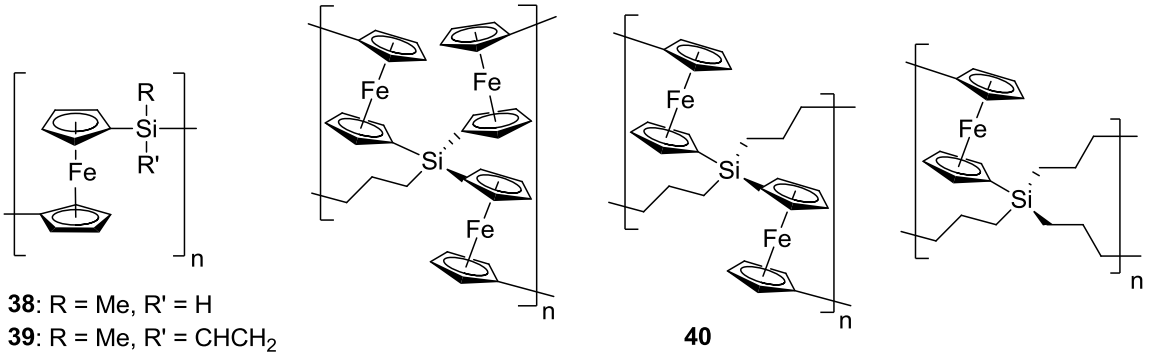


**38**: R = Me, R' = H
**39**: R = Me, R' = $CHCH_2$

**40**

**Figure 1-14.** PFS starting materials for ceramics **38** and **39** and possible linkages of the cross-linked PFS **40**.

The swelling of PFS upon oxidation was utilized for applications in redox-tunable capsules[75] and for photonic crystal displays.[76]

Vancso *et al.* reported the synthesis of capsules that can be opened by oxidation.[75] These capsules were made by repeated deposition of PFS-based polyanions and polycations in turns to give a layered structure. Application of the chemical oxidant iron trichloride resulted in swelling of the capsules to first increase their permeability until they finally disappeared. The swelling of the capsules was explained by the increase of positive charge on the chains leading to a stronger repulsion of like-charged chains and, thus, an expansion along the chain as well as in the direction of the layer growth. After full oxidation, a highly charged PFS for the former cationic PFS and a neutral PFS for the former anionic PFS was expected. The loss of electrostatic neutrality was assumed to lead

to a complete break up of the capsules. The oxidation process can be interrupted by adding a chemical reducing agent, leading to capsules with the desired permability.[75]

The possible application that is closest to commertial realization is the utilization of PFSs as the tunable component in photonic-crystal displays. The company OPALUX is working in this field.[77] The principle of operation of the PFS as the tunable component of photonic crystals is explained here based on a publication by Arsenault, Manners, and Ozin *et al*.[76] In the cell described below, the color change is based on the cross-linked PFS showing a redox-active swelling by incorporating solvent molecules or electrolyte anions. Depending on the applied voltage and the degree of oxidation of the PFS, different colors can be obtained. The material was constructed by first introducing a low-molecular-weight PFS with pendant C=C bonds to an inactive structural scaffold consisting of silica microspheres on an indium tin oxide coated glass plate. Subsequently polymerization was carried out in the presence of a multifunctional thiol to cross link the PFS. Upon oxidation, electrons are withdrawn from the iron centers and anions from the electrolyte as well as solvent molecules are entering the polymer matrix. Through the resulting swelling of the metallopolymer, the silica spheres are pushed away from each other and the color of the material shifts to red. The obtained color is also depending on the amount of cross linking and on the solvent. The color will turn back to its original green state, when electrons are pushed back into the polymer network and the solvent and anion is getting ejected.[76]

## 1.4 The Redox Properties of [1.1]Metallocenophanes and Oligo(ferrocenylsilane)s

The redox behavior is an important property of metallopolymers, since their redox properties differentiate the metallopolymers from many other, particularly organic non-redox active polymers. Therefore, the redox properties of metallopolymers may play a crucial role in their applications. For ferrocenyl-based polymers generally two reversible oxidation waves are observed. However, the concrete potentials and differences between two oxidation / reduction events are depending on the bridging elements and their ligands. In addition to that, the conditions of the electrochemical measurement including solvents and electrolytes can have a considerable influence as shown by Geiger *et al.* with the example of bis(fulvalene)dinickel.[78] The strongest interactions between the two metal centers were found for solvents of low polarity and low donor strength and for weakly coordinating electrolyte anions in contrast with the stronger coordinating traditional electrolyte anions.[78] [1.1]Metallacylophanes are commonly utilized as model compounds for the redox properties of respective polymers, since [1.1]metallacyclophanes posses two metal centers that can electrochemically interact with each other.

In a typical cyclic voltammetry measurement, one metal center is getting oxidized first at a certain potential. If the charge of this metal center shows no interaction with the second metal center, then the second metal center should be oxidized at the same potential. This behavior would be characterized as Type I according to the Robin-Day classification.[79] If there is some delocalization of the charge, then the other metal can feel the presence of the oxidized species and gets oxidized at a higher potential than the first one. This is referred to as Type II behavior. If the charge is delocalized on both metal centers, one would expect a substantially higher potential for the second oxidation, which

is classified as Type III according to Robin-Day. For [1.1]FCPs typically a Type II behavior is found. A similar behavior is observed for other [1.1]metallarenophanes like [1.1]chromarenophanes ([1.1]CAP) and [1.1]molybdarenophanes ([1.1]MAPs), if the bis(benzene)metal complexe shows a reversible one-electron oxidation. However, the redox behavior of ruthenocene is significantly different and not completely understood. The redox properties of ruthenocene and [1.1]RCPs will be described in more detail below, due to its relevance for the results discussed in Chapter 5.

### 1.4.1 The Redox Properties of [1.1]Ferrocenophanes

The results of cyclic voltammetry studies are commonly reported in the form of their halfwave potential $E_{1/2}$ with $E_{1/2} = ½ (E_{pc} + E_{pa})$. The difference between the two halfwave potentials ($\Delta E_{1/2}$) is then used to evaluate the strength of the electronic interactions. The halfway potentials are usually referenced to the ferrocene/ferrocenium couple. It should be noted that these values should be more correctly referred to as $E^0$ and $\Delta E^0$ or $E^{0'}$.[80] However, since in most publications the notation $E_{1/2}$ was used, this term will be used in this thesis. Table 1-3 shows representative $\Delta E_{1/2}$ values of [1.1]FCPs with different bridging elements including additional data.

An often raised question considering the redox behavior of [1.1]FCPs is whether the electronic interaction occurs through bonds or through space. In 1998, Manners *et al.* suggested that the interaction occurs through bonds, arguing that for group-14-element-bridged [1.1]FCPs the $\Delta E_{1/2}$ values increase with increasing iron-iron distance (Table 1-3).[17] However, different electrolytes or solvents were used in the measurements. Therefore, it is arguable, if the measured data can be conclusive enough to attest this suggestion.

**Table 1-3.** $\Delta E_{1/2}$ values for selected [1.1]FCPs referenced to the $Fc/Fc^+$ redox couple.

| $ER_x$ | $CH_2$ | $SiMe_2$ | $SiCl_2$ | $Sn\textit{n}Bu_2$ | $Sn\textit{t}Bu_2$ | $SnMes_2$ | GaAr′ |
|---|---|---|---|---|---|---|---|
| Fe-Fe[Å] | 4.816(2) | 5.171(9) | 5.930 | 5.50 | 5.474(1) | 5.248(1) | 5.462 |
| $E_{1/2}^1$ [V] | -0.09 | 0.01 | 0.13 | 0.50 | -0.06 | 0.01 | 0.05 |
| $E_{1/2}^2$ [V] | 0.11 | 0.26 | 0.48 | 0.70 | 0.21 | 0.29 | 0.35 |
| $\Delta E_{1/2}$[V] | 0.20 | 0.25 | 0.35 | 0.20 | 0.27 | 0.28 | 0.30 |
| Solvent | $C_6H_5CN$ | DCM | MeCN | DCM | DCM | DCM | DCM |
| Electro- | $[Bu_4N]$ | $[Bu_4N]$ | $[Bu_4N]$ | $[Bu_4N]$ | $[Bu_4N]$ | $[Bu_4N]$ | $[Bu_4N]$ |
| lyte | $[BF_4]$ | $[PF_6]$ | $[ClO_4]$ | $[BF_4]$ | $[PF_6]$ | $[PF_6]$ | $[PF_6]$ |
| reference | 53 | 43a | 43c | 44b | 17 | 17 | 41b |

### 1.4.2 The Redox Properties of Ruthenocene, [1.1]Ruthenocenophanes and [1.1]Ruthenoferrocenophanes

*The redox behavior of ruthenocene*

The redox chemistry of ruthenium is complex, particularly in comparison with ferrocene, which is the standard reference for electrochemical measurements in non-aqueous solvents.[81] The first study of the redox behavior of ruthenocene was carried out by Wilkinson alongside its synthesis in 1952.[82] Page and Wilkinson reported a one-electron oxidation for ruthenocene[83] and the isolation of $[Cp_2Ru]ClO_4$ after electrochemical oxidation.[82] The one-electron oxidation measured by Wilkinson on a mercury electrode was doubted, when Gray *et al.* characterized the product of the ruthenocene oxidation on a mercury electrode as $Hg[RuCp_2]_2^{2+}$, which suggests a two-electron oxidation of ruthenocene.[84] Other older reports also assigned a two-electron oxidation to ruthenocene.[85] The two-electron oxidation of ruthenocene is also supported by the fact that ruthenium(IV) salts of the type $[RuCp_2X]^+Y^-$ were isolated after electrochemical[86] or chemical oxidation.[87] The oxidation of ruthenocene was found to be not electrochemically reversible until Mann *et al.* reported a reversible one-electron oxidation of ruthenocene, when the weak coordinating anion $[B\{C_6H_3(CF_3)_2\}_4]^-$ was used

as the anion of the electrolyte.[88] Geiger *et al.* found a similar redox behavior of ruthenocene with another weak coordinating electrolyte anion, $[B(C_6F_5)_4]^-$.[89] Moreover, Geiger *et al.* studied the chemical fate of the ruthenocenium cation in the presence of $[B\{C_6H_3(CF_3)_2\}_4]^-$ and $[B(C_6F_5)_4]^-$ at low temperatures.[90] At temperatures of 256 K, the simple one-electron oxidation of ruthenocene to ruthenocenium is accompanied by two other oxidations at higher potentials and the respective products were identified to be the bis(ruthenocenium) dication **41** and the unusual species **42** (Figure 1-15). The respective osmocenium species had been previously characterized including their solid-state structures.[91]

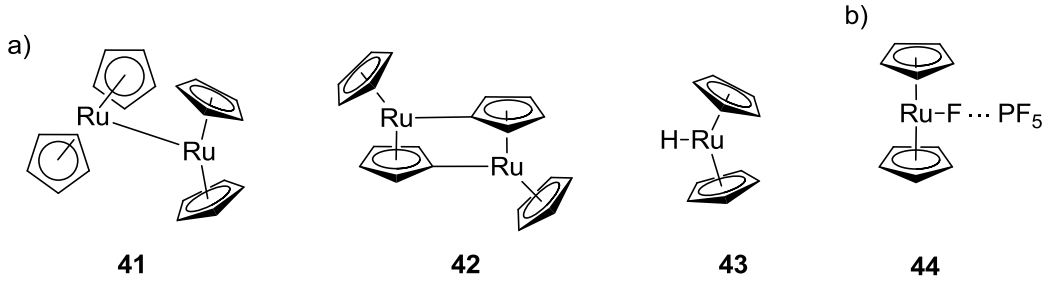


**Figure 1-15.** Products formed by further reactions of the electrochemically obtained ruthenocenium cation a) in the presence of the weakly coordinating electrolyte anions $[B(C_6F_5)_4]^-$ and $[B(C_6H_3(CF_3)_2)_4]^-$, **41**, **42**, and **43** and b) in the presence of the traditional electrolyte anion $[PF_6]^-$, **44**.

Geiger *et al.* showed that a temperature dependent equilibrium exists between the ruthenocenium cation, its dimer **41**, and the product **42** in combination with ruthenoceniumhydride (**43**) (Figure 1-15). All those products were able to re-form ruthenocene upon reduction. Moreover, the addition of the traditional electrolyte anion $[PF_6]^-$ to the previous electrolyte, $[Bu_4N][B(C_6F_5)_4]$ or $[Bu_4N][B\{C_6H_3(CF_3)_2\}_4]$, led to a significant decrease in the reversibility of the oxidation. With an increasing amount of added $[PF_6]^-$, the oxidation of ruthenocene became less and less reversible. Geiger *et al.*

suggested that a direct adduct of ruthenocenium with the anion occurs and that a fluorine bond forms *as* shown for **44** (Figure 1-15). The resulting $PF_5$ species may or may not be in proximity of the fluorine. An isolation of species **44** was not pursued.

Ruthenium-ruthenium bond formation subsequent to the oxidation of ruthenocene-based species was also reported for the carbon-bridged [1.1]RCP **24** (that will be discussed in more detail later)[92] and the carbon-bridged [2]RCP **45**[93] based on the molecular structures of the oxidized products. The ruthenium-ruthenium bond formation and the reversible one-electron oxidation of **45** was observed in the presence of the weakly coordinating electrolyte anion $[B(C_6F_5)_4]^-$. Calculations showed that **45** is more reactive towards dimerization than ruthenocene.[93]

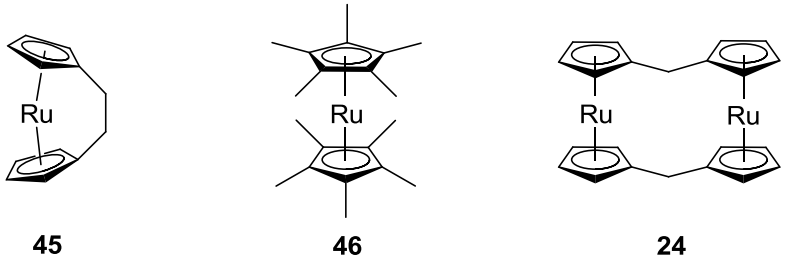


**Figure 1-16.** Depiction of ruthenocene-based compounds exhibiting interesting redox properties, **45**, **46**, and **24**.

Interestingly, when decamethylated ruthenocene (**46**) was electrochemically oxidized, a reversible one-electron oxidation was observed showing that the methyl groups protect the ruthenium(III) center from nucleophilic attacks (Figure 1-16).[94] Based on this fact, it was concluded that the different redox behavior of ruthenocene in contrast with ferrocene is likely based on the larger size of ruthenium, leading to a larger separation of the cyclopentadienyl rings and rendering the ruthenium(III) vulnerable toward nucleophiles.

Recent studies of the redox properties of ruthenocene in aqueous media showed an electrochemically irreversible one-electron oxidation to ruthenocenium, which underwent dimerization to **41**.[95] Large counter anions were found to stabilize **41**, while in the presence of small counter anions, disproportionation to ruthenocene and the ruthenocenium dication occurred.[95] Based on their study of the redox behavior of ruthenocene in different room temperature ionic liquids, Rogers *et al*. suggested that under these conditions first an one-electron oxidation of ruthenocene to ruthenocenium took place.[96] The ruthenocenium cation was then highly susceptible to either undergo dimerization to **41** or nucleophilic attack by an anion of the ionic liquid. In the latter case, further oxidation of the ruthenium centers occured. Since Rogers *et al.* measured a two-electron oxidation, they concluded that a nucleophilic attack occurred.[96]

*The redox behavior of [1.1]RCPs*

In 1982, Mueller-Westerhoff *et al.* reported the only electrochemical study of a [1.1]RCP, namely, of the methylene-bridged [1.1]RCP **24** (Scheme 1-7).[52] Surprisingly, not the expected two irreversible two-electron oxidation waves were observed for **24**, but one reversible two-electron oxidation wave in the presence of the traditional electrolyte anion $BF_4^-$ was found. Moreover, the oxidation potential of **24** was significantly lower than that of ruthenocene (**24**: $E_{1/2}$ = 380 mV, ruthenocene: E = 920 mV).[52] Based on NMR measurements of the oxidized **24**, it was suggested that one of the ruthenocene moieties is in a dicationic form, while the other ruthenocene moiety remains in its original oxidation state. Ten years later, Mueller-Westerhoff *et al.* isolated **47** after chemical oxidation and studied **47** by single-crystal X-ray analysis (Figure 1-17).[92] The

molecular structure of [**47**][$BF_4$]$_2$ in the solid state clearly showed the presence of a ruthenium-ruthenium bond with a bond-length of 2.953(1) Å (Figure 1-17).

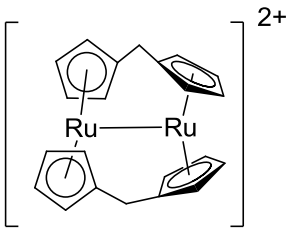


**47**

**Figure 1-17.** Depiction of the oxidized carbon-bridged [1.1]RCP (**47**) exhibiting a ruthenium-ruthenium bond.

Species **47** exhibited an unusually twisted conformation in which the ruthenocene moieties have a twist angle α' of 75° and a tilt angle α of 28°. Based on the proximity of the ruthenium centers in **24** with 4.701(1) Å in the solid state and an estimated ruthenium-ruthenium distance of 3.6 Å during the *syn*-to-*syn* exchange, the authors suggested that a non-bonding interaction between the atomic orbitals of the ruthenium centers occurs in **24**. The authors illustrate the idea with a molecular orbital diagram in which first the atomic orbitals of ruthenium facing each other are split to form a bonding and an antibonding orbital. Therefore, the first electron is removed from the antibonding orbital at a lower oxidation potential and at the same time the bond order is increased to 0.5. This increases the splitting of the molecular orbitals and the next electron could be removed at an even lower potential leading to a bond order of 1. A direct two-electron oxidation of one ruthenium center and a subsequent donor bonding of the other ruthenium center was ruled out by the authors, since in this case, a similar oxidation potential of **24** and ruthenocene would be expected. Based on the latest studies of the redox properties of ruthenocene (see above), it can be assumed that the proximity of the

two ruthenium centers facilitates the dimerization of the ruthenocenium cations so that even in the presence of an $[BF_4]^-$ electrolyte anion dimerization occurs, while with a traditional electrolyte anion a nucleophilic attack and subsequent second oxidation at the same potential would be expected.

*The redox behavior of [1.1]RFCPs*

Mueller-Westerhoff *et al.* also investigated the electrochemical behavior of the methylene-bridged [1.1]RFCP (**29**).[53] A reversible one-electron oxidation for the iron center was observed at 400 mV, which is close to the potential of the first oxidation wave of the methylene-bridged [1.1]FCP **13** ($E_{1/2}$ = 410 mV). At a potential of 940 mV, an electrochemically irreversible two-electron oxidation of the ruthenium center occurs, which is close to the oxidation potential of ruthenocene at 920 mV. Watanabe *et al.* reported the same behavior for the carbonyl-bridged [1.1]RFCP **30**.[57]

### 1.4.3 The Redox Properties of Oligo(ferrocenylsilane)s

In depth studies of the redox properties of the cyclic and linear oligo(ferrocenylsilane)s **$34_n$c** and **$34_n$l** were carried out by Manners *et al.* (Figure 1-18).[97] In both cases, a general trend was observed, which is different for odd compared to even numbered ferrocenediyl moieties.

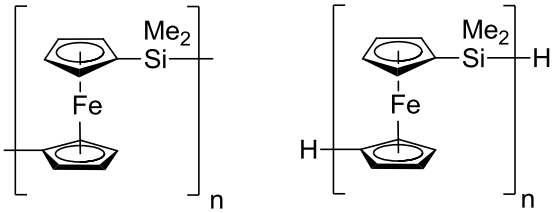


**$34_n$c** **$34_n$l**

**Figure 1-18.** Electrochemically studied cyclic and linear oligo(ferrocenylsilane)s (**$34_n$c** and **$34_n$l**).

For linear oligomers with odd numbers of repeating units, two reversible redox waves were observed (Figure 1-19).[97a] For **34$_3$l** it was clearly seen that the first oxidation is a two-electron oxidation (Figure 1-19 a, x=1). The given rationale is that every other ferreocenyl moiety and the remaining end group are getting oxidized at the same potential and the other iron centers that are now surrounded by oxidized species are getting oxidized at a higher potential. The typical pattern for linear oligomers with an even number of repeating units is that of three redox waves, of which the second redox wave always belongs to one electron. However, if the number of repeating units is increasing to those of polymers, the middle peak decreases so much in relative intensity that only two oxidation waves can be seen similar to the odd numbered species.

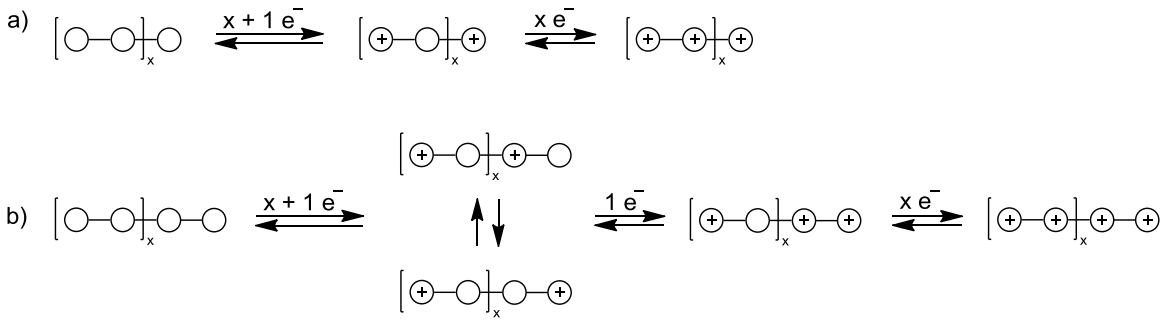


**Figure 1-19.** Interpretation of the redox behavior of a) odd numbered and b) even numbered linear oligo(ferrocenylsilane)s **34$_n$l**.

An opposite behavior considering the redox events with an odd or even number of ferrocenediyl moieties for cyclic oligo(ferrocenylsilane)s **34$_n$c** was observed when compared to linear oligo(ferrocenylsilane)s **34$_n$l** (Figure 1-20).[97b] Cyclic oligo(ferrocenylsilane)s with an even number of repeating units exhibited two oxidation waves, that might be due to overlaps of more redox waves. The cyclic tetramer **34$_4$c** showed indications thereof by exhibiting two shoulders that can be found on the two

major redox waves. Odd numbered cyclic oligo(ferrocenylsilane)s like **34$_7$c** gave three oxidation waves with the middle one referring to a one-electron oxidation (Figure 1-20 b).

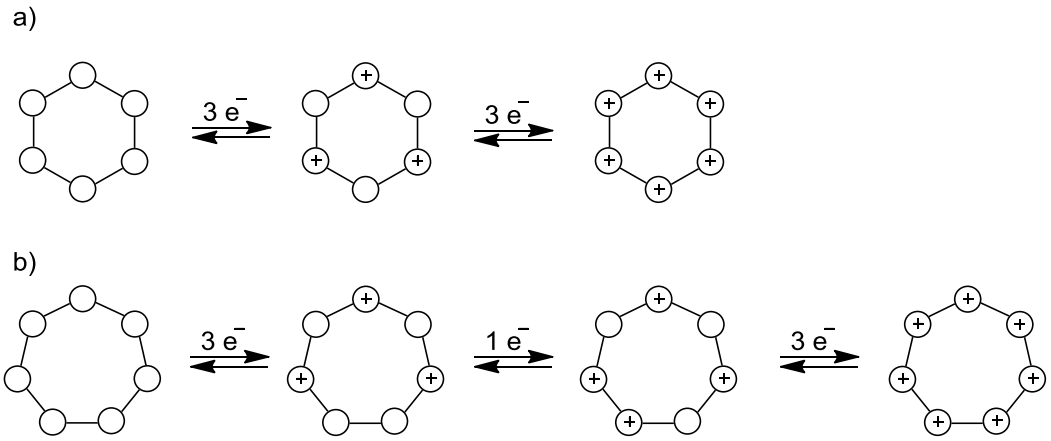


**Figure 1-20.** Explanation for the redox behavior of cyclic oligo(ferrocenylsilanes) shown for the examples of a) **34$_6$c** and b) **34$_7$c**.

## 1.5 Group-13-Element-Bridged [1]Metallocyclophanes, [1.1]Metallocyclophanes, and Metallopolymers

The major focus of this thesis is on aluminum- and gallium-bridged MCPs and their polymeric species. Therefore, the literature of metallacyclophanes that are bridged by group-13 elements and related species is reviewed.

Of course, boron as a second period element shows a chemistry that is significantly different from its heavier group members. The difference manifests itself in its small size and high electronegativity (Table 1-4).[98] As a consequence of its different properties, boron needs significantly different ligands than aluminum and gallium in order to be stabilized in metallocyclophanes. Aluminum and gallium have similar sizes and electronegativities with aluminum being generally more Lewis-acidic than gallium (Table 1-4). Due to their similar properties, aluminum and gallium show a similar reactivity during the synthesis of metallacyclophanes. Indium is the largest in size, has a similar electronegativity to aluminum and gallium and has the least Lewis acidity among the four elements (Table 1-4). Moreover, indium prefers a higher coordination number than the smaller group-13 elements. It is presumed that the larger size of indium compared to aluminum and gallium is the major reason for its different reactivity in salt-metathesis reactions. Thallium was never investigated as a bridging element for metallacyclophanes. One of the most important reasons would be that the majority of thallium(III) compounds are not stable and decompose to thallium(I) species.

**Table 1-4.** Properties of group-13 elements.

| | boron | aluminum | gallium | indium | thallium |
|---|---|---|---|---|---|
| Metal radius /pm | (80-90) | 143 | 135 | 167 | 170 |
| Ionic radius /pm* | 27 | 53.5 | 62.0 | 80 | 88.5 |
| EN | 2.0 | 1.5 | 1.6 | 1.7 | 1.8 |

* in the oxidation state 3+, hexacoordinated.

### 1.5.1 Boron-bridged [1]Metallacyclophanes, Borata[1.1]ferrocenophane, Metallopolymers and Bis(ferrocenyl) Species

*Boron-bridged [1]metallacyclophanes*

The first boron-bridged metallacyclophanes were the [1]FCPs **48** and **49**, which were reported in a short communication in 1997 by Braunschweig and Manners *et al.* (Scheme 1-15).[10] The boron bridge in these species is part of an aminoborane fragment. The nitrogen in the aminoborane is equipped with sterically bulky ligands and the bond length between boron and nitrogen is in the range of a double bond (Scheme 1-15). Boron is the only element from the first row for which a [1]FCP could be isolated. Because of the small radius of boron, boron-bridged [1]FCPs have highly tilted Cp rings and tilt angles α as high as 32° were determined by crystallography. Species **48** was investigated for thermal ROP initiated at 190 °C, but mainly insoluble material was obtained. $^{1}$H NMR spectroscopy of the soluble part of the materials showed the presence of oligomers and mass spectrometry revealed peaks for the boron-bridged [1.1]FCP and [1.1.1]FCP.[10]

**Scheme 1-15.** Synthesis of the boron-bridged [1]FCPs **48**, **49**, and **50**.

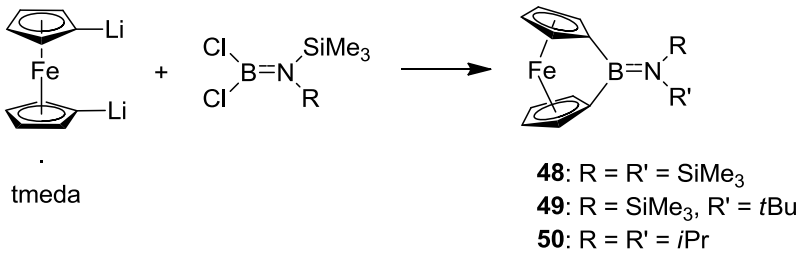


Braunschweig, Green, and Manners *et al.* reported the synthesis and characterization of **50** and the reactivity of **49** and **50** in a full article in 2000 (Scheme 1-15 and Figure 1-21).[99] Species **50** reacted with $[Fe(CO)_5]$ by insertion of the iron center into the Fe-Cp bond and the formation of an iron-iron bond, while **49** reacted with $[Co_2(CO)_8]$ by ring-opening via an insertion of the cobalt center into the Fe-Cp bond (Figure 1-21).

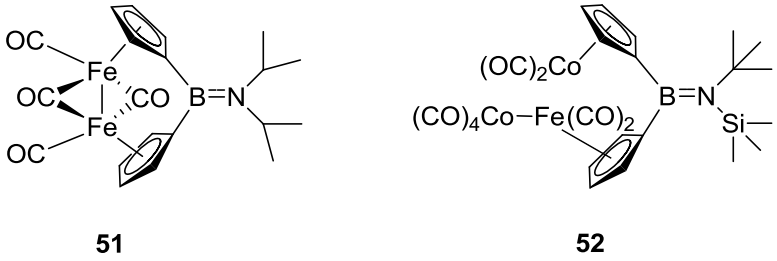


**Figure 1-21.** Species **51** and **52** obtained from reactions of the boron-bridged [1]FCPs **49** and **50** with metal carbonyls.

Boron-bridged [1]CAPs can be obtained from salt-metathesis reactions of dilithio(bisbenzenechromium) with the respective aminodihaloboranes in moderate yields of 42 – 48% (Scheme 1-16).[100] As expected, the very sensitive boron-bridged [1]CAPs **55** exhibited a large tilt angle of 26.6(3)°. Preliminary results of the thermal ROP lead to decomposition of the boron-bridged [1]CAPs to Cr(0) metal. The addition of BuLi to **53** resulted in ring-opening and [1.1]CAPs were observed by mass spectrometry.[100]

**Scheme 1-16.** Synthesis of the boron-bridged [1]CAPs, **53**, **54**, and **55** and the boron-bridged [1]vanadarenophane **56**.

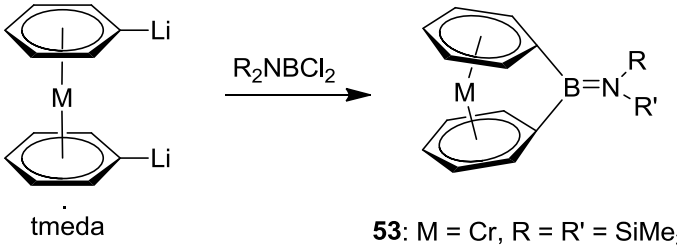


**53**: M = Cr, R = R' = $SiMe_3$
**54**: M = Cr, R = R' = *i*Pr
**55**: M = Cr, R = $SiMe_3$, R' = *t*Bu
**56**: M = V, R = R' = $SiMe_3$

The boron-bridged [1]vanadarenophane ([1]VAP) **56** equipped with the bulky bis(trimethylsilyl)amino group on boron was synthesized by salt-metathesis reaction in a good yield of 75% (Scheme 1-16).[101] A large tilt angle of 31.1° was determined for **56**. Attempted ROP of **56** with a platinum catalyst resulted in the ring-opened species **57**.[102] The platinum catalyst reacted stochiometrically with **56** by ring-opening it, followed by the addition of one molecule of deuterated benzene to vanadium (Figure 1-22).[102]

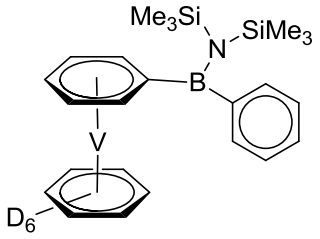


**57**

**Figure 1-22.** Species **57**, obtained by ring-opening of the [1]VAP **56** in the presence of platinum.

The boron-bridged [1]trochrocenophanes **58** and **59**[103] and the boron-bridged [1]trovacenophane **60**[104] were synthesized by salt-metathesis reactions in yields of 63%, 70%, and 37%, respectively (Scheme 1-23). Based on the larger size of the sandwiched metal, the [1]trovacenophane **60** has a higher tilt angle with 28.23° than the respective [1]trochrocenophane **58** with 23.87(13)° (Scheme 1-17).

**Scheme 1-17.** Synthesis of boron-bridged [1]trochrocenophanes **58** and **59** and the [1]trovacenophane **60**.

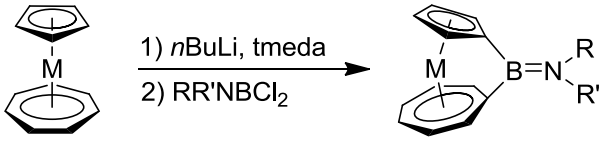


**58**: M = Cr, R = R' = $SiMe_3$
**59**: M = Cr, R = $SiMe_3$, R' = *t*Bu
**60**: M = V, R = R' = $SiMe_3$

*Diborata[1.1]ferrocenophane*

The formation of [1.1]metallacyclophanes as one of the products of attempted ROP was observed by mass spectrometry, but none of these species was isolated.[10,100] The only isolated boron-bridged [1.1]FCP is anionic as a consequence of its synthesis via a condensation reaction (Scheme 1-18).[105] Species **61** showed the expected *syn* conformation as well as a fast *syn*-to-*syn* isomerization. The solid-state structure displayed a considerable twist of the ferrocenediyl moieties to each other of 22°. Cyclic voltammetry of this compound showed an irreversible oxidation at a negative potential of -0.58 V (vs $FcH/FcH^+$), which was attributed to the high electron density in the anionic [1.1]FCP.

**Scheme 1-18.** Synthesis of the diborata[1.1]ferrocenophane **61**.

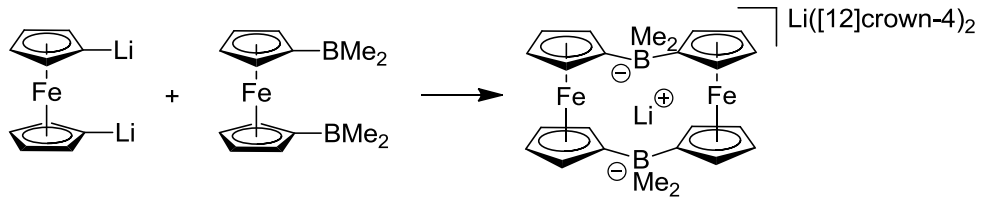


**61**

*Poly(ferrocenylborane)s*

Boron-bridged polymers can be obtained by condensation reactions. Jäkle, Holthausen, and Wagner *et al.* reported in a short communication the synthesis of the

mesitylboron-bridged polyferrocenes **62** and **63** (Scheme 1-18).[106] Species **62** was obtained from condensations of 1,1'-bis(dibromoboryl)ferrocene in a very good yield of 92% (Scheme 1-19). Since **62** was quite sensitive to air and moisture, it was treated with mesitylcopper to give the more stable species **63** in an overall yield of 75% starting from the monomer (Scheme 1-19). The average molecular weight of **63** was determined by GPC to be 5.16 kDa, referring to a low-molecular-weight polymer. Heating of the polymer **63** to 403 °C resulted in a ceramic material with a ceramic yield of only 28%. Cyclic voltammetry measurement of **63** showed two reversible oxidation waves with a separation of 705 mV. This separation is significantly larger than for bis(ferrocenyl)mesitylborane (see below).

**Scheme 1-19.** Synthesis of the boron-bridged polymers **62** and **63**.

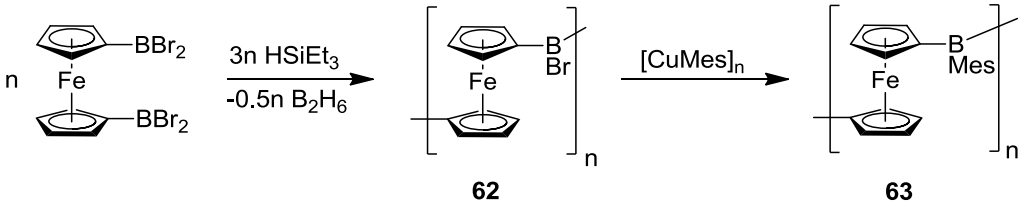


**62** **63**

Jäkle and Wagner *et al.* reported in a full paper the synthesis of the boron-bridged polymer **64**, which was obtained by condensation reactions of 1,1'-ferrocenylene-hydridoborates (Scheme 1-20).[107] The air- and moisture sensitive polymeric species **64** was then converted by hydroborations with phenylacetylene or *tert*-butylacetylene into the polymers **65** and **66** (Scheme 1-20). The molecular weights of **65** and **66** could not be determined since the species were too sensitive for GPC analysis and the scattering intensity of the DLS measurements was too small to give reliable results.

**Scheme 1-20.** Synthesis of the poly(ferrocenylborane)s **64**, **65**, and **66** via condensation reactions.

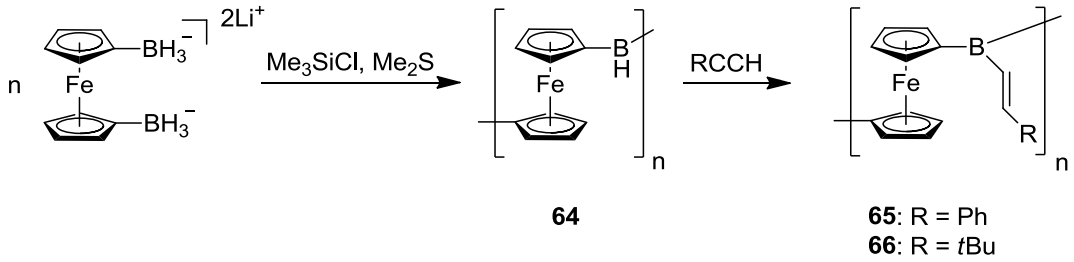


**64**

**65**: R = Ph
**66**: R = *t*Bu

*Bis(ferrocenyl)boranes*

The bis(ferrocenyl)boranes **67**-**72** were studied as model compounds for the respective polymers **62**-**66** (Scheme 1-21). Similar to the respective polymers, the bis(ferrocenyl)boranes **67** and **68** were obtained directly from condensation reactions of ferrocenylborates (Scheme 1-21).[106,107] These were subsequently transferred into the more stable compounds **69**, **70**, and **71** (Scheme 1-21).[106,107] Species **72** was obtained, when the condensation of lithium ferrocenylhydridoborate was carried out in the presence of cyclohexane (Scheme 1-21).[107] The electrochemical behavior of **69** was studied by cyclic voltammetry and a pronounced interaction between the two ferrocenediyl moieties was found with $\Delta E_{1/2}$ = 422 mV.[106] These bis(ferrocenyl)borane model compounds were also used to investigate if a π-conjugation of the Cp rings via the empty orbital on boron would be possible. The molecular structures of **69**, **70**, and **71** indicated an overlap of the π-clouds based on the dihedral angles that were observed between boron and the carbon atoms bonded to it (**69**: 21.8 and 14.1°, **70**: 12.3 and 21.1°, **71**: 17°).[106,107]

**Scheme 1-21.** Synthesis of the bis(ferrocenyl)boranes **67**-**72**.

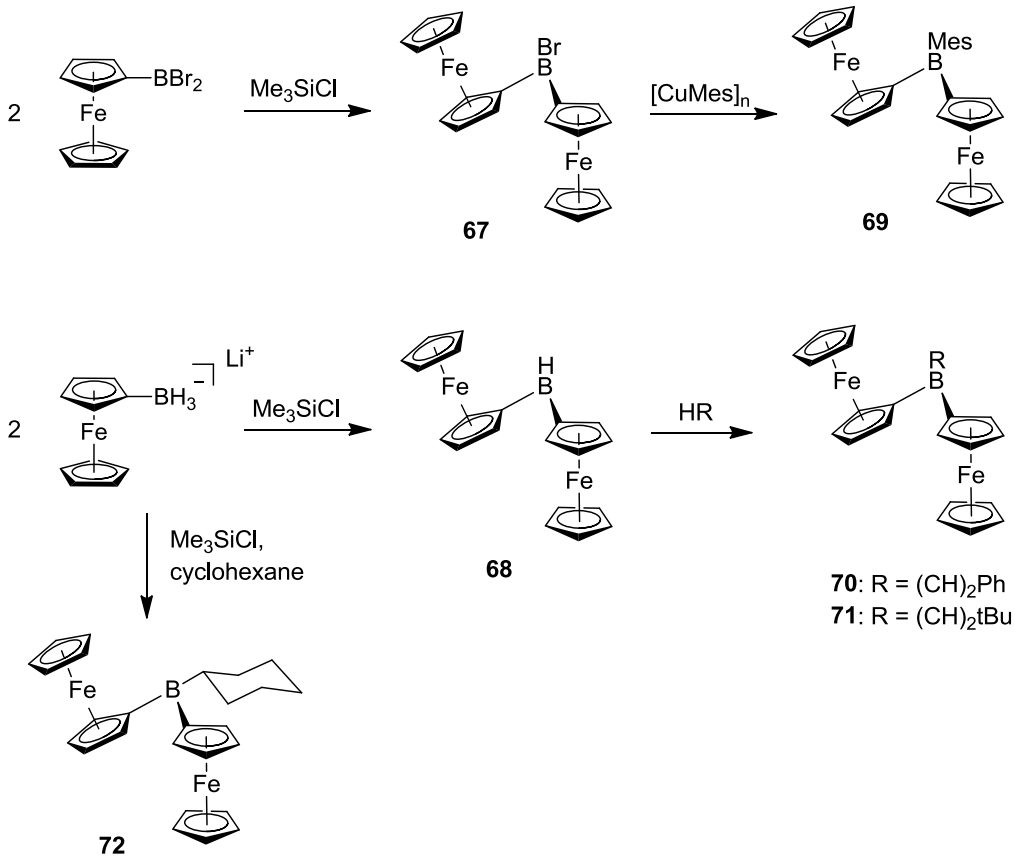


### 1.5.2 Aluminum- and Gallium-bridged [1]Metallacyclophanes, [1.1]Metallacyclophanes, and Metallopolymers

In contrast to the boron species, for which only the [1]metallacyclophanes were obtained by salt-metathesis reaction, for aluminum- and gallium-bridged species salt-metathesis is the route to give any of the products ([1]metallacyclophanes, [1.1]metallacyclophanes, metallopolymers and bis(ferrocenyl) species), depending on the ligand. As the more detailed discussion below will show, ligands with more steric bulk tend to give aluminum- and gallium-bridged [1]MCPs, whereas ligands with less steric protection yield aluminum- and gallium-bridged [1.1]MCPs. As a salt-metathesis reaction has to be kinetically controlled, the size of the ligand must have an influence on the

energy of the transition state, most likely in combination with an electronic effect. There are two considerable differences between aluminum and gallium. On the one hand, aluminum species show commonly more Lewis acidity than gallium species, and on the other hand, gallium is generally less sensitive towards moisture. Gallium and aluminum prefer to be four- or even five-coordinate. Therefore, the aluminum- or gallium-centers prefer an additional donor that was incorporated in some ligands.

*Aluminum- and gallium-bridged [1.1]FCPs*

The first structurally characterized, gallium-bridged [1.1]FCP (**73**) equipped with the bis(trimethylsilyl)methyl ligand was reported in 2001 by Uhl *et al.* (Scheme 1-22).[41a] Species **73** was obtained in 47% yield from a salt-metathesis reaction (Scheme 1-22). The solid-state structure of **73** showed the expected *anti* conformation of **73**. Only two signals for the cyclopentadienyl protons were displayed in the $^{1}$H NMR spectrum, thus indicating that an *anti*-to-*anti* isomerization occurred.

**Scheme 1-22.** Synthesis of the gallium-bridged [1.1]FCP **73**.

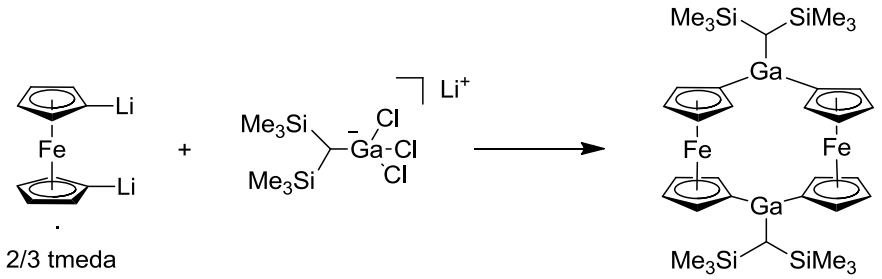


**73**

In 2001, the formation of **74$^{Py}$** as a minor product from a condensation reaction of 1,1'-bis(dimethylgallyl)ferrocene was mentioned by Jutzi *et al.* (Scheme 1-23).[41c] The full characterization of **74$^{Py}$** as well as optimized reaction conditions were reported two years later.[41d] In species **74$^{Py}$**, the gallium atom is equipped with a methyl group and an

additional pyridine donor. Methylgallium-bridged [1.1]FCPs with different donors (Do) or without a donor on gallium were also investigated. Investigated donors include diethylether, pyridine, pyrimidine, quinoxaline, pyrazine and dioxane. The solid-state structures of **74**, **74**$^{\mathbf{Et_2O}}$, **74**$^{\mathbf{Py}}$, **74**$^{\mathbf{pyrimidine}}$, and **74**$^{\mathbf{quinoxaline}}$ revealed the *anti* conformation of these species in which the methyl group occupied the *endo* position. The donor – if present –occupied the *exo* position. The $^{1}$H NMR spectra of **74** and all other measured adducts showed only two peaks for the cyclopendadienyl protons. This is assumed to be caused by an *anti*-to-*anti* isomerization. Cyclic voltammetry measurements of **74** in pyridine with tetrabutylammonium fluoride as the electrolyte exhibited two reversible redox waves at -314 mV and -114 mV ($\Delta E_{1/2}$= 200 mV).

**Scheme 1-23.** Synthesis of methylgallium-bridged [1.1]FCPs with different donors (**74**$^{\mathbf{Do}}$).

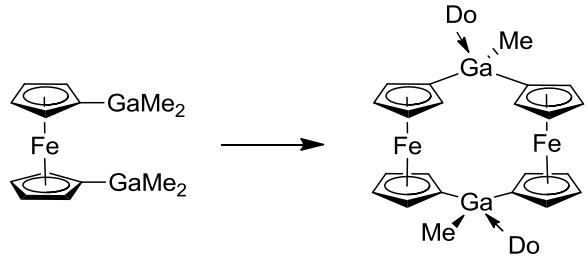


**74**$^{\mathbf{Do}}$

A similar aluminum-bridged [1.1]FCP (**75**) with an ethyl group as a ligand and an additional pyridine donor was described in 2009 by Wrackmeyer *et al.* (Scheme 1-24).[40c] Species **75** was obtained from a condensation reaction of 1,1'-dialuminaferrocenes in 41% yield (Scheme 1-24). The solid-state structure of **75** showed the typical *anti* isomer, in which the ethyl group takes the *endo* position and the pyridine donor occupies the *exo* position. The $^{1}$H NMR spectrum of **75** did not indicate any *anti*-to-*anti* isomerization,

which was attributed to the more Lewis-acidic aluminum forming a stronger bond with the donor.

**Scheme 1-24.** Synthesis of the aluminum-bridged [1.1]FCP **75** by condensation reaction.

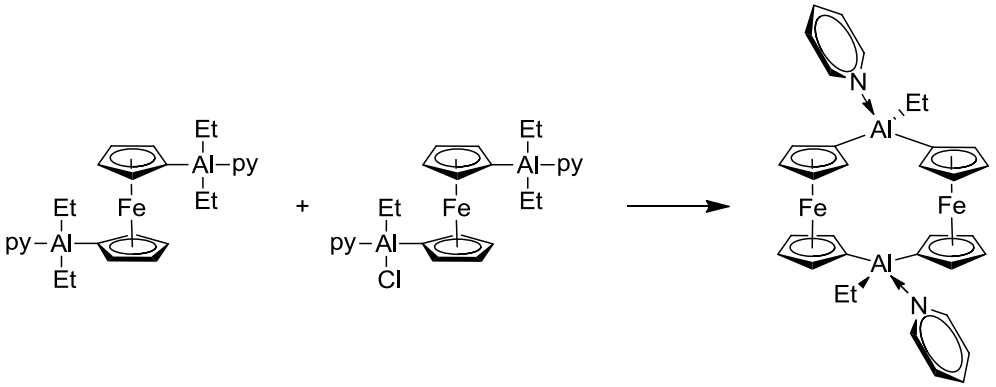


**75**

The first aluminum-bridged [1.1]FCP (**76**) with a chlorido ligand and a tmeda donor was reported by our group in 2005 (Scheme 1-25).[40a] Species **76** resulted from an attempt to improve the synthesis of the aluminum-bridged [1]FCP equipped with the Pytsi ligand (Pytsi =-$C(SiMe_3)_2(SiMe_2C_6H_4N\text{-}2)$) by changing the solvent from toluene to hexanes (Scheme 1-25). No explanation for the formation of the [1.1]FCP in hexanes was given. The solid-state structure presented the *anti* conformation of **76** with the chloride in the *endo* position. No indication for an *anti*-to-*anti* isomerization in solution was observed by $^1$H NMR spectroscopy.

**Scheme 1-25.** Synthesis of the first aluminum-bridged [1.1]FCP (**76**).

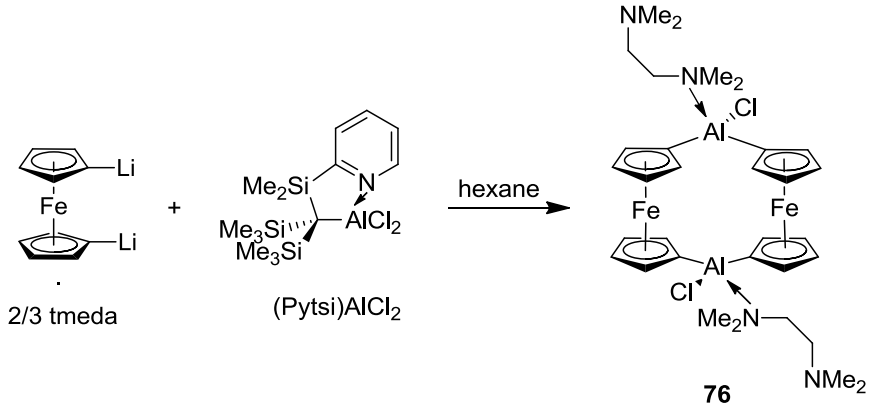


The Ar′ ligand with a dimethylamino group as an intramolecular nitrogen donor was utilized by Braunschweig *et al.* for the synthesis of the aluminum-bridged [1.1]FCP **77** (Scheme 1-26).[40b] Our group used the Ar′ ligand for the synthesis of the aluminum- and gallium-bridged [1.1]FCPs **77** and **78** (Scheme 1-26). In 2005, Braunschweig *et al.* reported the synthesis of the aluminum-bridged [1.1]FCP **77** by a salt-metathesis reaction in 86% yield (Scheme 1-26).[40b] This was shortly followed by the report of the gallium-bridged [1.1]FCP **78**, obtained in 15% yield, by our group (Scheme 1-26).[41b] The solid-state structures of **77** and **78** exhibited the *anti* conformation of these species with the nitrogen donor in *exo* position. No indication for a fast *anti*-to-*anti* isomerization was observed by $^1$H NMR spectroscopy. The redox behavior of **77** and **78** in $CH_2Cl_2$ and with $[Bu_4N][PF_6]$ as an electrolyte was studied by our group. Species **78** showed the expected two reversible redox waves with $\Delta E_{1/2}$ = 300 mV. However, the reported cyclic voltammogram of **77** displayed two oxidation waves and only one reduction wave and **77** was assigned to be a class I compound according to Robin-Day classification.

**Scheme 1-26**. Synthesis of the aluminum- and gallium-bridged [1.1]FCPs **77**-**80**, equipped with the Ar′ or the *p*-$SiMe_3$Ar′ ligand.

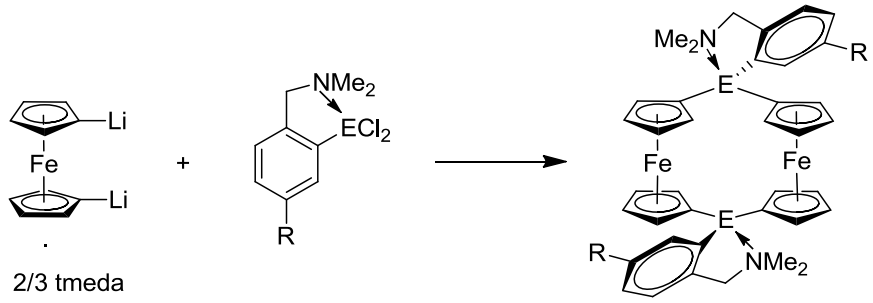


**77**: E = Al, R = H
**78**: E = Ga, R = H
**79**: E = Al, R = $SiMe_3$
**80**: E = Ga, R = $SiMe_3$

The unexpected redox behavior of **77** encouraged our group to further investigate aluminum- and gallium-bridged [1.1]FCPs and their redox properties. The *p*-$SiMe_3$Ar′ (*p*-$SiMe_3$Ar′ = 3-$SiMe_3$-6($Me_2NCH_2$)$C_6H_3$) ligand with a similar steric bulk as that of the Ar′ ligand was chosen to stabilize the aluminum or gallium center (Scheme 1-26). However, compounds with the *p*-$SiMe_3$Ar′ ligand have a higher solubility in organic solvents than compounds with the Ar′ ligand. Employing the salt-metathesis route, the aluminum- and gallium-bridged [1.1]FCPs **79** and **80** were synthesized in 43 and 47% yield respectively. Single-crystal X-ray analysis of **79** and **80** showed the expected *anti* conformation of these species in the solid state, whereas $^1$H NMR spectroscopy of **79** and **80** showed that no fast *anti*-to-*anti* isomerization occurred on the NMR timescale. The redox behavior of **80** in $CH_2Cl_2$ with [$Bu_4N$][$PF_6$] as an electrolyte exhibited the expected two reversible one-electron waves that were separated by 0.309 V. The $\Delta E_{1/2}$ value of **80** was decreased to 0.218 V, when thf was used as a solvent instead of $CH_2Cl_2$. The cyclic voltammogram of **79** in $CH_2Cl_2$ with [$Bu_4N$][$PF_6$] as an electrolyte showed two major redox waves of which the second one had a higher intensity and two additional minor

reduction waves. Based on these irregularities, the measured difference between the redox waves in **79** with 0.332 V has to be viewed with caution. Moreover, the observed redox behavior of **77** was assumed to be caused by ferrocene that would be formed after hydrolysis of **77**.

*Aluminum- and gallium-bridged [1]FCPs and [1]RCPs*

The synthesis of the first aluminum- and gallium-bridged [1]FCPs (**81** and **82**) was described in 2005 by our group (Scheme 1-27).[11,109] A sterically bulky, *trisyl*-based ligand, with an intramolecular pyridine donor, Pytsi, was employed for this synthesis (*trisyl* stands for tris(trimethysilyl)methyl; Scheme 1-27). Salt-metathesis reactions gave the aluminum- and gallium-bridged [1]FCPs in moderate yields of 31%[11] for **81** and of 59% for **82** (Scheme 1-27).[109] The α angles of these species are around 15° and are expectedly lower than for boron-bridged [1]FCPs (32°)[10] or the silicon-bridged [1]FCPs (21°).[12]

**Scheme 1-27.** Synthesis of the aluminum- and gallium-bridged [1]MCPs **81-86**.

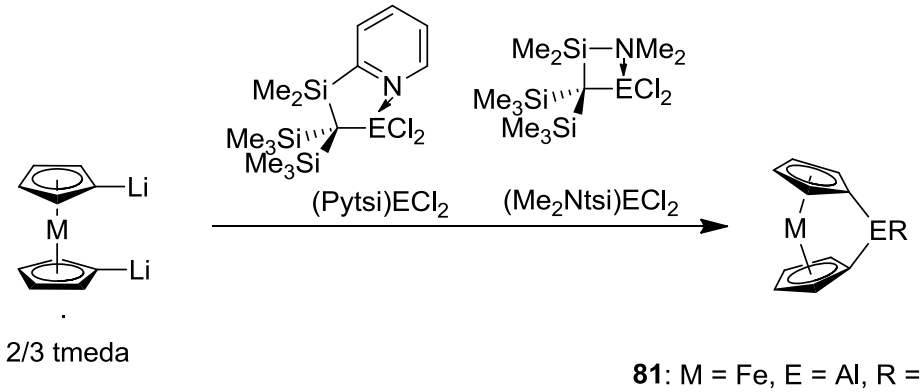


**81**: M = Fe, E = Al, R = Pytsi
**82**: M = Fe, E = Ga, R = Pytsi
**83**: M = Fe, E = Al, R = $Me_2$Ntsi
**84**: M = Fe, E = Ga, R = $Me_2$Ntsi
**85**: M = Ru, E = Al, R = $Me_2$Ntsi
**86**: M = Ru, E = Ga, R = $Me_2$Ntsi

Another trisyl derived ligand with a dimethylamino group as intramolecular donor, $Me_2$Ntsi, was subsequently chosen to stabilize aluminum and gallium during salt-metathesis reactions. Aluminum- and gallium-bridged [1]FCPs equipped with this ligand were isolated in an excellent yield of 97% for aluminum and in a good yield of 68% for gallium.[15] The aluminum- and gallium-bridged [1]RCPs **85** and **86**, equipped with the $Me_2$Ntsi ligand were isolated from the salt-metathesis reaction in yields of 80% and 36%, respectively (Scheme 1-27).[110] Species **85** and **86** exhibited the expected, significantly higher tilt angles than **83** and **84** due to the larger size of the sandwiched metal (Table 1-5).

**Table 1-5.** Tilt angles α of aluminum- and gallium-bridged [1]metallacyclophanes.

| metal | Fe[11,109] | Fe[15] | Ru[110] | Cr[15] | V[15] | Mo[112] |
|---|---|---|---|---|---|---|
| ligand | Pytsi | $Me_2$Ntsi | $Me_2$Ntsi | $Me_2$Ntsi | $Me_2$Ntsi | $Me_2$Ntsi |
| aluminum | 14.9(3)° | 14.3(1)° | 20.3(2)° | 11.8(1)° | 14.7(1)° | 18.3(2)° |
| gallium | 15.7° | 15.8(2)° | 20.9(2)° | 13.2(1)° | 15.6(1)° | 21.2(1)° |

Species **81**-**86** were tested for polymerizations with different methods including thermal, anionic, photo-controlled and transition-metal-catalyzed ROP.[110] It was found that **83** and **84** underwent thermal ring-opening at 210-220 °C to give oligomers with $M_w$ = 1.5 kDa, referring to 3-4 repeating units. Species **83**-**86** were irresponsive to *n*-butylithium or LiCp under irradiation and species **81** and **82** did similarly not undergo ROP. However, in the case of *n*-butyllithium as an initiator for the polymerization of **81** and **82**, alkylation of the *para* position of the pyridine ring was observed. When a Pd(0) catalyst was employed for ROP of **82**, metallopolymers with a $M_w$ of 21 kDa were obtained along with unreacted monomers. It was concluded that the steric bulk of the

trimethylsilyl groups was blocking anionic attacks and therefore highly reduced their reactivity toward ROP.

*Aluminum- and gallium-bridged metallocene-based polymers*

During the time of my research, my colleague Bidraha Bagh synthesized and isolated the first aluminum- and gallium-bridged metallocene-based polymers, employing the Mamx (Mamx = 4,6-di*t*Bu-2($Me_2NCH_2$)$C_6H_3$) ligand for the salt-metathesis reaction.[26b,111] Compared to the Ar′ ligand, the steric bulk of the Mamx ligand is increased by two *tert*-butyl groups, one in *ortho* and one in *para* position. In a short communication, the salt-metathesis reaction of 1,1'-dilithioferrocene with (Mamx)$GaCl_2$ giving rise to the [1]FCP **87** was reported (Scheme 1-28).[111] Species **87** was not isolable, but underwent ROP to give the high-molecular-weight polymer $\mathbf{87_n}$ (Table 1-4) that was isolated in 45% yield (Scheme 1-28).

**Scheme 1-28.** Synthesis of the poly(ferrocenylgallane) $\mathbf{87_n}$, the poly(ferrocenylalumane) $\mathbf{88_n}$, the poly(ruthenocenylgallane) $\mathbf{89_n}$, and the poly(ruthenocenylalumane) $\mathbf{90_n}$.

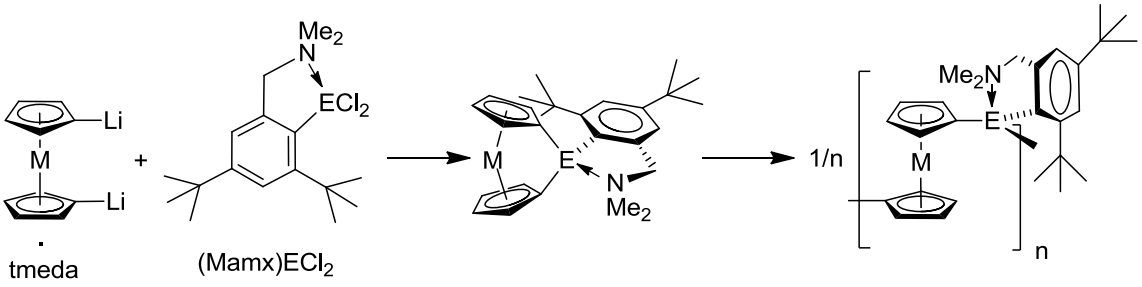


In the successive full article, similar results were described for salt-metathesis reactions of 1,1'-dilithioferrocene and 1,1'-dilithioruthenocene with (Mamx)$GaCl_2$ and (Mamx)$AlCl_2$ (Scheme 1-28).[26b] However, the molecular weights of $\mathbf{87_n}$-$\mathbf{90_n}$ were highly

dependant on the bridging element and the metal (Table 1-6). The highest molecular weight was observed for **88$_n$** with >100 kDa. Ruthenocene-based polymers were found to have only low molecular weights. The gallium-bridged [1]RCP **89** was isolated and submitted to transition-metal-catalyzed ROP, which led to a threefold increase of the molecular weight (Table 1-6).

**Table 1-6.** Molecular weights and repeating units of aluminum- and gallium-bridged metallopolymers equipped with the Mamx ligand (**87$_n$-90$_n$**) determined by dynamic light scattering (DLS).

| E/M | Ga/Fe | Al/Fe | Ga/Ru | Al/Ru |
|---|---|---|---|---|
| Nr | **87$_n$** | **88$_n$** | **89$_n$** | **90$_n$** |
| $M_w$ in kDa | 36(±8) | 106(±8) | 10(±5)/29(±6)* | 8(±3) |
| $DP_w$ | 72(±17) | 232(±18) | 19(±9)/52(±12)* | 16(±6) |

*****second value refers to polymers obtained from controlled ROP.

Moreover, DFT calculations were carried out to investigate the influence of the *tert*-butyl group for the reactivity of the [1]MCPs **87**-**90**. Therefore, the Mamx$^{-t\text{Bu}}$ (Mamx$^{-t\text{Bu}}$ = 4-*t*Bu-2-($Me_2NCH_2$)$C_6H_4$) ligand in which the *ortho tert*-butyl group of the Mamx ligand was replaced by hydrogen, was utilized (Figure 1-23). The calculated tilt angles of **87**-**90** were similar to those calculated for the respective species equipped with the Mamx$^{-t\text{Bu}}$ ligand. However, calculations showed that species **87**-**90** exhibited a significantly higher energy release during a ring-opening than the respective species equipped with the Mamx$^{-t\text{Bu}}$ ligand. Therefore, the steric bulk of the *ortho tert*-butyl group on the ligand substantially increased the strain in the [1]MCP in addition to the strain originating from the tilt of the Cp rings.

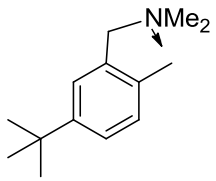


Mamx-*t*Bu

**Figure 1-23.** Depiction of the Mamx$^{-tBu}$ ligand.

*Aluminum- and gallium-bridged metallarenophanes*

The synthesis of [1]MAPs, [1]CAPs, and [1]VAPs with aluminum and gallium in bridging position was described by our group (Scheme 1-29).[15,112] Salt-metathesis reactions of aluminum and gallium dichlorides equipped with the $Me_2$Ntsi ligand with the respective dilithiated sandwich compounds gave aluminum- and gallium-bridged [1]metallarenophanes in good to moderate yields (**91**: 81%, **92**: 69%; **93**: 75%, **94**: 52%; **95**: 54%, **96**: 58%). The tilt angles α increased from chromium to vanadium to molybdenum, which is in agreement of molybdenum being the largest in size (Table 1-5). Investigations into transition-metal-catalyzed ROP showed that **94** underwent ring-opening with benzene in the presence of a platinum catalyst.The ring-opened product of **94** is similar to **57** and was reported prior to **57** (Figure 1-22).

**Scheme 1-29.** Synthesis of the aluminum- and gallium-bridged [1]metallarenophanes **91**-**96**.

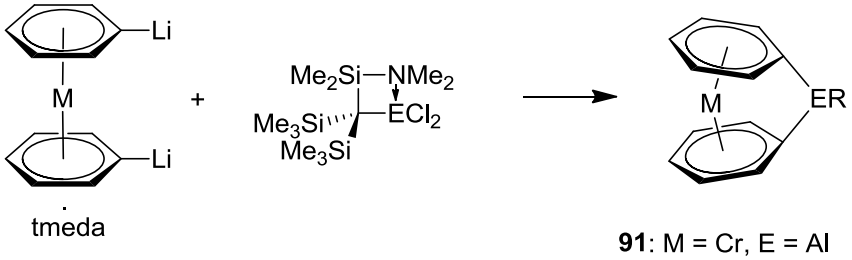


**91**: M = Cr, E = Al
**92**: M = Cr, E = Ga
**93**: M = V, E = Al
**94**: M = V, E = Ga
**95**: M = Mo, E = Al
**96**: M = Mo, E = Ga

Since aluminum- and gallium-bridged [1.1]FCPs with the Ar′ ligand were successfully synthesized, the same ligand was chosen for the synthesis of aluminum- or gallium-bridged [1.1]CAPs and [1.1]MAPs.[113] However, during the synthesis of the aluminum-bridged [1.1]CAP **97**, equipped with the Ar′ ligand, the very low solubility of this species hampered its characterization (Scheme 1-30). Therefore, a *tert*-butyl group was introduced in *para* position of the Ar′ ligand in order to increase the solubility of the targeted [1.1]MCPs and facilitate their characterization. The aluminum- and gallium-bridged [1.1]metallarenophanes **98**-**101**, equipped with the *p*-*t*BuAr′ ligand, were obtained in low to moderate yields (**98**: 30%, **99**: 28%, **100**: 29%, **101**: 20%) from salt-metathesis reactions (Scheme 1-30). The solid-state structures revealed the expected *anti* conformations of species **97**-**101**. The electrochemical behavior of **98**-**101** in thf with $[Bu_4N][PF_6]$ as an electrolyte was studied, however, only the gallium-bridged [1.1]metallarenophanes gave reproducible results. Species **99** and **101** exhibited two reversible redox waves with $\Delta E_{1/2}$ values of 0.215 V for **99** and 0.220 V for **101**. These values are very similar to that of the gallium-bridged [1.1]FCP **80** in thf of 0.218 V.[108]

**Scheme 1-30.** Synthesis of the aluminum- and gallium-bridged [1.1]metallarenophanes **97**-**101**.

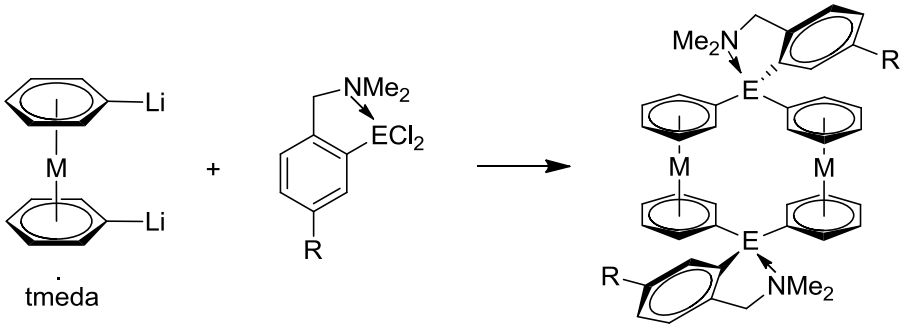


**97**: M = Cr, E = Al, R = H
**98**: M = Cr, E = Al, R = *t*Bu
**99**: M = Cr, E = Ga, R = *t*Bu
**100**: M = Mo, E = Al, R = *t*Bu
**101**: M = Mo, E = Ga, R = *t*Bu

*Bis(ferrocenyl)aluminum and bis(ferrocenyl)gallium compounds*

Bis(ferrocenyl)aluminum and bis(ferrocenyl)gallium compounds **102**-**105** were synthesized in moderate yields (**102**: 51%, **103**: 49%, **104**: 47%, **105**: 41%) by our group (Scheme 1-31).[26b,108] The molecular structures in the solid state of **102** and **103** as well as the redox properties of **102**-**105** will be discussed in detail in Chapter 3.2.3.

**Scheme 1-31.** Synthesis of the bis(ferrocenyl)aluminum and bis(ferrocenyl)gallium compounds **102-105**.

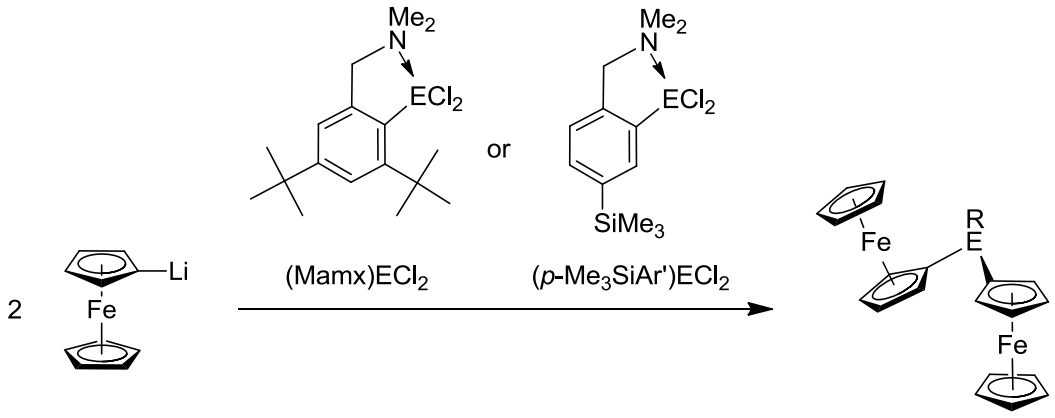


**102**: E = Al, R = Mamx
**103**: E = Ga, R = Mamx
**104**: E = Al, R = *p*-$Me_3$SiAr'
**105**: E = Ga, R = *p*-$Me_3$SiAr'

### 1.5.3 Indium-bridged [1.1]Ferrocenophanes

The first reported indium-bridged [1.1]FCP (**106**) equipped with the Ar′ ligand, was synthesized by a salt-metathesis reaction (Scheme 1-32).[41b] In contrast to aluminum and gallium, salt-metathesis reactions of indium dihalides equipped with the sterically bulky ligand $Me_2$Ntsi gave rise to the indium-bridged [1.1]FCP **107** (Scheme 1-32).[42] The steric repulsion of the Cp protons with the ligand is presumed to favor the formation of aluminum- and gallium-bridged [1]MCP over [1.1]FCPs with sterically bulky ligands like $Me_2$Ntsi.[42] With an increased size of the element, indium in comparison to aluminum and gallium, the distance between the ligand and the Cp-protons increases and the steric repulsion decreases. The increased distance between the ligand and the Cp protons in **107** in comparison to **84** was observed by their molecular structures in the solid state.[42]

**Scheme 1-32.** Synthesis of the indium-bridged [1.1]FCPs **106** and **107**.

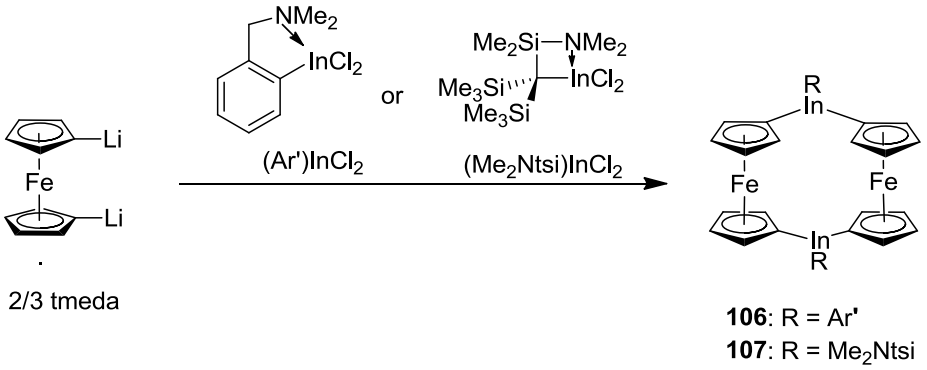


Species **106** and **107** showed the expected *anti* conformation in the solid state. The $^{1}$H NMR spectrum of **107** displayed only two signals for the Cp protons at room temperature. This is consistent with $D_{2h}$ symmetry of **107** on time average which was explained by an *anti*-to-*anti* isomerization occuring fast at room temperature (r.t.) on the NMR timescale. At -30 °C two sets of four signals for the cyclopentadienyl protons in **107** were observed in the $^{1}$H NMR spectrum and were assigned to an *anti* and a less pronounced *syn* isomer. The redox properties of **106** and **107** were studied with $[Bu_4N][PF_6]$ as an electrolyte. For species **106** a complex spectrum was observed using $CH_2Cl_2$ that showed two major reversible redox waves, but also some unidentifiable redox waves. For species **107** in thf, only an irreversible oxidation was recorded.

Salt-metathesis reactions of dilithioferrocene with $[(Pytsi)InCl_2]_2$ yielded an unusual indium species (**108**) in which the cyclopentadienyl rings are bridged by the chlorine bridged indium dimer (Scheme 1-33).[109] No further reaction of **108** with 1,1'-dilithioferrocene occurred. Species **108** might be too stable to react or the bridging chlorine atoms are too well sterically protected.

**Scheme 1-33.** Synthesis of the unusual indium species **108**.

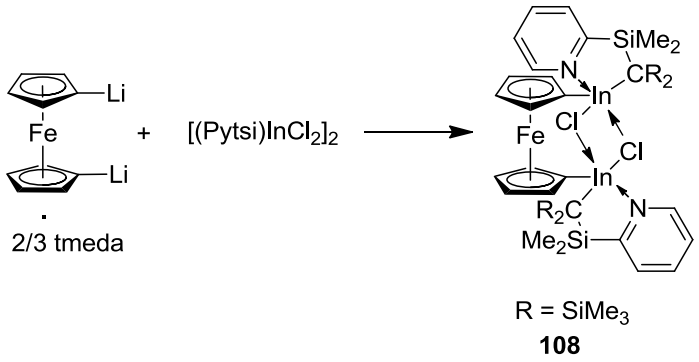


**108**

## 1.6 Research Objective

The first research objective was to synthesize and characterize new aluminum- and gallium-bridged [1]MCPs that are reactive toward ROP. Salt-metathesis reactions of dilithiometallocenes with aluminum and gallium dihalides yield [1]MCPs or [1.1]MCPs depending on the steric bulk of the ligand. When slim ligands on aluminum and gallium were employed, [1.1]MCPs were obtained, whereas sterically bulky ligands attached to aluminum or gallium dihalides gave rise to [1]MCPs. However, attempted ROPs of the aluminum- and gallium-bridged [1]MCPs were found to be unsuccessful or at best sluggish, since the sterically bulky ligand was overly protecting the species. Based on these results it was speculated that employing ligands of moderate steric bulk might result in [1]MCPs that are still able to polymerize. The choice of ligands with moderate steric bulk was based on the idea of decreasing the steric bulk of the Pytsi and the Mamx ligand (Figure 1-24). The Pytsi and the Mamx ligand were successfully employed for the synthesis of aluminum- and gallium-bridged [1]MCPs.

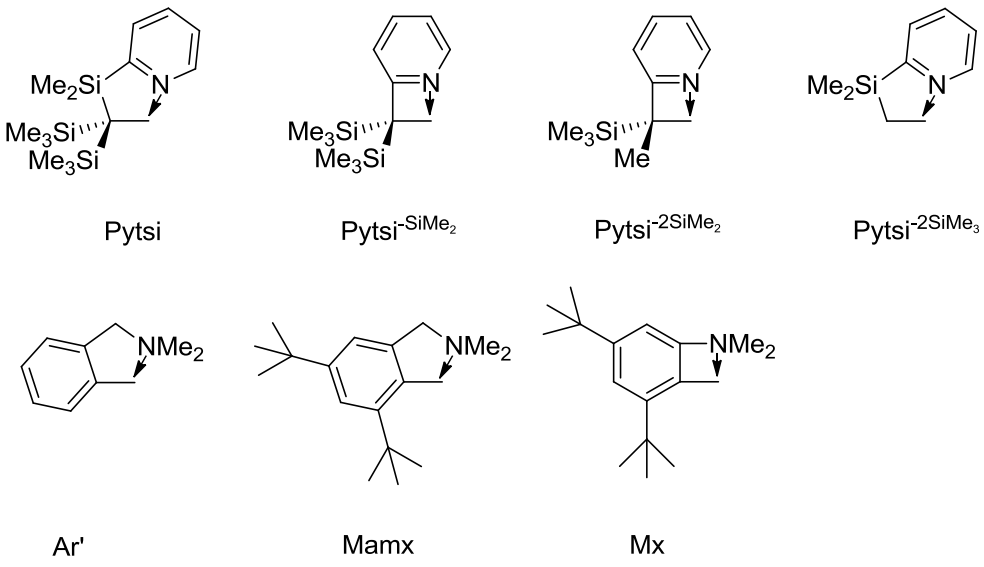


**Figure 1-24.** Different ligands that were or should be used to stabilize aluminum or gallium in MCPs.

The first part of this research objective was the synthesis and characterization of new aluminum and gallium dihalides equipped with the four ligands Pytsi$^{-SiMe_2}$, Pytsi$^{-2SiMe_2}$, Pytsi$^{-2SiMe_3}$, and Mx that are required for subsequent salt-metathesis reactions with dilithiometallocenes (Figure 1-24). The results obtained for this part are described in Chapter 2.

The second part of this research objective was the study of the reactivity of the new aluminum and gallium dihalides with dilithiometallocenes. Besides the intended aluminum-and gallium-bridged [1]MCPs, [1.1]MCPs and metallocenyl-based oligomers can form. We wanted to extend our knowledge and understanding about the steric bulk of the ligand that is required to yield [1]MCPs in salt-metathesis reactions. Moreover, the ROP of the new aluminum- and gallium-bridged [1]MCPs should be investigated and the polymers should be characterized. During the course of this research, another objective was included in this part: the synthesis and characterization of bis(ferrocenyl)aluminum and gallium species as model compounds for aluminum- and gallium-bridged ferrocenyl-based polymers. A detailed discussion of the results obtained from salt-metathesis reactions with the new aluminum and gallium dihalides is given in Chapter 3.

The experience and knowledge gained from the synthesis of aluminum- and gallium-bridged bis(ferrocenyl) compounds was used to explore methods to synthesize [1.1]FCPs that contain two different bridging elements as well as polyferrocenes with alternating bridging elements. Neither of these species was previously known. The two different element combinations silicon/tin and silicon/gallium were chosen. Chapter 4 focuses on the results obtained from this project.

As described in the introduction (Chapter 1.2), little is known about [1.1]RCPs. The silicon-bridged [1.1]RCP **28** was the only heteroatom-bridged [1.1]RCP known in the literature. For **28**, neither the solid-state structure nor its redox behavior was reported. Only one solid-state structure of a [1.1]RCP (**24**) was published. Therefore, we wanted to explore, if new [1.1]RCPs could be synthesized. As discussed before, the known [1.1]RCP **24** (Scheme 1-7) showed an unexpected redox chemistry. We wanted to address the question, if the respective aluminum- and gallium-bridged species exhibit similar redox events. Aluminum and gallium dihalides equipped with a slim ligand were reacted with dilithioruthenocene to give the first aluminum- and gallium-bridged [1.1]RCPs. The results of these investigations are discussed in Chapter 5.

## 1.7 References


(1) (a) Kealy, T. J.; Pauson, P. T. *Nature*, **1951**, 1039. (b) Miller, S. A.; Tebboth, J. A.; Tremaine, J. F. *J. Chem. Soc.* **1952**, 632-633.

(2) Greenwood, N. N.; Earnshaw, A.*Chemistry of the Elements*, 2nd ed.; Elsevier: Burlington, 2006, 1298.

(3) Rinehart, K. L.; Frerichs, Jr. A. K.; Kittle, P. A.; Westman, L. F.; Gustafson, D. H.; Pruett, R. L.; McMahon, J. E. *J. Am. Chem. Soc.* **1960**, *82*, 4111-4112.

(4) Osborne, A. G.; Whiteley, R. H. *J. Organomet. Chem.* **1975**, *101*, C27-C28.

(5) Bellas, V.; Rehahn, M. *Angew. Chem. Int. Ed.* **2007**, *46*, 5082-5104.

(6) Foucher, D.A.; Tang, B.Z.; Manners, I. *J. Am. Chem. Soc.* **1992**, *114*, 6246-6248.

(7) a) Whittell, G.R.; Partridge, B. M.; Presly, O. C.; Adams, C. J.; Manners, I. *Angew. Chem. Int. Ed.* **2008**, *47*, 4354-4357. b)Matas, I.; Whittell, G. R.; Partridge, B. M.; Holland, J. P.; Haddow, M. F.; Green, J. C.; Manners, I. *J. Am. Chem. Soc.* **2010**, *132*, 13279-13289.

(8) Barlow, A.; Drewitt, M. J.; Dijkstra, T.; Green, J. C.; O'Hare, D.; Whittingham, C.; Wynn, H. H.; Gates, D. P.; Manners, I.; Nelson, J. M.; Pudelski, J. K. *Organometallics* **1998**, *17*, 2113-2120.

(9) Green, J. C. *Chem. Soc. Rev.* **1998**, *27*, 263-272.

(10) Braunschweig, H.; Dirk, R.; Müller, M.; Nguyen, P.; Resendes, R.; Gates, D. P.; Manners, I. *Angew. Chem.* **1997**, *109*, 2433-2435.

(11) Schachner, J. A.; Lund, C. L.; Quail, J. W.; Müller, J. *Organometallics* **2005**, *24*, 785-787.

(12) Finckh, W. Tang, B.-Z.; Foucher, D. A.; Zamble, D. B.; Ziembinski, R.; Lough, A.; Manners, I. *Organometallics* **1993**, *12*, 823-829.

(13) Butler, I. R.; Cullen, W. R.; Einstein, F. W. B.; Rettig, S. J.; Willis, A. J. *Organometallics* **1983**, *2*, 128-135.

(14) Rulkens, R.; Gates, D. P.; Balaishis, D.; Pudelski, J. K.; McIntosh, D. F.; Lough, A. J.; Manners, I. *J. Am Chem. Soc.* **1997**, *119*, 10976-10986.

(15) Lund, C. L.; Schachner, J. A.; Quail, J. W.; Müller, J. *Organometallics* **2006**, *25*, 5817-5823.

(16) Foucher, D. A.; Edwards, M.; Burrow, R. A.; Lough, A. J.; Manners, I. *Organometallics* **1994**, *13*, 4959-4966.

(17) Jäkle, F.; Rulkens, R.; Zech, G.; Foucher, D. A.; Lough, A. J.; Manners, I. *Chem–Eur. J.* **1998**, *4*, 2117-2128.

(18) Broussier, R.; Da Rold, A.; Gautheron, B.; Dromzee, Y.; Jeannin, Y. *Inorg. Chem.* **1990**, *29*, 1817-1822.

(19) a) Nguyen, P.; Lough, A. J.; Manners, I. *Macromol. Rapid Commun.* **1997**, *18*, 953-959. b) Nguyen, P.; Stojcevic, G.; Kulbaba, K. MacLachlan, M. J.; Liu, X.-H.; Lough, A. J.; Manners. I. *Macromolecules* **1998**, *31*, 5977-5983.

(20) Hatanaka, Y.; Okada, S.; Minami, T.; Goto, M.; Shimada, K. *Organometallics* **2005**, *24*, 1053-1055.

(21) MacLachlan, M. J.; Lough, A. J.; Geiger, W. E.; Manners, I. *Organometallics* **1998**, *17*, 1873-1883.

(22) Sharma, H. K.; Cervantes-Lee, F.; Mahmoud, J. S.; Pannell, K. H. *Organometallics* **1999**, *18*, 399-403.

(23) Clearfield, A.; Simmons, C. J.; Withers, Jr., H. P.; Seyferth, D. *Inorg. Chim. Acta.* **1983**, *75*, 139-144.

(24) a) Sheridan, J. B.; Temple, K.; Lough, A. J.; Manners, I. *J. Chem Soc., Dalton Trans.* **1997**, 711-713. b) Berenbaum, A.; Jäkle, F.; Lough, A. J.; Manners, I. *Organometallics* **2002**, *21*, 2359-2361.

(25) Vogel, U.; Lough, A. J.; Manners, I. *Angew. Chem. Int. Ed.* **2004**, *43*, 3321-3325.

(26) a) Schachner, J. A.; Tockner, S.; Lund, C. L., Quail, J. W.; Rehan, M.; Müller, J. *Organometallics* **2007**, *26*, 4658-4662. b) Bagh, B.; Schatte, G.; Green, J. C. ; Müller, J. *J. Am. Chem. Soc.* **2012**, *134*, 7924-7936.

(27) Nesmeyanov, A. N.; Kritskaya, I. I. *Bull. Acad. Sci. USSR Div. Chem. Sci (Engl. Transl.)* **1956**, 243-244.

(28) Bitterwolf, T. E.; Ling, A.C. *J. Organomet. Chem.* **1973**, *57*, C15-C18.

(29) a) Hillman, M.; Michaile, S.; Feldberg, S. W.; Eisch, J. J. *Organometallics* **1985**, *4*, 1258-1263. b) Michaile, S.; Hillman, M.; Eisch, J. J. *Organometallics* **1988**, *7*, 1059-1065.

(30) Watts, W. E. *J. Am. Chem. Soc.* **1966**, *88*, 856-857.

(31) Löwendahl, M.; Davidson, Ö.; Ahlberg, P.; Håkansson, M. *Organometallics* **1993**, *12*, 2417-2419.

(32) Mizuta, T. Imamura, Y.; Miyoshi, K.; Yorimitsu, H.; Oshima, K. *Organometallics*, **2005**, *24*, 990-996. PPh[1.1]FCP anti to syn

(33) Imamura, Y.; Mizuta, T.; Miyoshi, K. *Organometallics* **2006**, *25*, 882-886.

(34) Kansal, V. K.; Watts, W. E.; Mueller-Westerhoff, U. T.; Nazzal, A. *J. Organomet. Chem.* **1983**, *243*, 443-449.

(35) Rudziński, J. M.; Ōsawa, E. *J. Phys. Org. Chem.* **1993**, *6*, 107-112.

(36) Löwendahl, M.; Davidson, Ö.; Ahlberg, P. *J. Chem. Res., Synop.* **1993**, 40-41.

(37) Perucha, A. S. Heilmann-Brohl, J.; Bolte, M.; Lerner, H.-W.; Wagner, M. *Organometallics* **2008**, *27*, 6170-6177.

(38) Kuz'mina, L. G.; Struchkov, Y. T.; Lemenovskii, D. A.; Urazovskii, I. F.; Nifant'ev, I. E.; Perevalova, E. G. *Koord. Khim.* **1983**, *9*, 1212-1219.

(39) Scheibitz, M.; Winter, R. F.; Bolte, M.; Lerner, H.-W.; Wagner, M. *Angew. Chem. Int. Ed.* **2003**, *42*, 924-927.

(40) a) Schachner, J. A.; Lund, C. L.; Quail, J. W.; Müller, J. *Acta. Cryst.* **2005,** *E61*, m682-m684. b) Braunschweig, H.; Burschka, C.; Clentsmith, G. K. B.; Kupfer, T.; Radacki, K. *Inorg. Chem.* **2005**, *44*, 4906-4908. c) Wrackmeyer, B.; Klimkina, E. V.; Milius, W. *Eur. J. Inorg. Chem.* **2009**, 3155-3162.

(41) a) Uhl, W.; Hahn, I.; Jantschak, A.; Spies, T. *J. Organomet. Chem.* **2001**, *637-639*, 300-303. b) Schachner, J.A.; Orlowski, G.A.; Quail, J.W.; Kraatz, H.-B.; Müller, J. *Inorg. Chem.* **2006**, *45*, 454-459. c) Jutzi, P.; Lenze, N.; Neumann, B.; Stammler, H.-G. *Angew. Chem. Int. Ed* **2001**, *40*, 1424-1427. d) Althoff, A.; Jutzi, P.; Lenze, N.; Neumann, B.; Stammler, A.; Stammler, H.-G. *Organometallics* **2003**, *22*, 2766-2774..

(42) Schachner, J. A.; Lund, C. L.; Burgess, I. J.; Quail, J. W.; Schatte, G.; Müller, J. *Organometallics*, **2008**, *27*, 4703-4710.

(43) a) Zechel, D. L.; Foucher, D. A.; Pudelski, J. K.; Yap, G. P. A.; Rheingold, A. L.; Manners, I. *J. Chem. Soc. Dalton Trans.* **1995**, 1893-1899. b) Park, J.; Seo, Y.; Cho, S.; Whang, D.; Kim, K.; Chang, T. *J. Organomet. Chem.* **1995**, *489*, 23-25. c) Calleja, G.; Carré, F.; Cerveau, G. *Organometallics* **2001**, *20*, 4211-4215. d) Berenbaum, A.; Lough,

A. J.; Manners, I. *Organometallics* **2002**, *21*, 4415-4424. e) Bao, M.; Hatanaka, Y.; Shimada, S. *Chem. Lett.* **2004**, *33*, 520-521.

(44) a) Seyferth, D.; Withers, H. P. *Organometallics* **1982**, *1*, 1275-1282. b) Dong, T.-Y.; Hwang, M.-Y.; Wen, Y.-s. *J. Organomet. Chem.* **1990**, *391*, 377-385. c) Jäkle, F.; rulkens, R.; Zech, G.; Foucher, D. A.; Lough, A. J.; Manners, I. *Chem.—Eur. J.* **1998**, *4*, 2117-2128.

(45) Utri, G.; Schwarzhans, K.-E.; Allmaier, G. M. *Z. Naturforsch., B: Chem. Sci.* **1990**, *45*, 755-762.

(46) Brunner, H.; Klankermayer, J.; Zabel, M. *J. Organomet. Chem.* **2000**, *601*, 211-219.

(47) Spang, C.; Edelmann, F. T.; Noltemeyer, M.; Roesky, H. W. *Chem. Ber.* **1989**, *122*, 1247-1254.

(48) Ieong, N. S.; Chan, W. Y.; Lough, A. J.; Haddow, M. F.; Manners, I. *Chem.—Eur. J.* **2008**, *14*, 1253-1263.

(49) Ni, Y.; Rulkens, R.; Pudelski, J. K.; Manners, I. *Macromol. Rapid Commun.* **1995**, *16*, 637-641. b) Reddy, N. P.; Choi, N.; Shimada, S.; Tanaka, M. *Chem. Lett.* **1996**, 649-650. c) Chan, W. Y.; Lough, A. J.; Manners, I. *Angew. Chem. Int. Ed.* **2007**, *46*, 9069-9072.

(50) Clearfield. A.; Simmons, C. J.; Withers Jr, H. P.; Seyferth, D. *Inorg. Chim. Acta.* **1983**, *75*, 139-144.

(51) Mueller-Westerhoff, U. T.; Nazzal, A.; Tanner, M. *J. Organomet. Chem.* **1982**, *236*, C41-C44.

(52) Diaz, A. F.; Mueller-Westerhoff, U. T.; Nazzal, A.; Tanner, M. *J. Organomet. Chem.* **1982**, *236*, C45-C48.

(53) Rheingold, A. L.; Mueller-Westerhoff, U. T.; Swiegers, G. F.; Haas, T. J. *Organometallics* **1992**, *11*, 3411-3417.

(54) Izumi, T.; Asakura, K.; Kasahara, A. *Bull. Yamagata Univ. (Engl.)* **1988**, *20*, 95-100.

(55) Sato, M.; Suzuki, M.; Okoshi, M.; Kurasina, M.; Watanabe, M. *J. Organomet. Chem.* **2002**, *648*, 72-80.

(56) Herberhold, M.; Bärtl, T. *Z. Naturforsch.* **1995**, *50b*, 1692-1698.

(57) Watanabe, M.; Sato, M.; Nagasawa, A.; Motoyama, I.; Takayama, T. *Bull. Chem. Soc. Jpn.* **1998**, *71*, 2127-2136.

(58) Watanabe, M.; Sano, H. *Chem. Lett.* **1988**, *17*, 1457-1460.

(59) Odian, G. *Principles of Polymerization*; 4 ed.; Wiley-Interscience: Hoboken, N. J., 2004.

(60) Bellas, V.; Rehahn, M. *Angew. Chem. Int. Ed.* **2007**, *46*, 5082-5104.

(61) Withers, Jr., H. P.; Seyferth, D.; Fellmann, J. D.; Garrou, P. E.; Martin, S. *Organometallics* **1982**, *1*, 1283-1288.

(62) Jäkle, F.; Rulkens, R.; Zech, G.; Massey, J. A.; Manners, I. *J. Am. Chem. Soc.* **2000**, *122*, 4231-4232.

(63) Rulkens, R.; Lough, A. J.; Manners, I. *J. Am. Chem. Soc.* **1994**, *116*, 797-798.

(64) Rulkens, R.; Ni, Y.; Manners, I. *J. Am. Chem. Soc.* **1994**, *116*, 12121-12122.

(65) a) Ni, Y.; Rulkens, R.; Pudelski, J. K.; Manners, I. *Macromol. Rapid Commun.* **1995**, *16*, 637-641. b) Reddy, N. P.; Yamashita, H.; Tanaka, M. *J. Chem. Soc., Chem. Commun.* **1995**, 2263-2264.

(66) Temple, K.; Jäkle, F.; Sheridan, J. B.; Manners, I. *J. Am. Chem. Soc.* **2001**, *123*, 1355-1364.

(67) Mizuta, T.; Onishi, M.; Miyoshi, K. *Organometallics*, **2005**, *19*, 5005-5009.

(68) Mizuta, T.; Imamura, Y.; Miyoshi, K. *J. Am. Chem. Soc.* **2003**, *125*, 2068-2069.

(69) Tanabe, M.; Manners, I. *J. Am. Chem. Soc.* **2004**, *126*, 11434-11435.

(70) Tanabe, M.; Vandermeulen, G. W. M.; Chan, W. Y.; Cyr, P. W.; Vanderark, L.; Rider, D. A.; Manners, I. *Nat. Mater.* **2006**, *5*, 467-470.

(71) Resendes, R.; Nguyen, P.; Lough, A. J.; Manners, I. *Chem. Comm.* **1998**, 1001-1002.

(72) a) Manners, I. *Science* **2001**, *294*, 1664-1666. b) Eloi, J.-C.; Chabanne, L.; Whittell, G. R.; Manners, I. *Materials Today* **2008**, *11*, 28-36. c) Manners, I. *J. Organomet. Chem.* **2011**, *696*, 1146-1149. d) Whittell, G. R.; Hager, M. D.; Schubert, U. S.; Manners, I. *Nature Mat.* **2011**, *10*, 176-188.

(73) Petersen, R.; Foucher, D. A.; Tang, B.-Z.; Lough, A.; Raju, N. P.; Greedan, J. E.; Manners, I. *Chem. Mater.* **1995**, *7*, 2045-2053.

(74) MacLachlan, M. J. Ginzburg, M.; Coombs, N.; Coyle, T. W.; Raju, N. P.; Greedan, J. E.; Ozin, G. A.; Manners, I. *Science* **2000**, *287*, 1460-1463.

(75) Ma, Y.; Dong, W.-F.; Hempenius, M. A.; Möhwald, H.; Vancso, G. J. *Nat. Mat.* **2006**, *5*, 724-729.

(76) Arsenault, A. C.; Puzzo, D. P.; Manners, I. Ozin, G. A. *Nat. Photon.* **2007**, 468-472.

(77) http://opalux.com/

(78) Barrière, F.; Geiger, W. E. *J. Am. Chem. Soc.* **2006**, *128*, 3980-3989.

(79) Robin, M. B.; Day, P. *Adv. Inorg. Chem. Radiochem.* **1967**, *10*, 247-422.

(80) Bard, A. J.; Faulkner, L. R. *Electrochemical Methods*, 2nd ed.; John Wiley & Sons, Inc.: New York, 2001, Chap. 6.

(81) Gritzner, G.; Kuta, J. *Pure Appl. Chem.* **1984**, *56*, 461-466.

(82) Wilkinson, G. *J. Am. Chem. Soc.* **1952**, *74*, 6146-6147.

(83) Page, J. A.; Wilkinson, G. *J. Am. Chem. Soc.* **1952**, *74*, 6149-6150.

(84) Hendrikson, D. N.; Sohn, Y. S.; Morrison, W. H.; Gray, H. B. *Inorg. Chem.* **1972**, *11*, 808-811.

(85) Gale, R. J.; Job, R. *Inorg. Chem.* **1981**, *20*, 42-45.

(86) a) Kuwana, T.; Bublitz, D. E.; Hoh, G. *J. Am. Chem. Soc.* **1960**, *82*, 5811-5817. b) Gubin, S. P.; Smirnova, S. A.; Denisovich, L. I.; Lubovich, A. A. *J. Organomet. Chem.* **1971**, *30*, 234-255. c) Denisovich, L. I.; Zakurin, N. V.; Bezrukova, A. A.; Gubin, S. P. *J. Organomet. Chem.* **1974**, *81*, 207-216.

(87) a) Sohn, Y. S.; Schlueter, A. W.; Hendrickson, D. N.; Gray, H. B. *Inorg. Chem.* **1974**, *13*, 301-304. b) Smith, T. P.; Kwan, K. S.; Taube, H.; Bino, A.; Cohen, S. *Inorg. Chem.* **1984**, *23*, 1943-1945. c) Watanabe, M.; Sano, H. *Chem. Lett.* **1991**, 555-558.

(88) Hill, M. G.; Lamanna, W. M.; Mann, K. R. *Inorg. Chem.* **1991**, *30*, 4687-4690.

(89) Trupia, S.; Nafady, A.; Geiger, W. E. *Inorg. Chem.* **2003**, *42*, 5480-5482.

(90) Swarts, J. C.; Nafady, A.; Roudebush, J. H.; Trupia, S.; Geiger, W. E. *Inorg. Chem.* **2009**, *48*, 2156-2165.

(91) Droege, M. W.; Harman, W. D.; Taube, H. *Inorg. Chem.* **1987**, *26*, 1309-1315.

(92) Mueller-Westerhoff, U. T.; Rheingold, A. L.; Swiegers, G. F. *Angew. Chem. Int. Ed. Engl.* **1992**, *31*, 1352-1354.

(93) Russell, A. D.; Gilroy, J. B.; Lam, K.; Haddow, M. F.; Harvey, J. N.; Geiger, W. E.; Manners, I. *Chem.–Eur. J.* **2012**, *18*, 8000-8003.

(94) a) Koelle, U.; Salzer, A. *J. Organomet. Chem.* **1983**, *243*, C27-C30. b) Kölle, U.; Grub, J. *J. Organomet. Chem.* **1985**, *289*, 133-139.

(95) Banks, C. E.; Robinson, K. L.; Laing, H.-P.; Meredith, A. W.; Lawrence, N. S. *Electroanalysis* **2007**, *19*, 555-560.

(96) Rogers, E. I.; Lawrence, N. S.; Compton, R. G. *J. Electroanal. Chem.* **2011**, *657*, 144-149.

(97) a) Rulkens, R.; Lough, A. J.; Manners, I.; Lovelace, S. R.; Grant, C.; Geiger, W. E. *J. Am. Chem. Soc.* **1996**, *118*, 12683-12695. b) Herbert, D. E.; Gilroy, J. B.; Chan, W. Y.; Chabanne, L.; Staubitz, A.; Lough, A. J.; Manners, I. *J. Am. Chem. Soc.* **2009**, *131*, 14958-14968.

(98) Greenwood, N. N.; Earnshaw, A. *Chemistry of the Elements*, 2nd ed.; Elsevier: Burlington, 2006, Chap. 7.

(99) Berenbaum, A.; Braunschweig, H.; Dirk, R.; Englert, U.; Green, J. C.; Jäckle, F.; Lough, A. J.; Manners, I. *J. Am. Chem. Soc.* **2000**, *122*, 5765-5774.

(100) Braunschweig, H.; Homberger, M.; Hu, C.; Zheng, X. Gullo, E. Clentsmith, G.; Lutz, M. *Organometallics* **2004**, *23*, 1968-1970.

(101) Braunschweig, H.; Adams, C. J.; Kupfer, T.; Manners, I.; Richardson, R. M.; Whittell, G. R. *Angew. Chem. Int. Ed.* **2008**, *47*, 3826-3829.

(102) Braunschweig, H.; Kaupp, M.; Adams, C. J.; Kupfer, T.; Radacki, K.; Schinzel, S. *J. Am. Chem. Soc.* **2008**, *130*, 11376-11393.

(103) Braunschweig, H.; Kupfer, T.; Lutz, M.; Radacki, K. *J. Am. Chem. Soc.* **2007**, *129*, 8893-8906.

(104) Braunschweig, H.; Lutz, M.; Radacki, K.; Schaumlöffel, A.; Seeler, F.; Unkelbach, C. *Organometallics* **2006**, *25*, 4433-4435.

(105) Scheibitz, M.; Winter, R. F.; Bolte, M.; Lerner, H.-W.; Wagner, M. *Angew. Chem. Int. Ed.* **2003**, *42*, 924-927.

(106) Heilmann, J. B.; Scheibitz, M.; Qin, Y.; Sundararaman, A.; Jäkle, F.; Kretz, T.; Bolte, M.; Lerner, H.-W.; Holthausen, M. C.; Wagner, M. *Angew. Chem. Int. Ed.* **2006**, *45*, 920-925.

(107) Scheibitz, M.; Li, H.; Schnorr, J.; Perucha, A. S.; Bolte, M.; Lerner, H.-W.; Jäkle, F.; Wagner, M. *J. Am. Chem. Soc.* **2009**, *131*, 16319-16329.

(108) Bagh, B.; Breit, N. C.; Harms, K.; Schatte, G.; Burgess, I. J.; Braunschweig, H.; Müller, J. *Inorg. Chem.* **2012**, *51*, 11155-11167.

(109) Schachner, J. A.; Lund, C. L.; Quail, J. W.; Müller, J. *Organometallics* **2005**, *24*, 4483-4488.

(110) Schachner, J. A.; Tockner, S.; Lund, C. L., Quail, J. W.; Rehahn, M.; Müller, J. *Organometallics* **2007**, *26*, 4658-4662.

(111) Bagh, B.; Gilroy, J. B.; Staubitz, A.; Müller, J. *J. Am. Chem. Soc.* **2010**, *132*, 1794-1795.

(112) Lund, C. L.; Schachner, J. A.; Quail, J. W.; Müller, J. *J. Am. Chem. Soc.* **2007**, *129*, 9313-9320.

(113) Lund, C. L.; Schachner, J. A.; Burgess, I. J.; Quail, J. W.; Schatte, G.; Müller, J. *Inorg. Chem.* **2008**, *47*, 5992-6000.

# CHAPTER 2
# SYNTHESIS OF NEW ALUMINUM AND GALLIUM DIHALIDES FOR REACTIONS WITH LITHIATED SANDWICH COMPLEXES

## 2.1 Introduction

*Ligands with medium steric bulk*

As described in more detail in Chapter 1.5, aluminum- and gallium-bridged [1]FCPs and [1]RCPs were obtained with the bulky ligands Pytsi and $Me_2$Ntsi, whereas salt-metathesis reactions with less bulky ligands, like Ar′, yielded [1.1]FCPs (Scheme 1-25 and Scheme 1-26).[1] Since ROP of the aluminum- and gallium-bridged [1]FCPs was not successful or at best sluggish and, for example, no reaction with the anionic initiator *n*BuLi occurred, it was concluded that the steric bulk of these ligand is hampering the polymerization.[1e] Therefore, the synthesis of aluminum and gallium dichlorides with ligands of moderate steric bulk for further reactions with dilithioferrocene or dilithioruthenocene were anticipated and will be discussed in this chapter. Some features of the previous ligands that led to [1]FCPs, like the nitrogen donor, should be retained in these new ligands of moderate steric bulk. For the first three ligands described here, steric bulk in the form of dimethylsilyl or trimethylsilyl groups was formally removed from the Pytsi ligand (Figure 2-1). These ligands were named Pytsi$^{-SiMe_2}$, Pytsi$^{-2SiMe_2}$, and Pytsi$^{-2SiMe_3}$ (Figure 2-1), indicating groups that were removed from the Pytsi ligand. In the Pytsi ligand, the steric bulk is mainly due to the trimethylsilyl groups, but also the dimethylsilyl group is adding a little bulk as it is not planar like the pyridine group. When this dimethylsilyl group is removed in Pytsi$^{-SiMe_2}$ the steric bulk experienced by the group-13 element should be reduced, which is also due to a four-membered ring being formed by the ligand and the group-13 element instead of a five-membered ring. In the four-membered ring, the trimethylsilyl groups are getting tilted further away from the

group-13 element. The steric bulk is getting further removed from Pytsi$^{-SiMe_2}$ as one of the trimethylsilyl groups is replaced with a methyl group in the Pytsi$^{-2SiMe_2}$ ligand. The major reason for keeping a methyl group in this position instead of a proton is that this proton could be so acidic that it would interfere in subsequent reactions with lithiated sandwich complexes. It is also worth mentioning that this ligand is less symmetric than the other ligands and possesses a stereogenic carbon atom. The new ligand with the least steric bulk is Pytsi$^{-2SiMe_3}$, in which both trimethylsilyl groups were formally removed from the Pytsi ligand.

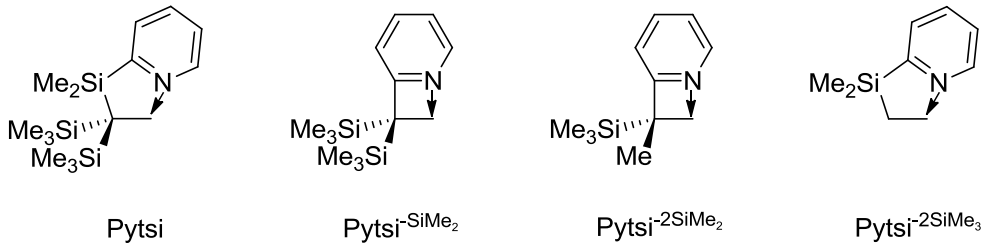


**Figure 2-1.** Depiction of the ligands Pytsi, Pytsi$^{-SiMe_2}$, Pytsi$^{-2SiMe_2}$, and Pytsi$^{-2SiMe_3}$.

Another option to obtain ligands with moderate steric bulk besides the removal of bulky groups from the Pytsi ligand is to increase the steric bulk of a non-bulky ligand like Ar′ (Figure 2-2). Bidraha Bagh from our group followed this approach and utilized the Mamx ligand that has a *tert*-butyl group in the *ortho* and *para* positions. However, with the Mamx ligand, [1]MCPs were obtained that were escaping their isolation by ROP (see Chapter 1.5 / Scheme 1-27).[2] Calculations showed that the *ortho tert*-butyl group adds additional strain to the system.[2b] The last ligand described in this chapter is the Mx ligand, which was derived from the Mamx ligand by a formal removal of one methylene group (Figure 2-2). Similar to the Pytsi$^{-SiMe_2}$ and Pytsi$^{-2SiMe_2}$ ligand, a transition from a

five-membered ring to a four-membered ring accompanies this change and the distance between the *tert*-butyl group and the group-13 element is expected to increase.

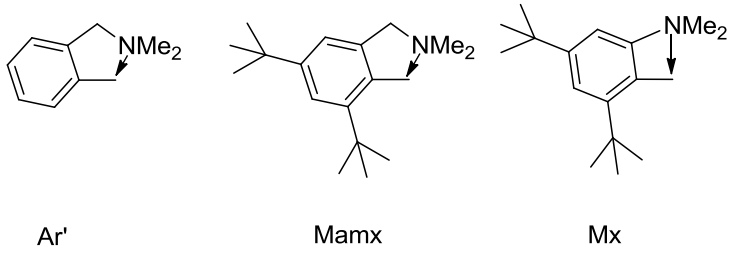


**Figure 2-2.** Depiction of the ligands Ar´, Mamx, and Mx.

*Known compounds with the Pytsi$^{-SiMe_2}$, Pytsi$^{-2SiMe_2}$, Pytsi$^{-2SiMe_3}$, and Mx ligands*

The Pytsi$^{-SiMe_2}$ ligand was already widely utilized since the 1980s by a variety of research groups. Pytsi$^{-SiMe_2}$-containing compounds with the main-group-elements Li,[3] Mg,[4] Al,[5] Ga,[6,5b] In,[7] Si,[8,3] Ge,[9] Sn,[10,9b] As,[11] Sb,[12,5c, 6, 11] Bi,[11] and Se[13], and the transition metal elements Cr,[14] Mn,[14] Fe, [14,15] Co,[16] Ni,[17] Cu,[18] Ag,[19] Au,[20] Zn,[4b] Cd,[4b] and Hg[4b,21] were reported. As illustrated in Figure 2-3, most common are bis(ligand) compounds of the type (Pytsi$^{-SiMe_2}$)$_2$E (E = Mg, Ge, Ni, Mn, Cr, Fe, Co, Zn, Cd, Hg) and (Pytsi$^{-SiMe_2}$)$_2$EX (E = Al, Ga, In, Sb, Ge), but also various compounds containing only one ligand per element like (Pytsi$^{-SiMe_2}$)EX (E = Ni, Se, Ge) and (Pytsi$^{-SiMe_2}$)EX$_2$ (E = Bi, As, Sb) or [(Pytsi$^{-SiMe_2}$)E]$_2$ (E = Ag, Au, Cu) are known (Figure 2-3).

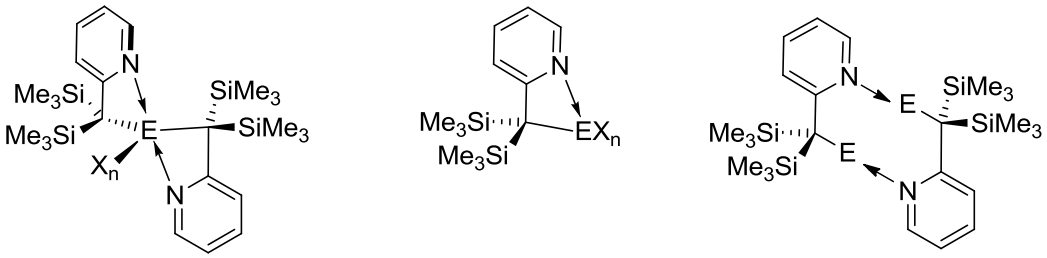


n = 0: E = Mg, Ge, Ni, Mn, Cr, Fe, Co, Zn, Cd, Hg
n = 1: E = Al, Ga, In, Sb, Ge

n = 1: E = Ni, Se, Ge
n = 2: E = Bi, As, Sb

E = Cu, Ag, Au

**Figure 2-3.** Most common types of compounds with the Pytsi$^{-SiMe_2}$ ligand.

For aluminum and gallium, compounds of the type (Pytsi$^{-SiMe_2}$)$_2$ECl and the respective salts [(Pytsi$^{-SiMe_2}$)$_2$E][ECl$_4$] were reported.[5a,5b] In the case of gallium, [(Pytsi$^{-SiMe_2}$)$_2$Ga][GaCl$_4$] was obtained during the synthesis of (Pytsi$^{-SiMe_2}$)$_2$GaCl, when the reactions were not carried out carefully. This showed that formation of the salt is preferred.

No complexes with the Pytsi$^{-2SiMe_2}$ ligand were known in literature prior to the investigations described below.

Palladium complexes equipped with the Pytsi$^{-2SiMe_3}$ ligand were first investigated by Hiraki *et al.* in 1988 (Figure 2-4).[22] Chlorido-bridged and acetato-bridged dimeric species of the type [(Pytsi$^{-2SiMe_3}$)PdX]$_2$ as well as donor (Do) stabilized monomeric species like (Pytsi$^{-2SiMe_3}$)PdCl(Do) were reported (Figure 2-4). In 2001, Yoshida *et al.* investigated palladium-catalyzed Stille couplings with (Pytsi$^{-2SiMe_3}$)SnR$_3$ (R = Me, Bu, Ph). These reactions were accelerated by the formation of (Pytsi$^{-2SiMe_3}$)PdCl(PPh$_3$), a compound that was isolated and structurally characterized (Figure 2-4).[23]

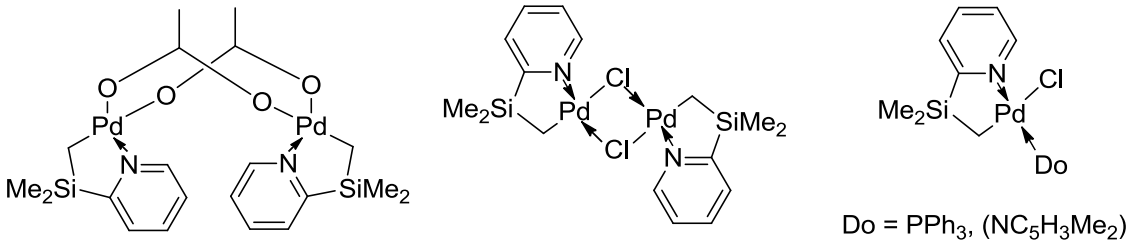


**Figure 2-4.** Palladium complexes equipped with the Pytsi$^{-2SiMe_3}$ ligand.

The Mx ligand was utilized by Yoshifugi *et al.* for the synthesis of a variety of phosphorus compounds (Scheme 2-1). MxBr was used as a starting material in order to assure the lithiation in the desired position and to facilitate this lithiation. $(Mx)PCl_2$, which was never isolated due to its high reactivity, was employed as a starting material for all other phosphorous compounds (Scheme 2-1).[24] In particular, phosphorus compounds with sulfur or selenium were studied (Scheme 2-1).[24,25] No molecular structure of any species with the Mx ligand was reported.

**Scheme 2-1.** Synthesis of phosphorus compounds with the Mx ligand.

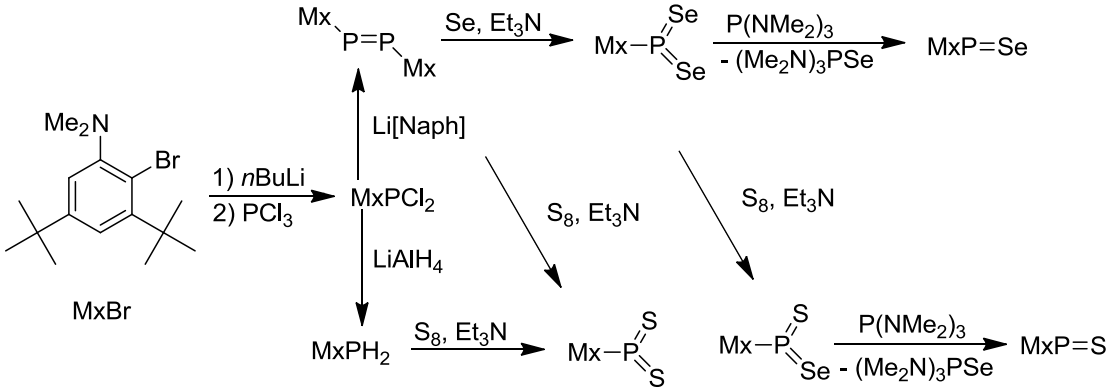

## 2.2 Results and Discussion

### 2.2.1 Synthesis of (Pytsi$^{-SiMe_2}$)AlBr$_2$, (Pytsi$^{-SiMe_2}$)AlCl$_2$, and (Pytsi$^{-SiMe_2}$)GaCl$_2$

Pytsi$^{-SiMe_2}$H can be synthesized in a one-step reaction starting from 2-methylpyridine following literature procedures.[3] Travis Ancelet, an undergraduate student who did his Chem 483 project in 2006/2007 in our lab, started the work with the Pytsi$^{-SiMe_2}$ ligand that is described here.[26] He obtained the initial results for the synthesis of (Pytsi$^{-SiMe_2}$)AlBr$_2$ and the crystals that were used for single crystal X-ray diffraction. The first approach was to synthesize (Pytsi$^{-SiMe_2}$)AlCl$_2$ by a reaction of the known Li(Pytsi$^{-SiMe_2}$)·tmeda[3] with aluminum trichloride (Scheme 2-2 (a)). However, by $^1$H NMR spectroscopy it was observed that the intended (Pytsi$^{-SiMe_2}$)AlCl$_2$ did not form as two singlets for the trimethylsilyl groups were observed. However, the mirror plane in monomeric (Pytsi$^{-SiMe_2}$)AlCl$_2$ should render the trimethylsilyl groups equivalent. Mass spectrometry revealed that (Pytsi$^{-SiMe_2}$)$_2$AlCl (**109**) was the product of this reaction, a species which was already known in literature (Scheme 2-2).[5a]

**Scheme 2-2.** Synthesis of (Pytsi$^{-SiMe_2}$)$_2$AlCl (**109**) instead of the intended (Pytsi$^{-SiMe_2}$)AlCl$_2$.

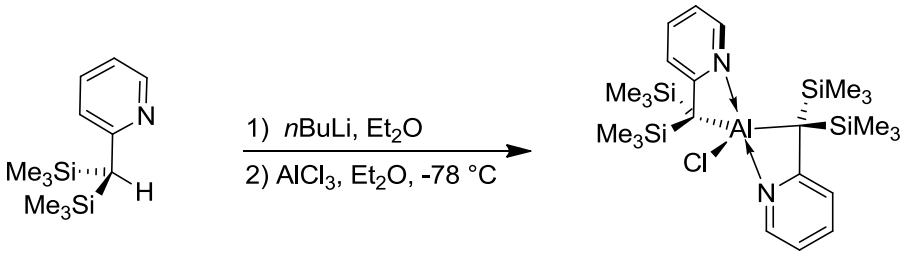


**109**

42%

This problem was circumvented by following an indirect route to obtain (Pytsi$^{-SiMe_2}$)AlBr$_2$ (**111**) via (Pytsi$^{-SiMe_2}$)AlMe$_2$ (**110**) (Scheme 2-3). The idea behind the indirect

route is that if only one chlorine atom is present on the aluminum, further reaction with Li(Pytsi$^{-SiMe_2}$) cannot occur, once the chlorine atom was replaced. Subsequently the methyl groups can be exchanged by bromine, chlorine or other halides. Similar strategies have been reported before for the synthesis of aluminum dihalides.[27] (Pytsi$^{-SiMe_2}$)$AlMe_2$ (**110**) was obtained in a nearly quantitative yield (Scheme 2-3). Species **110** showed four multiplets for the aromatic protons and one singlet for the aliphatic protons in the $^1H$ NMR spectrum, which is expected for this $C_s$ symmetric species. The elemental analysis data of this species was slightly off, probably due to the high air sensitivity of this compound and the difficulties in handling this sticky oil.

**Scheme 2-3.** Synthesis of (Pytsi$^{-SiMe_2}$)$AlMe_2$ (**110**).

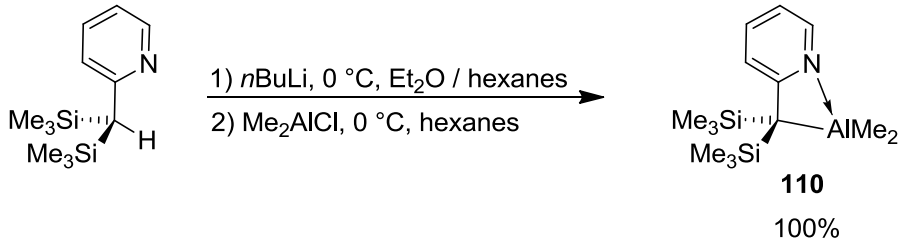


Bromination of (Pytsi$^{-SiMe_2}$)$AlMe_2$ (**110**) with molecular bromine gave (Pytsi$^{-SiMe_2}$)$AlBr_2$ (**111**) in a good yield of 75% (Scheme 2-4). Characterization of this species was similar to (Pytsi$^{-SiMe_2}$)$AlMe_2$ (**110**).

**Scheme 2-4.** Synthesis of (Pytsi$^{-SiMe_2}$)$AlBr_2$ (**111**).

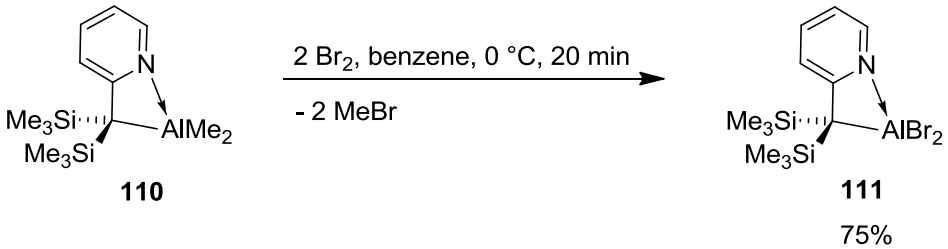

The molecular structures of (Pytsi$^{-SiMe_2}$)$AlMe_2$ (**110**) and (Pytsi$^{-SiMe_2}$)$AlBr_2$ (**111**) were determined by Dr. J. Wilson Quail from the Saskatchewan Structural Sciences Center (SSSC) (Figure 2-5 and Figure 2-6).

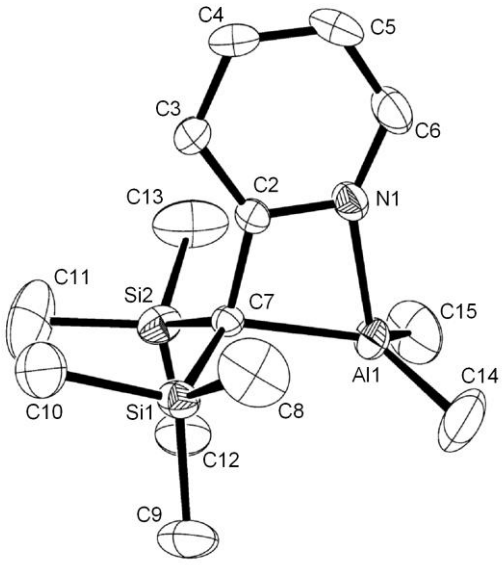


**Figure 2-5.** Molecular structure of (Pytsi$^{-SiMe_2}$)$AlMe_2$ (**110**) with thermal ellipsoids at the 50% probability level. Hydrogen atoms are omitted for clarity. One of two independent molecules is shown. Selected atom-atom distances [Å] and bond angles [°] (values in braces refer to the second independent molecule that is not shown): Al1–N1 = 1.984(2) {1.996(2)}, Al1–C7 = 2.064(2) {2.052(2)}, Al1–C14 = 1.968(3) {1.968(3)}, Al1–C15 = 1.962(3) {1.970(3)}, C2–C7 = 1.495(3) {1.490(3)}, C7–Al1–N1 = 70.66(8) {70.62(8)}, C7–Al1–C14 = 121.85(12) {117.59(11)}, C7–Al1–C15 = 121.11(13) {123.091(11)}, N1–Al1–C14 = 112.07(12) {106.71(10)}, N1–Al1–C15 = 110.80(12) {118.31(12)}, C14–Al1–C15 = 111.80(16) {112.57(12)}, C7–C2–N1 = 110.45(18) {110.30(19)}, C7–C2–C3 = 130.4(2) {130.5(2)}. Reprinted with permission from Breit, N. C.; Ancelet, T.; Quail, W.; Schatte, G.; Müller, J. *Organometallics* **2011**, *30*, 6150-6158. Copyright 2011 American Chemical Society.

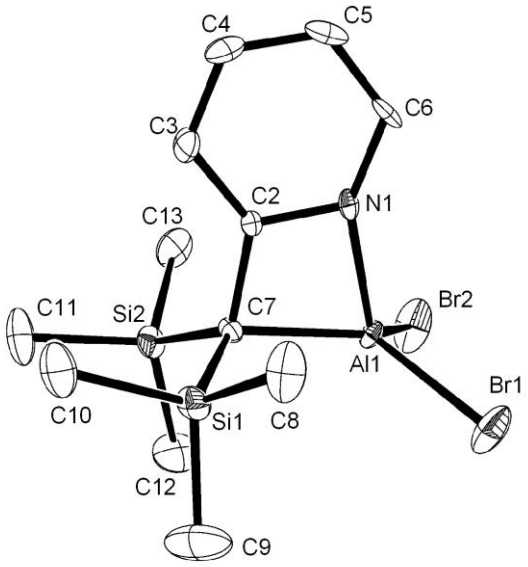


**Figure 2-6.** Molecular structure of (Pytsi$^{-SiMe_2}$)$AlBr_2$ (**111**) with thermal ellipsoids at the 50% probability level. Hydrogen atoms are omitted for clarity. Selected atom-atom distances [Å] and bond angles [°]: Al1–N1 = 1.936(4), Al1–C7 = 2.002(5), Al1–Br1 = 2.2784(14), Al1–Br2 = 2.2738(15), C2–C7 = 1.510(6), C7–Al1–N1 = 73.38(18), C7–Al1–Br1 = 124.54(15), C7–Al1–Br2 = 121.60(15), N1–Al1–Br1 = 116.35(13), N1–Al1–Br2 = 111.32(15), Br1–Al1–Br2 = 105.66(6), C7–C2–N1 = 110.9(4), C7–C2–C3 = 130.2(4). Reprinted with permission from Breit, N. C.; Ancelet, T.; Quail, W.; Schatte, G.; Müller, J. *Organometallics* **2011**, *30*, 6150-6158. Copyright 2011 American Chemical Society.

The molecular structures of both species are very similar. As expected, both species are monomers in the solid state and the aluminum has a distorted tetrahedral coordination sphere. The carbon-aluminum bond length and the nitrogen-aluminum bond length are very similar to other aluminum complexes with the Pytsi ligand like (Pytsi)$AlEt_2$[28] and (Pytsi)$AlCl_2$[29] (Table 2-1). Generally the carbon-aluminum and nitrogen-aluminum bond lengths are longer for the alkyl complexes than for the halide complexes, because the alkyl groups are better donors and thus the aluminum requires less electron density from the ligand. The bite angle of the Pytsi$^{-SiMe_2}$ ligand is with 70.66(8) and 70.62(8)° in (Pytsi$^{-SiMe_2}$)$AlMe_2$ (**110**) and 73.38(18)° in (Pytsi$^{-SiMe_2}$)$AlBr_2$

(**111**) significantly smaller than in similar compounds decorated with the Pytsi ligand [96.02(8)° for (Pytsi)$AlEt_2$, and 100.07(7)° for (Pytsi)$AlCl_2$]. This decrease of the bite angle can be explained by the decrease of the five-membered ring formed by the Pytsi ligand with aluminum to the four-membered ring formed by the Pytsi$^{-SiMe_2}$ ligand with aluminum. However, four-coordinate aluminum prefers tetrahedral coordination with an angle of 109.5°. Therefore, the change of the bite angle of the ligand from up to 100° to only 70° might decrease the ability of this ligand to stabilize the aluminum center. The bite angle is also significantly smaller than that in ($Me_2$Ntsi)$AlCl_2$ of 88.28(7)°.[30] In spite of the presence of a four-membered ring with the $Me_2$Ntsi ligand, this ligand has a larger bite angle than the Pytsi$^{-SiMe_2}$ ligand. This can be based on the larger ideal angle of the $sp^2$ hybridized atoms in comparison to the $sp^3$ hybridized atoms as well as the higher flexibility of angles on silicon atoms. Moreover, the C7-C2-C1 angle is deviates by 10° from the preferred 120° angle of $sp^2$ hybridized carbon centers (Table 2-1). The distances of the silicon atoms and the aluminum in (Pytsi)$AlEt_2$ and (Pytsi$^{-SiMe_2}$)$AlMe_2$ were compared in order to see if the trimethylsilyl groups are further away from the aluminum center in the Pytsi$^{-SiMe_2}$ ligand than in the Pytsi ligand. This comparison clearly showed the expected increasing distance from silicon to aluminum as the five-membered ligand is reduced to a four-membered ring (Si-Al = 3.1960(9), 3.2070(9) Å in (Pytsi)$AlEt_2$ and 3.265, 3.281, 3.292, 3.305 Å in (Pytsi$^{-SiMe_2}$)$AlMe_2$ (**110**)). This change would be more apparent, if the distance between the protons on the methyl groups and the aluminum center could be directly compared. However, this is not possible due to the fixed position of the methyl-carbon atoms that might be in different proximity to the aluminum center.

**Table 2-1.** Bond lengths and bond angles of (Pytsi)$AlEt_2$, (Pytsi)$AlCl_2$, (Pytsi$^{-SiMe_2}$)$AlMe_2$ (**110**), and (Pytsi$^{-SiMe_2}$)$AlBr_2$ (**111**).

| | C7-Al | N-Al | C7-Al-N | C7-C2-N1 |
|---|---|---|---|---|
| (Pytsi)$AlEt_2$ | 2.043(2) | 2.004(2) | 96.02(8) | 114.6 |
| (Pytsi$^{-SiMe_2}$)$AlMe_2$ | 2.064(2) | 1.984(2) | 70.66(8) | 110.5(2) |
| | 2.052(2) | 1.996(2) | 70.62(8) | 110.3(2) |
| (Pytsi$^{-SiMe_2}$)$AlBr_2$ | 2.002(5) | 1.936(4) | 73.38(18) | 110.9(4) |
| (Pytsi)$AlCl_2$ | 1.978(2) | 1.938(2) | 100.07(7) | |

Reactions of (Pytsi$^{-SiMe_2}$)$AlBr_2$ (**111**) with $(LiC_5H_4)_2Fe{\cdot}2/3$tmeda were expected to lead to the formation of lithium bromide that would easily coordinate to tmeda. This tmeda adduct of lithium bromide shows a higher solubility in organic solvents than the respective lithium chloride, which could hamper the isolation of the desired product. Therefore, an exchange of the methyl groups with chlorine instead of bromine atoms were carried out. (Pytsi$^{-SiMe_2}$)$AlCl_2$ (**112**) was obtained in a good yield by reacting (Pytsi$^{-SiMe_2}$)$AlMe_2$ (**110**) with an excess of trimethyltin chloride (Scheme 2-5). Without the more than two-fold excess of $Me_3SnCl$, a mixture of (Pytsi$^{-SiMe_2}$)$AlCl_2$ (**112**) and (Pytsi$^{-SiMe_2}$)AlMeCl was obtained. All characterizations were similar to **111**.

**Scheme 2-5.** Synthesis of (Pytsi$^{-SiMe_2}$)$AlCl_2$ (**112**).

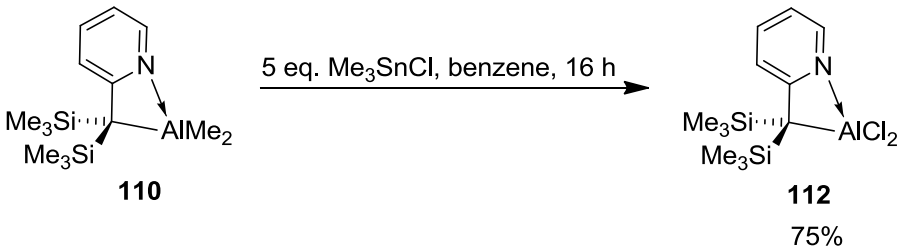


The synthesis of (Pytsi$^{-SiMe_2}$)$GaCl_2$ (**113**) was achieved by a direct reaction of Li(Pytsi$^{-SiMe_2}$) with gallium trichloride (Scheme 2-6). However, the intended (Pytsi$^{-SiMe_2}$)$GaCl_2$ was only formed as a minor product. The major product of this reaction was [(Pytsi$^{-SiMe_2}$)$_2$Ga][$GaCl_4$]. As mentioned in Chapter 2.1, [(Pytsi$^{-SiMe_2}$)$_2$Ga][$GaCl_4$] is

preferentially formed from (Pytsi$^{-SiMe_2}$)$_2$GaCl in the presence of gallium trichloride.[5b] [(Pytsi$^{-SiMe_2}$)$_2$Ga][GaCl$_4$] was identified by IR spectroscopy and comparison of the measured stretching frequency of the Ga-Cl vibration with the literature value ($\upsilon_{GaCl}$: 380 cm$^{-1}$ and 375 cm$^{-1}$ for literature 5b). Moreover, (Pytsi$^{-SiMe_2}$)$_2$Ga$^+$ was found by ESI mass spectrometry. The salt was insoluble in the organic solvent mixture and precipitated out of the reaction mixture, which facilitated its separation from (Pytsi$^{-SiMe_2}$)GaCl$_2$ (**113**). Species **113** can be isolated by crystallization from the solvent mixture in a low yield of 21%. Characterizations of this species were similar to **111** and **112**. No attempts were carried out to improve the yield by going through a route similar to that used for aluminum, because in contrast to dimethylaluminum chloride no similar species is commercially available for gallium. The results described in Chapter 2.2.1 were published in 2011 in Organometallics.[31]

**Scheme 2-6.** Synthesis of (Pytsi$^{-SiMe_2}$)GaCl$_2$ (**113**).

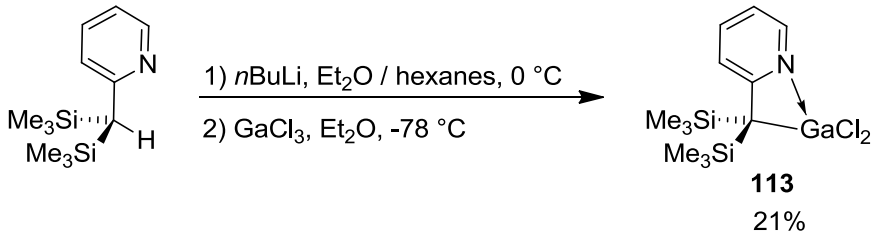


### 2.2.2 Synthesis of (Pytsi$^{-2SiMe_2}$)$_2$AlMe and (Pytsi$^{-2SiMe_2}$)$_2$AlCl Instead of the Intended (Pytsi$^{-2SiMe_2}$)AlCl$_2$

The synthesis of Pytsi$^{-2SiMe_2}$H (**114**) was described in literature prior to our investigations. The first procedure has two steps and starts from 2-methylpyridine to give Pytsi$^{-2SiMe_2}$H via 2-(trimethylsilyl)methylpyridine in 49% overall yield.[3] The second procedure starts from 2-ethylpyridine utilizing *n*-butyllithium and chlorotrimethylsilane.

However, a yield for this procedure was not reported.[32] The procedure used during the research described in this thesis was a slight variation of the second procedure in which tmeda and hexanes was used instead of the reported thf, resulting in Pytsi$^{-2SiMe_2}$H in 76% yield (Scheme 2-7).

**Scheme 2-7.** Synthesis of Pytsi$^{-2SiMe_2}$H (**114**).

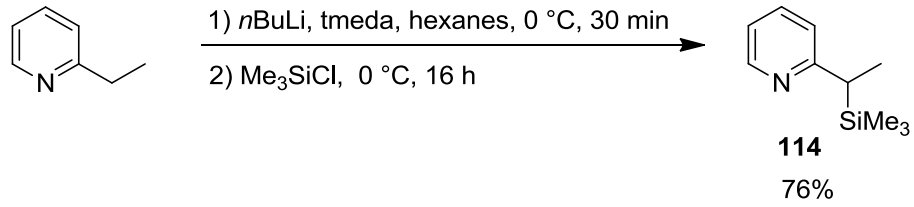


**114**

76%

The starting point for the intended synthesis of (Pytsi$^{-2SiMe_2}$)$AlCl_2$ was a direct reaction of Li(Pytsi$^{-2SiMe_2}$) with aluminum trichloride. Subsequent to a lithiation of **114** with *tert*-butyllithium in diethyl ether at -78 °C, a solution of aluminum trichloride at low temperatures was added (Scheme 2-8). $^1$H NMR spectroscopy revealed that only one major compound formed that was isolated by crystallization in a moderate yield of 42% (Scheme 2-8). The $^1$H NMR spectrum of the product could not be used to verify whether (Pytsi$^{-2SiMe_2}$)$AlCl_2$ or (Pytsi$^{-2SiMe_2}$)$_2$AlCl formed, because the obtained spectrum could fit with both species. However, mass spectrometry clearly showed that the product was (Pytsi$^{-2SiMe_2}$)$_2$AlCl (**115**).

**Scheme 2-8.** Synthesis of (Pytsi$^{-2SiMe_2}$)$_2$AlCl (**115**) instead of the intended (Pytsi$^{-2SiMe_2}$)AlCl$_2$.

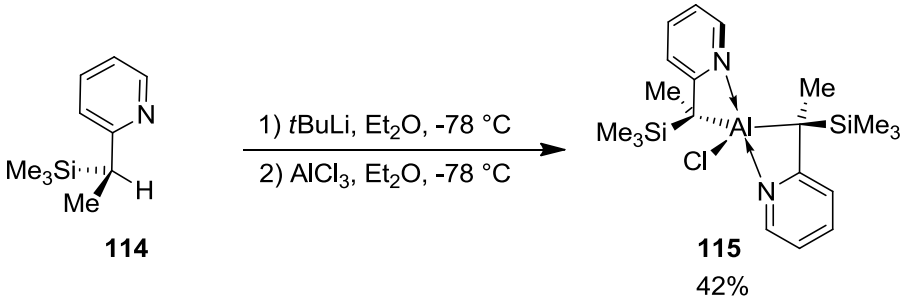


Based on the success to synthesize (Pytsi$^{-SiMe_2}$)AlCl$_2$ (**112**) by an indirect route via (Pytsi$^{-SiMe_2}$)AlMe$_2$ (**110**) (see Chapter 2.2.1, Scheme 2-3 and Scheme 2-5), a similar route to obtain the intended (Pytsi$^{-2SiMe_2}$)AlCl$_2$ via (Pytsi$^{-2SiMe_2}$)AlMe$_2$ was envisioned. We anticipated that (Pytsi$^{-2SiMe_2}$)AlMe$_2$ (**116**) would be the only product in the reaction of Li(Pytsi$^{-SiMe_2}$) with Me$_2$AlCl as no further reactions of a lithiated ligand with another chloride could occur (Scheme 2-9). However, when Pytsi$^{-2SiMe_2}$H was reacted with *n*-butyllithium in the presence of tmeda and subsequently dimethylaluminum chloride was added, an unexpected product was obtained (Scheme 2-9).

**Scheme 2-9.** Isolation of (Pytsi$^{-2SiMe_2}$)$_2$AlMe (**117**) instead of the intended (Pytsi$^{-2SiMe_2}$)AlMe$_2$ (**116**).

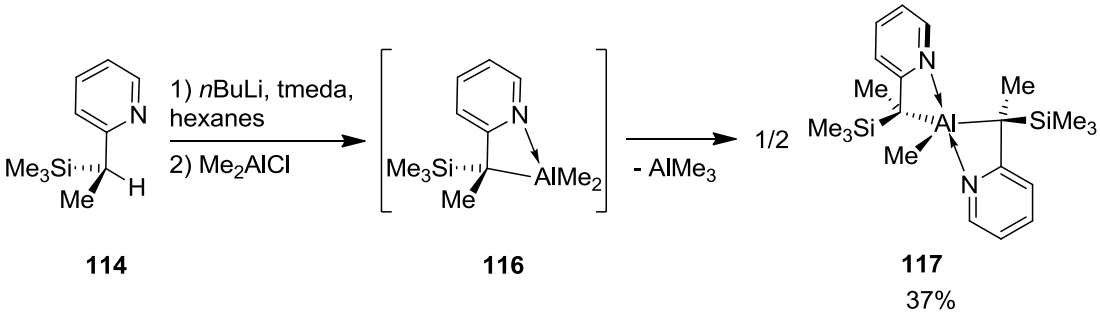


The $^1$H NMR spectrum of the reaction mixture showed only one product that contained two ligands and one methylaluminum group. Moreover, a trimethylaluminum tmeda adduct was observed as a side product. It can be assumed that in a first step the

intended (Pytsi$^{-2SiMe_2}$)AlMe$_2$ (**116**) formed and then a ligand exchange occurred to give the thermally more stable products, (Pytsi$^{-2SiMe_2}$)$_2$AlMe (**117**) and the trimethyl aluminum tmeda adduct (Scheme 2-9). If reactions were carried out in the absence of tmeda, for example with diethylether as a solvent, the formation of two major species was observed by $^1$H NMR spectroscopy. One of these major species was the previously isolated (Pytsi$^{-2SiMe_2}$)$_2$AlMe (**117**) and the other one can be tentatively assigned to be (Pytsi$^{-2SiMe_2}$)AlMe$_2$ (**116**). The signals observed in the $^1$H NMR spectrum fit with the expected set of signals for (Pytsi$^{-2SiMe_2}$)AlMe$_2$ (**116**). When this mixture of species was treated with tmeda, the equilibrium between these species shifted in favor of (Pytsi$^{-2SiMe_2}$)$_2$AlMe (**117**). A similar case was reported for an exchange between a dimethyl gallium species (**118**) with trimethylgallane and the respective methyl gallium compound **119** (Scheme 2-10).[33]

**Scheme 2-10.** Example for a ligand exchange of the dimethylgallium compound **118** to the methylgallium compound **119**.

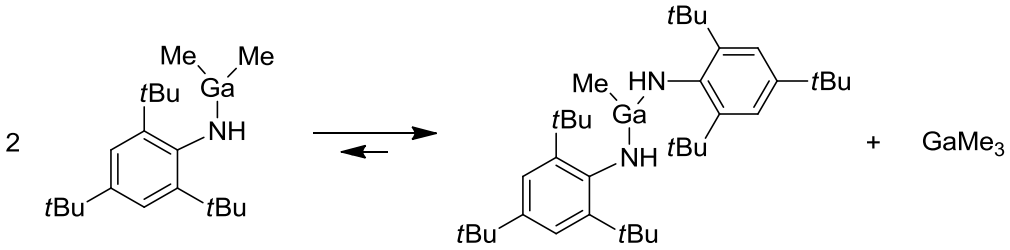


**118** **119**

For the gallium species shown in Scheme 2-10, only trimethylgallane and **119** were found, when diethyl ether was utilized as solvent, but in pentane a mixture of all three species was found. In analogy to these findings it is suggested for the (Pytsi$^{-2SiMe_2}$)$_x$AlMe$_y$ compounds that there is an equilibrium between the (Pytsi$^{-2SiMe_2}$)AlMe$_2$ (**116**) and (Pytsi$^{-2SiMe_2}$)$_2$AlMe (**117**) with a trimethylalumane donor adduct. In the presence of a better donor, like tmeda in comparison with diethyl ether, this equilibrium

is shifted toward the trimethylalumane donor adduct. However, reactions of lithiated ligands with dimethylaluminum chloride in the presence of tmeda commonly yield the expected dimethyl aluminum species without any ligand exchange. For example T. Ancelet obtained (Pytsi$^{-SiMe_2}$)AlMe$_2$ (**110**) in the presence of tmeda. Therefore, it can be concluded that the ligand Pytsi$^{-2SiMe_2}$ has a particular affinity for the formation of bisligand species that can be reinforced in the presence of strong donors.

Repeated attempts to synthesize the obtained products (Pytsi$^{-2SiMe_2}$)$_2$AlCl (**115**) and (Pytsi$^{-2SiMe_2}$)$_2$AlMe (**117**) from reactions with the correct stoichiometry in the case of **115** or with methylaluminum dichloride for species **117** were unsuccessful. Even though the same products formed as observed by $^1$H NMR spectroscopy, it was not possible to isolate any crystals under these conditions.

In the $^1$H NMR spectra of both species, (Pytsi$^{-2SiMe_2}$)$_2$AlCl (**115**) and (Pytsi$^{-2SiMe_2}$)$_2$AlMe (**117**) only one set of signals was observed for the ligand, showing four multiplets for the aromatic protons and two singlets for the aliphatic protons. This is surprising as a racemic ligand was used and each compound has two stereogenic carbon centers. Therefore, six different isomers giving two sets of signals in the $^1$H NMR spectrum would be expected to be present (Scheme 2-11). On the one hand a differentiation of *rac* and *meso* isomers with R,R and S,S combinations being the *rac* isomers and R,S and S,R combinations for the *meso* isomers can be made (Scheme 2-11). On the other hand, for trigonal bipyramids the two possible geometrical isomers, Λ and Δ, are expected (Scheme 2-11). This renders three sets of enantiomers (Scheme 2-11). The nitrogen donor can detach from the aluminum in solution, the ligand can rotate and the nitrogen donor can coordinate from the opposite direction. Therefore, the two racemic

sets of enantiomers are connected to each other and one set of signals is expected for all the *rac* species. One set of signals is expected for the *meso* species, because the *meso* isomers are enantiomers and in equilibrium with each other (Scheme 2-11). As mentioned above, only one set of signals was found in the $^{1}$H NMR spectra of both species. Hence, the stereoselective formation of one type of isomer over the other occurred. The molecular structure in the solid state of (Pytsi$^{-2SiMe_2}$)$_2$AlMe (**117**) clearly showed that the *rac* species formed selectively. If we assume an equilibrium between *rac* and *meso* species (based on the equilibrium between **116** and **117**), then the isolated *rac* species ought to be more thermodynamically stable than the *meso* species. A rationale for this selectivity and the higher thermodynamic stability of the *rac* isomers is offered based on steric interactions. Two groups of different steric bulk, the trimethylsilyl and the methyl group from the ligand, are found in equatorial positions. The steric repulsion between these groups in the different species is decreasing in the order of R,R-Δ/S,S-Λ > R,S-Δ/S,R-Λ > S,S-Δ/R,R-Λ. The isomers with the least steric interactions, that are expected to be thermally favored, are only available for the *rac* compounds. Hence, the *rac* isomers would be favored to form. No single-crystal X-ray analysis data was obtained for (Pytsi$^{-2SiMe_2}$)$_2$AlCl (**115**) therefore, it can only be assumed that this species formed as a *rac* isomer. The same argument of steric repulsion used for (Pytsi$^{-2SiMe_2}$)$_2$AlMe (**117**) should also be valid for this strongly related compound (**115**). Moreover, the similarity of the NMR data of **115** and **117** speaks in favor of the same type of isomers in both.

**Scheme 2-11.** Different possible isomers of (Pytsi$^{-2SiMe_2}$)$_2$AlX (X = Cl, Me) (**115** and **117**). The dotted line separates enantiomers, solid lines separate diastereomers, and double arrows indicate equilibria. Reprinted with permission from Breit, N. C.; Ancelet, T.; Quail, W.; Schatte, G.; Müller, J. *Organometallics* **2011**, *30*, 6150-6158. Copyright 2011 American Chemical Society.

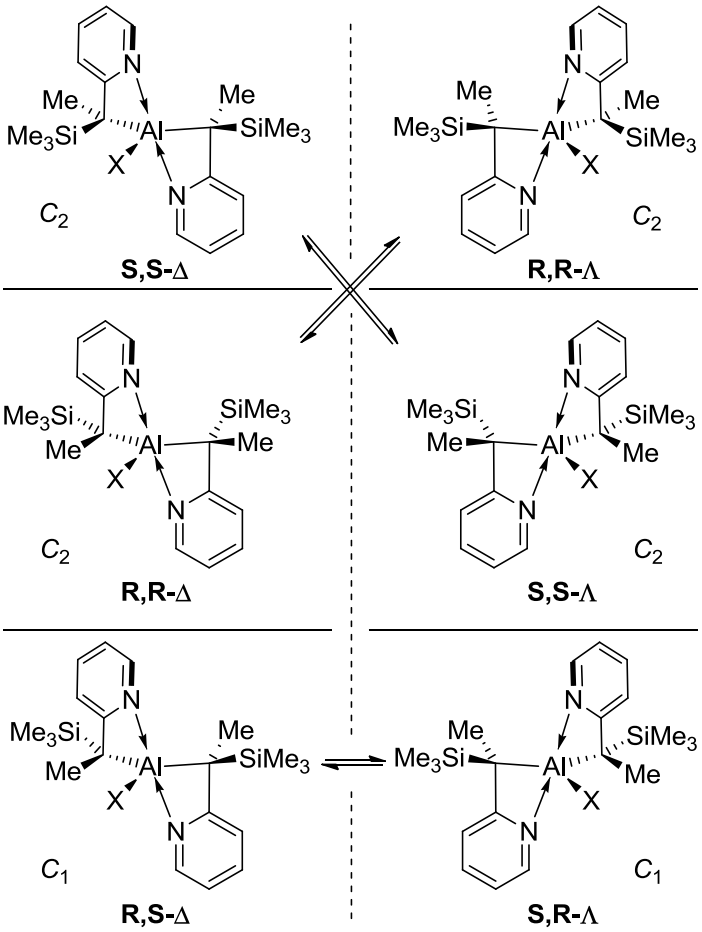


Crystals suitable for single-crystal X-ray analysis were grown of (Pytsi$^{-2SiMe_2}$)$_2$AlMe (**117**) from the diethyl ether / hexanes solvent mixture. Dr. Gabriele Schatte (SSSC) carried out the measurement and determined the molecular structure of **117** (Figure 2-7). The molecular structure revealed the presence of R,R-Λ and S,S-Δ isomers. The aluminum has a distorted trigonal-bypyramidal coordination sphere in which the nitrogen atoms occupy the axial positions. The distortion can be illustrated by the N-Al-N angle that deviates from 180° in a perfect trigonal bypyramid about

26.93(14)° [153.07(14)°]. Similar distortions from linearity were reported for (Pytsi$^{-SiMe_2}$)$_2$GaCl [167.1(1), 161.0(1), and 159.8(1)°]. The nitrogen-donor bond in (Pytsi$^{-2SiMe_2}$)$_2$AlMe (**117**) is significantly longer than that in (Pytsi$^{-SiMe_2}$)AlMe$_2$ (**110**) (2.1280(19) Å for **117** and 1.984(2) and 1.996(2) Å for **110**). The longer donor-bond of **117** in comparison to **110** is expected, based on the five-coordinate aluminum center in **117** and the four-coordinate aluminum center in **110**. The five-coordinate aluminum center is less Lewis-acidic toward each of the nitrogen donors than the four-coordinate aluminum center. The bite angle of the Pytsi$^{-2SiMe_2}$ ligand is very similar to that of the Pytsi$^{-SiMe_2}$ ligand [67.70(7)° for **117**; 70.66(8) and 70.62(8)° for **110**]. Also a tilt of the pyridyl group toward the acceptor atom by almost 10° similar to that in (Pytsi$^{-SiMe_2}$)AlMe$_2$ was found [C7–C2–N1 = 110.2(2)° for **117**; C7–C2–N1 = 110.45(18) {110.30(19)}° for **110**].

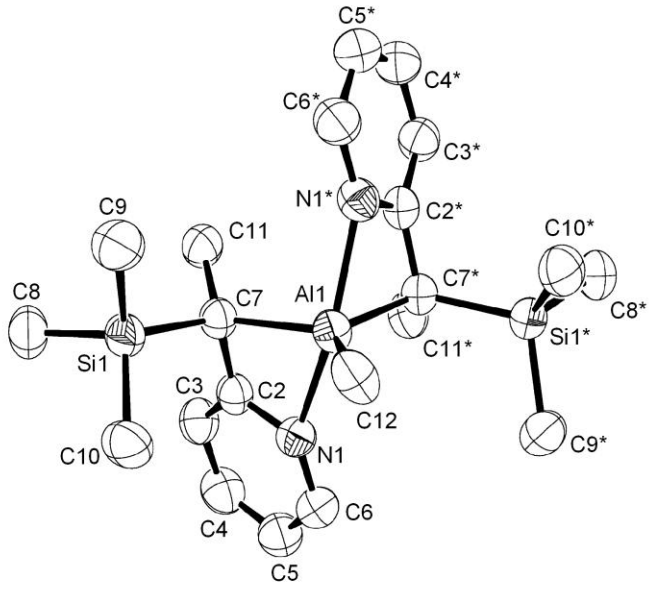


**Figure 2-7.** Molecular structure of (Pytsi$^{-2SiMe_2}$)$_2$AlMe (**117**) with thermal ellipsoids at the 50% probability level (only the R,R-Λ isomer is shown). Hydrogen atoms are omitted for clarity. Selected atom-atom distances [Å] and bond angles [°]: Al1–N1 = 2.1280(19), Al1–C7 = 2.056(2), Al1–C12 = 1.992(4), C2–C7 = 1.487(3), C7–Al1–N1 = 67.70(7), C7–Al1–C12 = 125.30(8), C7–Al1–N1$^*$ = 96.34(8), N1–Al1–C12 = 103.46(7), N1–Al1–

N1* = 153.07(14), C7–C2–N1 = 110.2(2), C7–C2–C3 = 129.7(2). Reprinted with permission from Breit, N. C.; Ancelet, T.; Quail, W.; Schatte, G.; Müller, J. *Organometallics* **2011**, *30*, 6150-6158. Copyright 2011 American Chemical Society.

In Chapter 2.2.1, it was shown for similar compounds that gallium trichloride can react significantly different than aluminum trichloride and (Pytsi$^{-SiMe_2}$)$GaCl_2$ (**113**) was obtained in a low yield, when respective reactions with aluminum trichloride yielded selectively (Pytsi$^{-SiMe_2}$)$_2$AlCl (**109**). Therefore, it was hoped that (Pytsi$^{-2SiMe_2}$)$GaCl_2$ could be obtained under the conditions that, in the case of aluminum, only gave (Pytsi$^{-2SiMe_2}$)$_2$AlCl (**115**). Therefore, reactions of (Pytsi$^{-2SiMe_2}$)H (**114**), butyllithium and gallium trichloride were carried out similarly to the respective reaction with aluminum trichloride (Scheme 2-8). This resulted in a mixture of two major compounds as observed by $^1$H NMR spectroscopy. It was not possible to isolate any of the species by sublimation, crystallization from various solvents, or by precipitation of a toluene solution into hexanes. Moreover, reactions were carried out with two equivalents of ligand and lithiation reagent with the aim to synthesize and isolate (Pytsi$^{-2SiMe_2}$)$_2$GaCl so that it can be identified as one of the products. According to $^1$H NMR data, this reaction led to similar mixtures like those with equimolar reactants. Therefore, it can only be speculated what the products are. The formation of any major amount of [(Pytsi$^{-2SiMe_2}$)$_2$Ga][$GaCl_4$] can be excluded, because [(Pytsi$^{-2SiMe_2}$)$_2$Ga][$GaCl_4$] is expected to precipitate out of the solution. However, the mass of the obtained product mixture after filtration and solvent removal is close to the theoretical yield expected for (Pytsi$^{-2SiMe_2}$)$GaCl_2$. One of the species, can be expected to be either (Pytsi$^{-2SiMe_2}$)$_2$GaCl or (Pytsi$^{-2SiMe_2}$)$GaCl_2$, because the $^1$H NMR spectra showed δ values that are similar to respective values of (Pytsi$^{-2SiMe_2}$)$_2$AlCl (**115**) and (Pytsi$^{-SiMe_2}$)$AlCl_2$ (**112**). However, the

$^1$H NMR signals of the other species exhibited δ values that are quite different from **115** or **112**, particularly for the trimethylsilyl group at δ -0.16 [δ 0.22 for **115** and δ 0.18 for **112**] and the 6-pyridyl-proton at δ 8.61 (δ 7.84 for **115** and δ 6.91 for **112**]. Therefore, the second species is expected to be neither (Pytsi$^{-2SiMe_2}$)$_2$GaCl nor (Pytsi$^{-2SiMe_2}$)GaCl$_2$ and no conclusion about its identity can be made.

The results described in Chapter 2.2.2 were published in 2011 in Organometallics.[31]

### 2.2.3 Synthesis of (Pytsi$^{-2SiMe_3}$)AlCl$_2$ and (Pytsi$^{-2SiMe_3}$)GaCl$_2$

The starting ligand Pytsi$^{-2SiMe_3}$H (**120**) is commercially available, but in the course of this research, **120** was synthesized by a lithiation of 2-bromopyridine and subsequent reaction with $Me_3SiCl$ in a good yield (Scheme 2-12). Similar synthesis routes were reported in literature;[34] however, the reaction conditions were altered in order to suit the starting materials at hand.

**Scheme 2-12.** Synthesis of Pytsi$^{-2SiMe_3}$H (**120**)

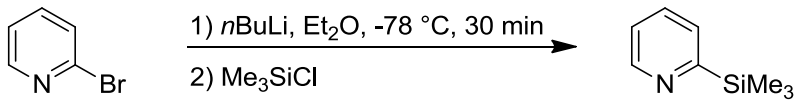


**120**
78%

The starting point for the synthesis of aluminum and gallium dichlorides equipped with the Pytsi$^{-2SiMe_3}$ ligand was a reaction of the lithiated ligand, Li(Pytsi$^{-2SiMe_3}$), with the element trichlorides. Yoshida *et al.* investigated different lithiation conditions for this ligand and obtained the best results utilizing *t*BuLi in diethyl ether at -78 °C.[35] Under these lithiation conditions Li(Pytsi$^{-2SiMe_3}$) was formed and reacted with the element

trichlorides at -78 °C (Scheme 2-13). $^{1}$H NMR spectra of the reaction mixtures indicated the formation of one major species along with some unknown minor species. After purification by sublimation or recrystallization the desired products (Pytsi$^{-2SiMe_3}$)$AlCl_2$ (**121**) and (Pytsi$^{-2SiMe_3}$)$GaCl_2$ (**122**) were obtained in moderate yields of 47 and 50%, respectively.

**Scheme 2-13.** Synthesis of (Pytsi$^{-2SiMe_3}$)$AlCl_2$ and (Pytsi$^{-2SiMe_3}$)$GaCl_2$ (**121** and **122**).

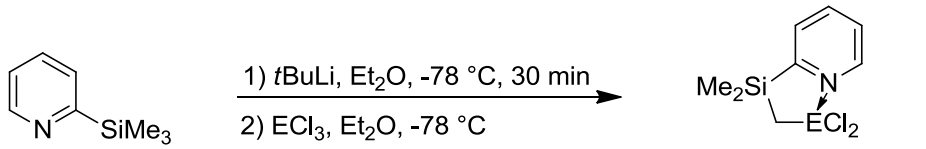


**120**

**121**: E = Al, 47%
**122**: E = Ga, 50%

The $^{1}$H NMR spectra of species **121** and **122** showed one singlet for the dimethylsilyl protons and one singlet for the methylene protons. In comparison with the $^{1}$H NMR data of the (Pytsi)$AlCl_2$ and (Pytsi)$GaCl_2$, the dimethylsilyl protons of Pytsi$^{-2SiMe_3}$ species are shifted downfield (δ 0.33 for (Pytsi)$AlCl_2$[29] and δ 0.02 for (Pytsi$^{-2SiMe_3}$)$AlCl_2$; δ 0.36 for (Pytsi)$GaCl_2$[36] and δ 0.05 for (Pytsi$^{-2SiMe_3}$)$GaCl_2$) thus showing that the dimethylsilyl protons are slightly more shielded in absence of the two trimethylsilyl groups. Crystals suitable for single-crystal X-ray analysis of (Pytsi$^{-2SiMe_3}$)$GaCl_2$ were obtained from a toluene solution. The X-ray analysis was carried out by Dr. Klaus Harms (University of Marburg) and the molecular structure is shown in Figure 2-8.

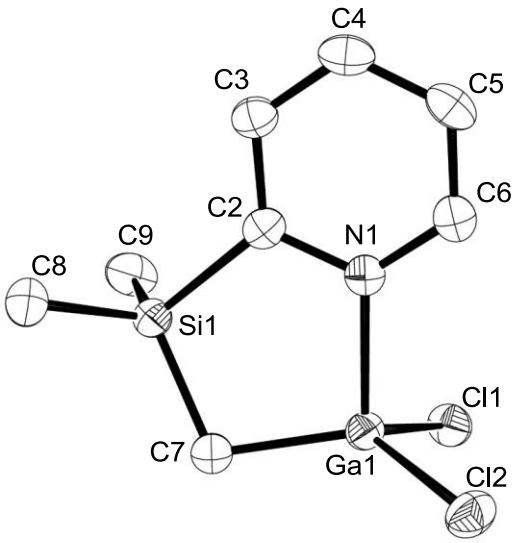


**Figure 2-8.** Molecular structure of (Pytsi$^{-2SiMe_3}$)$GaCl_2$ (**122**) with thermal ellipsoids at the 50% probability level. Hydrogen atoms are omitted for clarity. Selected atom-atom distances (Å) and bond angles (°): Ga-N = 2.0126(16), Ga-C = 1.949(2), Ga-Cl1 = 2.2024(5), Ga-Cl2 = 2.1927(6), N-Ga-C = 98.79(7), N1-C2-Si: 116.02(14), Cl1-Ga-Cl2 = 108.54(2), C7-Ga-Cl1 = 118.10(7), C7-Ga-Cl2 = 121.94(7), N1-Ga-Cl1 = 103.42(5), N1-Ga-Cl2 = 102.16(5). Reprinted with permission from Bagh, B.; Breit, N. C.; Harms, K.; Schatte, G.; Burgess, I.; Braunschweig, H.; Müller, J. *Inorg. Chem.* **2012**, *51*, 11155-11167. Copyright 2012 American Chemical Society.

The gallium atom has the expected distorted tetrahedral coordination sphere. The bite angle of the ligand is 98.79(7)°, which is significantly larger than 86.6(2)° found in (Pytsi$^{-2SiMe_3}$)PdCl($PPh_3$) with a planar coordination sphere around palladium. This shows the flexibility of the Pytsi$^{-2SiMe_3}$ ligand. The bite angle of (Pytsi$^{-2SiMe_3}$)$GaCl_2$ (**122**) fits well to the bite angle in (Pytsi)$GaCl_2$ with 98.03(9)°.[1b] Further similarities of the structural parameters of both species are illustrated in Table 2-2. The most interesting difference is the decrease of the carbon-gallium bond length as the two trimethylsilyl groups are getting formally removed [1.988(2) Å for (Pytsi)$GaCl_2$ and 1.949(2) Å for (Pytsi$^{-2SiMe_3}$)$GaCl_2$]. The trimethylsilyl groups increase the electron density on the *ipso*-carbon and therefore the bond should be stronger and the bond length shorter. However, the

opposite trend is observed here, which is presumably due to the steric hindrance introduced by the trimethylsilyl groups. The steric requirement of the trimethylsilyl groups also leads to a decrease of the Cl-Ga-Cl angle in their presence from 108.54(2)° to 103.73(3)°. Moreover, a change in the coordination geometry of the gallium is observed. The coordination geometry of (Pytsi)$GaCl_2$ can be described as a trigonal pyramid with nitrogen on the top, because the sum of the angles C7-Ga1-Cl1, C7-Ga1-Cl2, and Cl1-Ga-Cl2 is 350.0°, which is closer to the expected 360° for a trigonal pyramid than to the expected 328.5° for a tetrahedral coordination environment, whereas in (Pytsi$^{-2SiMe_3}$)$GaCl_2$ the sum of these angles is 335.4°, which is close to a tetrahedral geometry.

**Table 2-2.** Bond length and angles from the molecular structures of (Pytsi)$GaCl_2$ and (Pytsi$^{-2SiMe_3}$)$GaCl_2$ (**122**).

| | Ga-N | Ga-C | Ga-Cl | | N-Ga-C | Cl-Ga-Cl |
|---|---|---|---|---|---|---|
| (Pytsi)$GaCl_2$ | 2.004(2) | 1.988(2) | 2.1816(7) | 2.2016(7) | 98.03(9) | 103.73(3) |
| **122** | 2.013(2) | 1.949(2) | 2.1927(6) | 2.2024(5) | 98.79(7) | 108.54(2) |

The results described in Chapter 2.2.3 have been recently published in Inorganic Chemistry.[36]

### 2.2.4 Synthesis of (Mx)$AlCl_2$ and (Mx)$GaBr_xCl_{2-x}$

Unlike the three previous ligands, the Mx ligand has a dimethylamino group as the nitrogen donor instead of a pyridyl group. The pyridyl group was shown to be able to assist the deprotonation of the ligand in the desired position.[3,35] It is known that MxBr can be used as starting material for lithiations.[24] The synthesis of MxBr (**123**) was already described by Yoshifuji *et al.* (Scheme 2-14).[37] In a first step, 3,5-di-*tert*-butyltoluene was oxidized by potassium permanganate.[38] The carboxylic acid was then treated with sodium

azide to give the aniline derivative.[39] The aniline was acetylated and the acetyl group directed the bromine in the following bromination to the desired position.[40] The acetyl group was removed from the amine,[41] which was then methylated with sodium borohydrate and formaldehyde.[37]

**Scheme 2-14.** Synthesis of MxBr (**123**). Yields refer to literature values.

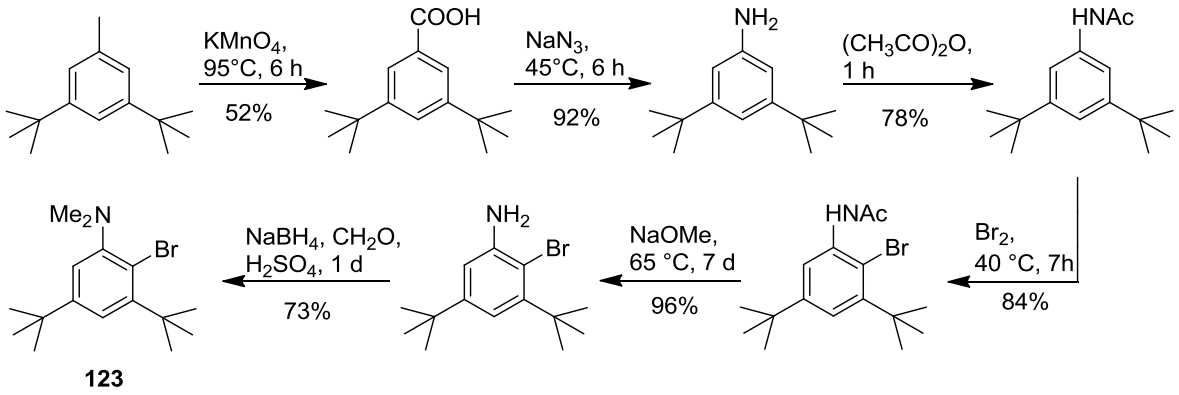


In the first reactions toward the synthesis of group-13 element dichlorides, MxBr (**123**) was lithiated with *tert*-butyllithium at low temperatures and subsequently a solution of aluminum trichloride was added (Scheme 2-15). The presence of (Mx)$AlCl_2$ (**124**) in the reaction mixture was revealed by $^1H$ NMR spectroscopy. However, it was only one of the products next to MxH and another unknown species. Purification of (Mx)$AlCl_2$ was attempted by crystallizations and sublimations, but it was not possible to remove all MxH from (Mx)$AlCl_2$. Therefore, reactions with $Me_2AlCl$ were explored.

**Scheme 2-15.** Direct reaction of MxBr with *t*BuLi and $AlCl_3$ to give (Mx)$AlCl_2$ (**124**).

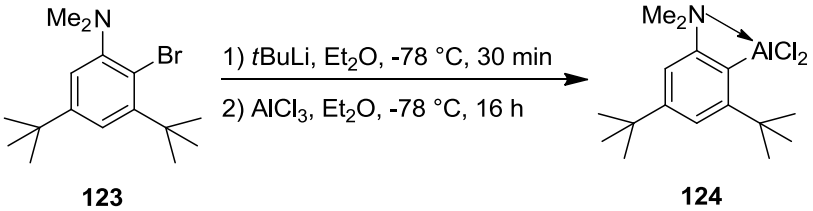

The synthesis of (Mx)$AlCl_2$ (**124**) in a very good yield was achieved by following the indirect route via (Mx)$AlMe_2$ (**125**) (Scheme 2-16). Similar to (Pytsi$^{-SiMe_2}$)$AlMe_2$ (**110**), the formation of (Mx)$AlMe_2$ (**125**) was quantitative. This attests the quality of the lithiation. The formation of (Mx)$AlCl_2$ (**124**) required prolonged heating to ensure a complete conversion, but no further excess of trimethyltin chloride was required. The product was isolated by crystallization from toluene in a very good yield of 94% (Scheme 2-16). $^1$H NMR spectra of both species showed two singlets for the *tert*-butyl groups, one singlet for the dimethylamino group and two broad singlets for the aromatic protons, which is expected for this $C_s$-symmetric species.

**Scheme 2-16.** Synthesis of (Mx)$AlCl_2$ (**124**) via (Mx)$AlMe_2$ (**125**).

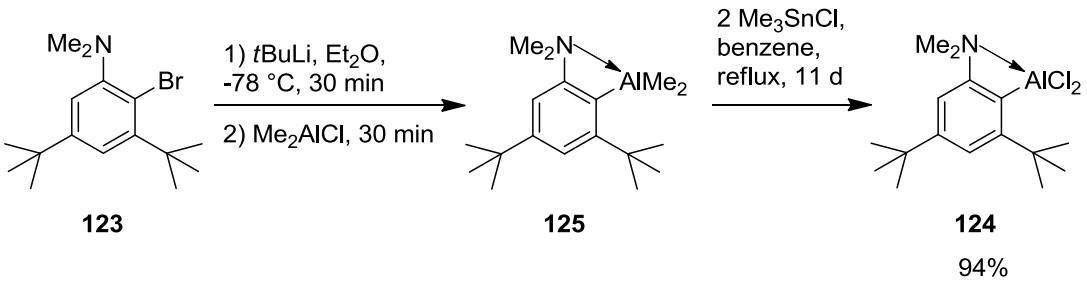


**123** **125** **124**

94%

Using the same lithiation procedure as before, LiMx was reacted with a solution of gallium trichloride at low temperatures to give a mixture of species from which (Mx)$GaBr_xCl_{2-x}$ (**126**) was isolated in a moderate yield of 43% (Scheme 2-17).

**Scheme 2-17.** Synthesis of (Mx)$GaBr_xCl_{2-x}$ (**126**).

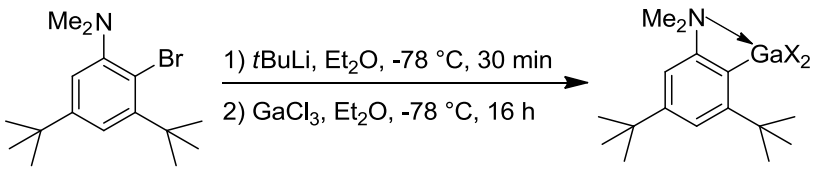


**126**

X = Br/Cl

43%

The $^{1}$H NMR spectrum of species **126** exhibited the same pattern as the aluminum species and no indication for any abnormality was observed. However, mass spectrometry and single-crystal X-ray analysis of this species clearly showed that the expected (Mx)$GaCl_2$ was only one of the obtained species, but also (Mx)GaBrCl and (Mx)$GaBr_2$ were present. Clearly, a chlorine-bromine exchange occurred.

It is difficult to give a value of x in (Mx)$GaBr_xCl_{2-x}$ (**126**) with absolute certainty. The values for x derived from mass spectrometry, single-crystal analysis and elemental analysis and their limitations will be discussed below. Mass spectrometry showed the peaks for (Mx)$GaCl_2^+$ : (Mx)$GaBrCl^+$ : (Mx)$GaBr_2^+$ in a 57 : 37 : 6 ratio. This results in a chlorine : bromine ratio of 3 : 1 with x = 0.5. However, the three species might have different volatilities, which would adulterate the values. Single-crystal X-ray analysis data gave a chlorine : bromine ratio of 2 : 1 which translates into an x-value of 0.66. This data is only valid for one crystal and it might not reflect the chlorine : bromine ratio of the whole product. Elemental analysis data gave a chlorine : bromine ratio of 3 : 1 and x = 0.5. This value for x was obtained, by calculating the amount of x for an analytically pure product. However, possibly minor impurities could have a significant influence on this result. In any case for two reactions different ratios are possible as slightly different conditions could influence the exchange and, therefore, the final chlorine to bromine ratio. However, based on the discussed data, it is fair to assume that overall more chlorine is present in (Mx)$GaBr_xCl_{2-x}$ than bromine.

Roesky *et al.* described a similar chlorine-bromine exchange in the course of the preparation of compound **127** starting from the brominated ligand **128** (Scheme 2-18).[42] The authors did not mention how much chlorine was exchanged by bromine, however, it

was suggested that the brominated ligand (**128**) had reacted with the gallium dichloride to exchange halides (Scheme 2-18).

**Scheme 2-18**. Literature precedence for a chlorine-bromine exchange on gallium in compound **127**.

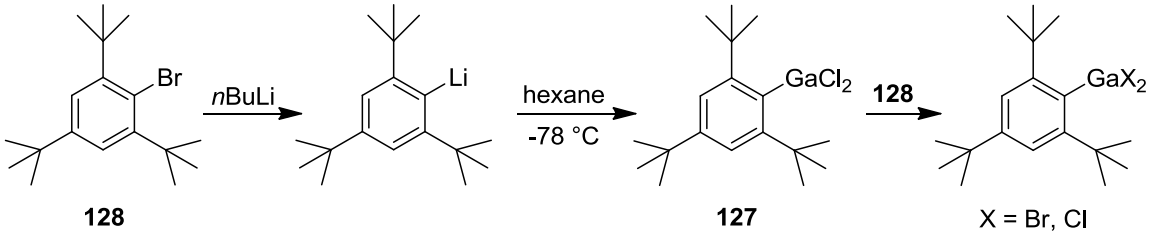


In the case of the Mx ligand, it is improbable that MxBr (**123**) reacted with (Mx)$GaCl_2$, because a complete lithiation was shown by the quantitative formation of (Mx)$AlMe_2$ (**125**). The only bromine containing species that is expected to be present in the reaction miture is *tert*-butylbromide, which formed during the lithiation of MxBr (**123**). However, it would be surprising, if *tert*-butylbromide would be able to react with (Mx)$GaCl_2$ in a chlorine-bromine exchange. A different solubility of two species, for example salts, in the solvent diethyl ether depending on the halide being bromide or chloride, was envisioned to be able to trigger a chlorine-bromine exchange. Lithium bromide is the only salt that could be present.

We wanted to study which of these three compounds, MxBr, *t*BuBr, and LiBr is able to exchange the chlorine atoms in (Mx)$GaBr_xCl_{2-x}$ (**126**) for bromine atoms. Therefore, (Mx)$GaBr_xCl_{2-x}$ (**126**) was separately stirred with five equivalents of MxBr, *t*BuBr and LiBr in diethyl ether for 16 hours. Mass spectrometry measurements were used to evaluate the exchange. In the case of MxBr and *t*BuBr as reagents, no significant change (> 5%) of the ratios between the different dihalides was observed. However, in the case of added lithium bromide, a significant change was identified: The most

prominent molecular mass of the gallium species with two halides belonged to (Mx)$GaBr_2$. (Mx)GaBrCl was still present as a minor compound, whereas no peaks were observed for (Mx)$GaCl_2$ by mass spectrometry.

Based on these results, it is likely that lithium bromide formed during the synthesis of (Mx)$GaCl_2$. It is probable that *tert*-butylbromide has reacted with Li(Mx) to give lithium bromide, MxH, and *iso*-butene. Similar reactions for *tert*-butylbromine and *tert*-butyllithium are well known in literature (Scheme 2-19).[43] A significant amount of MxH was found in the $^1$H NMR spectra of the reaction mixtures of the direct reaction with group-13-element trichlorides, which supports this rationale.

**Scheme 2-19.** Reaction of *t*BuLi with *t*BuBr to give LiBr, *iso*-butene and *iso*-butane.

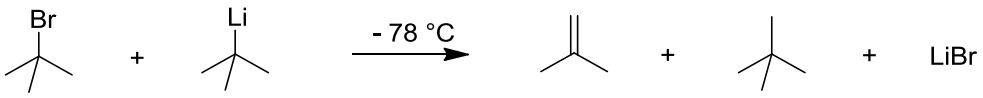


Under this premise, the slightly impure (Mx)$AlCl_2$ obtained from the direct reaction with aluminum trichloride was investigated by mass spectrometry and the presence of bromine containing aluminum species was found. This demonstrates that the chlorine-bromine exchange also occurred with aluminum.

The scope of the chlorine-bromine exchange was investigated by submitting the 4 different gallium dichlorides (Mamx)$GaCl_2$, (*p*-*t*BuAr′)$GaCl_2$, (Ar′)$GaCl_2$, and (Pytsi$^{-2SiMe_3}$)$GaCl_2$ to the same conditions, namely, stirring with 5 equivalents of lithium bromide in diethyl ether for 16 h (Figure 2-9). In all cases, mass spectrometry clearly showed that a complete conversion to the dibromides had occurred. It is unknown why the gallium dichlorides shown in Figure 2-9 showed an even higher reactivity with lithium bromide than (Mx)$GaBr_xCl_{2-x}$.

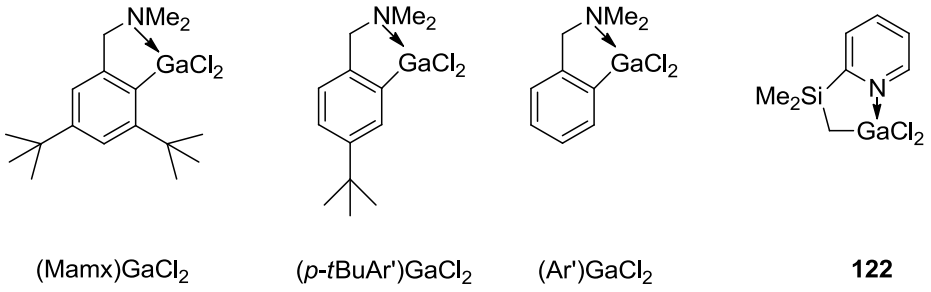


(Mamx)$GaCl_2$ (*p*-*t*BuAr')$GaCl_2$ (Ar')$GaCl_2$ **122**

**Figure 2-9.** Different gallium dichlorides that were tested for chlorine-bromine exchange with lithium bromide.

Some authors suggest to use two equivalents of *tert*-butyllithium so that *tert*-butyl bromide can react with the remaining *tert*-butylithium.[44] The synthesis of (Mx)$GaBr_xCl_{2-x}$ (**126**) could potentially be improved by using two equivalents of *tert*-butyllithium, because the formation of MxH from Li(Mx) could be inhibited. However, when reactions were carried out with two equivalents of *tert*-butyllithium, there was no formation of (Mx)$GaBr_xCl_{2-x}$, but instead another unknown product was observed by $^1$H NMR spectroscopy. Moreover, a higher amount of lithium bromide is expected to be present in these reactions that should lead to a stronger chlorine-bromine exchange. Attempts were made to isolate Li(Mx) by precipitation at -78 °C and thus eliminate the *tert*-butylbromide from the reaction mixture. However, the formed precipitate was so fine that it did not settle over a time frame of many hours. Therefore, it was not possible to isolate pure (Mx)$GaCl_2$. For all subsequent reactions with 1,1'-dilithiometallocenes described in Chapter 3.2, (Mx)$GaBr_xCl_{2-x}$ (**126**) was used.

Crystals of **126** that were suitable for single-crystal X-ray analysis were obtained from acetonitrile and the molecular structure was determined by Dr. Klaus Harms (University of Marburg) (Figure 2-10). The gallium compound **126** is a monomeric species in the solid state with a distorted tetrahedrally surrounded gallium center.

Initially, the presence of only (Mx)$GaCl_2$ was expected, but the molecular structure in the solid state displayed bromine atoms close to the chlorine atoms. The chlorine : bromine ratio was found to be 67:33. The molecular structure does not exhibit, which of the three species (Mx)$GaCl_2$, (Mx)GaBrCl, and (Mx)$GaBr_2$ are present. Based on the chlorine to bromine ratio, it would be possible that only (Mx)$GaCl_2$ and (Mx)GaBrCl or (Mx)$GaCl_2$ and (Mx)$GaBr_2$ are present. However, based on the presence of all three species revealed by mass spectrometry in the powdered samples, is most likely that (Mx)$GaCl_2$, (Mx)GaBrCl, and (Mx)$GaBr_2$ were all present in the crystal. The bite angle of the Mx ligand is 70.93(9)°, which is very similar to the other ligands Pytsi$^{-SiMe_2}$ [70.66(8), 70.62(8), and 73.38(18)°] and Pytsi$^{-2SiMe_2}$ [67.70(7)°] that form four-membered rings with rigid aromatic bonds. Similarly a distortion by 9.3° from the 120° angle of the aromatic C2 atom was exhibited. The parent (Mamx)$GaCl_2$, that forms a five-membered ring with the gallium, showed a bite angle of 89.26(9)° as well as a minor distortion from the 120° angle of the C2 atom by 2.1°. The gallium-carbon and gallium-nitrogen bond lengths of **126** and (Mamx)$GaCl_2$ are in a similar range (Ga–C = 1.935(3) Å for **126**, Ga–C = 1.956(2) Å for (Mamx)$GaCl_2$; Ga–N = 2.126(2) Å for **126**, Ga–C = 2.066(2) Å for (Mamx)$GaCl_2$). The slightly longer gallium-nitrogen bond in **126** might be due to the higher strain of the four-membered ring forcing a larger distance. An increase of the distance between the *tert*-butyl group in the *ortho* position and the gallium atom by going from the Mamx ligand to the Mx ligand can be deduced from their molecular structures (C7-Ga1 = 3.641(3) Å for (Mamx)$GaCl_2$ and C7-Ga1 = 3.852 Å for (Mx)$GaBr_xCl_{2-x}$).

Single-crystal X-ray analysis data showed the presence of a disordered gallium chloride species in the crystal. The ratio of the disordered gallium chloride species to

(Mx)$GaBr_xCl_{2-x}$ is 3:97. It is likely that the disordered species contains $GaCl_3$ or $GaBrCl_2$ or $GaBr_2Cl$. An additional coordination of a species to the gallium trihalide is assumed. The distances of Ga1A to C2 and N1 are significantly longer than those for Ga1 [Ga1A–N1 = 2.975 Å and Ga1–N1 2.126(2) Å; Ga1A–C2 = 2.172(11) Å and Ga1A–C2 = 1.935(3) Å], therefore, a coordination of Mx in this position is unlikely.

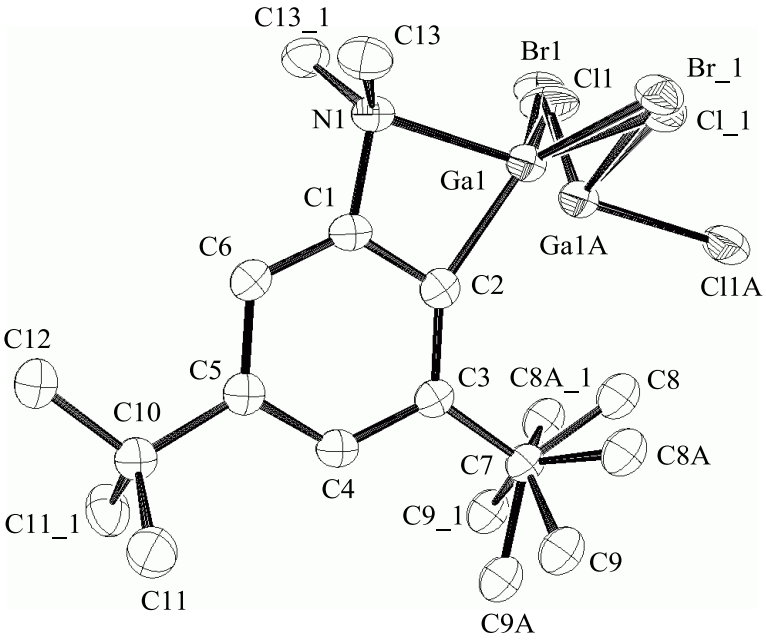


**Figure 2-10.** Molecular structure of (Mx)$GaBr_xCl_{2-x}$ with thermal ellipsoids at the 50% probability level. There is a disorder of gallium trichloride in a 97:3 ratio in the crystal lattice. Moreover, the ratio of Br1 to Cl1 is 30:67. Hydrogen atoms are omitted for clarity. Selected atom-atom distances (Å) and bond angles (°): C2—Ga1 = 1.935(3), C2—Ga1A = 2.172(11), N1—Ga1 = 2.126(2), N1—Ga1A = , Cl1—Ga1 = 2.157(8), Cl1—Ga1A = 2.127(9), Cl1A—Ga1A = 2.20(3), Ga1—Br1 = 2.271(7), Ga1A—Br1 = 2.317(9), C2-Ga1-N1 = 70.93(9), C2-C1-N1 = 110.7(2), Cl1_1-Ga1-Cl1 = 108.6(4), Br1-Ga1-Br1_1 = 110.0(3), N1-Ga1-Cl1 = 111.7(2), N1-Ga1-Br1 = 106.36(19), C2-Ga1-Cl1 = 123.18(18), C2-Ga1-Br1 = 124.33(14).

## 2.3 Summary and Conclusion

Different aluminum and gallium dichlorides that are expected to give interesting results in salt metathesis reactions with dilithiometallocenes were synthesized. The outcome of reactions of LiR with $ECl_3$ (E = Al, Ga) was highly depending on the ligand R. The ligands equipped with a pyridine donor that form four-membered rings with the group-13 element, Pytsi$^{-SiMe_2}$ and Pytsi$^{-2SiMe_2}$, show a tendency to form bisligand compounds (**109**, **115**, and **117**). Species (Pytsi$^{-2SiMe_2}$)$AlMe_2$ (**116**) is in a remarkable donor depending equilibrium with (Pytsi$^{-2SiMe_2}$)$_2$AlMe (**117**). It might be interesting to further study this equilibrium with different donors and also the time dependence in order to gain a better understanding of this process. In reactions of MxBr (**123**) with *tert*-butyllithium and the group-13-element trichlorides a chlorine-bromine exchange was observed. Preliminary studies revealed that lithium bromide could be the source of bromine and that other gallium dichlorides also underwent reactions with lithium bromide. However, this exchange reaction could be investigated in more detail including the actual amount of lithium bromide that would be required for a complete conversion, the time dependence of this reaction, if there is a difference for different ligands considering the required amounts of LiBr or the time dependence of the exchange. Moreover, this reaction could be tested on a preparative scale.

For the Pytsi$^{-SiMe_2}$ and the Mx ligand, a clean aluminum dichloride could be obtained in a good to very good yield by following the indirect route via a dimethyl aluminum species. Therefore, it is worth to investigate this reaction, whenever the direct synthesis yields problems.

## 2.4 Experimental

**General information.** Manipulations were done using standard Schlenk and glovebox techniques ($N_2$ as inert gas), unless noted differently. Solvents were dried using a MBraun solvent purification system ($Et_2O$, thf, toluene, hexanes) or distilled from sodium and benzophenone ($C_6H_6$) and stored under nitrogen over 3 or 4 Å molecular sieves. Solvents for NMR measurements were prepared through freeze-pump-thaw procedures and stored under nitrogen over 3 and 4 Å molecular sieves. Mass spectra were measured on a VG 70SE and are reported in the form m/z (rel intens) [$M^+$] where 'm/z' is the mass observed, 'rel intens' is the intensity of the peak relative to the most intense peak and '$M^+$' is the molecular ion or fragment; only characteristic mass peaks are reported. For isotopic patterns, only the mass peak of the isotope with the highest natural abundance is listed. Mass spectra with electron spray ionization were recorded using a QSTAR XL system (Applied Biosystem). Elemental analyses were carried out at the SSSC at the University of Saskatchewan using a Perkin-Elmer 2400 CHN elemental analyzer; $V_2O_5$ was added to the samples to promote combustion. $^1H$ and $^{13}C$ NMR spectra were recorded at 25 °C on a 500 MHz Bruker Avance spectrometer ($^1H$: 500.2 MHz; $^{13}C$: 125.8 MHz). $^1H$ NMR chemical shifts were referenced to the residual protons of the deuterated solvent ($C_6D_6$: δ 7.15; $CDCl_3$: δ 7.26); $^{13}C$ chemical shifts were referenced to δ 128.00 ($C_6D_6$) and 77.00 ($CDCl_3$), respectively. C atoms directly bound to Al or Ga were not detected by $^{13}C$ NMR spectroscopy. The absence of signals is presumably due to the effect of the electric quadrupole moment of Al or Ga on the relaxation times of directly bound carbon atoms. The IR spectrum was recorded on a Bruker Tensor 27 FTIR spectrometer.

**Chemicals.** The following reagents were used without further purification: 2-picoline (98%, Alfa Aesar), *n*BuLi (2.5 M in hexanes, Acros Organics or Aldrich), *t*BuLi (1.7 M in pentane, Aldrich), $Me_3SiCl$ (98%, Alfa Aesar), $GaCl_3$ (99.999%, Alfa Aesar), $Br_2$ (99.8%, Alfa Aesar), $Me_3SnCl$ (97%, Aldrich), $Me_2AlCl$ (1 M in hexanes, Aldrich), 2-bromopyridine (99%, Alfa Aesar), 3,5-di*tert*-butyltoluene (98%, Alfa Aesar), $KMnO_4$ (99%, EMD), sodium azide (99.5%, Aldrich), $(Ac)_2O$ (99.5%, Fluka), NaOMe (97%, Fluka), $NaBH_4$ (98%, Aldrich), $H_2CO$ (37% in MeOH, Aldrich), and 2-ethylpyridine (97%, Alfa Aesar).

Aluminum trichloride (99.985%, Alfa Aesar) was sublimed prior to use; tmeda (99%, Alfa Aesar) was distilled from sodium and stored over 4 Å molecular sieves. MxBr and Pytsi$^{-SiMe_2}$H were synthesized according to literature procedures.[3,37] Pytsi$^{-2SiMe_2}$H and Pytsi$^{-2SiMe_3}$H were synthesized with some variations from literature procedures;[32,34] therefore their syntheses are reported here.

**Synthesis of (Pytsi$^{-SiMe_2}$)AlMe$_2$ (110).** *n*BuLi in hexanes (13.0 mL, 20.8 mmol) was added dropwise to a solution of (Pytsi$^{-SiMe_2}$)H (4.68 g, 19.7 mmol) in diethylether (20 mL) at 0 °C. After stirring for 1 h at r.t., $Me_2AlCl$ in hexanes (21 mL, 21 mmol) was added at 0 °C. After the reaction mixture was stirred for 16 h at room temperature, diethyl ether was removed in vacuum. The product was dissolved in hexanes (40 mL) and the solid residue was filtered off. Volatiles were removed in vacuum and (Pytsi$^{-SiMe_2}$)$AlMe_2$ was obtained as an orange oil with minor impurities (6.03 g, ~100%). Single crystals suitable for single-crystal X-ray analysis were obtained from a toluene solution at -15 °C. $^1$H NMR ($C_6D_6$): δ -0.16 (s, 6H, $AlMe_2$), 0.16 (s, 18H, $SiMe_3$), 6.13 (pst, 1H, 5-H), 6.69 (d, 1H, 3-H), 6.81 (pst, 1H, 4-H), 7.12 (d, 1H, 6H). $^{13}$C NMR ($C_6D_6$): δ -5.9 ($AlMe_2$), 2.4

($SiMe_3$), 118.5 (5-C), 125.7 (3-C), 139.7 (4-C), 144.0 (6-C), 173.8 (*ipso*-C). MS (70 eV, $EI^+$): *m/z* (%) 278 (9) [$M^+$ – Me], 190 (21) [$C_9H_{13}AlNSi^+$], 73 (100) [$SiMe_3^+$], 57 (15) [$AlMe_2^+$]. HRMS ($EI^+$; *m/z*): [M – Me]$^+$ calcd for $C_{13}H_{25}AlNSi_2$, 278.1341; found 278.1340 (Δppm = 0.3). Anal calcd for $C_{14}H_{28}AlNSi_2$ (293.531): C, 57.29; H, 9.61; N, 4.77. Found: C, 54.45; H, 9.05; N, 4.44.

**Synthesis of (Pytsi$^{-SiMe_2}$)AlBr$_2$ (111).** A solution of $Br_2$ (0.69 g, 4.3 mmol) in benzene (7 mL) was added dropwise to a solution of (Pytsi$^{-SiMe_2}$)$AlMe_2$ (0.63 g, 2.1 mmol) in benzene (7 mL) at 0 °C. After 20 min of stirring, the volatiles were removed in vacuum. The resulting oil was washed with hexanes (15 mL) to yield a Btsmp$AlBr_2$ with minor impurities (0.69 g, 76%). Single crystals suitable for single-crystal X-ray analysis were obtained from a diethyl ether solution at -15 °C. $^1$H NMR ($C_6D_6$): δ 0.21 (s, 18H, $SiMe_3$), 6.00 (pst, 1H, 5-H), 6.57 (d, 1H, 3-H), 6.71 (pst, 1H, 4-H), 6.98 (d, 1H, 6-H). $^{13}$C NMR ($C_6D_6$): δ 2.2 ($SiMe_3$), 120.1 (5-C), 124.8 (3-C), 142.0 (4-C), 143.7 (6-C), 171.8 (2-C). MS (70 eV, $EI^+$): *m/z* (%) 408 (33) [$M^+$ – Me], 206.12 (24) [$C_{10}H_{17}AlNSi^+$], 206.08 (100) [$C_{10}H_{16}NSi_2^+$], 132 (23) [$C_6H_5AlSi^+$], 73 (42) [$SiMe_3^+$]. HRMS ($EI^+$; *m/z*): calcd for $C_{12}H_{22}AlBr_2NSi_2$, 422.9452; found 422.9451 (Δppm = 0.4). Anal. Calcd for $C_{12}H_{22}AlBr_2NSi_2$ (423.270): C, 34.05; H, 5.24; N, 3.31. Found: C, 33.02; H, 5.22; N, 3.01.

**Synthesis of (Pytsi$^{-SiMe_2}$)AlCl$_2$ (112).** A solution of $Me_3SnCl$ (3.9 g, 20 mmol) in benzene (10 mL) was added to a solution of crude (Pytsi$^{-SiMe_2}$)$AlMe_2$ (3.84 mmol) in benzene (20 mL) at room temperature. The reaction mixture was stirred for 16 h, before the volatiles were removed in vacuum. The obtained solid was washed with hexanes (2 x 10 mL) and dried in vacuum to yield product (0.96 g, 75%). $^1$H NMR ($C_6D_6$): δ 0.18 (s,

18H, $SiMe_3$), 5.99 (pst, 1H, 5-H), 6.61 (d, 1H, 3-H), 6.71 (pst, 1H, 4-H), 6.91 (d, 1H, 6-H). $^{13}C$ NMR ($C_6D_6$): δ 2.0 ($SiMe_3$), 120.0 (C-5), 124.6 (C-3), 142.0 (C-4), 143.7 (C-6), 172.1 (C-2). MS (70 eV, $EI^+$): *m/z* (%) 333 (1) [$M^+$], 318 (43) [$M^+$ – Me], 237 (30) [Pytsi$^{-SiMe_2}H^+$], 236 (18) [Pytsi$^{-SiMe_2^+}$], 222 (99) [Pytsi$^{-SiMe_2}H^+$ – Me], 206 (100) [$C_{10}H_{16}NSi_2^+$], 150 (11) [$C_8H_{12}NSi^+$], 149 (14) [$C_8H_{11}NSi^+$], 132 (13) [$C_6H_5AlSi^+$], 73 (38) [$SiMe_3^+$]. HRMS (EI; *m/z*): calcd for $C_{12}H_{22}AlCl_2NSi_2$, 333.0483; found 333.0477 (Δppm = 2.0). Anal. Calcd for $C_{12}H_{22}AlCl_2NSi_2$ (334.368): C, 43.10; H, 6.63; N, 4.19. Found: C, 43.54; H, 6.62; N, 3.99.

**Synthesis of (Pytsi$^{-SiMe_2}$)$GaCl_2$ (113).** (Pytsi$^{-SiMe_2}$)H (6.36 g, 26.8 mmol) was added to a solution of *n*BuLi in hexanes (9.5 mL, 27 mmol) and diethyl ether (10 mL) at 0 °C. After 2.5 h of stirring at room temperature, the reaction mixture was cooled down to -78 °C and a -78 °C cold solution of $GaCl_3$ (4.72 g, 26.8 mmol) in diethyl ether (20 mL) was added. The cold bath was removed and the reaction mixture was stirred for 16 h at room temperature. After the precipitate was filtered off, the amount of solvent was reduced in vacuum, and compound (Pytsi$^{-SiMe_2}$)$GaCl_2$ crystallized at -25 °C (2.08 g, 21%). $^1H$ NMR ($C_6D_6$): δ 0.16 (s, 18H, $SiMe_3$), 6.08 (pst, 1H, 5-H), 6.55 (d, 1H, 3-H), 6.74 (pst, 1H, 4-H), 7.02 (br, 1H, 6-H). $^{13}C$ NMR ($C_6D_6$): δ 1.4 ($SiMe_3$), 120.6 (C-5), 122.6 (C-3), 141.2 (C-4), 144.7 (C-6), 170.1 (*ipso*-C). MS (70 eV, $EI^+$): *m/z* (%) 362 (18) [$M^+$ – Me], 237 (31) [Pytsi$^{-SiMe_2}H^+$], 236 (18) [Pytsi$^{-SiMe_2^+}$], 222 (100) [Pytsi$^{-SiMe_2}H^+$ – Me], 206 (86) [$C_{10}H_{16}NSi_2^+$], 150 (21) [$C_8H_{12}NSi^+$], 149 (14) [$C_8H_{11}NSi^+$], 73 (45) [$SiMe_3^+$]. HRMS ($EI^+$; *m/z*): calcd for $C_{12}H_{22}Cl_2GaNSi_2$, 376.9894; found 376.9914 (Δppm = 5.2). Anal. Calcd for $C_{12}H_{22}Cl_2GaNSi_2$ (377.110): C, 38.22; H, 5.88; N, 3.71. Found: C, 38.79; H, 6.23; N, 3.62.

Identification of the byproduct [(Pytsi$^{-SiMe_2}$)$_2$Ga][GaCl$_4$]: IR (KBr) $\upsilon_{GaCl}$: 380 cm$^{-1}$ (literature value: 375 cm$^{-1}$). MS (ESI): *m/z* (%) 541 (52) [R′$_2$Ga]$^+$, 238 (100) [R′HH]$^+$.

**Synthesis of Pytsi$^{-2SiMe_2}$H (114).** *n*BuLi in hexanes (20.5 mL, 51.3 mmol) was diluted with hexanes (45 mL) and cooled to 0 °C, followed by addition of tmeda (7.0 mL, 47 mmol) and 2-ethylpyridine (5.00 g, 46.4 mmol). After stirring at room temperature for 30 min, the reaction mixture was cooled down to 0 °C, before $Me_3SiCl$ (5.40 g, 49.7 mmol) was slowly added, followed by stirring at room temperature for 16 h. Hexanes (60 mL) and deionized water (80 mL) were added and the phases were separated. The aqueous phase was washed with hexanes (3 x 50 mL) and the united organic phases were washed with deionized water (3 x 60 mL). Volatiles were removed in vacuum and distillation in vacuum at an oil bath temperature of 70 °C gave a colorless oil (6.73 g, 76%). $^1$H NMR ($CDCl_3$): δ -0.04 (s, 9H, $SiMe_3$), 1.41 (d, J = 7.5 Hz, 3H, $CH_3$), 2.44 (q, J = 7.4 Hz, 1H, CH), 6.98 (m, 2H, 3-H, 5-H), 7.52 (pst, 1H, 4-H), 8.47 (d, 1H, 6-H). $^{13}$C NMR ($CDCl_3$): δ -3.2 ($SiMe_3$), 13.7 ($CH_3$), 32.7 ($CHMeSiMe_3$), 119.3, 121.1 (5-C and 3-C), 135.5 (4-C), 148.7 (6-C), 165.7 (2-C).

**Synthesis of (Pytsi$^{-2SiMe_2}$)$_2$AlMe (117).** For the attempted synthesis of (Pytsi$^{-2SiMe_2}$)$AlMe_2$, a solution of *n*BuLi in hexanes (1.8 mL, 5.1 mmol) was diluted with hexanes (5 mL) and tmeda (0.55 g, 4.7 mmol) was added, followed by the addition of Pytsi$^{-2SiMe_2}$H (0.92 g, 4.7 mmol) at 0 °C. After stirring at room temperature for 4 h, the reaction mixture was cooled down to 0 °C, and a solution of $Me_2AlCl$ in hexanes (5.2 mL, 5.2 mmol) was added. After removal of the ice bath, the reaction mixture was stirred for 16 h at room temperature. The precipitate was filtered off and crystallization from hexanes at -25 °C yielded the product (Pytsi$^{-2SiMe_2}$)$_2$AlMe (0.35 g, 37%). $^1$H NMR ($C_6D_6$):

δ 0.13 (s, 18H, $SiMe_3$), 0.19 (s, 3H, AlMe), 0.84 (s, 6H, Me), 6.38 (pst, 1H, 5-H), 6.76 (d, 1H, 3-H), 6.94 (m, 1H, 4-H), 7.77 (d, 1H, 6-H). $^{13}$C NMR ($C_6D_6$): δ -1.8 ($SiMe_3$), 14.9 (Me), 118.0 (5-C), 120.7 (3-C), 137.3 (4-C), 144.5 (6-C), 176.5 (*ipso*-C) ($C_5H_4$). MS (70 eV, $EI^+$): *m/z* (%) 398 (14) [$M^+$], 383 (9) [$M^+$ – Me], 220 (74) [$M^+$ – $Pytsi^{-2SiMe_2}$], 219 [$M^+$ – $Pytsi^{-2SiMe_2}H$], 162 (39) [$C_9H_{13}AlN^+$], 146 (53) [$C_6H_{18}Si_2^+$], 132 (16) [$MeCAl(C_5H_4N)^+$], 73 (100) [$SiMe_3^+$]. HRMS ($EI^+$; *m/z*): calcd for $C_{21}H_{35}AlN_2Si_2$, 398.2154; found 398.2152 (Δppm = 0.5). Anal. Calcd for $C_{21}H_{35}AlN_2Si_2$ (398.669): C, 63.27; H, 8.85; N, 7.03. Found: C, 64.71; H, 9.63; N, 7.17.

**Synthesis of a mixture of ($Pytsi^{-2SiMe_2}$)$_2$AlMe (117), and ($Pytsi^{-2SiMe_2}$)AlMe$_2$ (116).** *n*BuLi in hexanes (3.45 mL, 9.76 mmol) was added to diethyl ether (4 mL). Then $Pytsi^{-2SiMe_2}H$ (1.74 g, 9.71 mmol) was added dropwise at 0 °C. The reaction mixture was stirred for 30 min at room temperature before it was cooled to -78 °C and $Me_2AlCl$ (10.0 mL, 10.0 mmol) in hexanes was added. The dry ice bath was removed and the reaction mixture was stirred for 40 min at room temperature. Part of the solvent (5 mL) was removed under vacuum. The precipitate was filtered off and washed with hexanes (3 x 10 mL). The volatiles were removed in vacuum and a $^1$H NMR spectrum of the product mixture was measured. $^1$H NMR ($C_6D_6$): δ -0.5 – 0.0 (br, 6H, $AlMe_2$), 0.01 (s, 9H, $SiMe_3$), 1.57 (s, 3H, Me), 6.19 (pst, 1H, 5-H), 6.73 (psd, 1H, 3-H), 6.88 (pst, 1H, 4-H), 7.21 (psd, 1H, 6-H).

**Synthesis of ($Pytsi^{-2SiMe_2}$)$_2$AlCl (115).** In an attempt to synthesize ($Pytsi^{-2SiMe_2}$)$AlCl_2$, *t*BuLi in pentane (2.8 mL, 4.8 mmol) was added to a solution of $Pytsi^{-2SiMe_2}H$ (0.89 g, 4.7 mmol) in a mixture of hexanes (5 mL) and diethyl ether (10 mL) at -78 °C. After 45 min of stirring at -78 °C the reaction mixture was added to a -78 °C cold

solution of $AlCl_3$ (0.62 g, 4.7 mmol) in diethyl ether (15 mL). The dry ice bath was removed and the reaction mixture stirred for 16 h at room temperature. The precipitate was filtered off and crystalline $(Pytsi^{-2SiMe_2})_2AlCl$ (0.41 g, 42% yield) was obtained from this solvent mixture at -25 °C. $^1H$ NMR ($C_6D_6$): δ 0.22 (s, 18H, $SiMe_3$), 0.85 (s, 6H, Me), 6.36 (pst, 2H, 5-H), 6.73 (d, 2H, 3-H), 6.93 (pst, 2H, 4-H), 7.84 (d, 2H, 6-H). $^{13}C$ NMR ($C_6D_6$): δ -1.8 ($SiMe_3$), 14.7 (Me), 118.8 (5-C), 120.9 (3-C), 138.3 (4-C), 144.1 (6-C), 174.7 (2-C). EIMS (70 eV): m/z (rel intens) 418 (48) [$M^+$], 240 (41) [$M^+ - Pytsi^{-2SiMe_2}$], 239 (26) [$M^+ - Pytsi^{-2SiMe_2}H$], 162 (100) [$(Pytsi^{-2SiMe_2})AlCl^+ - C_5H_3N$], 146 (28) [$C_6H_{18}Si_2^+$], 132 (16) [$(Pytsi^{-2SiMe_2})Al^+ - SiMe_3$], 73.0 (18) [$SiMe_3^+$]. HRMS ($EI^+$; *m/z*): calcd for $C_{20}H_{32}AlClN_2Si_2$, 418.1608; found 418.1615 (Δppm = 1.6). Anal. Calcd for $C_{20}H_{32}AlClN_2Si_2$ (419.087): C, 57.32; H, 7.70; N, 6.68. Found: C, 55.35; H, 8.32; N, 6.24.

**Synthesis of $(Pytsi^{-2SiMe_2})_xGaCl_y$ mixture.** *t*BuLi in pentane (1.6 mL, 2.7 mmol) was added to a solution of $Pytsi^{-2SiMe_2}H$ (0.49 g, 2.7 mmol) in diethyl ether (6 mL) at -78 °C. The reaction mixture was stirred for 20 min at -78 °C, then a solution of $GaCl_3$ (0.47 g, 2.7 mmol) in diethyl ether (6 mL) at -78 °C was added. The mixture was allowed to warm up to room temperature and was stirred for 16 h. The solvent was removed in vacuum and the product was dissolved in toluene (8 mL). Solid LiCl was filtered off and washed with toluene (2 x 3 mL). The solvent was removed and the resulting product mixture was dried in vacuum (0.84 g). $^1H$ NMR ($C_6D_6$): -0.16 (s, 9H, $SiMe_3$-B), 0.30 (s, 9H, $SiMe_3$-A), 1.10 (s, 3H, Me-A), 1.21 (s, 3H, Me-B), 6.08 (m, 1H, Ar-H-B), 6.43 (m, 1H, Ar-H-A), 6.53 (m, 1H, Ar-H-B), 6.71 (m, 1H, Ar-H-A), 6.75 (m, 1H, Ar-H-B), 6.96 (m, 1H, Ar-H-A), 7.89 (m, 1H, Ar-H-A), 8.61 (m, 1H, Ar-H-B).

**Synthesis of (Pytsi$^{-2SiMe_3}$)H (120).** *n*BuLi in hexanes (75 mL, 80.5 mmol) was added to a solution of 2-bromopyridine (12.1 g, 76.6 mmol) in diethyl ether (50 mL) at -78 °C. The reaction mixture was stirred for 30 min at -78 °C, before $Me_3SiCl$ (8.7 g, 80.1 mmol) was added at -78 °C. The reaction mixture was warmed to room temperature and stirred for 16 h. $H_2O$ (100 mL) was added and the phases were separated. The aqueous phase was washed with diethyl ether (3 x 100 mL) and the united organic phases were washed with water (3 x 100 mL) and dried over $MgSO_4$. The organic solvents were removed by vacuum distillation (26 mbar) at 95 °C. The product was isolated by condensation into a flask at -196 °C in high vacuum (9.03 g, 78%). $^1$H NMR ($CDCl_3$): δ 0.28 (s, 9H, $SiMe_3$), 7.16 (m, 1 H, Ar-H), 7.48 (m, 1H, Ar-H), 7.55 (m, 1H, Ar-H), 8.76 (m, 1H, Ar-H).

**Synthesis of (Pytsi$^{-2SiMe_3}$)$AlCl_2$ (121).** *t*BuLi in pentane (11.8 mL, 20.1 mmol) was added dropwise to a solution of (Pytsi$^{-2SiMe_3}$)H (2.89 g, 19.1 mmol) in diethyl ether (30 mL) at -78 °C. After 40 min of stirring at -78 °C, a suspension of $AlCl_3$ (2.44 g, 18.3 mmol) in diethylether (30 mL) was slowly added at -78 °C. It was stirred for 16 h at r.t., and then the solvent was removed of in vacuum. The product was dissolved in toluene (35 mL) and the precipitate was filtered off and washed with toluene (10 x 5 mL). The volatiles were removed at high vacuum at 90 °C and crystallization from toluene (5 mL) yielded colorless crystals (2.60 g, 47%). $^1$H NMR ($C_6D_6$): δ -0.32 (s, 2H, $CH_2$), 0.02 (s, 6H, $SiMe_2$), 6.27 (m, 1H, Ar-H), 6.70 (m, 2H, Ar-H), 8.28 (m, 1H, Ar-H). $^{13}$C NMR ($C_6D_6$): δ -0.6 ($CH_2$), 1.4 ($SiMe_2$), 124.9, 130.3, 139.4, 146.9, 171.0 ($C_5H_4N$). EIMS (70 eV): *m/z* (rel intens) 247 (7) [$M^+$], 232 (100) [$M^+$ – Me], 212 (11) [$M^+$ – Cl], 151 (11)

[$MH^+$ – $AlCl_2$], 150 (15) [$M^+$ – $AlCl_2$], 106 (14) [$C_5H_4NSi^+$]. Anal. Calcd for $C_8H_{12}AlCl_2NSi$ (248.16): C, 38.72; H, 4.87; N, 5.64. Found: C, 39.66; H, 5.32, N, 5.51.

**Synthesis of (Pytsi$^{-2SiMe_3}$)$GaCl_2$ (122).** *t*BuLi in pentane (8.60 mL, 14.6 mmol) was added dropwise to a solution of 2-(trimethylsilyl)pyridine in $Et_2O$ (25 mL) at -78 °C. After 40 min at -78 °C the solution was slowly added to a solution of $GaCl_3$ (2.38 g, 13.5 mmol) in $Et_2O$ (35 mL) at -78 °C. After the reaction mixture was stirred for 16 h at r.t., all volatiles were removed under vacuum. The crude product was dissolved in toluene (40 mL) and the precipitate was filtered off and washed with toluene (4 x 10 mL). Sublimation (120 °C; high vacuum) gave the colorless crystalline product (2.00 g, 50%) that contained only very minor impurities. Analytically pure product (1.36 g, 35%) was obtained by crystallization from toluene (4 mL). Crystals suitable for single-crystal X-ray analysis were obtained from toluene solution at -25 °C. $^1$H NMR ($C_6D_6$): δ -0.07 (s, 2H, $CH_2$), -0.02 (s, 6H, $SiMe_2$), 6.42 (m, 1H, Ar-H), 6.77 (d, 1H, Ar-H), 6.82 (m, 1H, Ar-H), 8.41 (d, 1H, Ar-H) $^{13}$C NMR (125.8 MHz): δ -6.8 ($CH_2$), -1.1 ($SiMe_3$), 125.5, 130.3, 139.2, 146.8, 167.2 ($C_5H_4N$). EIMS (70 eV): *m/z* (rel intens) 291 (7) [$M^+$], 276 (100) [$M^+$ – Me], 256 (54) [$M^+$ – Cl], 170 (11) [$(NC_5H_4)SiMeCH_2Cl^+$], 149 (14) [$C_8H_7NSi^+$], 120 (16) [$C_6H_6NSi^+$], 106 (12) [$C_5H_4NSi^+$], 92 (11) [$C_5H_4Si^+$], 91 (15) [$C_5H_3Si^+$], 69 (14) [Ga]. Anal. Calcd for $C_8H_{12}Cl_2GaNSi$ (290.90): C, 33.03; H, 4.16; N, 4.81. Found: C, 33.82; H, 4.33; N, 4.61.

**Synthesis of (Mx)$AlMe_2$ (125).** *t*BuLi in pentane (2.65 mL, 4.51 mmol) was added dropwise to a solution of MxBr (1.27 g, 4.08 mmol) in diethyl ether (30 mL) at -78 °C. The reaction mixture was stirred for 30 min at -78 °C before $Me_2AlCl$ in hexanes (4.50 mL, 4.50 mmol) was added dropwise. The dry ice bath was removed and the

solution was stirred for 30 min was observed. The volatiles were removed in vacuum. The product was dissolved in toluene (15 mL) and the precipitate was filtered off and washed with toluene (3 mL). Removal of toluene led to a fairly pure product (1.17 g, 99%). $^{1}$H NMR ($C_6D_6$): δ -0.21 (s, 6 H, $AlMe_2$), 1.32 (s, 9 H, *t*Bu), 1.45 (s, 9 H, *t*Bu), 2.16 (s, 6 H, $NMe_2$), 6.78 (m, 1 H, Ar-H), 7.54 (m, 1 H, Ar-H). $^{13}$C NMR ($C_6D_6$): δ -9.2 ($Me_2Al$), 31.7 (*t*Bu), 32.1 (*t*Bu), 35.3 ($\underline{C}(CH_3)_3$), 36.6($\underline{C}(CH_3)_3$), 46.7 ($NMe_2$), 109.4, 121.6, 152.6, 158.5, 159.6 (Ar-H). EIMS (70 eV): *m/z* (rel intens) 274 (100) [$M^+$-Me]. HRMS (EI; *m/z*): [M – Me]$^+$ calcd for $C_{17}H_{29}AlN$, 274.2115; found 274.2115 (Δppm = 0.2). Anal. Calcd for $C_{18}H_{32}AlN$ (289.44): C, 74.69; H, 11.14; N, 4.84. Found: C, 72.89; H, 10.54; N, 4.77.

**Synthesis of (Mx)$AlCl_2$ (124).** A solution of $Me_3SnCl$ (3.58 g, 18.0 mmol) in benzene (15 mL) was added to a solution of (Mx)$AlMe_2$ (5.9 mmol) in benzene (30 mL) at 10 °C. After reflux for 11 days, the volatiles were removed under vacuum and the resulting solid was washed with hexanes (5 mL). The product was dissolved in warm toluene (11 mL) and crystallization at -25 °C gave the pure product (1.84 g, 94 %). $^{1}$H NMR ($C_6D_6$): δ 1.23 (s, 9H, *t*Bu-4), 1.38 (s, 9H, *t*Bu-6), 2.17 (s, 6H, $NMe_2$), 6.69 (m, 1H, Ar-H), 7.54 (m, 1H, Ar-H). $^{13}$C NMR ($C_6D_6$): δ 31.4 (*t*Bu), 31.8 (*t*Bu), 35.5 ($\underline{C}(CH_3)_3$), 36.1 ($\underline{C}(CH_3)_3$), ($Me_2N$), 109.4, 123.5, 128.7, 155.6, 156.9, 159.9 (Ar-H). EIMS (70 eV): *m/z* (%) 329 (59) [Mx$AlCl_2^+$], 314 (52) [Mx$AlCl_2^+$ – Me], 287 (100) [$C_{13}H_{20}AlCl_2N$], 232 (46) [$Mx^+$], 216 (46) [$Mx^+$ – $CH_4$], 57 (21) [*t*$Bu^+$]. HRMS ($EI^+$; *m/z*): calcd for $C_{16}H_{26}Cl_2AlN$, 329.1258; found 329.1255 (Δppm = 0.7). Anal. Calcd for $C_{16}H_{26}AlCl_2N$ (330.27): C, 58.19; H, 7.93; N, 4.24. Found: C, 57.68; H, 7.62; N, 4.16.

**Synthesis of (Mx)GaBr$_x$Cl$_{2-x}$ (126).** *t*BuLi in pentane (7.75 mL, 13.2 mmol) was added to a solution of MxBr (4.06 g, 13.0 mmol) in diethyl ether (25 mL) at -78 °C. After the reaction was stirred for 30 min at -78 °C, it was added to a solution of $GaCl_3$ (2.29 g, 13.0 mmol) in diethyl ether (20 mL) at -78 °C. The first flask was washed with diethyl ether (5 + 2 mL) to ensure a complete transfer. The dry ice bath was removed and the mixture was stirred at room temperature for 16 h. The solid was filtered off and washed with diethyl ether (8 + 5 mL). The volatiles were removed in vacuum. The product was dissolved in toluene (30 mL) and the precipitate was filtered off and was washed with toluene (3 x 5 mL). The volatiles were removed in vacuum. Sublimation at 105 °C under high vacuum yielded **126** (2.08 g, 43%). $^1$H NMR ($C_6D_6$): δ 1.21 (s, 9H, *t*Bu-4), 1.33 (s, 9H, *t*Bu-6), 2.23 (s, 6H, $Me_2N$), 6.67 (s, 1H, CH-3), 7.52 (s, 1H, CH-5). $^{13}$C NMR ($C_6D_6$): δ 31.5 (*t*Bu), 31.6 (*t*Bu), 35.5 ($\underline{C}(CH_3)_3$), 35.7 ($\underline{C}(CH_3)_3$), 46.9 ($NMe_2$), 111.1, 124.4, 154.0, 155.7, 156.0, 158.4 (Ar-H). EIMS (70 eV): *m/z* (%) 461 (5) [$MxGaBr_2^+$], 417 (30) [$MxGaBrCl^+$], 373 (47) [$MxGaCl_2^+$], 232 (100) [$Mx^+$], 57 (44) [$t Bu^+$]. HRMS ($EI^+$; *m/z*): calcd for $C_{16}H_{26}Cl_2GaN$, 373.0669; found 373.0687 (Δppm = 5.0). Anal. Calcd for $C_{16}H_{26}Cl_2GaN$ (373.01): C, 51.52; H, 7.03; N, 3.76. Found: C, 48.49; H, 6.60; N, 3.30. Anal. Calcd for $C_{16}H_{26}Br_2GaN$ (461.92): C, 41.60; H, 5.67; N, 3.03. Anal Calcd for $C_{16}H_{26}Br_{0.5}Cl_{1.5}GaN$ (395.24): C, 48.62; H, 6.63; N, 3.54.

**Reactions of RGaBr$_x$Cl$_{2-x}$, with LiBr, *t*BuBr or MxBr.** RGaBr$_x$Cl$_{2-x}$ (0.1 mmol) and LiBr or *t*BuBr or MxBr (0.5 mmol) were stirred for 16 h in diethyl ether (2 mL). All volatiles were removed in vacuum.

**(Mx)GaBr$_x$Cl$_{2-x}$ (126) with LiBr.** EIMS (70 eV): *m/z* (%) 461 (55) [MxGaBr$_2^+$], 417 (12) [MxGaBrCl$^+$], 382 (15) [MxGaBr$^+$], 366 (17) [MxGaBr$^+$-CH$_4$], 232 (100) [Mx$^+$], 176 (36) [C$_{13}$H$_{20}^+$ or C$_{12}$H$_{18}$N$^+$], 57 (44) [$^t$Bu$^+$].

**(Mamx)GaCl$_2$ with LiBr.** EIMS (70 eV): *m/z* (%) 475 (25) [(Mamx)GaBr$_2^+$], 460 (9) [(Mamx)GaBr$_2^+$ – Me], 433 (19) [(Mamx)GaBr$_2^+$ – C$_3$H$_6$ or – NC$_2$H$_4$], 396 (100) [(Mamx)GaBr$^+$], 380 (44) [(Mamx)GaBr$^+$ – CH$_4$], 246 (24) [Mamx$^+$], 203 (33) [MamxH$^+$ – NMe$_2$], 58 (44) [C$_4$H$_{10}^+$ or C$_3$H$_8$N$^+$], 57 (28) [C$_4$H$_9^+$].

**(*p*-*t*BuAr′)GaCl$_2$ with LiBr.** EIMS (70 eV): *m/z* (%) 419 (15) [(*t*BuAr′)GaBr$_2^+$], 404 (14) [(*t*BuAr′)GaBr$_2^+$ – Me], 340 (100) [(*t*BuAr′)GaBr$^+$], 190 (16) [*t*BuAr′$^+$], 147 (23) [*t*BuAr′H$^+$ – NMe$_2$], 132 (26) [*t*BuAr$^+$ – NMe$_2$], 131 (25) [*t*BuAr$^+$ – HNMe$_2$], 91 (26) [C$_7$H$_7^+$], 58 (71) [C$_4$H$_{10}^+$ or C$_3$H$_8$N$^+$].

**(Ar′)GaCl$_2$ with LiBr.** EIMS (70 eV): *m/z* (%) 363 (9) [(Ar′)GaBr$_2^+$], 284 (100) [(Ar′)GaBr$^+$], 91 (57) [Ar′H$^+$ – NMe$_2$], 58 (72) [C$_3$H$_8$N$^+$].

**(Pytis$^{-2SiMe_3}$)GaCl$_2$ with LiBr.** EIMS (70 eV): *m/z* (%) 381 (0.3) [(Pytsi$^{-2SiMe_3}$)GaBr$_2^+$], 300 (100) [(Pytsi$^{-2SiMe_3}$)GaBr$^+$], 120 (10) [C$_6$H$_6$NSi$^+$].

## 2.5 References

(1) a) Schachner, J. A.; Lund, C. L.; Quail, J. W.; Müller, J. *Organometallics* **2005**, *24*, 785-787. b) Schachner, J. A.; Lund, C. L.; Quail, J. W.; Müller, J. *Organometallics* **2005**, *24*, 4483-4488. c) Lund, C. L.; Schachner, J. A.; Quail, J. W.; Müller, J. *Organometallics* **2006**, *25*, 5817-5823. d) Schachner, J.A.; Orlowski, G.A.; Quail, J.W.; Kraatz, H.-B.; Müller, *J. Inorg. Chem.* **2006**, *45*, 454-459. e) Schachner, J. A.; Tockner, S.; Lund, C. L., Quail, J. W.; Rehan, M.; Müller, J. *Organometallics* **2007**, *26*, 4658-4662.

(2) a) Bagh, B.; Gilroy, J. B.; Staubitz, A.; Müller, J. *J. Am. Chem. Soc.* **2010**, *132*, 1794-1795. b) Bagh, B.; Schatte, G.; Green, J. C. ; Müller, J. *J. Am. Chem. Soc.* **2012**, *134*, 7924-7936.

(3) Papasergio, R. I.; Skelton, B. W.; Twiss, P.; White, A. H. *J. Chem. Soc., Dalton Trans.* **1990**, *4*, 1161-1172.

(4) a) Andrews, P. C.; Brym, M.; Jones, C.; Junk, P. C.; Kloth, M. *Inorg. Chem. Acta.* **2006**, *359*, 355-363. b) Henderson, M. J.; Papasergio, R. I.; Raston, C. L.; White, A. H.; Lappert, M. F. *J. Chem. Soc., Chem. Commun.* **1986**, 672-674.

(5) a) Engelhardt, L.; Kynast, U.; Raston, C. L.; White, A. H. *Angew. Chem.* **1987**, *26*, 681-682. b) Kynast, U.; Skelton, B. W.; White, A. H.; Henderson, M. J.; Raston, C. L. *J. Organomet. Chem.* **1990**, *384*, C1-C5. c) Andrews, P. C.; Raston, C. L.; Skelton, B. W.; White, A. H. *Chem. Commun.* **1997**, *13*, 1183-1184.

(6) Andrews, P. C.; Nichols, P. J. *Organometallics* **2000**, *19*, 1277-1281.

(7) Kümmel, C.; Meller, A.; Noltemeyer, M. *Z. Naturforsch., B: Chem. Sci.* **1996**, *51*, 209-219.

(8) a) Van den Ancker, T.; Jolly, B. S.; Lappert, M. F.; Raston, C. L.; Skelton, B. W.; White, A. H. *Chem. Commun.* **1990**, *15*, 1006-1008. b) Van den Ancker, T. R.; Raston, C. L.; Skelton, B. W.; White, A. H. *Organometallics* **2000**, *19*, 4437-4444.

(9) a) Ossig, G.; Meller, A.; Brönneke, C.; Müller, O.; Schäfer, M.; Herbst-Irmer, R. *Organometallics* **1997**, *16*, 2116-2120. b) Benet, S.; Cardin, C. J.; Cardin, D. J.; Constantine, S. P.; Heath, P.; Rashid, H.; Teixeira, S.; Thorpe, J. H.; Todd, A. K. *Organometallics*, **1999**, *18*, 389-398.

(10) a) Cardin, C. J.; Cardin, D. J.; Constantine, S. P.; Todd, A. K.; Teat, S. J. *Organometallics* **1998**, *17*, 2144-2146. b) Cardin, C. J.; Cardin, D. J.; Constantine, S. P.; Drew, M. G. B.; Rashid, H.; Convery, M. A.; Fenske, D. *J. Chem. Soc., Dalton Trans* **1998**, *16*, 2749-2756. c) Engelhardt, L. M.; Jolly, B. S.; Lappert, M. F.; Raston, C. L.; White, A. H. *J. Chem. Soc., Chem. Commun.* **1988**, 336-338. d) Molter, A.; Mohr, F. *Z. Anorg. Allg. Chem.* **2009**, *635*, 134-138. e) Cardin, C. J.; Cardin, D. J.; Convery, M. A.; Devereux, M. M. *J. Chem. Soc., Chem. Commun.* **1991,** 687-688.

(11) Jones, C.; Engelhardt, L. M.; Junk, P. C.; Hutchings, D. S.; Patalinghug, W. C.; Raston, C. L.; White, A. H. *J. Chem. Soc., Chem. Commun.* **1991**, *21*, 1560-1562.

(12) a) Andrews, P. C.; Nichols, P. J.; Raston, C. L.; Roberts, B. A. *Organometallics* **1999**, *18*, 4247-4249. b) Andrews, P. C.; McGrady, J. E.; Nichols, P. J. *Organometallics* **2004**, *23*, 446-453.

(13) Skelton, B. W.; Tolhurst, V.-A.; White, A. H.; Williams, A. M.; Wilson, A. J. *J. Organomet. Chem.* **2003**, 674, 38-44.

(14) Hursthouse, M. B.; Izod, K. J.; Motevalli, M.; Thornton, P. *Polyhedron* **1996**, *15*, 135-145.

(15) Lee, H. K.; Luo, B.-S.; Mak, T. C. W.; Leung, W.-P. *J. Organomet. Chem.* **1995**, *489*, C71-C73.

(16) Leung, W.-P.; Lee, H.-K.; Zhou, Z.-Y.; Mak, T. C. W. *J. Organomet. Chem.* **1993**, *443*, C39-C40.

(17) a) Izod, K. J.; Thornton, P. *Polyhedron* **1993**, *12*, 1613-1620. b) Leung, W.-P.; Lee, H.-K.; Zhou, Z.-Y.; Mak, T. C. W. *J. Organomet. Chem.* **1998**, *564*, 193-200.

(18) Papasergio, R.; Raston, C. L.; White, A. H. *J. Chem. Soc., Chem. Commun.* **1983**, 1419-1420.

(19) Papasergio, R. I.; Raston, C. L.; White, A. H. *J. Chem. Soc., Chem. Commun.* **1984**, 612-613.

(20) Papasergio, R. I.; Raston, C. L.; White, A. H. *J. Chem. Soc., Dalton Trans.* **1987**, 3085-3091.

(21) Van den Ancker, T. R.; Engelhardt, L. M.; Henderson, M. J.; Jacobsen, G. E.; Raston, C. L.; Skelton, B. W.; White, A. H. *J. Organomet. Chem.* **2004**, *689*, 1991-1995.

(22) Fuchita, Y.; Nakashima, M.; Hiraki, K.; Kawatani, M.; Ohnuma, K. *J. Chem. Soc., Dalton Trans.* **1988**, 785-789.

(23) Itami, K.; Kamei, T.; Yoshida, J.-i. *J. Am. Chem. Soc.* **2001**, *123*, 8773-8779.

(24) Yoshifuji, M.; Hirano, M.; Toyota, K. *Tetrahedron Lett.* **1993**, *34*, 1043-1046.

(25) Yoshifuji, M.; Sangu, S.; Hirano, M.; Toyota, K. *Chem. Lett.* **1993**, 1715-1718.

(26) Ancelet, T. group report accessible from Müller, J.

(27) (a) Veith, M.; Lange, H.; Belo, A.; Recktenwald, O. *Chem. Ber.* **1985**, *118*, 1600-1615. (b) Schnitter, C.; Klimek, K.; Roesky, H. W.; Albers, T.; Schmidt, H. G.; Röpken, C.; Parisini, E. *Organometallics* **1998**, *17*, 2249-2257. (c) Schormann, M.; Klimek, K. S.;

Hatop, H.; Varkey, S. P.; Roesky, H. W.; Lehmann, C.; Röpken, C.; Herbst-Irmer, R.; Noltemeyer, M. *J. Solid State Chem.* **2001**, *162*, 225-236. (d) Schiefer, M.; Hatop, H.; Roesky, H. W.; Schmidt, H. G.; Noltemeyer, M. *Organometallics* **2002**, *21*, 1300-1303.

(28) Stanga, O.; Lund, C. L.; Liang, H.; Quail, J. W.; Müller, J. *Organometallics* **2005,** *24*, 6120-6125.

(29) Howson, J.; Eaborn, C.; Hitchcock, P. B.; Hill, M. S.; Smith, J. D. *J. Organomet. Chem.* **2005**, *690*, 69-75.

(30) Al-Juaid, S.; Eaborn, C.; El-Hamruni, S. M.; Hitchcock, P. B.; Smith, J. D. *Organometallics* **1999**, *18*, 45-52.

(31) Breit, N. C.; Ancelet, T.; Quail, W.; Schatte, G.; Müller, J. *Organometallics* **2011**, *30*, 6150-6158.

(32) Andrews, I. P.; Lewis, N. J.; McKillop, A.; Wells, A. S. *Heterocycles* **1996**, *43*, 1151-1158.

(33) Beachley, Jr. O. T.; Rosenblum, D. B.; MacRae, D. J. *Organometallics* **2001**, *20*, 945-949.

(34) Anderson, D. G.; Bradney, M. A. M.; Webster, D. E. *J. Chem. Soc. B* **1968**, 450-452.

(35) Itami, K.; Toshiyuki, K.; Mitsudo, K.; Nokami, T.; Yoshida, J. *J. Org. Chem*. **2001**, *66*, 3970-3976.

(36) Bagh. B.; Breit, N. C.; Harms, K.; Schatte, G.; Burgess, I.; Braunschweig, H.; Müller, J. submitted on August 13 (ic-2012-01777y).

(37) Yosifuji, M.; Hirano, M.; Toyota, K.; Niitsu, T.; Shiomi, D.; Inamoto, N. *Science Reports Tohoku Univ., Ser. 1* **1991**, *74*, 1-7.

(38) Beets, M. G. J.; Meerburg, W.; Van Essen, H. *Recl. Trav. Chim. Pays-Bas* **1959**, *78*, 570-585.

(39) Roy, N.; Sproules, S.; Bill, E.; Weyhermüller, T.; Wieghardt, K. *Inorg. Chem.* **2008**, *47*, 10911-10920.

(40) Burgers, J.; Van Hartingsveldt, W.; Van Keulen, J.; Verkade, P. E.; Visser, H.; Wepster, B. M. *Recl. Trav. Chim. Pays-Bas* **1956**, *75*, 1327-1342.

(41) de Koning, A. J. *Recl. Trav. Chim. Pays-Bas* **1973**, *92*, 839-844.

(42) Schulz, S.; Pusch, S.; Pohl, E.; Dielkus, S.; Herbst-Irmer, R.; Meller, A.; Roesky, H. W. *Inorg. Chem.* **1993**, *32*, 3343-3346.

(43) Seebach, D.; Neumann, H. *Chem. Ber.* **1974**, *107*, 847-853.

(44) Bailey, W. F.; Luderer, M. R.; Jordan, K. P. *J. Org. Chem.* **2006**, 71, 2825-2828.

# CHAPTER 3
# REACTION OF THE NEW ALUMINUM AND GALLIUM DIHALIDES WITH LITHIATED SANDWICH COMPLEXES

## 3.1 Introduction

Ferrocenyl-based polymers have attracted a lot of attention due to their interesting properties related to their metal centers like their redox behavior (see Chapter 1.3). PFS polymers have been well-investigated and many possible applications have been reported.[1] These polymers were synthesized by ROP of strained silicon-bridged [1]FCPs (see Chapter 1.3). Ferrocenyl-based polymers with different bridging elements would enrich this field as more modulations and different properties become available. Our group focuses on the chemistry of heavier group-13 elements and metallocenophanes. We want to open the field of aluminum- and gallium-bridged metallocenyl-based polymers by ROP of respective [1]MCPs. We were also interested to gain a deeper understanding of the principles behind the formation of aluminum- and gallium-bridged [1]MCPs, [1.1]MCPs, metallopolymers and oligomers. When the research described in this thesis was started, only the well-characterized aluminum- and gallium-bridged [1]MCPs **81**-**86** and [1.1]MCPs **73**-**78** as described in Chapter 1.5 were known. Only when sterically bulky ligands on aluminum or gallium were utilized, the salt-metathesis reaction led to the formation of [1]MCPs, whereas aluminum and gallium dihalides equipped with slim ligands selectively gave [1.1]MCPs (Scheme 3-1).[2]

**Scheme 3-1.** Formation of aluminum- and gallium-bridged [1]FCPs or [1.1]FCPs in dependence of the steric bulk of the ligand on aluminum or gallium.

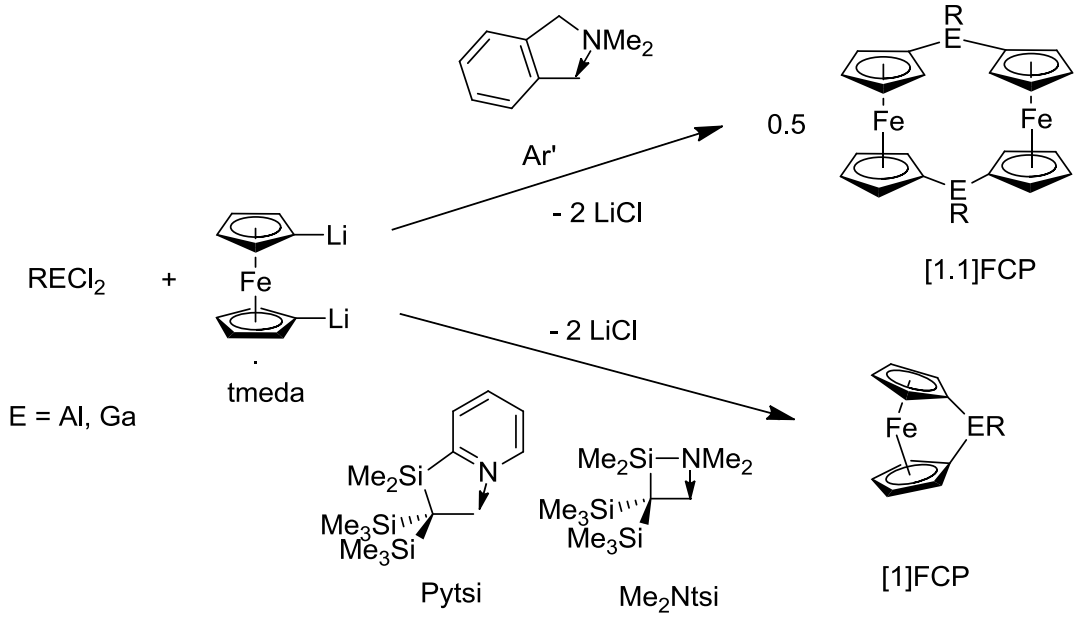


ROP of aluminum- and gallium-bridged [1]FCPs and [1]RCPs was unsuccessful or at best sluggish, which was attributed to the shielding of the sterically bulky ligands.[2e] Therefore, selected aluminum- and gallium dichlorides with ligands of moderate steric bulk and a nitrogen donor arm were synthesized (see Chapter 2). It was hoped that these ligands, on the one hand, will still have enough steric bulk to afford the formation of [1]MCPs over [1.1]MCP and, on the other hand, will result in little protection of the bonds between the Cp rings and the group-13 element, so that the [1]FCPs can be polymerized (Scheme 3-2). However, reactions of the new aluminum and gallium dichlorides with dilithiated metallocenes can also yield other products than the targeted [1]MCPs: [1.1]MCPs and other oligomers.

**Scheme 3-2.** Anticipated synthesis of aluminum- and gallium-bridged [1]MCPs and subsequent controlled ROP.

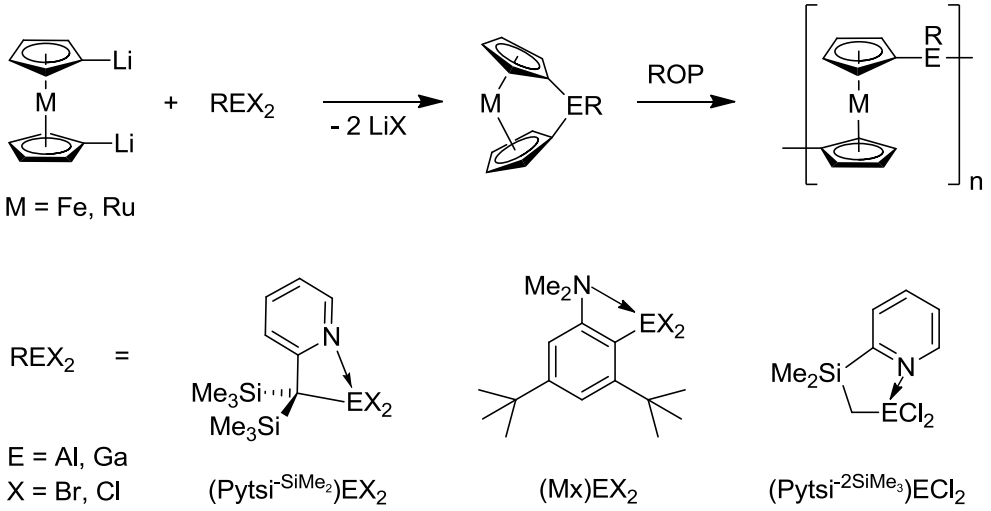

## 3.2 Results and Discussion

### 3.2.1 Reactions of (Pytsi$^{-SiMe_2}$)$AlBr_2$, (Pytsi$^{-SiMe_2}$)$AlCl_2$ and (Pytsi$^{-SiMe_2}$)$GaCl_2$ with 1,1'-Dilithioferrocene

Reactions of (Pytsi$^{-SiMe_2}$)$AlBr_2$, (Pytsi$^{-SiMe_2}$)$AlCl_2$, and (Pytsi$^{-SiMe_2}$)$GaCl_2$ with 1,1'-dilithioferrocene in benzene or toluene yielded the gallium- and aluminum-bridged [1]FCPs **129** and **130** respectively, as main products as shown by $^1$H NMR spectroscopy (Scheme 3-3).

**Scheme 3-3.** Reactions of (Pytsi$^{-SiMe_2}$)$AlBr_2$ (**111**), (Pytsi$^{-SiMe_2}$)$AlCl_2$ (**112)**, and (Pytsi$^{-SiMe_2}$)$GaCl_2$ (**113)** with 1,1'-dilithioferrocene to give the gallium- and aluminum-bridged [1]FCPs **129** and **130**.

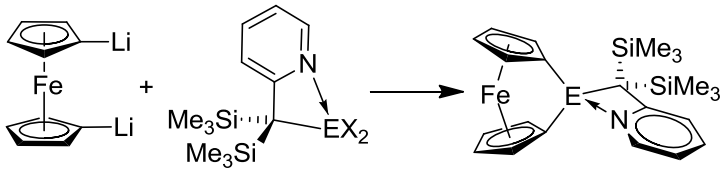


**111**: E = Al, X = Br
**112**: E = Al, X = Cl
**113**: E = Ga, X = Cl

**129**: E = Ga
**130:** E = Al

Aluminum- and gallium-bridged [1]FCPs with $C_s$-symmetric ligands show two signals for the α-protons and two signals for β-protons. The typical pattern of these Cp protons is that the two signals for β-protons are close together or even overlapping downfield of the well-separated signals for the α-protons. The $^1$H NMR spectra of **129** exhibited the cyclopentadienyl proton signals at δ 4.22 (2 α-H), 4.29 (2 α-H), 4.62 (4 β-H), while the $^1$H NMR spectrum of the aluminum compound **130** displayed four signals for the Cp protons at δ 4.10 (2 α-H), 4.28 (2 α-H), 4.66 (2 β-H), 4.68 (2 β-H). The isolated aluminum- or gallium-bridged [1]FCPs with the parent Pytsi ligand (**81** and **82**) showed similar shifts [δ 4.08 (2 α-H), 4.45 (2 α-H), 4.61 (2 β-H), 4.65 (2 β-H) for

(Pytsi)Ga[1]FCP (**82**);[2b] and δ 3.91 (2 α-H), 4.31 (2 α-H), 4.64 (2 β-H), 4.68 (2 β-H) for (Pytsi)Al[1]FCP (**81**)[2a]].

Unfortunately, it was not possible to isolate the [1]FCPs **129** and **130**. The isolation of the [1]FCPs **129** and **130** was attempted by crystallization from various solvents (toluene, hexane and diethyl ether) and precipitations into hexane. Moreover, diverse reaction conditions were chosen including different solvents (benzene, toluene, and diethyl ether), and different temperatures (r.t., 0 °C, -20 °C, -30 °C, -50 °C, and -78 °C) in order to optimize the reaction conditions and minimize impurities. In addition to that, salt-metathesis reactions were also carried out with $(LiC_5H_4)_2Fe{\cdot}3thf$ as an alternative for the common staring material $(LiC_5H_4)_2Fe{\cdot}2/3$ tmeda in order to avoid the presence of tmeda. One of the major problems concerning the isolation of species **129** and **130** was their reactivity. $^1$H NMR spectroscopy showed that over the course of 2 weeks, the signals for the Cp-protons in the [1]FCPs decreased and finally disappeared and only signals for species that exhibit very broad signals in the $^1$H NMR spectrum were found. The newly formed species were the aluminum- and gallium-bridged ferrocenyl-based oligomers or low-molecular-weight polymers $\mathbf{129_n}$ and $\mathbf{130_n}$ (Figure 3-1).

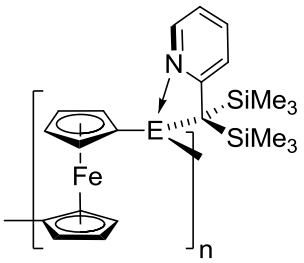


$\mathbf{129_n}$ (E = Ga)
$\mathbf{130_n}$ (E = Al)

**Figure 3-1.** Aluminum- and gallium-bridged ferrocenyl-based oligomers or low-molecular-weight polymers equipped with the Pytsi$^{\text{-SiMe}_2}$ ligand ($\mathbf{130_n}$ and $\mathbf{129_n}$).

Precipitation of toluene solutions into hexane were used to purify the low-molecular-weight polymers **129$_n$** and **130$_n$**. However, the isolation of an analytically pure polymer (elemental analysis) was only possible for **130$_n$** and only if $(LiC_5H_4)_2Fe{\cdot}3thf$ was used in the salt-metathesis reaction. One of the reasons for replacing $(LiC_5H_4)_2Fe{\cdot}2/3$ tmeda with $(LiC_5H_4)_2Fe{\cdot}3thf$ for the attempted isolation of **129** and **130** was that ROPs of tin-bridged [1]FCPs were known to be initiated by amines.[3] Reactions carried out between (Pytsi$^{-SiMe_2}$)$AlCl_2$ (**112**) and $(LiC_5H_4)_2Fe{\cdot}3thf$ did not react to form the expected products for unknown reasons. Possibly the difficulties of isolating **129$_n$** and **130$_n$** in an analytically pure form from reactions with $(LiC_5H_4)_2Fe{\cdot}2/3$tmeda are connected to problems separating tmeda or the tmeda adduct of lithium halides. $^1$H NMR spectra of both polymeric species exhibited only broad, structureless signals. The chemical composition of **129$_n$** and **130$_n$** was verified by hydrolysis experiments. When **129$_n$** and **130$_n$** were hydrolyzed in $CDCl_3$ containing $H_2O$, only ferrocene, and Pytsi$^{-SiMe_2}$H and tmeda - in case of **130$_n$** - were found by $^1$H NMR spectroscopy.

DLS and gel permeation chromatography (GPC) are the standard tools to investigate the size of polymers. Since GPC analysis was not available for our studies, the size of the gallium-bridged polymeric species **129$_n$** was studied by DLS resulting in a hydrodynamic radius $R_h$ of 1.35 ± 0.20 nm. In order to determine the $M_w$ from the $R_h$, the relationship between $R_h$ and $M_w$ would need to be known. However, this relationship is not known for poly(ferrocenylgallane)s. Therefore, the estimation of the molecular weight of all ferrocenyl- or ruthenocenyl-based polymers that are discussed in this thesis is based on the following assumptions: a) The polymer behaves like a random coil in a good solvent which gives a relationship between the $R_h$ and the radius of gyration ($R_g$) of

$R_g$ / $R_h$ = 2.05.[4] b) The correlation between $R_g$ and the molecular weight of the polymer is similar to the known correlation for dimethylsilyl-bridged PFS **34** and its absolute $M_w$.[5] Therefore, the $M_w$ of the polymers can be estimated from a calibration curve of log($M_w$) / log($R_g$) of the PFS **34**. Based on these assumptions, the $R_g$ of **129$_n$** was determined as 2.77 ± 0.41 and $M_w$ was estimated to be 8.3 ± 2.5 kDa which translates into 17 ± 5 repeating units ($DP_w$).

It is not clear, how and why the low-molecular-weight polymers formed. One of the possibilities is that the low-molecular-weight polymers exclusively formed by ring-opening of the [1]FCPs similar to Mamx ligand, for which an exclusive ROP of the [1]FCPs was suggested.[6] The other possibility is the formation of oligomers alongside the [1]FCPs during the salt-metathesis reaction and the subsequent attack of the living end-groups of the oligomers on the [1]FCPs. Thus the oligomers would have been growing to low-molecular-weight polymers by ROP of the [1]FCPs. One more possibility would be the formation of low-molecular-weight polymers during the reaction by polycondensation and the separate formation of more low-molecular-weight polymers from ROP of the [1]FCPs. It is also possible that tmeda catalyzed the ring-opening of **130** like in reactions described for tin.[3] Irrespective of the way of ring-opening by attack of lithium-containing oligomers or by ring-opening exclusively based on the instability of the [1]FCP, this ROP is slow. This shows that the aluminum- and gallium-bridged [1]FCPs equipped with the Pytsi$^{-SiMe_2}$ ligand are more stable than the respective species with the Mamx ligand which are stable for a maximum of 30 min.[6] Moreover, the slowness of the ROP of the [1]FCPs highly suggests that the oligomers or low-molecular-weight polymers that were already

present to a significant amount a few hours after the reaction was started, have been formed by polycondensation reactions.

Aluminum- and gallium-bridged [1]FCPs equipped with the parent Pytsi ligand (**81** and **82**) were well protected from anionic attack. When **81** and **82** were reacted with the anionic initiator *n*BuLi, only an alkylation in the *para*-position of the pyridine moiety was observed and the [1]FCPs retained their structure.[2e] However, by transition metal-catalyzed ROP of **82** an incomplete ROP was observed.[2e] Since **129** and **130** showed a higher reactivity than **81** and **82** towards ROP and the steric bulk of the ligand in **129** and **130** is smaller than in **81** and **82**, it would be interesting to probe if a transition metal catalyst could accelerate the ring-opening of **129** and could afford polymers with higher molecular weights. Subsequent to the salt-metathesis reaction and filtration, one part of **129** was treated with Karstedt's catalyst, whereas another part was left untreated as a blank sample. However, the transition-metal catalyst containing sample showed only a little less [1]FCP in the $^{1}$H NMR spectrum than the respective blank sample and after 3 days significant amounts of [1]FCP were left. This suggests that ring-opening attacks are still significantly blocked in **80**.

The results described in Chapter 3.2.1 were published in 2011 in Organometallics.[7]

### 3.2.2 Reactions of (Mx)$AlCl_2$ and (Mx)$GaBr_xCl_{2-x}$ with 1,1'-Dilithioferrocene and 1,1'-Dilithioruthenocene

Reactions of (Mx)$GaBr_xCl_{2-x}$ (**126**) with 1,1'-dilithioferrocene in diethyl ether lead to the formation of the [1]FCP **131** as a major product (Scheme 3-4).

**Scheme 3-4.** Reactions of $(Mx)GaBr_xCl_{2-x}$ (**126**) with $(LiC_5H_4)_2Fe \cdot 2/3tmeda$ or $(LiC_5H_4)_2Ru \cdot tmeda$ yielding the [1]FCP **131** or the [1]RCP **132**.

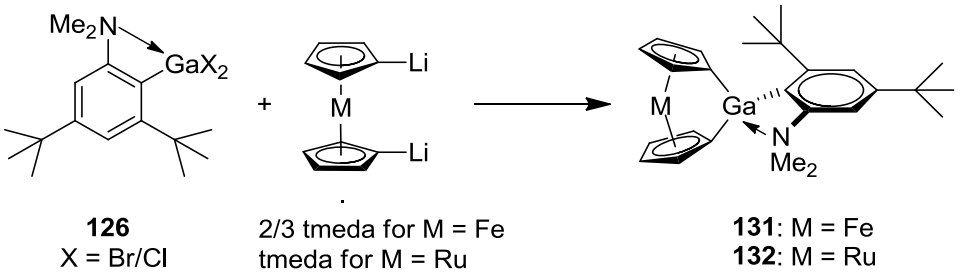


**126**
X = Br/Cl

2/3 tmeda for M = Fe
tmeda for M = Ru

**131**: M = Fe
**132**: M = Ru

Similarly to **129** and **130**, the gallium-bridged [1]FCP **131** was identified by the pattern of the signals for the cyclopentadienyl protons in the $^1$H NMR spectrum at 4.06 (2H, α-Cp), 4.43 (2H, α-Cp), 4.67 (2H, β-Cp), 4.68 (2H, β-Cp). Moreover, two singlets for the *t*Bu groups, one singlet for the $Me_2N$ group and two signals for the aromatic protons were assigned to the [1]FCP **131**. $^1$H NMR spectroscopy of the reaction mixture after 1 h also revealed the concomitant presence of oligomers or low-molecular-weight polymers $\mathbf{131_n}$ (Figure 3-2).

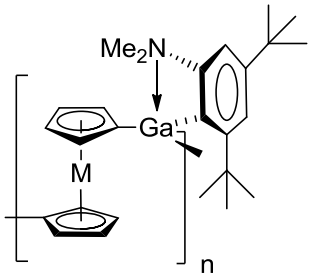


**131$_n$**: M = Fe
**132$_n$**: M = Ru

**Figure 3-2.** Poly(ferrocenylgallane) and poly(ruthenocenylgallane) equipped with the Mx ligand ($\mathbf{131_n}$ and $\mathbf{132_n}$).

All $^1$H NMR signals of the oligomers or low-molecular-weight polymers are broad, but the signals are not as broad as the signals observed for $\mathbf{129_n}$. Particularly the cyclopentadienyl protons show some features like three broad signals (Figure 3-3).

Moreover, the singlets for the *tert*-butyl groups do not have the same height. The upfield singlet assigned to the *ortho tert*-butyl group is shorter and slightly broader than the singlet for the *para tert*-butyl group (Figure 3-3).

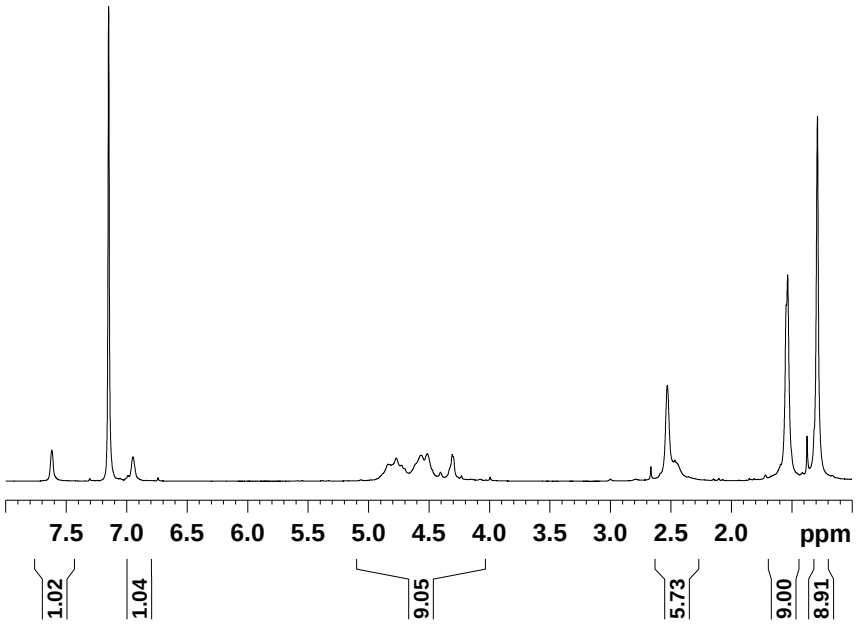


**Figure 3-3.** $^{1}$H NMR spectrum of the poly(ferrocenylgallane) equipped with the Mx ligand (**131$_n$**).

For the poly(ferrocenylgallane) equipped with the Mamx ligand (**87$_n$**) a fine-structure was observed for the *ortho tert*-butyl group in the $^{1}$H NMR spectrum.[6a] The *ortho tert*-butyl group of the Mamx ligand experiences the tacticity of the neighboring groups due to its proximity to the ferrocenediyl moieties. It is fair to assume that as the five-membered ring formed by the Mamx ligand and the group-13 element is reduced to a four-membered ring for the Mx ligand, the *ortho tert*-butyl group is moved away from the gallium atom and at the same time from ferrocenediyl moieties. The increased distance from the central *ortho tert*-butyl carbon to the gallium atom by 0.2 Å was discussed in Chapter 2.2.4 for (Mx)GaBr$_x$Cl$_{2-x}$ (**126**) compared to (Mamx)GaCl$_2$. This might explain the missing fine structure of the *ortho tert*-butyl group in **131$_n$**. Similar to

the aluminum- and gallium-bridged [1]FCPs equipped with the Mamx or the Pytsi$^{-SiMe_2}$ ligand, the [1]FCPs with the Mx ligand are not stable and after three days their signals were not be observed anymore by $^1$H NMR spectroscopy. The aluminum- and gallium-bridged [1]FCPs with the Mamx ligand (**87** and **88**) were consumed after 30 min, whereas the complete reaction of related species with the Pytsi$^{-SiMe_2}$ ligand (**129**) took two weeks. Therefore, **131** showed a medium stability in comparison with **87**, **88**, and **129**, **130**. Similarly as discussed in Chapter 2.2.1 for the Pytsi$^{-SiMe_2}$ ligand, there is no data available that would allow one to conclude how the formation of the oligomers or low-molecular-weight polymers occured.

Interestingly, the formation of a gallium-bridged [1.1]FCP equipped with the Mx ligand (**131$_2$**) as a minor product was observed (Figure 3-4). Species **131$_2$** was isolated in a very low yield of 5% by precipitation of a toluene solution into hexanes and washing the solid with toluene.

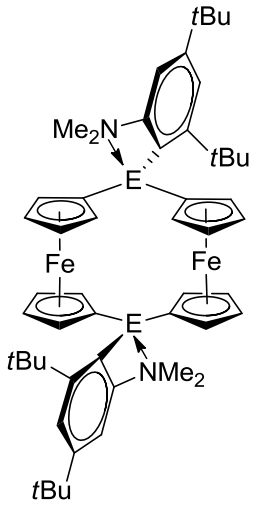


**131$_2$**: E = Ga
**133$_2$**: E = Al

**Figure 3-4.** Gallium- and aluminum-bridged [1.1]FCPs equipped with the Mx ligand (**131$_2$** and **133$_2$**).

The $^{1}$H NMR spectrum of **131$_2$** showed the typical pattern of Cp protons in aluminum- and gallium-bridged [1.1]FCPs with $C_s$-symmetric ligands. The two α-Cp protons appear far apart from each other, while the β-Cp protons give rise to signals in between the α-protons [3.94 (α-H), 4.24 (β-H), 4.29 (β-H), 4.64 (α-H)]. Moreover, the expected two singlets for the aliphatic protons and the two signals for the aromatic protons were displayed in the $^{1}$H NMR spectrum. A $^{13}$C NMR spectrum could not be recorded due to the compound's very limited solubility. The identity of **131$_2$** was confirmed by mass spectrometry, in which the molecular ion peak showed the highest intensity. It would be very interesting to see the molecular structure of **131$_2$** and the distance between the α-Cp protons and the *ortho tert*-butyl group, particularly because it was unexpected that a gallium-bridged [1.1]FCP could form with such a sterically bulky ligand. However, it was not possible to grow crystals from this species.

Reactions of (Mx)GaBr$_x$Cl$_{2-x}$ (**126**) with (LiC$_5$H$_4$)$_2$Ru·tmeda in toluene yielded, similarly to the reactions with (LiC$_5$H$_4$)$_2$Fe·2/3tmeda, a gallium-bridged [1]RCP (**132**) as observed by $^{1}$H NMR spectroscopy (Scheme 3-4). The $^{1}$H NMR spectrum, showed the β-Cp protons overlapping at δ 5.34 and the α-Cp protons being well separated at δ 4.12 and 4.54. Similar shifts were observed for the gallium-bridged [1]RCP equipped with the Mamx ligand [δ 4.05 (α-Cp), 4.59 (α-Cp), 5.34 (β-Cp), 5.36 (β-Cp)].[6b] Species **132** was not isolable and it was consumed within a few days most likely by ROP. The oligomers **132$_n$** were formed during these reactions and they were isolated by precipitation into hexane (Figure 3-2). The $^{1}$H NMR spectrum of the oligomers exhibited very broad peaks, for example, a featureless broad signal for the Cp-protons that resembles rather the spectra of **129$_n$** and **130$_n$** than that of **131$_n$**. For the Mamx ligand, a similar broadening of

the $^1$H NMR peaks was observed when the ferrocenediyl moieties were replaced with ruthenocenediyl moieties.[6] However, in both cases the $^1$H NMR spectra of the oligomers / polymers with Mamx ligand **87$_n$** and **89$_n$** showed sharper signals than in the respective species with the Mx ligand, **131$_n$** and **132$_n$**. In the reaction of (Mx)GaBr$_x$Cl$_{2-x}$ (**126**) with $(LiC_5H_4)_2Ru\cdot$tmeda a formation of a [1.1]RCP was not found.

Reactions between (Mx)AlCl$_2$ (**124**) and 1,1'-dilithiometallocenes (M = Fe, Ru) yielded polymeric materials similar to the respective reactions with (Mx)GaBr$_x$Cl$_{2-x}$ (**126**) (Scheme 3-5).

**Scheme 3-5.** Reactions of (Mx)AlCl$_2$ (**124**) with $(LiC_5H_4)_2M\cdot$tmeda (M = Fe, Ru) affording the aluminum-bridged ferrocenyl-based polymer **133$_n$** and ruthenocenyl-based oligomers **134$_n$**.

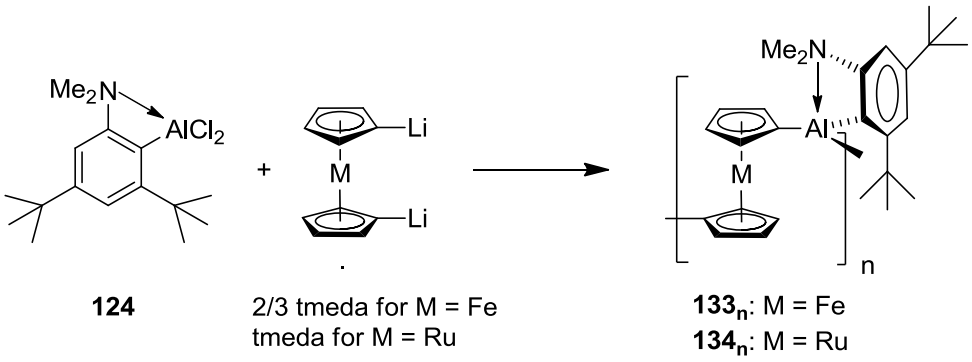


In contrast to the salt-metathesis reactions carried with (Mx)GaBr$_x$Cl$_{2-x}$ (**126**) in reactions of 1,1'-dilithiometallocenes (M = Fe, Ru) with (Mx)AlCl$_2$ (**124**) no aluminum-bridged [1]MCP could be identified by $^1$H NMR spectroscopy even 15 min after the reaction was started. Either the aluminum-bridged [1]MCPs are so reactive that they could not be observed or the oligomeric / polymeric species formed exclusively by the condensation reaction. A similarity of the aluminum-bridged metallocenyl-based polymers to the gallium-bridged species was observed in the $^1$H NMR spectra of **133$_n$** and **134$_n$**, with **134$_n$** exhibiting significantly broader peaks than **133$_n$**. The aluminum-

bridged ruthenocene-based oligomers could be separated from more soluble compounds like MxH by precipitation of a toluene solution into hexane. However, this separation was not possible for the poly(ferrocenylalumane) **133$_n$**, because it is soluble under these conditions. The poly(ferrocenylgallane) **131$_n$** showed the same solubility during the precipitation into hexane and it was isolated by precipitations of a toluene solution into methanol. However, when the precipitation into methanol was attempted for **133$_n$**, only MxH and ferrocene were found by $^1$H NMR spectroscopy. This was attributed to the higher sensitivity of aluminum than gallium toward moisture or alcohols. Gallium species with small ligands show also high sensitivities toward moisture or alcohols. However, the Mx ligand seems to be protecting the gallium atom with its steric bulk. The poly(ferrocenylgallane) **131$_n$** showed a half life time (till half of the species was degraded by moisture) of one week in atmosphere. The poly(ferrocenylgallane) **87$_n$** has an even higher stability towards moisture than **131$_n$** and no degradation was observed when **87$_n$** was handled in air. No pure ferrocenyl-based polymers **133$_n$** were isolable; the amount of impurities could only be decreased by sublimation of some volatile impurities.

The formation of an aluminum-bridged [1.1]FCP equipped with the Mx ligand (**133$_2$**) was observed (Figure 3-4). Species **133$_2$** was clearly identified by the typical pattern of the cyclopentadienyl $^1$H NMR signals [3.86 (α-Cp), 4.22 (β-Cp), 4.28 (β-Cp), 4.69 (α-Cp)]. The separation of **133$_2$** from the polymers **133$_n$** was achieved similarly to **131$_n$** by precipitation of the reaction mixture in toluene into hexanes. However, a separation of **133$_2$** from all impurities was not possible to date.

No clear sign for the formation of any aluminum-bridged [1.1]RCP equipped with the Mx ligand was observed. The formation of aluminum- and gallium-bridged [1.1]FCPs

equipped with the Mx ligand and the absence of related [1.1]RCPs suggests that the different sizes in sandwiched metals have an influence on activation energies of [1.1]RCPs and ruthenocenyl-based oligomers. Chapter 5 focuses on the reactions of 1,1'-dilithioruthenocene with aluminum and gallium dihalides equipped with the slim ligands Ar′ and *p*-*t*BuAr′. These reactions lead to the formation of ruthenocenyl-based oligomers next to [1.1]RCPs, whereas no formation of ferrocenyl-based oligomers was observed for these ligands on aluminum or gallium in respective reactions with dilithiated sandwich complexes. This clearly exhibits the same trend that the same steric bulk of ligands on aluminum and gallium leads to the formation of more ruthenocenyl-based oligomers in relation to [1.1]RCPs than in respective [1.1]FCPs and ferrocenyl-based polymers.

The molecular weights of all the ferrocenyl- or ruthenocenyl-based oligomers or polymers with the Mx ligand were determined by DLS (Table 3-1). The molecular weights were determined similar to those of **129$_n$** (Chapter 2.2.1). Only the poly(ferrocenylalumane) **133$_n$** was found to be a high-molecular-weight polymer with a molecular weight of 66 (± 13) kDa, which translates to 149 (± 29) repeating units. The molecular weights of **131$_n$**, **132$_n$**, and **134$_n$** are ranging between 4.2 and 6.0 kDa referring to 8-12 repeating units (Table 3-1). The aluminum- and gallium-bridged polymers in which the Mamx ligand was utilized (**87$_n$**-**90$_n$**) exhibited a similar trend with the poly(ferrocenylalumane) **88$_n$** having the highest molecular weights and the polyruthenocenes **89$_n$** and **90$_n$** being low-molecular weight polymers (Table 3-1). However, in contrast to **131$_n$**, the poly(ferrocenylgallane) **87$_n$** is a high-molecular-weight polymer. The reason for these different molecular weights is unknown to date.

**Table 3-1.** Molecular weights of aluminum- and gallium-bridged ferrocenyl- and ruthenocenyl-based polymers and oligomers with the Mamx and the Mx ligand determined by DLS.

| ligand | Mamx | | | | Mx | | | |
|---|---|---|---|---|---|---|---|---|
| Fe/Ru | Fe | | Ru | | Fe | | Ru | |
| Al/Ga | Al[6b] | Ga[6a] | Al[6b] | Ga[6b] | Al | Ga | Al | Ga |
| **Nr** | **$88_n$** | **$87_n$** | **$90_n$** | **$89_n$** | **$133_n$** | **$131_n$** | **$134_n$** | **$132_n$** |
| $M_w$[kDa] | 106±8 | 36±8 | 8±3 | 10±5 | 66±13 | 5.5±0.7 | 6.0±0.7 | 4.2±1 |
| $DP_w$ | 232±18 | 72±17 | 16±6 | 19±9 | 149±29 | 11±1 | 12±2 | 8±2 |

### 3.2.3 Reactions of (Pytsi$^{-2SiMe_3}$)$AlCl_2$ and (Pytsi$^{-2SiMe_3}$)$GaCl_2$ with 1,1'-Dilithioferrocene and Lithioferrocene

*Reactions of (Pytsi$^{-2SiMe_3}$)$AlCl_2$ and (Pytsi$^{-2SiMe_3}$)$GaCl_2$ with Dilithioferrocene*

Reactions of the aluminum and gallium dichlorides, equipped with the least sterically bulky ligand (Pytsi$^{-2SiMe_3}$) with 1,1'-dilithioferrocene were carried out in benzene or diethyl ether and gave the aluminum- and gallium-bridged [1.1]FCPs **$135_2$** and **$136_2$** in a mixture with the ferrocenyl-based oligomers **$135_n$** and **$136_n$** (Scheme 3-6).

**Scheme 3-6.** Reactions of 1,1'-dilithioferrocene with (Pytsi$^{-2SiMe_3}$)$AlCl_2$ (**121**) and (Pytsi$^{-2SiMe_3}$)$GaCl_2$ (**122**) yielding the aluminum- and gallium-bridged [1.1]FCPs **$135_2$** and **$136_2$** and ferrocenyl-based oligomers **$135_n$** and **$136_n$**.

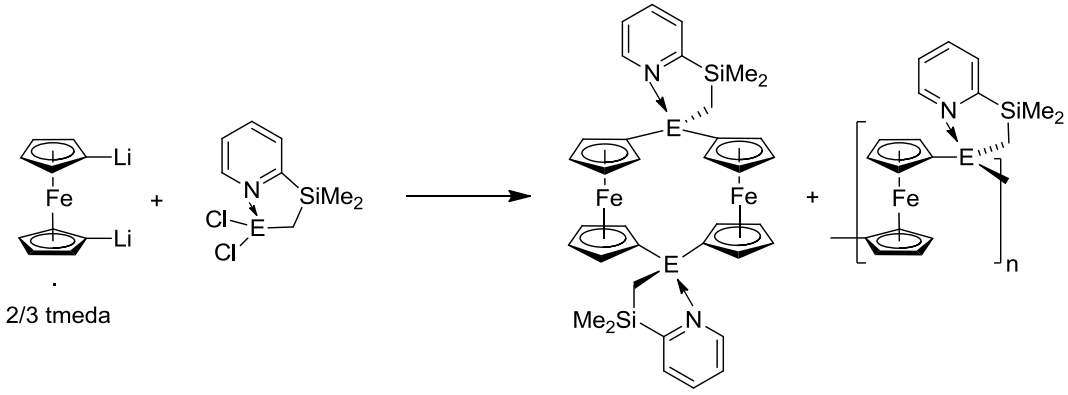


The formation of the [1.1]FCPs **$135_2$** and **$136_2$**, respectively, was observed by $^1H$ NMR spectroscopy by the typical pattern of the Cp protons in [1.1]FCPs. The Cp protons

of **136$_2$** were found at δ 4.16, 4.48, 4.69, and 5.30 and the Cp protons of **135$_2$** appeared at δ 4.18, 4.41, 4.64, and 5.17. The $^1$H NMR spectrum also revealed the formation of other species that were mainly exhibiting broad signals similar to **129$_n$** and **130$_n$**. Therefore, the species exhibiting these broad signals were assigned to the polycondensation products **135$_n$** and **136$_n$** respectively. In spite of our best efforts, it was not possible to isolate any of these species.

However, **121** and **122** could be utilized for reactions with lithioferrocene to yield bis(ferrocenyl)aluminum and gallium compounds (see below).

*Introduction to bis(ferrocenyl)compounds*

Bis(ferrocenyl) compounds are well known in the literature since Nesmeyanov described bis(ferrocenyl)mercury (**137**) in 1954 (Figure 3-5).[8] In analogy with [1]FCPs and [1.1]FCPs, most bis(ferrocenyl) compounds are known with carbon[9] and silicon[10]. Phosphorous-,[11] boron-,[12] and tin-containing[13] bis(ferrocenyl) compounds are less studied and for gold,[14] platinum,[15] zinc,[16] mercury,[8] aluminum,[17] germanium,[18] lead,[19] nitrogen,[20] sulfur,[21] selenium,[22] and tellurium[22] only a few examples are known. Wrackmeyer *et al.* described the only bis(ferrocenyl)aluminum species, a bis(ferrocenyl)methylaluminum pyridine donor adduct, which could not be isolated in a pure form.[17]

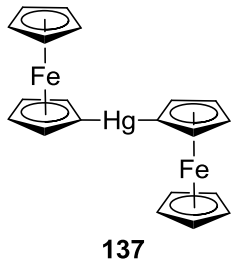


**137**

**Figure 3-5.** The first bis(ferrocenyl) compound (**137**).

The redox behavior of bis(ferrocenyl) compounds with different bridging elements was previously studied and type II as well as some type I behavior according to Robin and Day was reported.[23] Table 3-2 displays measured redox potentials ($E_{1/2}$), if applicable, the difference between two redox potentials ($\Delta E_{1/2}$), as well as some additional information about the solvent and electrolyte. For some species, like bis(ferrocenyl)amines or bis(ferrocenyl)mercury only one redox event was reported, whereas for others, with the exemption of boron, low $\Delta E_{1/2}$ values were measured.

**Table 3-2.** Redox behavior of known bis(ferrocenyl) compounds $R_xEFc_2$.

| E | B[12b] | C[9h] | C[9h] | Ge[18b] | P[11b] | N[20] | N[20] | Hg[24] |
|---|---|---|---|---|---|---|---|---|
| $R_x$ | Mes | $H_2$ | $Me_2$ | $Me_2$[a)] | Ph | H | Ph | |
| $E_{1/2}$ [V] | 0.045 | -0.04 | -0.06 | -0.26 | 0.175 | -0.36 | -0.28 | -0.13 |
| $E_{1/2}$ [V] | 0.467 | 0.06 | 0.10 | -0.20 | 0.340 | | | |
| $\Delta E_{1/2}$[V] | 0.422 | 0.10 | 0.16 | 0.074 | 0.165 | | | |
| Solvent | $CH_2Cl_2$ | EtOH | EtOH | thf | $CH_2Cl_2$ | MeCN | MeCN | MeCN |
| electrolyte | $Bu_4N$ | Na | Na | $Bu_4N$ | $Bu_4N$ | Na | Na | $Et_4N$ |
| | $B(C_6F_5)_4$ | $ClO_4$ | $ClO_4$ | $PF_6$ | $ClO_4$ | $ClO_4$ | $ClO_4$ | $ClO_4$ |

a) compound is $[(C_5Me_5)Fe(C_5H_4)]GeMe_2$.

*Motivation for the synthesis of bis(ferrocenyl)aluminum and gallium compounds*

The synthesis of new bis(ferrocenyl)aluminum and gallium compounds and the study of their redox behavior was one of the research objectives of our group member Bidraha Bagh. Bis(ferrocenyl)aluminum and gallium compounds are model compounds for aluminum- and gallium-bridged ferrocenyl-based polymers. The molecular structure of bis(ferrocenyl) compounds can give information about the probable arrangement of the ferrocenyl moieties in the polymers, which cannot be seen from the rigid model compounds [1.1]FCPs. Moreover, no redox behavior of aluminum- and gallium-bridged bis(ferrocenyl) compounds was previously studied and it would be interesting to compare the interactions of its iron centers to those in aluminum- and gallium-bridged [1.1]FCPs.

B. Bagh synthesized bis(ferrocenyl)aluminum and gallium compounds with the *p*-$SiMe_3Ar'$ ligand and the Mamx ligand **102-105** (Scheme 3-7).[25,6b] While **102** and **103** were directly synthesized as model compounds for the respective ferrocenyl-based polymers, species **104** and **105** were synthesized for a direct comparison with the respective [1.1]FCPs.

**Scheme 3-7.** Synthesis of bis(ferrocenyl) compounds with aluminum and gallium as bridges **102-105**.

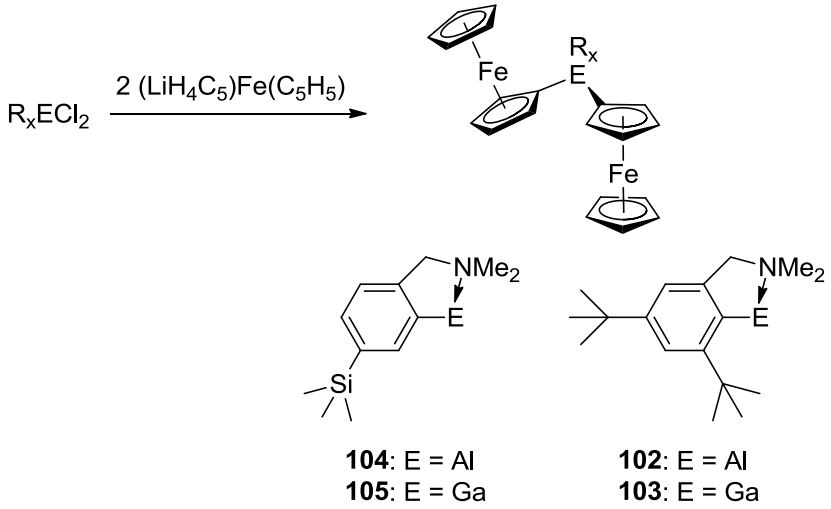


I joined this project by synthesizing and characterizing (Pytsi$^{-2SiMe_3}$)$AlFc_2$ and (Pytsi$^{-2SiMe_3}$)$GaFc_2$. The Pytsi$^{-2SiMe_3}$ ligand was assumed to have more steric bulk than the *p*-$SiMe_3Ar'$ ligand, but less steric bulk that the Mamx ligand. Moreover, the Pytsi$^{-2SiMe_3}$ ligand has a pyridine donor instead of a dimethylamine donor and a different backbone. This is likely to result in different structural features and redox properties of bis(ferrocenyl)aluminum and gallium species equipped with the Pytsi$^{-2SiMe_3}$ ligand compared to the related compounds synthesized by B. Bagh (**102-105**). The results obtained are described below considering the context of B. Baghs work and his results.

*Reactions of (Pytsi$^{-2SiMe_3}$)$AlCl_2$ and (Pytsi$^{-2SiMe_3}$)$GaCl_2$ with Lithioferrocene*

(Pytsi$^{-2SiMe_3}$)$AlFc_2$ (**138**) and (Pytsi$^{-2SiMe_3}$)$GaFc_2$ (**139**) were synthesized similar to **102-105** by a reaction of (Pytsi$^{-2SiMe_3}$)$AlCl_2$ (**121**) or (Pytsi$^{-2SiMe_3}$)$GaCl_2$ (**122**) with two equivalents of lithioferrocene (Scheme 3-8). (Pytsi$^{-2SiMe_3}$)$AlFc_2$ (**138**) and (Pytsi$^{-2SiMe_3}$)$GaFc_2$ (**139**) formed as the major species in these reactions as observed by $^1$H NMR spectroscopy. However, isolation of the pure species proved to be challenging and only low yields of 21% for **138** and 33% for **139** could be obtained. These yields are lower than the yields of **102-105** [51% for (Mamx)$AlFc_2$ (**102**), 49% for (Mamx)$GaFc_2$ (**103**), 47% for (*p*-$SiMe_3Ar'$)$AlFc_2$ (**104**), and 41% for (*p*-$SiMe_3Ar'$)$GaFc_2$ (**105**)].

**Scheme 3-8.** Synthesis of (Pytsi$^{-2SiMe_3}$)$AlFc_2$ (**138**) and (Pytsi$^{-2SiMe_3}$)$GaFc_2$ (**139**).

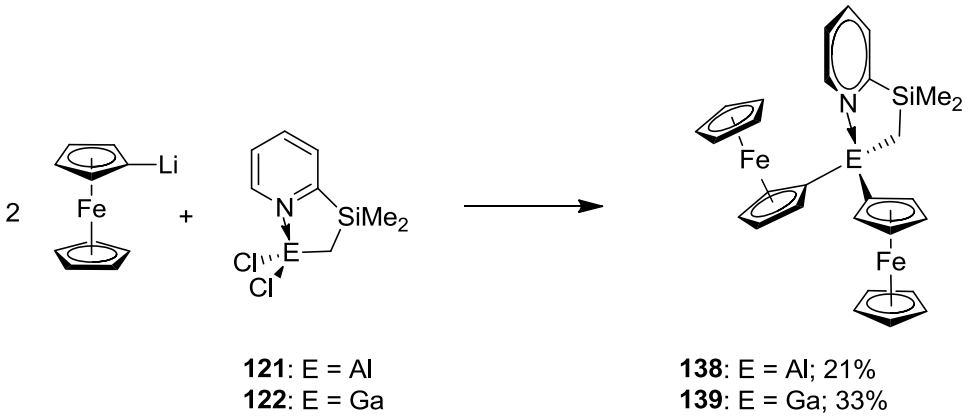


**121**: E = Al
**122**: E = Ga

**138**: E = Al; 21%
**139**: E = Ga; 33%

The $^1$H NMR spectra of **138** and **139** displayed one singlet for the dimethylsilyl group, one singlet for the methylene group and four multiplets for the aromatic protons of the ligand. In the $^1$H NMR spectrum of **139**, one signal was observed for all protons of the unsubstituted Cp rings and two signals were found for the α-protons and two for the β-protons of the Cp rings that are connected to aluminum or gallium. In the case of **138**, two signals overlapped to give four signals in a 2:1:1:5 ratio. The $^1$H and $^{13}$C NMR spectra of **138** and **139** are consistent with $C_s$-symmetry of these species in solution.

Therefore, it was concluded that the ferrocenyl groups rotate fast. The identity of both species (**138** and **139**) was also confirmed by mass spectrometry and their purity was determined by elemental analysis. Elemental analysis revealed **139** to be analytically pure. However, the elemental analysis of **138** showed the presence of minor impurities, possibly hydrolysis products due to the higher sensitivity towards water of aluminum in comparison with gallium. However, it was possible to grow crystals suitable for single-crystal X-ray analysis of **138** from a hexane solution. Dr. K. Harms (University of Marburg) determined the molecular structure of **138** (Figure 36).

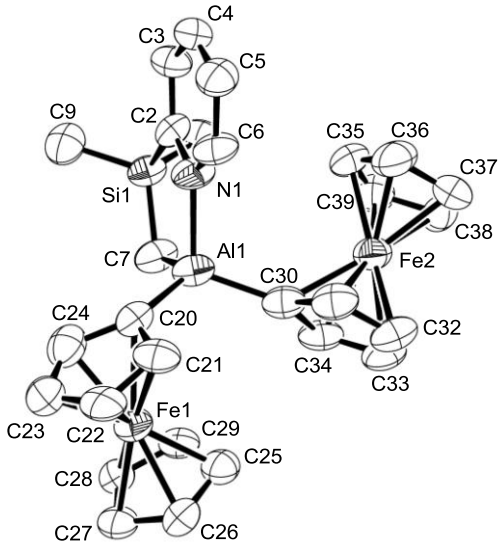


**Figure 3-6.** Molecular structure of (Pytsi$^{-2SiMe_3}$)AlFc$_2$ (**138**) with thermal ellipsoids at the 50% probability level. Hydrogen atoms are omitted for clarity. Selected atom-atom distances [Å] and bond angles [°] (values in braces refer to the second independent molecule that is not shown): Al1-N1 = 2.000(7) {2.034(7)}, Al1-C7 = 1.977(8) {1.980(7)}, Al1-C20 = 1.962(9) {1.962(9)}, Al1-C30 = 1.930(9) {1.950(8)}, Al1···Fe1 = 3.416(3) {3.403(3)}, Al1···Fe2 = 3.667(3) {3.680(3)}, Fe1···Fe2 = 6.045 {6.125}, C7-Al1-C20 = 115.3(4) {114.8(3)}, C7-Al1-C30 = 117.1(3) {118.4(3)}, C7-Al1-N1 = 96.1(3) {94.8(3)}, N1-Al1-C20 = 106.8(3) {106.4(3)}, N1-Al1-C30 = 108.1(3) {108.4(3)}, C20-Al1-C30 = 111.5(3) {111.7(3)}, Al1- C20-Centr$^{C20-C24}$ = 166.7(5) {168.1(5)}, Al1-C30-Centr$^{C30-C34}$ = 177.2(6) {176.3(6)}. Reprinted with permission from Bagh, B.; Breit, N. C.; Harms, K.; Schatte, G.; Burgess, I.; Braunschweig, H.; Müller, J. *Inorg. Chem.* **2012**, *51*, 11155-11167. Copyright 2012 American Chemical Society.

Species **138** crystallized with two independent molecules in the unit cell. The bond length between aluminum and nitrogen or carbon are similar to other aluminum-bridged [1.1]FCPs or bis(ferrocenyl) compounds [Al1–N1 = 2.000(7), 2.034(7) Å in **138**, Al1–N1 = 2.071(2) Å in [(*p*-SiMe$_3$Ar´)Alfc]$_2$ (**79**);[25] Al1–N1 = 2.038(3) Å in (Mamx)AlFc$_2$ (**102**);[6b] Al1–C7 = 1.977(8), 1.980(7)Å in **138**, Al1–C1 = 1.985(3) Å in **79**,[25] and Al1–C = 2.012(3) Å in (Mamx)AlFc$_2$ (**102**)[6b]]. In comparison with (Pytsi$^{-2SiMe_3}$)GaCl$_2$ (**122**) the bite angle of the ligand slightly decreases from 98.79(7)° in (Pytsi$^{-2SiMe_3}$)GaCl$_2$ (**122**) to 96.1(3) and 94.8(3)° in **138**. A similar decrease in the bite angle was exhibited by the Mamx ligand [C1–Ga–N1 = 89.26(9)° in (Mamx)GaCl$_2$, C1–Ga1–N1 = 84.11(15)° in (Mamx)GaFc$_2$ (**103**) and C1–Al1–N1 = 86.87(12)° in (Mamx)AlFc$_2$ (**102**)].[6] It can be presumed that the larger steric requirements of the ferrocenyl groups in comparison with chlorine induce the decrease of the bite angle. An interesting feature exhibited by the molecular structure of **138** is the dip angle α* (Figure 3-7). The dip angle α* is only 2.8(6) and 3.7(6)° for the ferrocenyl moiety (Fe2) close to the pyridyl group, while the dip angle α* is 13.3(5) and 11.9(5)° for the other ferrocenyl moiety (Fe1). The significant bending displayed by Fe1-ferrocenyl moiety can be explained by a direct bonding interaction between the Lewis-acidic aluminum atom and the iron center. Similar bending was previously described for borylferrocenes and increase with an increasing Lewis-acidity of the boron atoms.[12a] The dip angles of Me$_2$BFc (α* = 13.0°) and (HO)MeBFc (α* = 10.3, 10.8, and 12.9°) are comparable to the dip angles of the Fe1-ferrocenyl moiety in **138** [11.9(5) and 13.3(5)°]. In species **102** and **103** the group-13-elements are bent away from the iron center because of the steric interactions with the Mamx ligand, whereas for respective species with the Mamx$^{-tBu}$ ligand dip angles of

5.92° and 2.98° were calculated.[6b] Species **138** is the first bis(ferrocenyl)aluminum compound for which this attraction was derived from single-crystal X-ray diffraction data.

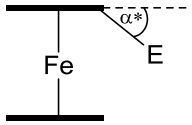


**Figure 3-7.** Definition of the dip angle $\alpha^* = 180 - \alpha(Cp^{centr}–C^{ipso}–E)$.

*Redox Behavior of (Pytsi$^{-2SiMe_3}$)AlFc$_2$ and (Pytsi$^{-2SiMe_3}$)GaFc$_2$*

As mentioned above, one of the major research objectives concerning the aluminum- and gallium-bridged bis(ferrocenyl) compounds was to study their redox behavior. Bis(ferrocenyl) compounds as well as [1.1]FCPs have two iron centers that can be oxidized. However, a significant difference between bis(ferrocenyl) compounds and [1.1]FCPs is that in [1.1]FCPs the ferrocenediyl moieties are rigid, whereas in bis(ferrocenyl) species the ferrocenyl moieties can rotate. If the ferrocenediyl moieties are flexible in ferrocenyl-based polymers, then it would be expected that the redox behavior of bis(ferrocenyl) compounds would be more similar to the redox behavior of ferrocenyl-based polymers than the redox behavior of [1.1]FCPs would be. However, for dimethylsilicon-bridged species the electrochemical communication of the iron-centers in the PFS **34** is more similar to the dimethylsilyl-bridged [1.1]FCP (**15**) than to bis(ferrocenyl)dimethylsilane [$\Delta E_{1/2}$ = 0.23 V for **34** in PhCN / $CH_2Cl_2$,[26] $\Delta E_{1/2}$ = 0.24 V for **15** in PhCN / $CH_2Cl_2$,[26] and $\Delta E_{1/2}$ = 0.15 V for $Me_2SiFc_2$ in $CH_2Cl_2$[10f]]. It will not be possible to directly compare the electrochemical communication of the iron centers ($\Delta E_{1/2}$) in bis(ferrocenyl) aluminum and gallium species and aluminum- and gallium-

bridged [1.1]FCPs with the electrochemical communication of the iron centers ($\Delta E_{1/2}$) in respective polymers. Only the redox behavior of the poly(ferrocenylgallane) equipped with the Mamx ligand (**87$_n$**) was reported and gave two poorly resolved oxidation waves and one broad reduction wave, from which no value for $\Delta E_{1/2}$ could be derived ($E_{1/2}$ = -0.047 V referenced to $FcH/FcH^+$).[6a] In order to conclude which model-compound, a gallium-bridged [1.1]FCP or a bis(ferrocenyl)gallane would have a more similar redox-behavior to the poly(ferrocenylgallane), more electrochemical data about poly(ferrocenylgallane)s would be required. However, we wanted to study the redox behavior of the bis(ferrocenyl)alumanes and bis(ferrocenyl)gallanes and compare them with the redox behavior of aluminum- and gallium-bridged [1.1]FCPs. Moreover, we intended to investigate the influence of different ligands on the group-13 element on the electrochemical communication between the ferrocenyl moieties in the bis(ferrocenyl) species.

The redox behavior of **138** and **139** was studied with glassy carbon as a working electrode, silver wire as a quasi reference electrode, gold as an auxiliary electrode, and $[Bu_4N][PF_6]$ as the electrolyte. During the course of the investigations, two different solvents (thf and $CH_2Cl_2$) were used and it was found that these solvents had a crucial effect on the observed behavior. The redox behavior of **138** and **139** is discussed separately, because **138** exhibited a complex redox behavior. The redox behavior of the gallium species **139** is described first. Cyclic voltammetry measurement of **139** in $CH_2Cl_2$ clearly showed two redox events (Figures 3-8).

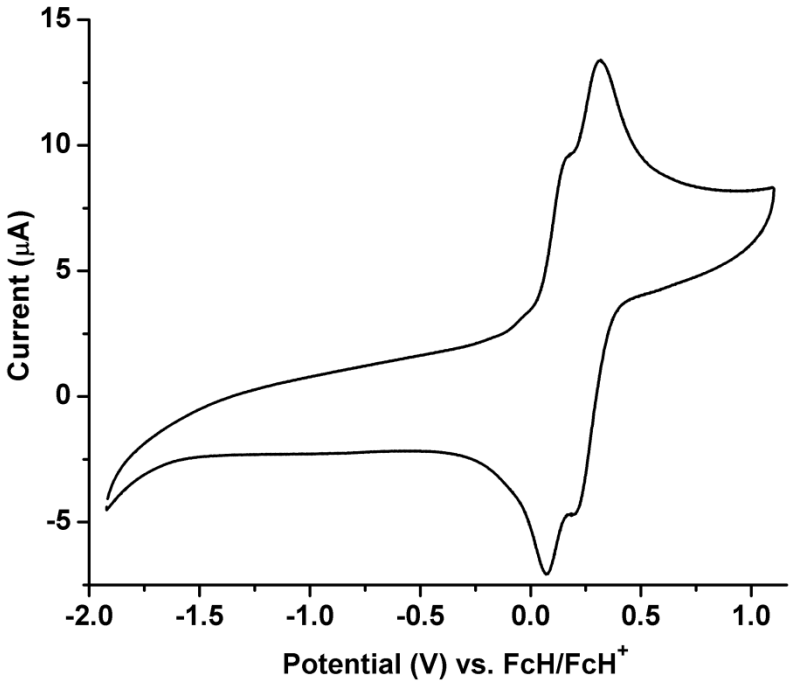


**Figure 3-8.** Cyclic voltammogram of (Pytsi$^{-2SiMe_3}$)$GaFc_2$ (**139**) in $CH_2Cl_2$ referenced to $FcH/FcH^+$. Reprinted with permission from Bagh, B.; Breit, N. C.; Harms, K.; Schatte, G.; Burgess, I.; Braunschweig, H.; Müller, J. *Inorg. Chem.* **2012**, *51*, 11155-11167. Copyright 2012 American Chemical Society.

The small value of $\Delta E_{1/2}$ for **139** with 0.139 V demonstrates that the ferrocenyl moieties are weakly interacting. This value is very close to the $\Delta E_{1/2}$ value of (*p*-$SiMe_3Ar'$)$GaFc_2$ (**105**) with 0.138 V and both are about 0.02 V smaller than those of (Mamx)$GaFc_2$ (**103**) (Table 3-3).

**Table 3-3.** Comparison of the electrochemical data of a variety of aluminum- and gallium-bridged [1.1]FCPs and bis(ferrocenyl) compounds in $CH_2Cl_2$ referenced to $FcH/FcH^+$.[25]

| | [1.1]FCPs | | | Bis(ferrocenyl) compound | | | | | |
|---|---|---|---|---|---|---|---|---|---|
| ligand | Ar′ | *p*-$SiMe_3$-Ar′ | | *p*-$SiMe_3$-Ar′ | | Pytsi$^{-2SiMe_3}$ | | Mamx | |
| E | Ga | Al | Ga | Al | Ga | Al | Ga | Al | Ga |
| **Nr** | **78** | **79** | **80** | **104** | **105** | **138** | **139** | **102** | **103** |
| $E_{1/2}^1$ [V] | 0.05 | -0.099 | -0.049 | 0.249 | -0.002 | 0.035 | 0.117 | -0.032 | 0.044 |
| $E_{1/2}^2$ [V] | 0.25 | 0.233 | 0.260 | - | 0.136 | 0.235 | 0.256 | 0.135 | 0.201 |
| $\Delta E_{1/2}$ [V] | 0.20 | 0.332 | 0.309 | - | 0.138 | 0.200 | 0.139 | 0.167 | 0.157 |

It was found that the degree of electrochemical communication between the iron centers is smaller in bis(ferrocenyl)gallium compounds than in gallium-bridged [1.1]FCPs, which is in agreement with the redox behavior observed for similar compounds with different element-bridges like silicon (see above) and carbon ($\Delta E_{1/2}$ = 0.20 V for **13**[27] and $\Delta E_{1/2}$ = 0.10 V for $Fc_2CH_2$[9h]). Bis(ferrocenyl) aluminum or gallium compounds equipped with the Mamx ligand, **102** and **103** show two different orientations of the ferrocenyl moieties in the solid-state structure.[6b] The Fe···Fe distances in the solid-state structures of **102** and **103** are very similar to each other (**102**: 5.683(7) Å; **103**: 5.594(9) Å).[6b] Therefore, it can be assumed that there are only minor changes in the Fe···Fe distance, when the ferrocenyl moieties rotate around the group-13-element-Cp bond. The Fe···Fe distance of (Mamx)$GaFc_2$ (**103**) is with 5.594(9) Å comparable to the respective distance in the gallium-bridged [1.1]FCPs **80** with 5.4277(8)Å.[25] For these species with similar Fe···Fe distances, significantly different $\Delta E_{1/2}$ values were observed ($\Delta E_{1/2}$ = 0.309 V for **80** and $\Delta E_{1/2}$ = 0.157 V for **103**).[25] The Fe···Fe distance of **139** is expected to be similar to its aluminum homologue **138** with 6.045(2) and 6.125(2) Å. For this increased Fe···Fe distance in comparison with **103**, the smallest $\Delta E_{1/2}$ value with 0.139 V was found.

In principle, this data can be interpreted in the way that a communication of the charge of the iron centers occurs through space as well as through bonds. The communication through space can be suggested based on the examples of **103** and **139**, for which a decreased electronic communication was observed with increasing Fe···Fe distance (see above). However, the Fe···Fe distance cannot be the only influence on the $\Delta E_{1/2}$ values as seen for the comparison of **103** and **80** above. One possible interpretation

for the observed stronger communication of the charge on the iron centers in [1.1]FCPs than in bis(ferrocenyl) compounds is the communication through bonds, since the [1.1]FCPs have two bonds between the ferrocenediyl moieties, whereas only one bond bridges the ferrocenyl moieties in bis(ferrocenyl) compounds. However, there are also other possible reasons for the decreased electrochemical communication between the iron centers in bis(ferrocenyl) compounds compared with [1.1]FCPs. The flexibility of the ferrocenyl moieties in bis(ferrocenyl) compounds can be reasoned to lead to a stronger solvation of the iron centers than in the rigid, less accessible iron centers of [1.1]FCPs. Particularly the space in between the iron centers is not available for solvents in [1.1]FCPs. This might lead to an increased screening of the charge in the monocationic bis(ferrocenyl) species and thus decreased electronic communication. Moreover, if the ferrocenyl moieties are in *trans* orientation like in **102** or **138**, the electron density of the Cp rings is in between the iron centers, which could increase the screening of charges.

The cyclic voltammogram of **139** measured with thf as a solvent displays only one redox wave (Figure 3-9). No communication between the iron centers and thus a class I behavior according to Robin-Day classification is observed.[23] A significant influence of the solvent on the redox properties of redox active compounds was previously described. Geiger *et al.* investigated the influence of a variety of parameters including different solvents on the redox behavior of bis(fulvalene)dinickel and found that solvents of low polarity and low donor number gave the highest $\Delta E_{1/2}$ values.[28] This led to an absolute decrease of $\Delta E_{1/2}$ by 0.073 V when thf was used as a solvent instead of $CH_2Cl_2$ in the presence of the electrolyte $[Bu_4N][PF_6]$.[28] For the gallium-bridged [1.1]FCP equipped with the *p*-$SiMe_3$Ar′ ligand, a decrease in the $\Delta E_{1/2}$ value of 0.091 V

was observed when thf was used instead of $CH_2Cl_2$.[25] This decrease of the $\Delta E_{1/2}$ value may even be higher for bis(ferrocenyl) compounds than for [1.1]FCPs, because bis(ferrocenyl) compounds have more space at the ferrocenyl moieties for the solvation of the stronger donor solvent and thus the effect might be increased. The bis(ferrocenyl)gallium compounds have low $\Delta E_{1/2}$ values between 0.138 and 0.157 in $CH_2Cl_2$ as a solvent (Table 3-4). Therefore, it can be understood that a decrease in the $\Delta E_{1/2}$ values by 0.07-0.09 V has a significant effect so that the redox events are getting so close that they overlap and only one broad redox wave is observed.

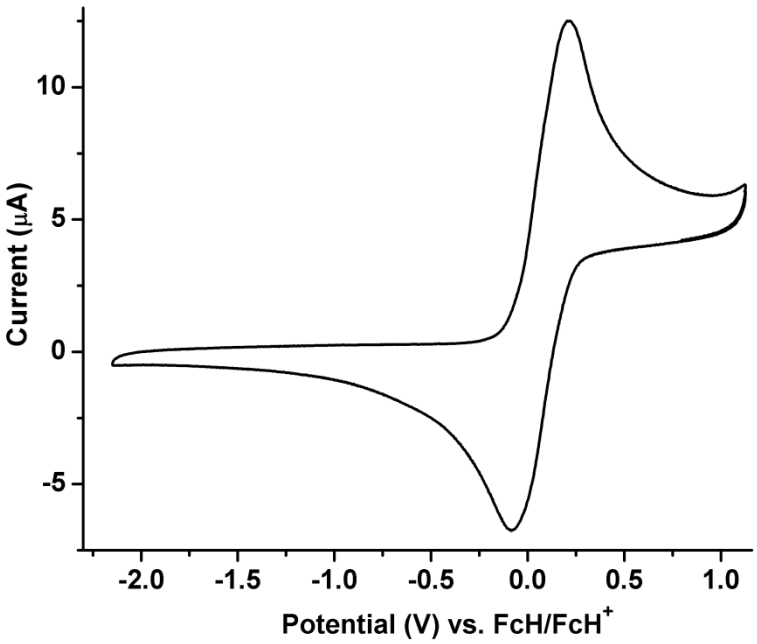


**Figure 3-9.** Cyclic voltammogram of (Pytsi$^{-2SiMe_3}$)$GaFc_2$ (**139**) in thf referenced to $FcH/FcH^+$. Reprinted with permission from Bagh, B.; Breit, N. C.; Harms, K.; Schatte, G.; Burgess, I.; Braunschweig, H.; Müller, J. *Inorg. Chem.* **2012**, *51*, 11155-11167. Copyright 2012 American Chemical Society.

Species **138** showed two major asymmetric redox waves of which the second redox wave was significantly more intense and a minor redox wave at higher potentials (Figure 3-10). This asymmetry of the first and second redox event was previously

observed for the aluminum-bridged [1.1]FCP **79**.[25] Possible reasons for this asymmetry, which was not observed for gallium, are the higher Lewis-acidity and altogether higher sensitivity of aluminum in comparison with gallium. Reactions of **138** or $\mathbf{138}^{+}$ with moisture or fluorine from the electrolyte $[Bu_4N][PF_6]$ could lead to a product that would get oxidized at similar oxidation potentials as $\mathbf{138}^{+}$. However, it can be excluded that a ferrocene impurity would have led to the higher intensity of the second redox wave since the half wave of the second redox wave of **138** is with 0.235 V significantly higher than the half wave potential of ferrocene at 0.000 V. The cyclic voltammogram of (Mamx)$AlFc_2$ (**102**) showed a significantly smaller asymmetry than the cyclic voltammogram of **138**.[25] The smaller asymmetry of **102** can be attributed to the more sterically bulky ligand Mamx in **102**. The sterical bulk of the Mamx ligand is close to the possible fifth coordination site of the aluminum, where an attack would be expected to occur. The cyclic voltammogram of (*p*-$SiMe_3$Ar´)$AlFc_2$ (**104**) exhibited for unknown reasons only one redox wave in $CH_2Cl_2$.[25]

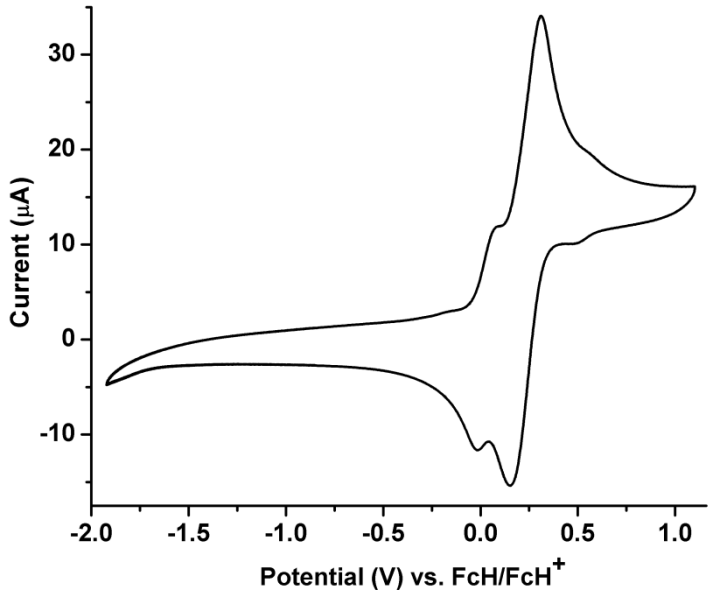


**Figure 3-10.** Cyclic voltammogram of (Pytsi$^{-2SiMe_3}$)$AlFc_2$ (**138**) in $CH_2Cl_2$ referenced to $FcH/FcH^+$. Reprinted with permission from Bagh, B.; Breit, N. C.; Harms, K.; Schatte, G.; Burgess, I.; Braunschweig, H.; Müller, J. *Inorg. Chem.* **2012**, *51*, 11155-11167. Copyright 2012 American Chemical Society.

Since the second oxidation wave of **138** is likely due to a combination of oxidation events, the $\Delta E_{1/2}$ value of **138** needs to be taken with caution. The $\Delta E_{1/2}$ value of **138** would amount to 0.200 V, which is significantly higher than for the respective gallium species **139** with $\Delta E_{1/2}$ = 0.139 V. Only a slightly higher $\Delta E_{1/2}$ value was observed for the related group-13 element bis(ferrocenyl) compounds equipped with the Mamx ligand [$\Delta E_{1/2}$ = 0.167 V for (Mamx)$AlFc_2$ (**102**) $\Delta E_{1/2}$ = 0.157 V for (Mamx)$GaFc_2$, **103**].[25] Similar reactions could be related to the minor redox wave observed for **138** at higher potentials. The aluminum-bridged [1.1]FCP **79** exhibited additional reactions as well, which became manifest in additional reduction waves.[25] Cyclic voltammetry measurements of **138** in thf gave rise to one redox wave similar to the respective gallium species **139**.

The results described in Chapter 3.2.3 were recently published in Inorganic Chemistry.[25]

### 3.2.4 Discussion about the Influence of the Steric Bulk of the Ligand on the Outcome of the Salt-Metathesis Reaction

Prior to the investigations reported in this thesis, it was found that salt-metathesis reactions of 1,1'-dilithiometallocenes and aluminum and gallium dichlorides gave rise to [1]MCPs, when sterically bulky ligands were utilized and [1.1]FCPs, when non sterically bulky ligands were used.[2] Salt-metathesis reactions between 1,1'-dilithiometallocenes and aluminum and gallium dichlorides equipped with the new ligands of moderate steric bulk gave rise to oligomers and polymers in all cases along with [1]MCPs or [1.1]FCPs depending on the ligand (see Chapters 2.2.1-2.2.3). Based on the presence of the poly(ferrocenes) **129$_n$-134$_n$** already at an early time of the reaction, it was assumed that at least a part of the poly(ferrocenes) formed by polycondensation reactions. The formation of polycondensation prodcuts was neither described for salt-metatheis reactions when the sterically bulky ligands $Me_2$Ntsi and Pytsi nor, when the non sterically bulky ligands Ar´ and *p*-Si$Me_3$Ar´ were employed. The polycondensation route appears to be only available in salt-metathesis reactions with 1,1'-dilithioferrocene, when ligands with moderate steric bulk are utilized.

The results discussed in Chapters 2.2.1-2.2.3 reinforce the theory that the outcome of salt-metathesis reactions between 1,1'-dilithiometallocenes with aluminum and gallium dihalides depends on the steric bulk of the ligand attached to the group-13 element. Based on the observations described above, the theory says that sterically bulky ligands give [1]FCPs, slim ligands give [1.1]FCPs, and ligands with moderate steric bulk give

preferably polycondensation products. This theory would suggest then, that the steric bulk of the Pytsi$^{-SiMe_2}$ ligand is larger than for the Mx ligand, which is larger than for the Pytsi$^{-2SiMe_3}$ ligand, because with the Pytsi$^{-SiMe_2}$ ligand [1]FCPs and polycondensation products were obtained, with the Mx ligand [1]FCPs, [1.1]FCPs and polycondensation products were obtained, and for the Pytsi$^{-2SiMe_3}$ ligand [1.1]FCPs and polycondensation products were obtained. This fits well with the assumed differences of the steric bulk of the different ligands.

Speculations about how the steric bulk of the ligands attached to aluminum and gallium could possibly influence the outcome of the salt-metathesis reaction are discussed below based on the crystallographic data and kinetical considerations. The electronic properties of the ligand might also have an influence on the outcome of the salt-metathesis reaction. However, no clear connection between the electronic properties of a ligand and the outcome of the salt-metathesis reaction was observed to date. Therefore, electronic contributions are not considered in the discussion below.

The distance of the ligand to the ferrocenyl moieties in the different products can be determined by single-crystal X-ray analysis. The shortest distances were found between the ligand and the α-protons of the cyclopentadienyl rings and they might have a significant influence on the formation of the product. Naturally, with an increasing steric bulk of the ligand, the repulsion increases as the distances between the ligand and the ferrocenyl moity decreases. The three products [1]FCP, [1.1]FCP and ferrocenyl-based oligomers have the ligands arranged in different ways (Figure 3-11). The arrangement of the ligands was observed by the solid-state structures of **77**-**80**, **81**-**86**, and **102**, **103**, and **138** and are shown for the example of the Mamx ligand in Figure 3-10.

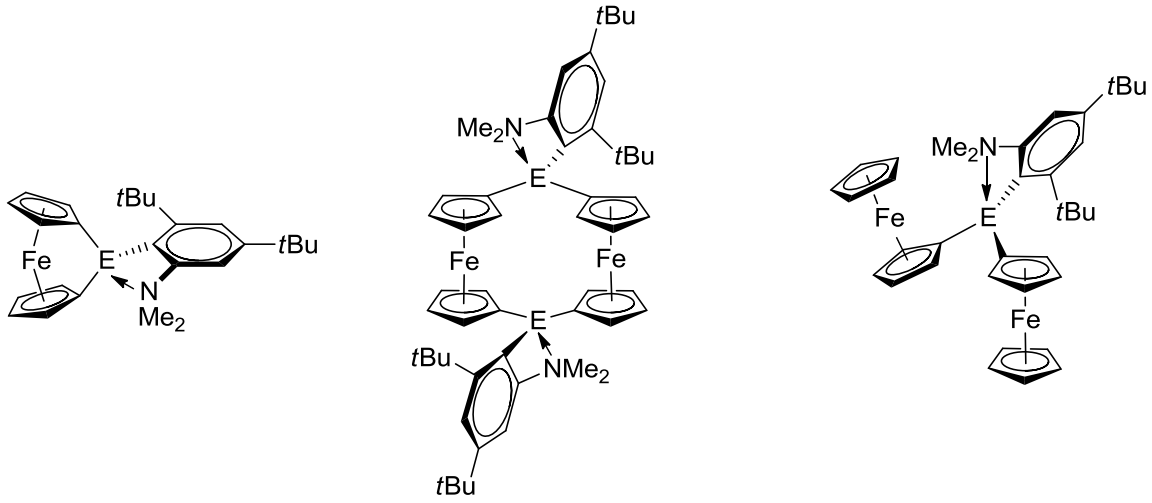


**Figure 3-11.** Different arrangement of ligands in [1]FCPs, [1.1]FCPs and bis(ferrocenyl) compounds as model compounds for oligomers shown with the Mx ligand.

In [1]FCPs, the ring formed between the ligand and the group-13 element is approximately parallel to the cyclopentadienyl-rings and their protons, whereas in [1.1]FCPs the ring formed between the ligand and the group-13 element is perpendicular to the cyclopentadienyl rings and their protons. That the perpendicular arrangement leads to closer proximities of the sterically bulky groups of the ligand and the protons of the Cp ring was neatly shown by our group for the $Me_2$Ntsi ligand (Figure 3-12).[29] For the $Me_2$Ntsi ligand, a [1.1]FCP was formed with indium as a bridging element, while with aluminum and gallium as bridging elements, [1]FCPs were obtained. Therefore, the closest distances between the ligand and the cyclopentadienyl protons that were detected in the molecular structures could be compared [H···H distances in ($Me_2$Ntsi)In[1.1]FCP (**107**) are 2.15, 2.35, 2.36, and 2.38 Å ($SiMe_3$···RH);[29] H···H distances in ($Me_2$Ntsi)Ga[1]FCP (**84**) are 2.28 and 2.44 Å ($SiMe_3$···R-H) and 2.35 and 2.53 Å ($NMe_2$···R-H)][2c] (Figure 3-11). In this comparison one needs to take into account that in a gallium-bridged [1.1]FCP equipped with the $Me_2$Ntsi ligand the distances would be even

shorter due to the gallium-carbon bonds being shorter than the indium-carbon bonds (In···C in **107**: 2.173(4), 2.160(5), and 2.291(4) Å; Ga···C in **84** 2.008(3), 2.017(3), and 2.048(3)Å). At least for the example of the $Me_2$Ntsi ligand, it can clearly be shown that the shortest distances between the ligand and the ferrocenyl moiety are larger in [1]FCPs than in [1.1]FCPs. This suggests that the unfavorable interactions of bulky ligands with Cp-protons is stronger in [1.1]FCPs than in [1]FCPs.

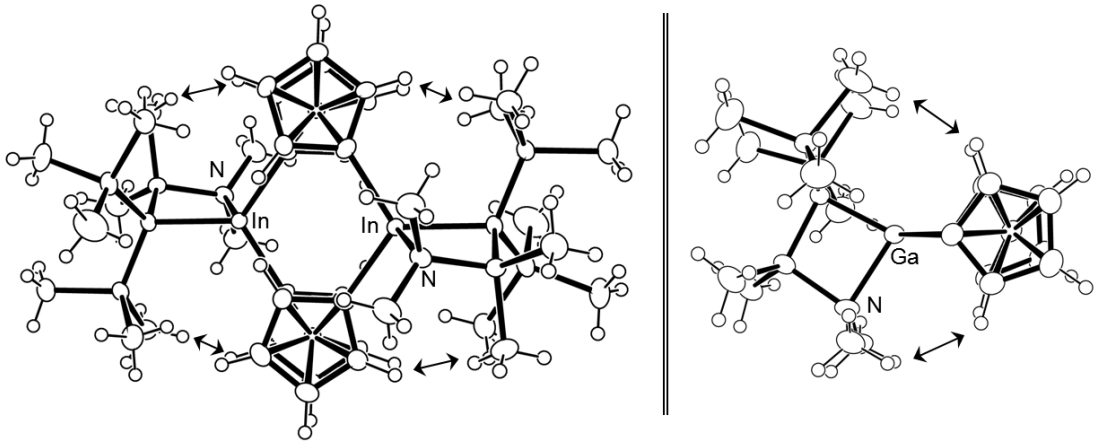


**Figure 3-12.** Comparison of the molecular structures in the solid state of the indium-bridged [1.1]FCP (**107**) and the gallium-bridged [1]FCP (**84**) equipped with the $Me_2$Ntsi ligand. Reprinted with permission from Schachner, J. A.; Lund, C. L.; Burgess, I. J.; Quail, J. W.; Schatte, G.; Müller, J. *Organometallics* **2008**, *27*, 4703-4710. Copyright 2008 American Chemical Society.

The arrangement of the ligand towards the ferrocenediyl moieties is more flexible in oligomers and bisferrocenyl compounds than in [1]FCPs or [1.1]FCPs. No molecular structure in the solid state was reported for any heavier group-13-element-bridged ferrocenyl-based oligomers. Therefore, bis(ferrocenyl) compounds are used as model compounds. Particularly interesting is the comparison of sterically bulky ligands on aluminum or gallium with slim ligands in bis(ferrocenyl) compounds, which was done

using DFT calculations in our group.[6b] In this publication, aluminum- and gallium-bridged bis(ferrocenyl) compounds with the Mamx ligand **102** and **103** were compared to similar species with the Mamx$^{-t\mathrm{Bu}}$ ligand, which is based on the Mamx ligand with the *ortho*-*tert*-butyl group being removed, **102**$^{-t\mathbf{Bu}}$ and **103**$^{-t\mathbf{Bu}}$ (Figure 3-13).

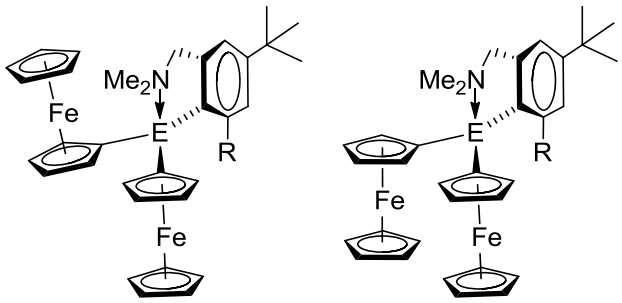


**102**: E = Al, R = *t*Bu
**103**: E = Ga, R = *t*Bu
**102**$^{-t\mathbf{Bu}}$: E = Al, R = H
**103**$^{-t\mathbf{Bu}}$: E = Ga, R = H

**Figure 3-13.** Depiction of the aluminum and gallium bis(ferrocenyl) compounds equipped with the Mamx or Mamx$^{-t\mathrm{Bu}}$ ligand, **102**, **103**, **102**$^{-t\mathbf{Bu}}$, and **103**$^{-t\mathbf{Bu}}$.

A sign for the larger strain in these aluminum- and gallium-bridged bis(ferrocenyl) compounds equipped with the Mamx ligand compared to those decorated with the Mamx$^{-t\mathrm{Bu}}$ ligand can be seen by the different dip angles α* observed for one of the ferrocenyl moieties (Figure 3-7).[6b] In the calculated structures of the bis(ferrocenyl) species with the Mamx$^{-t\mathrm{Bu}}$ ligand (**102**$^{-t\mathbf{Bu}}$ and **103**$^{-t\mathbf{Bu}}$) the group-13 element is bent towards one of the iron centers, whereas in the bis(ferrocenyl) species with the Mamx ligand, the group-13 element is bent away from the iron center. It is not possible any longer for the group-13 element to act upon the favorable attraction to the iron center due to the repulsion of the *ortho tert*-butyl group and the ferrocenyl moiety. The difference of the dip angles with aluminum equals 14.27°, whereas in the less Lewis-acidic gallium species the difference in dip angles amounts to 10.46°. For the other ferrocenyl moiety no

major change was observed when the Mamx-containing compound was compared with the Mamx$^{-t\text{Bu}}$ species, which shows that only one ferrocenyl moiety has steric interactions with the ligand.

The crystallographic data discussed above shows that more space for the ligands is available in [1]FCPs, followed by oligomers and after that [1.1]FCPs. Neglecting any entropic effect, this can explain that for sterically bulky ligands, oligomers are more thermally stable than [1.1]FCPs. Whereas for slim ligands on aluminum or gallium, for which no or only little steric interaction with the α-Cp protons in [1.1]FCPs occurs, the [1.1]FCPs are reasoned to be more thermodynamically stable than [1]FCPs. [1]FCPs are less thermally stable than [1.1]FCPs, because [1]FCPs incorporate ring strain based on the tilting of the Cp rings.

However, the salt-metathesis reaction is not an equilibrium reaction and the product formation is kinetically controlled. No kinetic study of this salt-metathesis reaction with aluminum or gallium was carried out. Therefore, it can only be speculated about the pathways of product formation and possible influences of the ligand. Scheme 3-9 shows the assumed basic steps of the kinetically controlled formation of [1]FCPs, [1.1]FCPs, ferrocenyl-based oligomers and polymers by salt-metathesis reactions and some considerations about these formations and the influence of the steric bulk of the ligand are given below.

**Scheme 3-9.** Suggested basic steps for the formation of [1]FCPs, [1.1]FCPs, metallopolymers and oligomers.

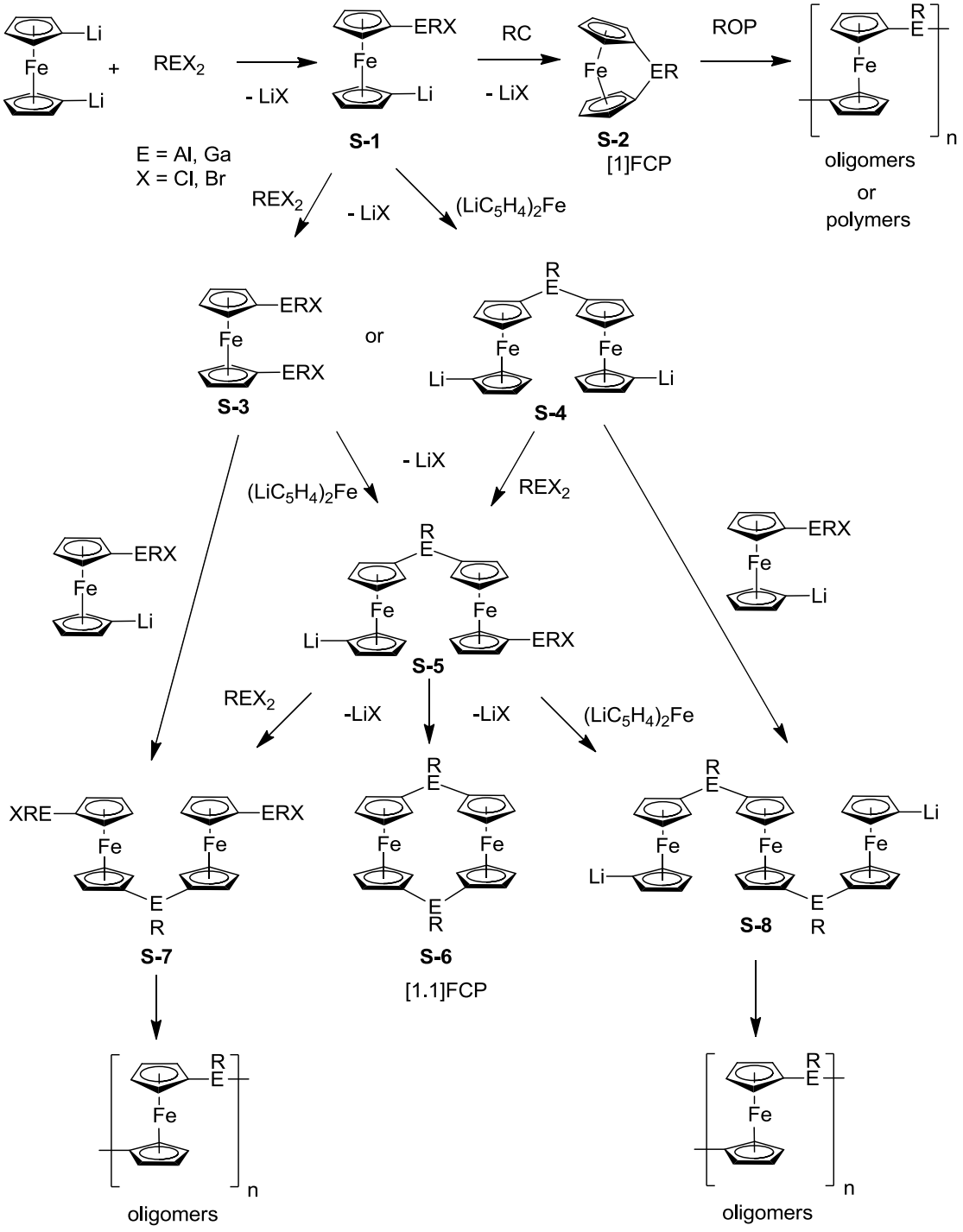


The first step is a reaction of 1,1'-dilithioferrocene with a group-13-element dihalide to form one group-13-element-carbon-bond in **S-1** and lithium halide. If the ring-

closing step has the transition state of the lowest energy, then a [1]FCP (**S-2**) is selectively formed. The [1]FCP can than undergo ROP to give metallopolymers or oligomers. The other option is a reaction of **S-1** with 1,1'-dilithioferrocene or the element dihalide. If any of these two reactions would have a significantly lower energy barrier than the ring-closing, no considerable amount of a [1]FCP could be obtained. As 1,1'-dilithioferrocene is usually suspended in solution and the element dihalide is dissolved in solution, the concentration of element dihalide is much higher. Therefore, it is more likely that the intermolecular reaction with the group-13-element dihalide competes with the intramolecular reaction. The steric bulk of the ligand can influence two factors. On the one hand, it can partly shield the lithium atom on **S-1** thus slow down the competing intermolecular reaction to give **S-3** or **S-4**. It is possible that the chlorine on the group-13 element is coordinating to the lithium atom. For example in the 1,1'-diindaferrocene **108**, a coordination between the chlorine and the indium was observed.[2b] This could leave the lithium atom in close proximity to the sterically bulky ligand and an incoming aluminum or gallium dihalide might cause some steric repulsion, which might increase the activation barrier for this step. This could explain why the formation of **S-3** is not favored with sterically bulky ligands. If the reaction of **S-1** would proceed by the reaction with 1,1'-dilithioferrocene, then a similar repulsion of the ligand with the ferrocenediyl moieties can be expected that renders the activation energy high. The absence of these repulsions with slim ligands might be expected to favor the intermolecular reaction. [1]FCP incorporate strain based on the tilting of the cyclopentadienyl rings[30] and it is likely, that the transition state also contains a part of that strain that increases its energy and kinetically disfavors this intramolecular reaction. The intramolecular reaction

generally has the advantage that the reactants are already present making it a first order reaction. In intermolecular reactions a delay occurs that is related to the two species having to meet each other in solution and a dependency on their concentration according to a second order reaction.

After an intermolecular reaction, the next step for the formation of a [1.1]FCP is the reaction of **S-3** or **S-4** with 1,1'-dilithioferrocene or the element dihalide to give **S-5**. At this point a competition between intra- and intermolecular reactions results in the formation of a [1.1]FCP or oligomeric species. The experiments with aluminum and gallium compounds equipped with slim ligands resulted selectively in the formation of [1.1]FCP and oligomeric species were not found.[2d] Therefore, it can be concluded that this pathway is kinetically favored. This could be due to the reacting groups being already in close proximity to each other. However, the ligand could have an influence on how fast the intramolecular reaction is in comparison with an intermolecular reaction. The outer α-protons of a [1.1]FCP experience steric repulsion from the ligand depending on the steric requirements of the ligand. If there is a strong interaction of these α-protons with a ligand, then the energy level of the [1.1]FCP should be higher than the one of the oligomer, which is likely to lead to a transition state of higher energy for the [1.1]FCP as well. Therefore, for a more sterically bulky ligand on aluminum or gallium, the formation of oligomers instead of [1.1]FCPs might be kinetically favored as it is assumed that the transition state to form the oligomers is experiencing less steric interactions of the ligand with the Cp-rings similar to the final products. Moreover, it is possible that already earlier from **S-3** or **S-4** a reaction with **S-1** occurs, which would lead to the formation of oligomers. However, the concentration of **S-1** in comparison with other reactive species

is expected to be significantly lower. Therefore, it is unlikely that the reaction of **S-3** or **S-4** with **S-1** has any major influence on the outcome of the salt-metathesis reaction and it can be neglected.

It was observed for the ligands of moderate steric bulk, that polycondensation products form. Based on the assumed mechanism (Scheme 3-3) and on the speculations above on influences of the steric bulk to different kinetic constants this observation can be reasoned the following: The moderate steric bulk of the ligand on aluminum or gallium is not enough to inhibit the intermolecular reaction of **S-1** to form **S-3** or **S-4** instead of the [1]FCP (**S-2**). However, the moderate steric bulk of the ligand is too high for [1.1]FCPs to form selectively over polycondensation products. The Pytsi$^{\text{-SiMe}_2}$ ligand is too sterically bulky to allow the formation of any [1.1]FCP (**S-5**).

### 3.3 Conclusion

Salt-metathesis reactions of 1,1'-dilithioferrocene with the different aluminum- and gallium dihalides, **111**-**113**, **124**, **126**, **120**, and **121** were carried out yielding aluminum- or gallium-bridged [1]FCPs, [1.1]FCPs, and polymers. The different outcome of these salt-metathesis reactions can be rationalized by the differences in the steric bulk of the ligand.

When the Pytsi$^{-SiMe_2}$ ligand with a moderate to high steric bulk was utilized during the salt-metathesis reaction, the [1]FCPs **129** and **130** and the low-molecular-weight polymers $\mathbf{129_n}$ and $\mathbf{130_n}$ were obtained. Since the [1]FCPs **129** and **130** were not isolable, the source of their assumed ROP could not be investigated. However, based on the $^1$H NMR data of the salt-metathesis reaction after a few hours, it appears that one part of the oligomers or low-molecular-weight polymers was formed by polycondensation reactions.

In the presence of the Mx ligand with a moderate steric bulk, salt-metathesis reactions gave rise to a gallium-bridged [1]FCP (**131**) and a gallium-bridged [1]RCPs (**132**), the aluminum- and gallium-bridged [1.1]FCPs $\mathbf{131_2}$ and $\mathbf{133_2}$ as well as the low-molecular-weight polymers $\mathbf{131_n}$, $\mathbf{132_n}$, and $\mathbf{134_n}$ and the high-molecular weight polymer $\mathbf{133_n}$. Similar to **129** and **130**, the [1]MCPs **131** and **132** were not isolable and reacted by ROP. An interesting difference was found in the outcome of these salt metathesis reactions depending on the bridging element and the metal center that was not previously observed with sterically bulky ligands.

The steric bulk of the Pytsi$^{-2SiMe_3}$ ligand was not enough to yield aluminum- and gallium-bridged [1]FCPs in salt-metathesis reactions. A mixture of aluminum- and gallium-bridged [1.1]FCPs (**136** and **135)** and ferrocenyl-based oligomers ($\mathbf{136_n}$ and $\mathbf{135_n}$) was formed. Neither of these products could be isolated.

The theory that the outcome of these salt-metathesis reactions depends on the steric bulk of the ligand was verified by these results and extended to ligands of moderate steric bulk. The formation of low-molecular-weight polymers or oligomers in all cases with the exception of **133$_n$** suggests that undesired polycondensation reactions are taking place. Moreover, the formed [1]MCPs are not stable under the applied conditions. These two facts lead to the conclusion that none of these ligands, Pytsi$^{-SiMe_2}$, Pytsi$^{-2SiMe_3}$, and Mx, is the right choice for the synthesis of isolable [1]MCPs that can be ring-open polymerized in a controlled manner. Moreover, it is suggested that future investigations into aluminum- and gallium-bridged [1]MCPs and their ROP will concentrate on other ways to reach this goal.

Bis(ferrocenyl) compounds with aluminum and gallium equipped with the Pytsi$^{-2SiMe_3}$ ligand (**138** and **139**) were synthesized and electrochemically studied. Similar to bis(ferrocenyl) species and [1.1]FCPs with other bridging elements, significantly smaller $\Delta E_{1/2}$ values were observed. It would be interesting to study the electrochemistry of another poly(ferrocenylgallane) for example **131$_n$** in order to check if gallium-bridged [1.1]FCPs are better model compound for the redox behavior of gallium-bridged polymers in comparison with bis(ferrocenyl)gallanes.

### 3.4 Experimental

**General information.** Manipulations were done using standard Schlenk and glovebox techniques ($N_2$ as inert gas), unless noted differently. Solvents were dried using a MBraun solvent purification system ($Et_2O$, thf, toluene, hexanes) or distilled from sodium and benzophenone ($C_6H_6$) and stored under nitrogen over 3 or 4 Å molecular sieves. Solvents for NMR measurements were degassed through freeze-pump-thaw procedures and stored under nitrogen over 4 Å molecular sieves. Mass spectra were measured on a VG 70SE and are reported in the form m/z (rel intens) [$M^+$] where 'm/z' is the mass observed, 'rel intens' is the intensity of the peak relative to the most intense peak and '$M^+$' is the molecular ion or fragment; only characteristic mass peaks are reported. For isotopic patterns, only the mass peak of the isotopoloque or isotope with the highest natural abundance is listed. Elemental analyses were carried out at the SSSC at the University of Saskatchewan using a Perkin-Elmer 2400 CHN elemental analyzer; $V_2O_5$ was added to samples to promote combustion. $^1H$ and $^{13}C$ NMR spectra were recorded at 25 °C on a 500 MHz Bruker Avance spectrometer ($^1H$: 500.2 MHz; $^{13}C$: 125.8 MHz). $^1H$ NMR chemical shifts were referenced to the residual protons of the deuterated solvent ($C_6D_6$: δ 7.15; $CDCl_3$: δ 7.26); $^{13}C$ chemical shifts were referenced to δ 128.00 ($C_6D_6$) and 77.00 ($CDCl_3$), respectively. C atoms directly bound to Al or Ga were not detected by $^{13}C$ NMR spectroscopy. The absence of signals is presumably due to the effect of the electric quadrupole moment of Al or Ga on the relaxation times of directly bound carbon atoms. Dynamic light scattering experiments were performed using a nano series Malvern zetasizer instrument (equipped with a 633 nm red laser). Samples were filtered twice through 0.2 μm syringe PTFE filters (Millex) before they were analyzed in 1 cm glass cuvettes at concentrations of 2.0 mg $mL^{-1}$, 3.0 mg $mL^{-1}$, and 4.0

mg $mL^{-1}$ in thf at 25 °C for $[(Pytsi^{-SiMe_2})Ga(C_5H_4)Fe(C_5H_4)]_n$ and in concentrations of 2.5 mg $mL^{-1}$ and 5.0 mg $mL^{-1}$ for the $[(Mx)E(C_5H_4)M(C_5H_4)]_n$ species (M = Fe, Ru; E = Al, Ga). The refractive index of the polymers was assumed to be 1.5.

**Chemicals.** The following chemicals were used without further purifications: ferrocene (98%, Aldrich), $RuCl_3 \cdot xH_2O$ (99%, Precious Metals Online), Zn dust (90%, BDH), dicyclopentadiene (95%, Fisher Scientific) and *n*BuLi (2.5 M in hexanes, Acros Organics or Aldrich). The species tmeda (99%, Alfa Aesar) was distilled from sodium and stored over 4 Å molecular sieves. $(LiC_5H_4)_2Fe \cdot 2/3tmeda$,[31] $(LiC_5H_4)_2Fe(thf)_3$,[32] $(LiC_5H_4)FeCp$,[33] $RuCp_2$,[34] and $(LiC_5H_4)_2Ru \cdot tmeda$[35] were synthesized according to literature procedures. The synthesis of the aluminum and gallium dihalides is described in Chapter 2.4.

**Electrochemical measurements.** A computer controlled system, consisting of a HEKA potentiostat PG590 (HEKA, Mahone Bay, NS, Canada) was used for the cyclic voltammetry experiments. Data was collected using a multifunction DAQ card (PCI 6251 M Series, National Instruments Austin, Texas) and in-house software written in the LabVIEW environment. Glassy carbon (BAS, 3mm) was used as the working electrode. The quasi-reference electrode (QRE) was a silver wire and all measurements were made against the QRE and subsequently rescaled to the ferrocene/ferrocenium couple. A loop of gold wire was used as the auxiliary electrode. Before each measurement, 1 mM solutions of were freshly prepared in dry thf or $CH_2Cl_2$ with 0.1 M $[Bu_4N][PF_6]$ as supporting electrolyte. The electrolyte, $[Bu_4N][PF_6]$, was dried overnight under high vacuum at 100 °C. The scan rate was 50 mV/s. All measurements were conducted inside a glovebox and taken at ambient temperature (24 – 25 °C).

**(Pytsi$^{-SiMe_2}$)Ga($C_5H_4$)$_2$Fe (129).** (Pytsi$^{-SiMe_2}$)$GaCl_2$ (0.59 g, 1.5 mmol) in benzene (7 mL) was added to a suspension of ($LiC_5H_4$)$_2$Fe·2/3tmeda (0.43 g, 1.5 mmol) in benzene (8 mL) at 0 °C. After stirring of the reaction mixture for 2.5 h at room temperature, the precipitate was filtered off and a $^1$H NMR spectrum was measured of the filtrate. $^1$H NMR ($C_6D_6$): δ 0.27 (s, 18 H, $SiMe_3$), 4.22 (m, 2 H, α-H, $C_5H_4$), 4.29 (m, 2 H, α-H, $C_5H_4$), 4.62 (m, 4 H, β-H, $C_5H_4$), 6.31 (m, 1 H, 5-H), 6.77 (m, 1 H, 3-H), 6.91 (m, 1 H, 4-H), 7.53 (m, 1 H, 6-H).

**Isolation of [(Pytsi$^{-SiMe_2}$)Ga($C_5H_4$)Fe($C_5H_4$)]$_n$ (129$_n$).** To (Pytsi$^{-SiMe_2}$)$GaCl_2$ (0.40 g, 1.1 mmol) and ($LiC_5H_4$)$_2$Fe(thf)$_3$ (0.49 g, 1.2 mmol) toluene (7 mL) was added. After stirring for 7 h, the precipitate was filtered off. Hexanes (15 mL) were added to the solution and the obtained precipitate was filtered and washed with hexanes (10 mL). After drying in vacuum a slightly orange powder, was obtained (0.12 g, 25%). $^1$H NMR ($CDCl_3$): δ 0.1 (br, 18 H, $SiMe_3$), 3.5–5.0 (br, 8 H, $C_5H_4$), 6.5–7.1 (br, 2 H, Ar-H), 7.05 (br, 2 H, Ar-H), 7.74 (br, 1 H, Ar-H), 8.22 (br, 1 H, Ar-H). Anal. Calcd for $C_{22}H_{30}FeGaNSi_2$ (490.219): C, 53.90; H, 6.17; N, 2.86. Found: C, 54.18; H, 6.12; N, 2.35.

**(Pytsi$^{-SiMe_2}$)Al($C_5H_4$)$_2$Fe (130).** A suspension of ($LiC_5H_4$)$_2$Fe·2/3tmeda (0.55 g, 2.0 mmol) in benzene (18 mL) was added to a solution of (Pytsi$^{-SiMe_2}$)$AlBr_2$ (0.72 g, 1.7 mmol) in benzene (12 mL) at 0 °C. After stirring at room temperature for 3 h a $^1$H NMR spectrum was measured. $^1$H NMR of **130** ($C_6D_6$): δ 0.30 (s, 18 H, $SiMe_3$), 4.10 (m, 2 H, α-H, $C_5H_4$), 4.28 (m, 2 H, α- H, $C_5H_4$), 4.66 (m, 2 H, *β*-H, $C_5H_4$), 4.68 (m, 2 H, *β*-H, $C_5H_4$), 6.24 (pst, 1 H, 5-H), 6.85 (d, 1 H, 3-H), 6.89 (m, 1 H, 4-H), 7.45 (m, 1 H, 6-H).

**(Mx)Ga[1]FCP and [(Mx)Ga($C_5H_4$)Fe($C_5H_4$)]$_n$ (131 and 131$_n$).** A solution of (Mx)$GaCl_2$ (0.755 g, 2.02 mmol) in diethyl ether (30 mL) was added to a suspension of ($LiC_5H_4$)$_2$Fe·2/3tmeda (0.570 g, 2.05 mmol) in diethylether (40 mL) at room temperature. After 1h of stirring an NMR was measured and a mixture of **131** and **131$_n$** was observed. After being stirred for 3 days, all volatiles were removed under vacuum and the product was dissolved in toluene. The precipitate was filtered off and volatiles were removed in vacuum. The product was dissolved in toluene (4 mL) and then it was added dropwise to strongly stirred hexanes (40 mL), in order to precipitate out smaller impurities. The volatiles were removed under vacuum and the product was extracted with hexanes (10 mL). A part of the precipitate (0.245 g) was dissolved in toluene (2 mL) and added dropwise to strongly stirred methanol (50 mL) to yield the pure compound as a powder (0.095 g, 18%). $^1$H NMR ($C_6D_6$) of **131**: δ 1.34 (s, 9H, *t*Bu), 1.48 (s, 9H, $^t$Bu), 2.46 (s, 6H, $Me_2N$), 4.06 (s, 2H, Cp-H), 4.43 (s, 2H, Cp-H), 4.67 (s, 2H, Cp-H), 4.68 (s, 2H, Cp-H), 6.84 (s, 1H, Ar-H), 7.61 (s, 1H, Ar-H). $^1$H NMR ($C_6D_6$) of **131$_n$**: δ 1.29 (s, 9H, $^t$Bu), 1.54 (s, 9H, $^t$Bu), 2.53 (br, 6H, $Me_2N$) 4.2-4.8 (m, 8H, Cp-H), 6.95 (s, 1H, Ar-H), 7.62 (s, 1H, Ar-H).

**[(Mx)Ga($C_5H_4$)Fe($C_5H_4$)]$_2$ (131$_2$).** A solution of (Mx)$GaBr_xCl_{2-x}$ (0.75 g, 2.0 mmol) in toluene (30 mL) was added dropwise to a solution of ($LiC_5H_4$)$_2$Fe·2/3tmeda (0.56 g, 2.0 mmol) in toluene (20 mL) at room temperature. The reaction mixture was stirred for 16 h and solid lithium salt was filtered off. The amount of solvent was reduced under vacuum to approx. 5 mL and the solution was added dropwise to strongly stirred hexane. The solid was filtered off and washed with hexane (6 x 4 mL) and toluene (3 x 2 mL) and died at 50 °C under high vacuum for 3 h to give pure **131$_2$** (0.045 g, 4.6%). $^1$H

NMR ($C_6D_6$) of **131$_2$**: δ 1.33 (s, 18H, *p*-*t*Bu), 1.68 (s, 18H, *o*-*t*Bu), 2.25 (s, 12H, $NMe_2$), 3.94 (pst, 4H, α-Cp), 4.24 (pst, 4H, β-Cp), 4.29 (pst, 4H, β-Cp), 4.64 (pst, 4H, α-Cp), 6.81 (s, 2H, CH-3), 7.42 (s, 2H, CH-5). EIMS (70 eV): *m/z* (rel intens) 972 (100) [$M^+$], 672 (9) [$MH^+$ – Ga(Mx)], 486 (41) [$M^+$ – $(C_5H_4)Fe(C_5H_4)Ga(Mx)$ or $M^{2+}$]. HRMS (EI; *m/z*): calcd for $C_{52}H_{68}Fe_2Ga_2N_2$, 972.2584; found 972.2591 (Δppm = 0.7).

**(Mx)Ga($C_5H_4$)$_2$Ru and [(Mx)Ga($C_5H_4$)Ru($C_5H_4$)]$_n$ (132 and 132$_n$).** A solution of $(Mx)GaCl_2$ (0.65 g, 1.7 mmol) in toluene (15 mL) was added to a suspension of $(LiC_5H_4)_2Ru$·tmeda (0.653 g, 1.75 mmol) in toluene (12 mL) at room temperature. The first flask was washed with toluene (4 mL). The reaction mixture was stirred for 30 min, and then an NMR sample was taken. After being stirred for 2 hours the reaction was filtered and the amount of solvent was reduced to 4 mL under vacuum. The solution was added dropwise to strongly stirred hexanes (20 mL). The precipitate was filtered off and washed with hexanes (4 x 3 mL). The obtained powder was the product (0.145 g, 16%). $^1$H NMR ($C_6D_6$) of **132**: δ 1.33 (s, 9H, $^t$Bu), 1.39 (s, 9H, $^t$Bu), 2.36 (s, 6H, $Me_2N$), 4.12 (s, 2H, Cp-H), 4.54 (s, 2H, Cp-H), 5.34 (s, 4H, Cp-H), 6.80 (s, 1H, Ar-H), 7.58 (s, 1H, Ar-H). $^1$H NMR ($C_6D_6$) of **132$_n$**: δ 1.1-1.8 (br, 18H, $^t$Bu), 2.5-2.9 (br, 6H, $Me_2N$), 3.8-5.5 (br, 8H, Cp-H), 7.60 (br, 1H, Ar-H).

**[(Mx)Al($C_5H_4$)Fe($C_5H_4$)]$_n$ (133$_n$).** A suspension of $(LiC_5H_4)_2Fe$·2/3tmeda (0.835 g, 3.00 mmol) in diethyl ether (40 mL) is added to a solution of $(Mx)AlCl_2$ (0.993 g, 3.01 mmol) in diethyl ether (30 mL) at room temperature. The reaction mixture was stirred for 3h, and then the solid was filtered off. The volatiles were removed under vacuum. The product is dissolved in toluene (4 mL) and the resulting solution is added dropwise to hexanes (40 mL). The solution was filtered and the volatiles were removed under

vacuum. The resulting solid was heated to 60 °C under vacuum for 8h in order to remove impurities. The remaining solid still contained 15% of MxH alongside with the polymeric product **133$_n$** (0.91g, 74% of the mixture; 63% of **133$_n$**). $^1$H NMR ($CDCl_3$): δ 1.34 (br, 9H, *t*Bu), 1.42 (br, 9H, *t*Bu), 2.7-2.9 (br, 6H, $NMe_2$), 4.0-4.6 (br m, 8H, Cp), 6.97 (br, 1H, CH-3), 7.41 (br, 1H, CH-5).

**[(Mx)Al($C_5H_4$)Fe($C_5H_4$)]$_2$ (133$_2$).** A solution of (Mx)$AlCl_2$ (0.533 g, 1.61 mmol) in toluene (22 mL) was added to a suspension of $(LiC_5H_4)_2Fe$·2/3tmeda (0.450 g, 1.61 mmol) in toluene (18 mL) at room temperature. The reaction mixture was stirred for 16 h and then the solid was filtered off. The amount of solvent was reduced under vacuum (6 mL) and the solution is added to hexanes (40 mL). The solid was filtered off and washed with hexane (4 mL). The volatiles of the filtrate were removed under vacuum. The product was dissolved in toluene (2 mL) and precipitated into hexane (20 mL). The two solids were united and toluene (8 mL) was added. The suspension was heated to reflux for 3h. The suspension is allowed to get to room temperature and the solution was separated. The solid was dried under vacuum to give **133$_2$** (0.025 g, 3.5%). $^1$H NMR ($CDCl_3$): δ 1.34 (s, 18H, *t*Bu), 1.70 (s, 18H, *t*Bu), 2.33 (s, 12H, $NMe_2$), 3.86 (pst, 4H, α-Cp), 4.22 (pst, 4H, β-Cp), 4.28 (spt, 4H, β-Cp), 4.69 (pst, 4H, α-Cp), 6.84 (s, 2H, CH-3), 7.43 (s, 2H, CH-5).

**[(Mx)Al($C_5H_4$)Ru($C_5H_4$)]$_n$ (134$_n$).** A solution of (Mx)$AlCl_2$ (0.520 g, 1.58 mmol) in toluene (15 mL) was added to a suspension of $(LiC_5H_4)_2Ru$·tmeda (0.566 g, 1.58 mmol) in toluene (16 mL) at room temperature. The reaction mixture was stirred for 16 h and the solid was filtered off. The amount of solvent was reduced under vacuum (2 mL) and the solution was added to hexanes (20 mL). Precipitation was encouraged by cooling

the suspension to -25 °C for 1h. The solid was filtered off and it was washed with hexane (3 x 4 mL) to give **$85_n$** (0.160 g, 21%). $^1$H NMR ($C_6D_6$): δ 1.1-1.4 (br, 9H, *t*Bu), 1.4-1.8 (br, 9H, *t*Bu), 2.1-2.8 (br, 6H, $NMe_2$), 3.8-5.7 (br, 8H, Cp), 6.8-7.1 (br, 1H, CH-3), 7.4-7.8 (br, 1H, CH-5).

**[(Pytsi$^{-2SiMe_3}$)Al($C_5H_4$)Fe($C_5H_4$)]$_2$ (135).** A solution of (Pytsi$^{-2SiMe_3}$)$AlCl_2$ (0.283 g, 1.03 mmol) in benzene (5 mL) is added to a suspension of ($LiC_5H_4$)$_2$Fe·2/3tmeda (0.310 g, 1.10 mmol) in benzene (7 mL) at room temperature. After being stirred for 16h, an NMR sample is taken. $^1$H NMR ($C_6D_6$): δ 0.24 (s, 4H, $CH_2$), 0.45 (s, 12H, $SiMe_2$), 4.16 (s, 4H, Cp-H), 4.48 (s, 4H, Cp-H), 5.30 (s, 4H, Cp-H), 5.99 (m, 2H, Ar-H), 6.58 (m, 2H, Ar-H), 6.88 (d, 2H, Ar-H), 8.09 (d, 2H, Ar-H).

**[(Pytsi$^{-2SiMe_3}$)Ga($C_5H_4$)Fe($C_5H_4$)]$_2$ (136).** A slurry of ($LiC_5H_4$)$_2$Fe·3thf (0.500 g, 1.21 mmol) in diethyl ether (15 mL) is added to solution of (Pytsi$^{-2SiMe_3}$)$GaCl_2$ (0.338 g, 1.33 mmol) in diethyl ether (15 mL) at 0 °C. The reaction mixture was stirred for 7 h at room temperature, and then an NMR sample was taken. $^1$H NMR ($C_6D_6$): δ 0.25 (s, 4H, $CH_2$), 0.45 (s, 12H, $SiMe_2$), 4.18 (s, 4H, Cp-H), 4.41 (s, 4H, Cp-H), 4.64 (s, 4H, Cp-H), 5.17 (s, 4H, Cp-H), 6.04 (m, 2H, Ar-H), 6.63 (m, 2H, Ar-H), 6.91 (d, 2H, Ar-H), 8.03 (d, 2H, Ar-H).

**(Pytsi$^{-2SiMe_3}$)AlFc$_2$ (138).** A solution of (Pytsi$^{-2SiMe_3}$)$AlCl_2$ (0.49 g, 2.0 mmol) in benzene (20 mL) was added to a suspension of ($LiC_5H_4$)CpFe (0.95 g, 5.0 mmol) in benzene (30 mL). After 16 hours, the precipitate was filtered off and the volatiles were removed in vacuum. The product was extracted with hexanes (105 mL) and crystallized at -25 °C (0.22 g, 21%). Crystals suitable for single crystal X-ray analysis were obtained from diethyl ether. $^1$H NMR ($C_6D_6$): δ -0.15 (s, 4H, $CH_2$), 0.37 (s, 12H, $SiMe_2$), 4.11 (m,

2H, $C_5H_4$), 4.15 (s, 10H, $C_5H_5$), 4.43 (m, 2H, $C_5H_4$), 4.47 (m, 4H, $C_5H_4$), 6.28 (m, 1H, Ar-H), 6.74 (m, 1H, Ar-H), 6.96 (m, 1H, NCCH), 8.28 (m, 1H, NCH). $^{13}$C NMR ($C_6D_6$) δ 0.7 ($SiMe_2$), 67.9 ($C_5H_5$), 71.2, 71.4, 75.9, 77.0 ($C_5H_4$), 123.9, 129.9, 137.9, 147.4, 172.2 (Ar-H). EIMS (70 eV): *m/z* (rel intens) 547 (15) [$M^+$], 187 (13) [$C_{10}H_{11}Fe^+$], 186 (100) [$C_{10}H_{10}Fe^+$], 150 (11) [$C_8H_{12}NSi^+$], 136 (24) [$C_7H_{10}NSi^+$], 121 (30) [$C_7H_6NSi^+$]. HRMS (EI; *m/z*): calcd for $C_{28}H_{30}AlFe_2NSi$, 547.0662; found 547.0665 (Δppm = 0.5). Anal. Calcd for $C_{28}H_{30}AlFe_2NSi$ (547.31): C, 61.45; H, 5.52; N, 2.56. Found: C, 59.90; H, 6.56; N, 2.26.

**(Pytsi$^{-2SiMe_3}$)GaFc$_2$ (139).** (Pytsi$^{-2SiMe_3}$)$GaCl_2$ (0.61 g, 2.1 mmol) and ($LiC_5H_4$)CpFe (1.00 g, 5.2 mmol) were stirred for two days in a mixture of hexanes (100 mL) and diethyl ether (30 mL). After the removal of a part of the solvent (30 mL) in vacuum, the precipitate was filtered off and washed with hexanes (3 x 10 mL). The volume of the solution was reduced in vacuum. Upon cooling to -25 °C a small amount of an orange coloured material deposited on the walls of the flask. The mother liquid was syringed off, cooling at -78 °C produced an orange coloured precipitate, which was separated and washed with hexanes (15 + 10 mL) at -78 °C. All volatiles were removed in vacuum at ambient temperature to leave **139** behind (0.41 g, 33%). $^1$H NMR ($C_6D_6$): δ 0.05 (s, 2H, $CH_2$), 0.38 (s, 6H, $SiMe_2$), 4.10 (m, 2H, $C_5H_4$), 4.17 (s, 10H, $C_5H_5$), 4.37 (m, 2H, $C_5H_4$), 4.44 (m, 2H, $C_5H_4$), 4.50 (m, 2H, $C_5H_4$), 6.29 (m, 1H, Ar-H), 6.76 (m, 1H, Ar-H), 6.97 (m, 1H, NCCH), 8.18 (m, 1H, NCH). $^{13}$C NMR ($C_6D_6$, 125.8 MHz) δ -10.0 ($CH_2$), 0.6 ($SiMe_2$), 68.0 ($C_5H_5$), 70.6; 70.8; 75.0; 75.9, 76.12 ($C_5H_4$), 124.0; 129.6; 137.0, 147.5, 170.1 (Ar-H). EIMS (70 eV): *m/z* (rel intens) 589 (100) [$M^+$], 404 (75) [$M^+$ - Fc], 69 (12) [$Ga^+$]. HRMS (EI; *m/z*): calcd for $C_{28}H_{30}Fe_2GaNSi$, 589.0102; found

589.0119 (Δppm = 2.9). Anal. Calcd for $C_{28}H_{30}Fe_2GaNSi$ (590.09): C, 57.00; H, 5.12; N, 2.37. Found: C, 56.65; H, 5.05; N, 2.44.

### 3.5 References

(1) Bellas, V.; Rehahn, M. *Angew. Chem. Int. Ed.* **2007**, *46*, 5082-5104.

(2) a) Schachner, J. A.; Lund, C. L.; Quail, J. W.; Müller, J. *Organometallics* **2005**, *24*, 785-787. b) Schachner, J. A.; Lund, C. L.; Quail, J. W.; Müller, J. *Organometallics* **2005**, *24*, 4483-4488. c) Lund, C. L.; Schachner, J. A.; Quail, J. W.; Müller, J. *Organometallics* **2006**, *25*, 5817-5823. d) Schachner, J. A.; Orlowski, G. A.; Quail, J. W.; Kraatz, H.-B.; Müller, J. *Inorg. Chem.* **2006**, *45*, 454-459. e) Schachner, J. A.; Tockner, S.; Lund, C. L., Quail, J. W.; Rehan, M.; Müller, J. *Organometallics* **2007**, *26*, 4658-4662.

(3) a) Jäkle, F.; Rulkens, R.; Zech, G.; Foucher, D. A.; Lough, A. J.; Manners, I. *Chem. Eur. J.* **1998**, *4*, 2117−2128. b) Jäkle, F.; Rulkens, R.; Zech, G.; Massey, J.; Manners, I. *J. Am. Chem. Soc.* **2000**, *122*, 4231−4232. c) Baumgartner, T.; Jäkle, F.; Rulkens, R.; Zech, G.; Lough, A. J.; Manners, I. *J. Am. Chem. Soc.* **2002**, *124*, 10062−10070.

(4) Burchard, W. In *Branched Polymers II*; Springer: New York, **1999**; Vol. *143*, pp 113−194.

(5) Massey, J. A.; Kulbaba, K.; Winnik, M. A.; Manners, I. *J. Polym. Sci., Part B: Polym. Phys.* **2000**, *38*, 3032−3041.

(6) a) Bagh, B.; Gilroy, J. B.; Staubitz, A.; Müller, J. *J. Am. Chem. Soc.* **2010**, *132*, 1794-1795. b) Bagh, B.; Schatte, G.; Green, J. C.; Müller, J. *J. Am. Chem. Soc.* **2012**, *134*, 7924-7936.

(7) Breit, N. C.; Ancelet, T.; Quail, J. W.; Schatte, G.; Müller, J. *Organometallics* **2011**, *30*, 6150-6158.

(8) Nesmeyanov, A. N.; Perevalova, E. G.; Golovvnya, R. V.; Nesmeyanova, O. A. *Doklady Akademii Nauk SSSR* **1954**, *97*, 459-461.

(9) a) Schlogl, K.; Mohar, A. *Monatsh. Chem.* **1961**, *92*, 219-235. b) Schloegl, K.; Pelousek, H.; Mohar, A. *Monatsh. Chem.* **1961**, *92*, 533-541. c) Pauson, P. L.; Watts, W. E. *J. Chem. Soc.* **1962**, 3880-3886. d) Xie, R.-J.; Han, L.-M.; Suo, Q.-L.; Hong, H.-L.; Luo, M.-H. *J. Coord. Chem.* **2010**, *63*, 1700-1710. e) Schottenberger, H.; Buchmeiser, M.; Polin, J.; Schwarzhans, K. E. *Z. Naturforsch, B: Chem. Sci.* **1993**, *48*, 1524-1532. f) Klimova, E. I.; García, M. M.; Klimova, T.; Stivalet, J. M.; Ortega, S. H.; Ramírez, L. H. *J. Organomet. Chem.* **2002**, *659*, 56-63. g) Bildstein, B.; Denifl, P.; Wurst, K. *J. Organomet. Chem.* **1995**, *496*, 175-186. h) Gorton, J. E.; Lentzer, H. L.; Watts, W. E. *Tetrahedron* **1971**, *27*, 4353-4360.

(10) a) Bocarsly, A. B.; Walton, E. G.; Bradeley, M. G.; Wrighton, M. S. *J. Electroanal. Chem. Interfacial Electrochem.* **1979**, *100*, 283-306. b) Liu, Y.-P.; Li, Z.-Q.; Tan Y.-X.; Zhang, Z.-J. *Acta Crystallogr., Sect. E* **2011**, *E67*, m635. c) Losada, J.; García-Armada, P.; Robles, V.; Martínez, A. M.; Casado, C. M.; Alonso, B. *New J. Chem.* **2011**, *35*, 2187–2195. d) MacLachlan, M. J.; Zheng, J.; Lough, A. J.; Manners, I. *Organometallics* **1999**, *18*, 1337-1345. e) Thieme, K.; Bourke, S. C.; Zheng, J.; MacLachlan, M. J.; Zamanian, F.; Lough, A. J.; Manners, I. *Can. J. Chem.* **2002**, *80*, 1469-1480. f) Rulkens, R.; Lough, A. J.; Manners, I.; Lovelace, S. R.; Grant, C.; Geiger, W. E. *J. Am. Chem. Soc.* **1996**, *118*, 12683-12695.

(11) a) Sollott, G. P.; Mertwoy, H. E.; Portnoy, S.; Snead, J. L. *J. Org. Chem.* **1963**, *28*, 1090-1092. b) Kotz, J. C.; Nivert, C. L.; Lieber, J. M. *J. Organomet. Chem.* **1975**, *91*, 87-95.

(12) a) Scheibitz, M.; Bolte, M.; Bats, J. W.; Lerner, H.-W.; Nowik, I.; Herber, R. H.; Krapp, A.; Lein, M.; Holthausen, M. C.; Wagner, M. *Chem.–Eur. J.* **2005**, *11*, 584-603.

b) Heilmann, J. B.; Scheibitz, M.; Qin, Y.; Sundararaman, A.; Jäkle, F.; Kretz, T.; Bolte, M.; Lerner, H.-W.; Holthausen, M. C.; Wagner, M. *Angew. Chem. Int. Ed.* **2006**, *45*, 920-925. c) Scheibitz, M.; Bats, J. W.; Bolte, M.; Lerner, H.-W.; Wagner, M. *Organometallics* **2004**, *23*, 940-942. d) Scheibitz, M.; Li, H.; Schnorr, J.; Perucha, A. S.; Bolte, M.; Lerner, H.-W.; Jäkle, F.; Wagner, M. *J. Am. Chem. Soc.* **2009**, *131*, 16319-16329.

(13) a) Nesmeyanov, A. N.; Tolstaya, T. P.; Korol'kov, V. V. *Dokl. Akad. Nauk* **1973**, *209*, 1113-1116. b) Bokii, N. G.; Struchkov, Yu. T.; Korol'kov, V. V.; Tolstaya, T. P. *Koord. Khim.* **1975**, *1*, 1144-1146. c) Kabouche, Z.; Nguyen, H. D. *J. Organomet. Chem.* **1989**, *375*, 191-195.

(14) Perevalova, E. G.; Grandberg, K. I.; Dyadchenko, V. P.; Kalinina, O. N. *J. Organomet. Chem.* **1988**, *352*, C37-C41.

(15) Herberhold, M.; Schmalz, T.; Milius, W.; Wrackmeyer, B. *Inorg. Chim. Acta* **2003**, *352*, 51-60.

(16) Barley, H. R. L.; Clegg, W.; Dale, S. H.; Hevia, E.; Honeyman, W.; Kennedy, A. R.; Mulvey, R. E. *Angew. Chem. Int. Ed.* **2005**, *44*, 6018-6021.

(17) Wrackmeyer, B.; Klimkina, E. V.; Ackermann, T.; Milius, W. *Inorg. Chim. Acta* **2009**, *362*, 3941-3948.

(18) a) Osborne, A. G.; Whiteley, R. H.; Meads, R. E. *J. Organomet. Chem.* **1980**, *193*, 345-357. b) Jones, S. C.; Barlow, S.; O'Hare, D. *Chem.–Eur. J.* **2005**, *11*, 4473-4481.

(19) Utri, G.; Schwarzhans, K. E.; Allmaier, G. M. *Z. f. Naturforsch., B: Chem. Sci.* **1990**, *45*, 755-762.

(20) Britton, W. E.; Kashyap, R.; El-Hashash, M.; El-Kady, M.; Herberhold, M. *Organometallics* **1986**, *5*, 1029-1031.

(21) Rausch, M. D. *J. Org. Chem.* **1961**, *26*, 3579-3580.

(22) Herberhold, M.; Leitner, P. *J. Organomet. Chem.* **1987**, *336*, 153-161.

(23) Robin, M. B.; Day, P. *Adv. Inorg. Chem. Radiochem.* **1967**, *10*, 247-422.

(24) Morrison, W. H.; Krogsrud, S.; Hendrickson, D. N. *Inorg. Chem.* **1973**, *12*, 1998-2004.

(25) Bagh, B.; Breit, N. C.; Harms, K.; Schatte, G.; Burgess, I.; Braunschweig, H.; Müller, J. *Inorg. Chem.* **2012**, *51*, 11155-11167.

(26) Herbert, D. E.; Gilroy, J. B.; Chan, W. Y.; Chabanne, L.; Staubitz, A.; Lough, A. J.; Manners, I. *J. Am. Chem. Soc.* **2009**, *131*, 14958-14968.

(27) Diaz, A. F.; Mueller-Westerhoff, U. T.; Nazzal, A.; Tanner, M. *J. Organomet. Chem.* **1982**, *236*, C45-C48.

(28) Barrière, F.; Geiger, W. E. *J. Am. Chem. Soc.* **2006**, *128*, 3980-3989.

(29) Schachner, J. A.; Lund, C. L.; Burgess, I. J.; Quail, J. W.; Schatte, G.; Müller, J. *Organometallics* **2008**, *27*, 4703-4710.

(30) Herbert, D. E.; Mayer, U. F. J.; Manners, I. *Angew. Chem. Int. Ed.* **2007**, *46*, 5060-5081.

(31) Butler, I. R.; Cullen, W. R.; Ni, J.; Rettig, S. J. *Organometallics* **1985**, *4*, 2196-2201.

(32) Perucha, A. S.; Heilmann-Brohl, J.; Bolte, M.; Lerner, H. W.; Wagner, M. *Organometallics* **2008**, *27*, 6170-6177.

(33) Bildstein, B.; Malaun, M.; Kopacka, H.; Wurst, K.; Mitterböck, M.; Ongania, K. H.; Opromolla, G.; Zanello, P. *Organometallics* **1999**, *18*, 4325-4336.

(34) Liu, D.; Xie, F.; Zhang, W. *J. Org. Chem.* **2007**, *72*, 6992-6997.

(35) Vogel, U.; Lough, A. J.; Manners, I. *Angew. Chem. Int. Ed.* **2004**, *43*, 3321-3325.

CHAPTER 4
[1.1]FERROCENOPHANES AND POLYFERROCENES WITH ALTERNATING BRIDGING ELEMENTS

## 4.1 Introduction

The synthesis and characterization of [1.1]FCPs has been well studied since 1956[1] and Chapter 1.2 gives an overview about these species. [1.1]FCPs with unsymmetrical bridges, the same bridging elements, but different ligands on the bridging element, are known in the literature (Figure 4-1).[2] Other [1.1]MCPs contain an element of asymmetry by having two different metal centers like in [1.1]RFCPs (Figure 4-1).[3] However, [1.1]FCP with different bridging elements were not described prior to our investigations (Figure 4-1).

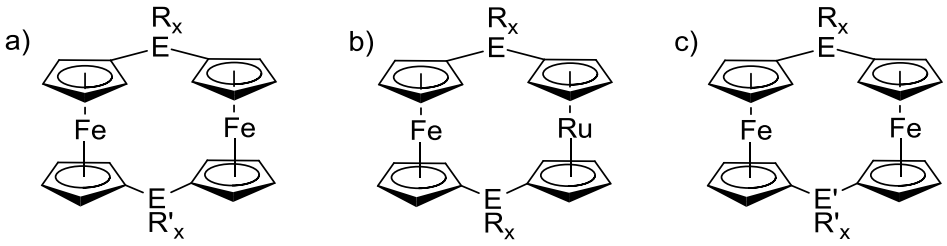


**Figure 4-1.** Depiction of a) an unsymmetrically bridged [1.1]FCP, b) a [1.1]RFCP, and c) a [1.1]FCP with different bridging elements.

[1.1]FCPs with different bridging elements are interesting as model compounds for copolymers and to study the influence of two different bridging elements on the geometry and properties of [1.1]FCPs. Moreover, it is a stimulating challenge to develop a synthetic strategy toward [1.1]FCPs with different bridging elements.

In a group project, Bidraha Bagh, Subhayan Dey, and I targeted the synthesis and characterization of the first [1.1]FCPs with two different elements as bridges. B. Bagh, the leader of this group project, developed the synthetic strategy (Scheme 4-1). The synthetic strategy starts with 1,1'-dibromoferrocene, from which one of the bromines is

replaced with lithium and the subsequent reaction with an element dichloride forms the first two bonds between one bridging element and the two cyclopentadienyl rings to give a bis(1'-bromoferrocenyl) species (Scheme 4-1). The use of brominated ferrocenediyl species was suggested in order to facilitate the lithiation in the desired position. In a second step, the remaining bromines are substituted by lithium and subsequent reactions with different element dichlorides can close the ring to give the targeted [1.1]FCPs (Scheme 4-1).

**Scheme 4-1**. Synthetic strategy to obtain [1.1]FCPs with different bridging elements.

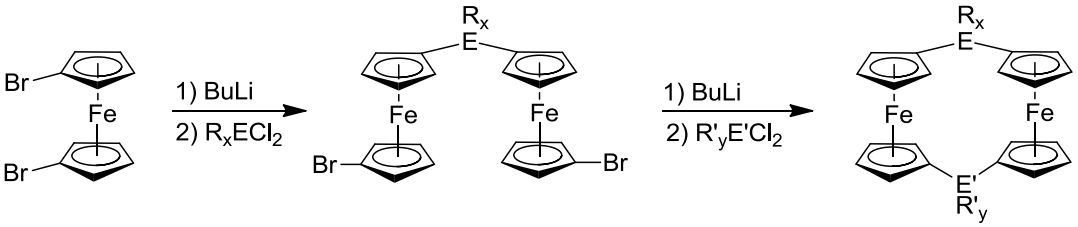


However, besides ring-closing to form a [1.1]FCP, in the second step a condensation reaction can also occur to give polyferrocenes with alternating bridging elements (Figure 4-2). Alternating bridging elements in polymers is an interesting structural motive that could not be obtained from an uncontrolled copolymerization. Therefore, these special polyferrocenes were also studied.

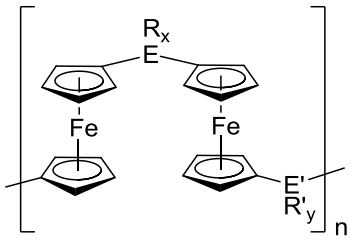


**Figure 4-2.** Polyferrocenes with alternating bridging elements.

Based on this synthetic strategy, the options for the first bridging element (E) were limited, since the E-Cp bonds that were formed in the first step need to be able to withstand the lithiation conditions. In Chapter 1 the various advantages of silicon as a bridging element were mentioned such as readily available, comparably cheap silicon dichloride starting materials and silicon compounds being less toxic than starting materials of other bridging elements (e.g. Hg, Sn). Moreover, silicon-bridged [1.1]FCPs or polyferrocenes are not air sensitive. Thus, purifications are facilitated and chromatographic treatment is possible. The use of silicon was also encouraged by the fact that PFS like **34** are the most intensely studied ferrocenyl-based polymers.[4] Therefore, silicon-bridged species might be of a higher interest to researchers working in this field than respective species with uncommon bridging elements.

S. Dey carried out the reactions between 1,1'-dibromoferrocene, *n*-butyllithium and dichlorodimethylsilane and dichlorodiethylsilane, respectively, to obtain the bis(1'-bromoferrocenyl)dialkylsilanes **140** or **141** in moderate yields (Scheme 4-2).[5] The $^1$H NMR spectra of **140** and **141** exhibited four signals for the cyclopentadienyl protons, one signal for all the α-protons and one signal for all the β-protons on each of the differently substituted Cp rings. This pattern of the $^1$H NMR signals fits with a $C_{2v}$ symmetry of **140** and **141** in solution.

**Scheme 4-2.** Synthesis of the bis(1'-bromoferrocenyl)dialkylsilanes **140** and **141**.

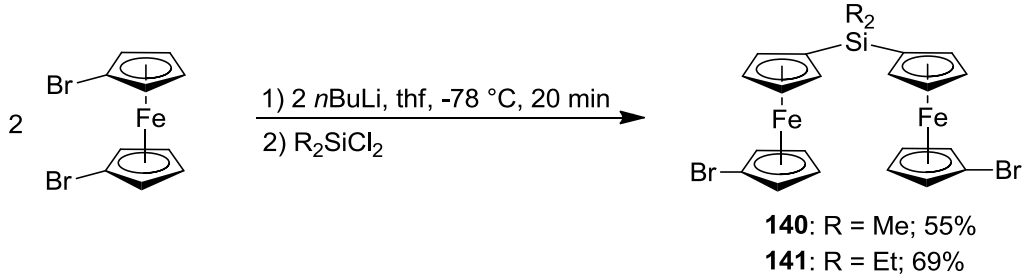


**140**: R = Me; 55%
**141**: R = Et; 69%

The first choice of a second bridging element (E') was tin. Similarly to silicon, tin dichlorides are commercially available and tin-bridged [1.1]FCPs or polyferrocenes are not air sensitive. Three tin compounds of the type $R_2SnCl_2$ with different steric bulk (R = Me, *n*Bu, *t*Bu) were reacted with the dilithio species of **140** and **141** in order to obtain the six mixtures **142-147** (Scheme 4-3). Both **140** and **141** were utilized for the reactions to attest any trend observed for the different ligands on tin and to investigate if the change of the dimethylsilyl-bridge to a diethylsilyl-bridge has an influence on the outcome of the reaction. Species **145-147** were synthesized by B. Bagh, whereas my contribution was the synthesis of **142-144**. The results of these reactions are described in Chapter 4.2.1 and Chapter 4.2.2 and the study of the redox behavior of these species is described in Chapter 4.2.4. The focus of these chapters is on my results, which are compared to those of **145-147**.

**Scheme 4-3.** Synthesis of the targeted silicon-tin-bridged [1.1]FCPs $\mathbf{142_1}$-$\mathbf{147_1}$ and polyferrocenes with alternating silicon and tin bridges $\mathbf{142_n}$-$\mathbf{147_n}$.

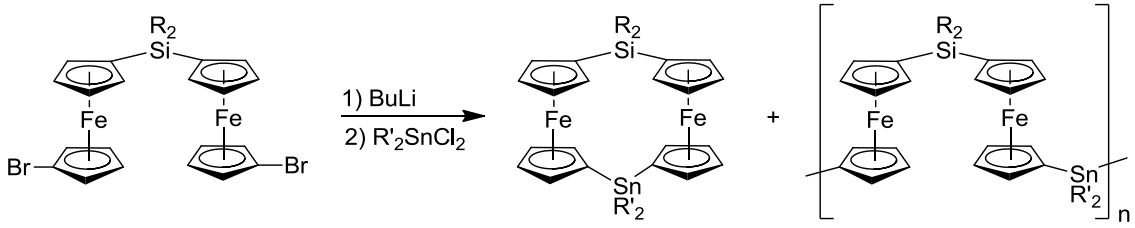


**140**: R = Me
**141**: R = Et

**$142_1$**: R = Et, R' = Me
**$143_1$**: R = Et, R' = *n*Bu
**$144_1$**: R = Et, R' = *t*Bu
**$145_1$**: R = Me, R' = Me
**$146_1$**: R = Me, R' = *n*Bu
**$147_1$**: R = Me, R' = *t*Bu

**$142_n$**: R = Et, R' = Me
**$143_n$**: R = Et, R' = *n*Bu
**$144_n$**: R = Et, R' = *t*Bu
**$145_n$**: R = Me, R' = Me
**$146_n$**: R = Me, R' = *n*Bu
**$147_n$**: R = Me, R' = *t*Bu

Since one of our main interests are aluminum- and gallium-bridged FCPs, we also wanted to investigate [1.1]FCPs with gallium and silicon as bridging elements. We concentrated on gallium as a bridging element instead of aluminum, because gallium

species are less sensitive than aluminum species. Moreover, previously no major difference between the solid-state structures of aluminum-bridged and gallium-bridged [1]metallacyclophanes or [1.1]metalla-cyclophanes was observed.[6] Gallium-bridged [1.1]FCPs are also preferred over aluminum-bridged [1.1]FCPs, because the redox behavior of the aluminum-bridged species is complex and not well understood (see Chapter 3.2.3). Gallium-bridged [1.1]FCPs were selectively formed when slim ligands like Ar′ or *p*-$SiMe_3$Ar′ were utilized in respective salt-metathesis reactions (see Chapter 1.4.2 and Chapter 3.2.3).[6d,6k] The results of the silicon-tin-bridged species, which are discussed in Chapter 4.2.1, showed that the respective [1.1]FCPs were not isolable in the intended, significant amount.[5] Based on the selectivity of gallium dichlorides equipped with slim ligands to yield [1.1]FCPs, it was hoped that reactions with (Ar′)$GaCl_2$ will yield a significantly higher amount of [1.1]FCP than the related tin species **142-144**. Only **140** was used as a starting material since no major difference for the dimethylsilyl- or diethylsilyl-mixed species **142-147** was observed. However, the two slightly different, slim ligands, Ar′ and *p*-$SiMe_3$Ar′, attached to gallium, were utilized. The [1.1]FCP $\mathbf{149_1}$ was synthesized by B. Bagh, while the [1.1]FCP $\mathbf{148_1}$ was synthesized by me (Figure 4-3). The results will be described in Chapter 4.2.3 and 4.2.4.

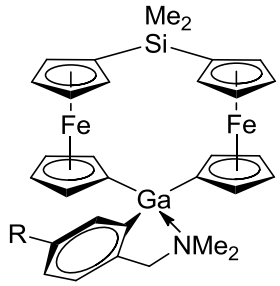


$\mathbf{148_1}$: R = H
$\mathbf{149_1}$: R = $SiMe_3$

**Figure 4-3.** Depiction of the intended silicon-gallium-bridged [1.1]FCPs $\mathbf{148_1}$ and $\mathbf{149_1}$.

## 4.2 Results and Discussion

### 4.2.1 Synthesis and Characterization of Polyferrocenes with Silicon and Tin as Alternating Bridges

Bis(1'-bromoferrocenyl)diethylsilane (**141**) was lithiated with *tert*-butyllithium and subsequently one of the dialkyltindichlorides, $Me_2SnCl_2$, $nBu_2SnCl_2$ or $tBu_2SnCl_2$ was added to give a mixture of ferrocenyl-based species with alternating tin and silicon groups as bridges (**142$_n$**-**144$_n$**) (Scheme 4-4).

**Scheme 4-4.** Synthesis of polyferrocenes with silicon and tin as alternating bridges **142$_n$**-**144$_n$**.

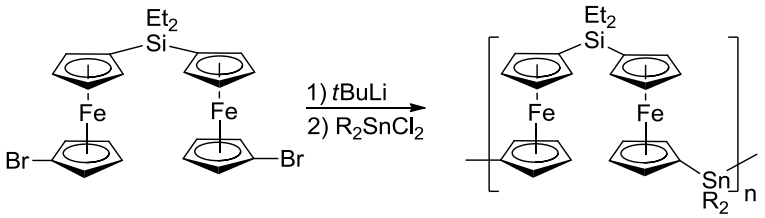


**141**

**142$_n$**: R = Me
**143$_n$**: R = *n*Bu
**144$_n$**: R = *t*Bu

No formation of the intended [1.1]FCPs as major compounds was observed by $^1$H NMR spectroscopy. The product mixture was purified by repeated precipitations of a toluene solution into methanol. MALDI-TOF mass spectrometry was utilized to gain insight into the formed species. MALDI-TOF data clearly revealed the presence of cyclic and linear oligomers for the dimethyltin- and di-*n*-butyltin-bridged species (**142$_n$** and **143$_n$**) (Figure 4-4).

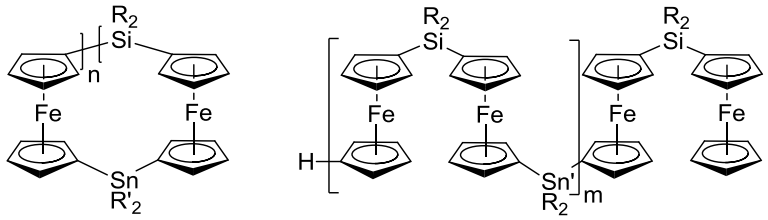


**$142_n$c**: R = Et, R' = Me
**$143_n$c**: R = Et, R' = *n*Bu
**$144_n$c**: R = Et, R' = *t*Bu
**$145_n$c**: R = Me, R' = Me
**$146_n$c**: R = Me, R' = *n*Bu
**$147_n$c**: R = Me, R' = *t*Bu

**$142_m$l**: R = Et, R' = Me
**$143_m$l**: R = Et, R' = *n*Bu
**$144_m$l**: R = Et, R' = *t*Bu
**$145_m$l**: R = Me, R' = Me
**$146_m$l**: R = Me, R' = *n*Bu
**$147_m$l**: R = Me, R' = *t*Bu

**Figure 4-4.** Cyclic and linear polyferrocenes with alternating tin and silicon-bridges, **$142_n$c-$147_n$c** and **$142_m$l-$147_m$l**.

The presence of cyclic oligomers is particularly interesting since cyclic ferrocenyl-based polymers are scarce compared with their linear counterparts. The dimethyltin- and diethylsilyl-bridged polyferrocenes (**$142_n$**) showed the highest numbers of repeating units in the MALDI-TOF spectrum. The cyclic oligomers **$142_n$c** had up to 10 repeating units, while the linear oligomers **$142_m$l** had up to 9 repeating units, which relates to 20 ferrocene moieties (Figure 4-5). The MALDI-TOF spectrum of **$143_n$** revealed species with repeating units up to m = 4, n = 5. The cyclic species **$143_n$c** showed a significantly higher intensity than the respective linear oligomers **$143_m$l**. The MALDI-TOF data of **$144_n$** showed only a peak for the [1.1]FCP **$144_1$** and possibly fragmentation of the longer chain oligomers occurred.

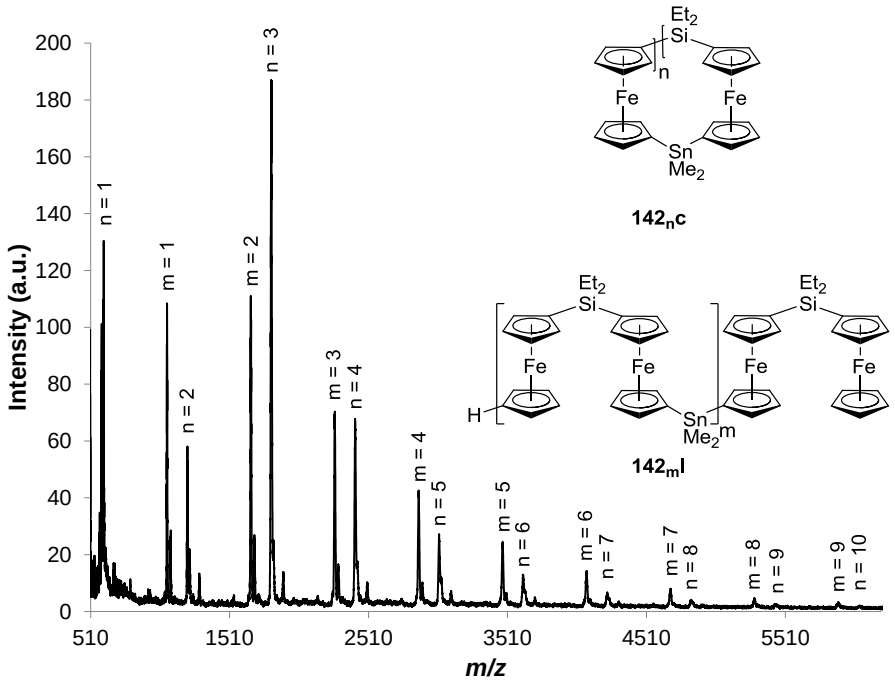


**Figure 4-5.** MALDI-TOF spectrum of **142$_n$**. Reprinted with permission from Bagh, B.; Breit, N. C.; Dey, S.; Gilroy, J. B.; Schatte, G.; Harms, K.; Müller, J. *Chem.–Eur. J.* **2012**, *18*, 9722-9733. Copyright 2012 Wiley VCH.

MALDI-TOF data of the respective dimethylsilyl-bridged species (**145$_n$-147$_n$**) showed the same trend as the diethylsilyl-bridged species **142$_n$-144$_n$**. The highest number of repeating units for the dimethylsilyl-bridged species was observed for **145$_n$** with n = 8 and m = 7, referring to 16 ferrocenyl moieties. Species **146$_n$** showed the presence of oligomers up to 14 ferrocenyl moieties and for **147$_n$** no meaningful data was obtained.

$^{1}$H NMR, $^{13}$C NMR, $^{29}$Si NMR, $^{119}$Sn NMR spectroscopy was measured for the mixtures of oligomers with diethylsilane bridges, **142$_n$-144$_n$**, and the assignment of peaks was based on data of known poly(ferrocenylsilane)s and poly(ferrocenylstannane)s.[7] The NMR data of the oligomers with diethylsilane bridges (**142$_n$**, **143$_n$**, and **144$_n$**) was very similar and, therefore, only those of **142$_n$** are discussed. The $^{1}$H NMR spectrum of **142$_n$** revealed one broad signal for the dimethyltin group and two broad, well-separated signals

for the diethylsilyl group (Figure 4-6). For the cyclopentadienyl protons, two signals would be expected for the Cp ring connected to silicon and two signals would be expected for the Cp ring connected to tin. Both α- or β-protons on one Cp ring are chemically equivalent. Moreover, one signal for the hydrogenated Cp end groups would be expected. The smallest signal at δ 4.03 was assigned the Cp protons of the end groups, since similar shifts were reported for Cp end groups of silicon-bridged ferrocenyl-based oligomers and polymers (Figure 4-6).[7c] Two signals for Cp rings overlapped at δ 4.30 in the case of **142$_n$**, whereas these signals are well separated in **143$_n$** and **144$_n$**. The signals at δ 4.10 and 4.30 were assigned to the protons of the Cp ring that is connected to silicon due to the similarity with the reported shifts of δ 4.10 and 4.30 for poly(ferrocenyldiethylsilane).[7a] The remaining two signals at δ 4.16 and 4.30 were assigned to the protons on the tin-bound Cp ring. These values are comparable to the shifts of δ 4.07 and 4.29 reported for poly(ferrocenyldimethylstannane).[7b]

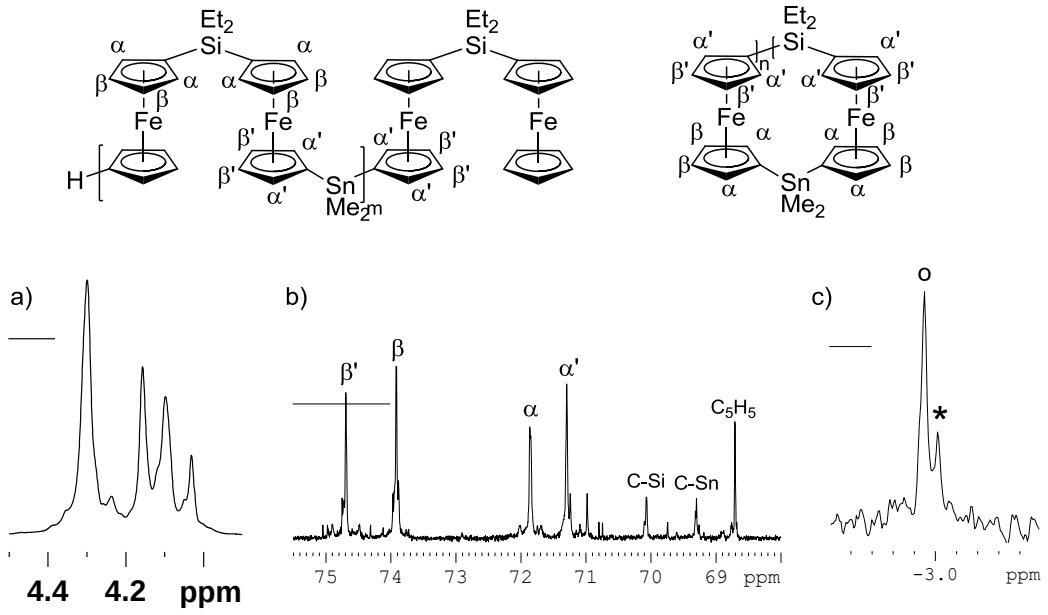


**Figure 4-6.** a) Excerpt of the $^{1}$H NMR spectrum of **142$_n$**. b) Excerpt of the $^{13}$C NMR spectrum of **142$_n$**. c) Excerpt of the $^{29}$Si NMR spectrum of **142$_n$**. Reprinted with

permission from Bagh, B.; Breit, N. C.; Dey, S.; Gilroy, J. B.; Schatte, G.; Harms, K.; Müller, J. *Chem.–Eur. J.* **2012**, *18*, 9722-9733. Copyright 2012 Wiley VCH.

In the $^{13}$C NMR spectrum of **142$_n$**, two additional peaks for the two *ipso*-carbons that are either connected to tin or to silicon are expected (Figure 4-6). Comparison with the reported chemical shifts of poly(ferrocenyldiethylsilane) at δ 74.4, 72.3, and 70.4[7a] led to the assignment of the signals at δ 74.0, 71.9, and 70.1 to the carbon atoms of the Cp ring connected to silicon. As a consequence, the other set of signals at δ 74.7, 71.3, and 69.3 was assigned to the carbon atoms of the tin-bound Cp ring.

The $^{29}$Si NMR spectrum of **142$_n$** showed only one major signal at δ -3.0 and one minor signal at δ -2.9 (Figure 4-6). Manners and Geiger *et al.* reported the $^{29}$Si NMR data of linear silicon-bridged oligomers with ferrocenyl end groups.[7c] These oligomers exhibited one peak for the silicon atoms that are connected to the ferrocenyl end groups and one peak for the 'inner' silicon atoms. $^{29}$Si NMR spectra of known dimethylsilyl-bridged linear and cyclic ferrocenyl based oligomers showed only minor differences with ranges between δ -6.4 and -6.8 and ranges between δ -6.2 and -6.4, respectively.[7c,8] Based on the strong intensity of the major peak and the very small intensity of the minor peak, it was assumed that the cyclic oligomers have the same shift as the 'inner' Si atoms in the linear oligomers. So, the signal with the strong intensity was assigned to the 'inner' Si atoms in the linear oligomers and the cyclic oligomers. The less intense signal in the $^{29}$Si NMR spectrum of **142$_n$** was assigned to the silicon atoms that are bound to a ferrocenyl end group.

The $^{119}$Sn NMR spectrum of **142$_n$** displayed one major signal at δ -15.8 and a few minor signals at δ -23.0, -10.1 and -7.5. $^{119}$Sn NMR spectroscopy covers a significantly larger range than the previously discussed three nuclei with the extremes at δ 2960 for

(2,6-$Mes_2C_6H_3$)Sn(*t*$Bu_3$Ge)[9] and at δ -2247 for ($\eta^5$-$Me_5C_5$)Sn[$BF_4$].[10] Moreover, the reported $^{119}$Sn NMR data for poly(ferrocenyldi-*tert*-butylstannane) and for the di-*tert*-butylstannyl-bridged [1.1]FCP are significantly different with δ -45.2 and -33.3, respectively.[7d] This clearly shows that $^{119}$Sn NMR spectroscopy is more sensitive towards smaller changes than $^{29}$Si NMR spectroscopy. These facts can explain that multiple signals were present in the $^{119}$Sn NMR spectrum of **142$_n$** while the $^{29}$Si NMR spectrum of **142$_n$** only displayed two signals. These small signals in the $^{119}$Sn NMR spectrum of **142$_n$** might originate from differentiations between cyclic and linear oligomers or from differentiations between species with different chain lengths. In the case of **144$_n$**, an additional weak signal was exhibited in the $^{119}$Sn NMR spectrum at δ 75.2. This signal was assigned to a tin chloride end group based on the reported compound Fc*Sn*t*$Bu_2$Cl with δ 72.3.[11] A similar signal was not observed in the $^{119}$Sn NMR spectrum of **142$_n$** and **143$_n$** and no peak for any tin end group was observed by MALDI-TOF analysis. However, MALDI-TOF measurements of **144$_n$** did not reveal the presence of any species larger than a [1.1]FCP. The $^{119}$Sn NMR signal at δ 75.2 indicated the presence of a species with a SnCl end group. This leads to the conclusion that the presence of tin end groups depends on the ligand on tin. The NMR data of dimethylsilyl-bridged polyferrocenes with alternating bridging elements (**145$_n$**, **146$_n$**, and **147$_n$**) was very similar to that of the respective diethylsilyl-bridged species (**142$_n$**, **143$_n$**, and **144$_n$**) discussed above.[5]

The average size of **142$_n$**, **143$_n$**, and **144$_n$** was studied by DLS and GPC analysis (Table 4-1). DLS data was evaluated similar to **129$_n$** (Chapter 3.2.1) and GPC analysis was carried out by Dr J. B. Gilroy (University of Bristol, U.K.). GPC and DLS results

exhibited the same order of average molecular weights for the diethylsilyl-bridged species **142$_n$**-**144$_n$** (Table 4-1). The di-*n*-butylstannyl-bridged polyferrocenes (**143$_n$**) displayed the highest molecular weight, followed by the dimethylstannyl-bridged species (**142$_n$**). Mixture **144$_n$** showed the lowest molecular weight, 2 kDa, which corresponds to three repeating units and six ferrocenyl moieties. The same trend was observed for the polyferrocenes with dimethylsilyl-bridges (**145$_n$**, **146$_n$**, and **147$_n$**) (Table 4-1). That the same tendency was observed for the diethylsilyl-bridged species (**142$_n$**-**144$_n$**) and the dimethylsilyl-bridged species (**145$_n$**-**147$_n$**) clearly shows that the ligand on tin has an influence on the formation of the oligomers. Dimethylsilyl-bridged species **145$_n$**-**147$_n$** show one or two more repeating units than the diethylsilyl-bridged species **142$_n$**-**144$_n$**. However, no major difference was found for dimethylsilyl- and diethylsilyl-bridged polyferrocenes with alternating silicon and tin atoms as bridging elements. This absence of a major change of the molecular weights of the diethylsilyl- and dimethylsilyl-bridged species could be due to the fact that the alkyl groups on silicon are already incorporated in the bis(1'-bromoferrocenyl)dialkylsilane and are further away from the center, where the reaction takes place. However, more data would be needed to verify this speculation.

**Table 4-1.** DLS and GPC data of the polyferrocenes **142$_n$**, **143$_n$**, **144$_n$**, **145$_n$**, **146$_n$**, and **147$_n$** with silicon and tin as alternating bridging elements.

| | GPC | | | | DLS | |
|---|---|---|---|---|---|---|
| | $M_n$ [Da] | $M_w$ [Da] | PDI | $DP_w$ | $M_w$ [Da] | $DP_w$ |
| **142$_n$** | 1800 | 2600 | 1.44 | 4 | 4300 | 7 |
| **143$_n$** | 2300 | 5200 | 2.26 | 8 | 6700 | 10 |
| **144$_n$** | 1600 | 2100 | 1.31 | 3 | 1800 | 3 |
| **145$_n$** | 2000 | 2900 | 1.45 | 5 | 3100 | 5 |
| **146$_n$** | 2500 | 6300 | 2.52 | 10 | 7200 | 11 |
| **147$_n$** | 1800 | 2500 | 1.39 | 4 | 5000 | 8 |

Even though GPC and DLS showed the same trend, DLS data always gave higher molecular weights. Manners *et al.* reported in an in-depth study on the molecular weight determination of PFSs that GPC analysis underestimated the molecular weight.[12] A similar underestimation of the molecular weights of **$142_n$-$144_n$** by GPC analysis might be the reason for the difference in molecular weights observed for GPS and DLS analysis of **$142_n$-$144_n$**. However, another option is that the assumptions made for the estimation of molecular weights by DLS do not fit with the properties of the polymers well enough, which would lead to wrong estimations of the $M_w$ by DLS.

Interestingly, the GPC and DLS data showed that **$143_n$** had a significantly higher molecular weight than **$142_n$**, twice as much by GPC, and also a higher PDI than **$142_n$**. However, MALDI-TOF analysis revealed fewer high-molecular-weight peaks and fewer peaks altogether. In MALDI-TOF, the peaks of the highest molecular weights and with very low intensities have n = 5 and m = 4 repeating units, which highly underestimates the average 8-10 repeating units determined by GPC and DLS with an PDI of 2.26 (GPC). Fragmentation of higher molecular weight polyferrocenes during the MALDI-TOF measurement could be a possible source. Therefore, it is debatable whether MALDI-TOF is able to give an accurate picture of the distribution of the oligomers for these species or if both the DLS and GPC data are wrong.

### 4.2.2 Isolation and Characterization of Tin-Silicon-Bridged Ferrocenophanes

Two tin-silicon-bridged FCPs with diethylsilyl bridges were isolated from the respective reaction mixture or purified product mixture. The [1.1]FCP with a dimethyltin bridge (**$142_1$**) was isolated by crystallization from a methanol-toluene solvent mixture in a very low yield of 3% (Figure 4-7).

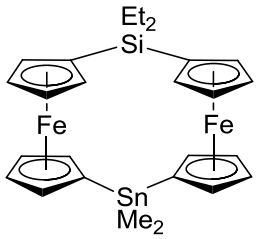


**142$_1$**

**Figure 4-7.** Depiction of the isolated diethylsilyl- and dimethylstannyl-bridged [1.1]FCP (**142$_1$**).

The $^{1}$H NMR spectrum of **142$_1$** showed overlapping multiplets for the Cp protons, a singlet for the dimethylstannyl group and a doublet and triplet for the diethylsilyl group. In the $^{13}$C NMR spectrum of **142$_1$**, the cyclopentadienyl protons exhibited four signals of higher intensity, assigned to the α- and β-carbon atoms, as well as two signals for the two different *ipso*-carbon atoms. The presence of the tin-satelites in the $^{13}$C NMR spectrum revealed which signals belong to the tin-bridged Cp rings and which signals belong to the silicon-bridged Cp rings [69.3 (*ipso*-C of Si-$C_5H_4$), 70.7, 74.3 (α- and β-C of Si-$C_5H_4$), 68.8 (*ipso*-C Sn-$C_5H_4$), 70.8, 75.0 (α- and β-C of Sn-$C_5H_4$)]. Species **142$_1$** consists of two inequivalent Cp rings that are either connected to silicon or to tin. All α- and β-carbons on one kind of ring are identical, which shows that **142$_1$** is $C_{2v}$ symmetric in solution. Therefore, a fast *anti*-to-*anti* isomerization must occur in solution (Scheme 4-5).

**Scheme 4-5.** Observed *anti*-to-*anti* isomerization of silicon-tin-mixed-bridged [1.1]FCP **142$_1$**.

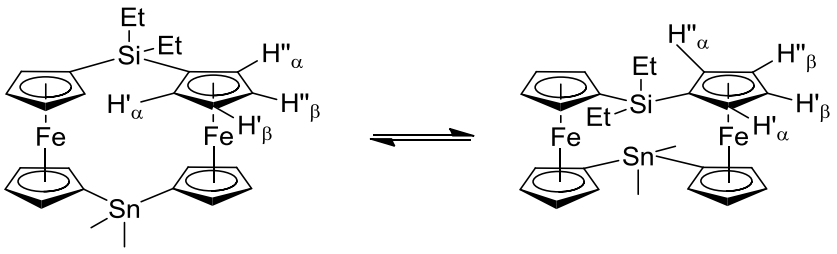

The *anti*-to-*anti* isomerization exchanges the positions of the H'$_\alpha$ protons and the H"$_\alpha$ protons so that both can be the inner or outer α-protons, rendering them equivalent on the NMR timescale. The same occurs for H'$_\beta$ protons and the H"$_\beta$ protons. Moreover, the dimethylstannyl groups or ethylsilyl groups change positions during this exchange so that each of the methyl groups on tin or ethyl groups on silicon can be in *endo* and in *exo* positions. Therefore, only one signal was observed for each of these groups. *anti*-to-*anti* exchanges were previously observed for tin- and silicon-bridged [1.1]FCPs.[13]

$^{29}$Si NMR spectroscopy of **142$_1$** revealed one signal at δ -2.3. This signal was not observed in the $^{29}$Si NMR spectrum of **142$_n$** (δ -2.9; -3.0), which indicates that **142$_1$** was only present in very minor amounts. The dimethylsilyl-bridged [1.1]FCP **15** has a significantly different shift in the $^{29}$Si NMR spectrum of δ -6.52.[13a]

$^{119}$Sn NMR spectroscopy of **142$_1$** gave one signal at δ -23.0, which is one of the minor signals observed for **142$_n$** (δ -23.0, -15.8, -10.0, -7.5). Conversely, this suggests that the presence of **142$_1$** in **142$_n$** can be seen by $^{119}$Sn NMR spectroscopy, but not by $^{29}$Si NMR spectroscopy. A possible reason would be that the $^{29}$Si NMR spectrum is not as resolved as the $^{119}$Sn NMR spectrum. The other minor peaks observed in the $^{119}$Sn NMR spectrum of **142$_n$** might also have corresponding signals in the $^{29}$Si NMR spectrum that cannot be observed because of a lower resolution and poorer signal to noise ratio.

Even though crystals of **142$_1$** were obtained by crystallization from a variety of solvents and solvent mixtures, it was not possible to determine a molecular structure by single-crystal X-ray analysis, because of twinning problems. Therefore, no proof of the *anti* conformation of **142$_1$** was obtained. However, since all silicon-bridged and all tin-bridged [1.1]FCPs display an *anti* conformation (see Chapter 1.2.2), there can be little

doubt about $\mathbf{142_1}$ being in the *anti* conformation. Mass spectrometry of this species confirmed the identity of $\mathbf{142_1}$. B. Bagh isolated the [1.1]FCP with dimethylsilyl and dimethylstannyl bridges ($\mathbf{145_1}$) which also showed an *anti*-to-*anti* isomerization in solution.

MALDI-TOF analysis of the oligomers with alternating diethylsilyl and di-*tert*-butystannyl bridges ($\mathbf{144_n}$) did not show the presence of oligomers with higher numbers of repeating units that would be expected to be present based on GPC and DLS analysis (Chapter 4.2.1). Therefore, $\mathbf{144_n}$ was treated by column chromatography in order to isolate oligomers. The column chromatography gave mixtures of species and only the [1.1.1.1]FCP $\mathbf{144_2c}$ was isolated in a low yield of 3% (Figure 4-8). The respective species with dimethylsilyl-bridges instead of diethylsilyl-bridges ($\mathbf{147_2c}$) was isolated by B. Bagh by crystallization (Figure 4-8). In contrast to the large number of known [1.1]FCPs, [1.1.1.1]FCPs are scarcely studied species. Carbon- and silicon-bridged [1.1.1.1]FCPs were the only [1.1.1.1]FCPs that have been known prior to our investigations.

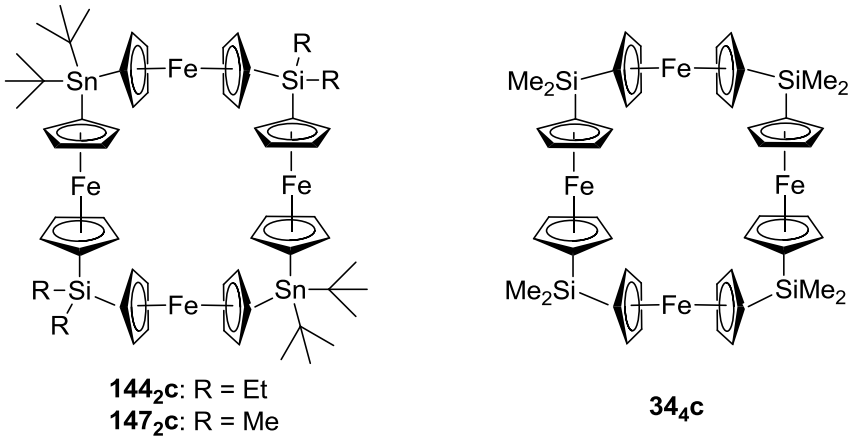


**Figure 4-8.** Depiction of the silicon-tin-bridged [1.1.1.1]FCP $\mathbf{144_2c}$ and $\mathbf{147_2c}$ and the dimethylsilyl-bridged [1.1.1.1]FCP ($\mathbf{34_4c}$).

Similarly to the [1.1]FCPs **142$_1$** and **145$_1$**, the $^1$H NMR spectrum of **144$_2$c** showed only four cyclopentadienyl protons at δ 4.11, 4.13, 4.28, and 4.32. This can be explained by assuming that a fast ring-inversion occurs that exchanges the inner and outer Cp protons rendering the α- or β-protons on one cyclopentadienyl ring equivalent on the NMR timescale. At the same time, only one singlet was observed for the di-*t*-butylstannyl groups and one triplet and one quartet for the diethylsilyl groups. The splitting of $^1$H NMR signals that are assigned to the Cp protons in **144$_2$c** is larger than in **142$_1$** with δ 4.25, 4.26, 4.29, and 4.30.

The $^{13}$C NMR spectrum of **144$_2$c** displayed six peaks for the Cp-protons and the signals of the α- and β-protons were assigned to the Cp rings, which are bound to silicon or tin depending on the presence or absence of tin satellites [70.0 (*ipso*-C of Si-$C_5H_4$ or Sn-$C_5H_4$), 70.5 (*ipso*-C of Si-$C_5H_4$ or Sn-$C_5H_4$), 71.7, 74.3 (α- and β-C of Si-$C_5H_4$), 71.4, 75.0 (α- and β-C of Sn-$C_5H_4$)]. The identity of **144$_2$c** was confirmed by mass spectrometry.

Crystals suitable for single crystal X-ray analysis of **144$_2$c** were grown from hexane solutions and the X-ray analysis was carried out by Dr. G. Schatte (SSSC). Figure 4-9 shows the ORTEP plot of molecular structure of **144$_2$c**.

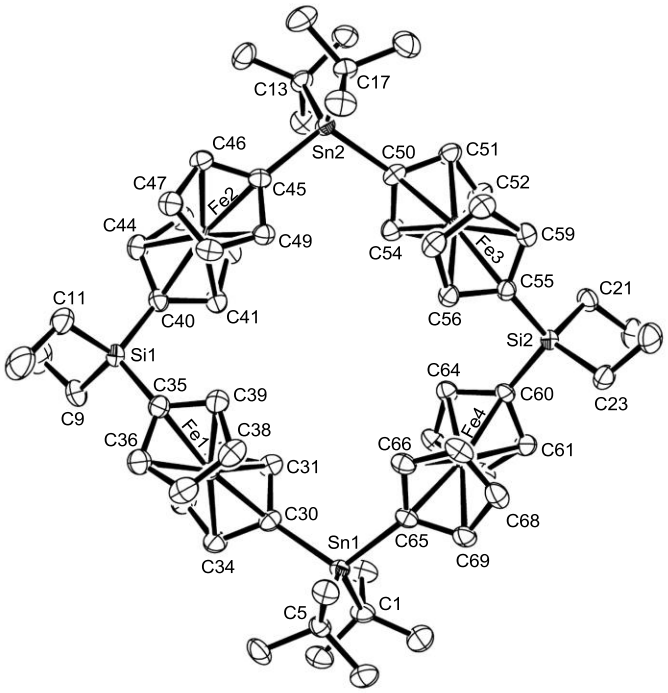


**Figure 4-9.** Molecular structure of **144$_2$c** with thermal ellipsoids at the 50% probability level. Hydrogen atoms are omitted for clarity. Selected atom-atom distances [Å] and bond angles [º]: Si1-C9 = 1.878(3), Si1-C11 = 1.877(3), Si1-C35 = 1.861(2), Si1-C40 = 1.857(3), Si2-C21 = 1.878(2), Si2-C23 = 1.880(2), Si2-C55 = 1.861(2), Si2-C60 = 1.859(2), Sn1-C1 = 2.185(2), Sn1-C5 = 2.187(2), Sn1-C30 = 2.129(2), Sn1-C65 = 2.132(2), Sn2-C13 = 2.195(2), Sn2-C17 = 2.193(2), Sn2-C45 = 2.127(2), Sn2-C50 = 2.135(2), Fe1-Fe2 = 5.5979(5), Fe1-Fe4 = 5.9956(5), Fe2-Fe3 = 5.9813(5), Fe3-Fe4 = 5.5652(4), Fe1-Fe3 = 8.2023(5), Fe2-Fe4 = 8.1558(5), C30-Sn1-C65 = 112.57(9), C35-Si1-C40 = 112.23(11), C45-Sn2-C50 = 111.17(9), Reprinted with permission from Bagh, B.; Breit, N. C.; Dey, S.; Gilroy, J. B.; Schatte, G.; Harms, K.; Müller, J. *Chem.–Eur. J.* **2012**, *18*, 9722-9733. Copyright 2012 Wiley VCH.

The Si-C or Sn-C bond length and related angles are in the expected range. The overall shape of the molecule is a square similar to the dimethylsilyl-bridged [1.1.1.1]FCP **34$_4$c** (Figure 4-8).[8] Interestingly, the molecular structure of **147$_2$c** exhibits an oval shape (Figure 4-10).

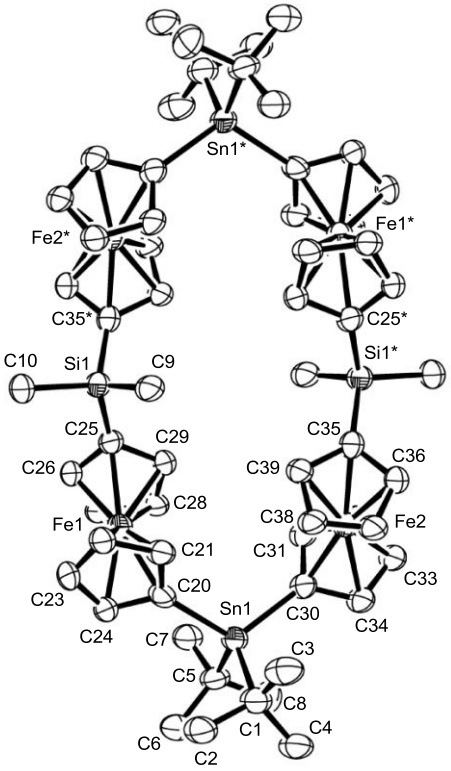


**Figure 4-10.** Molecular structure of **147$_2$c** with thermal ellipsoids at the 50% probability level. Hydrogen atoms are omitted for clarity. Reprinted with permission from Bagh, B.; Breit, N. C.; Dey, S.; Gilroy, J. B.; Schatte, G.; Harms, K.; Müller, J. *Chem.–Eur. J.* **2012**, *18*, 9722-9733. Copyright 2012 Wiley VCH.

The difference in the shape of the diethylsilyl-bridged species **144$_2$c** and the dimethylsilyl-bridged **147$_2$c** can be exemplified by their Fe···Fe distances. Species **144$_2$c** exhibits similar Fe···Fe distances between neighboring iron atoms in the range of 5.5652(4) and 5.9956(5) Å, whereas **147$_2$c** has a long Fe···Fe distance of 6.948(4) Å (Fe1···Fe2*) and a short Fe···Fe distance of 5.440(4) Å (Fe1···Fe2). The difference between the shapes can be described as the orientation of the ferrocenediyl groups around the silicon and tin centers. A staggered conformation of the ferrocenediyl moieties is preferred to an eclipsed arrangement due to steric repulsions. Figure 4-11 shows a Newman projection along the silicon-Cp or tin-Cp bond. The ferrocenediyl moieties can

be opposite to each other, *trans*, or in a 60° angle to each other, *gauche*. Each silicon or tin atom is bonded to two ferrocenediyl moieties, therefore, combinations of *trans,trans*, *trans,gauche* and *gauche,gauche* are possible. The solid-state structure of **144$_2$c** exhibited only *gauche,gauche* orientations, while the solid-state structure of **147$_2$c** revealed *trans,trans* orientations at the silicon centers and *gauche,gauche* orientations at the tin centers. This different arrangement leads directly to the different shapes of the solid-state structures of **144$_2$c** and **147$_2$c**.

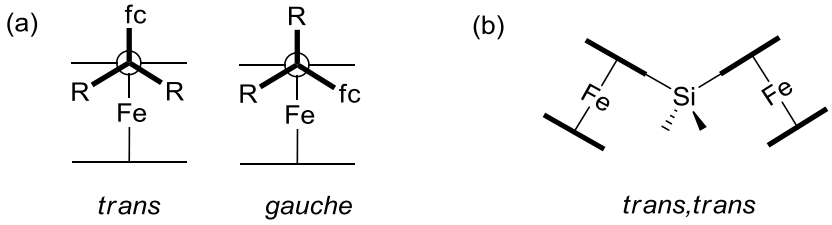


**Figure 4-11.** Possible orientations of groups on the bridging atom in [1.1.1.1]FCPs. a) Newman projection along Si-Cp or Sn-Cp bonds. *trans* and *gauche* describe the position of the $Cp^{centr}$–Fe–$Cp^{centr}$ axis of the two ferrocenediyl moieties to each other. b) $fc_2SiMe_2$ moiety in *trans,trans* conformation. Reprinted with permission from Bagh, B.; Breit, N. C.; Dey, S.; Gilroy, J. B.; Schatte, G.; Harms, K.; Müller, J. *Chem.–Eur. J.* **2012**, *18*, 9722-9733. Copyright 2012 Wiley VCH.

### 4.2.3 Gallium-Silicon-Mixed-Bridged [1.1]Ferrocenophanes and Polyferrocenes

Species **141** was lithiated with *n*-butyllithium and subsequently treated with (Ar′)$GaCl_2$ to give the anticipated silicon-gallium-mixed-bridged [1.1]FCP **148$_1$** as the main product (Scheme 4-6).

**Scheme 4-6.** Synthesis of silicon-gallium-mixed-bridged [1.1]FCP **148$_1$** and polyferrocenophanes with alternating silicon and gallium bridging elements **148$_n$**.

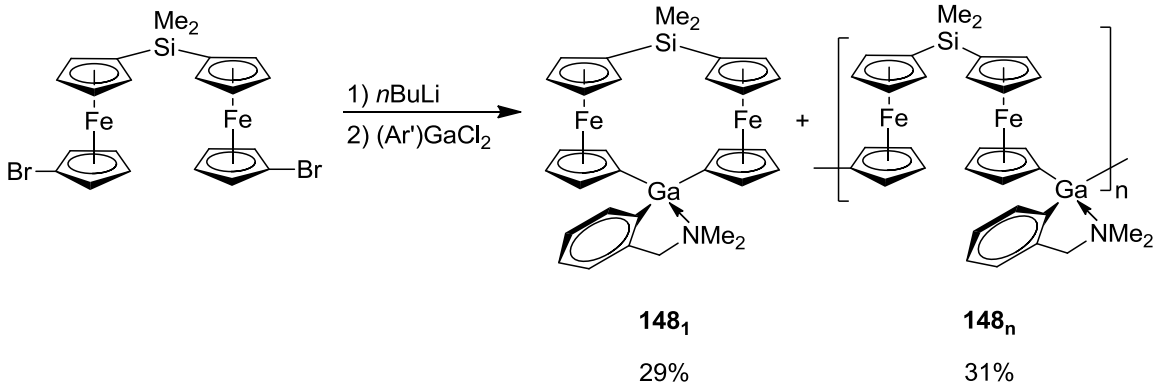


**148$_1$** 29%

**148$_n$** 31%

Species **148$_1$** was isolated by extractions into hexanes in a low yield of 29%. The major factor diminishing the yield of **148$_1$** was the formation of oligomers **148$_n$** as side products. These oligomers will be discussed later separately. $^1$H NMR spectroscopy of **148$_1$** revealed eight signals for the cyclopentadienyl protons and two singlets for the dimethylsilyl protons in addition to the expected 6 signals for the Ar′ ligand. This clearly shows the $C_s$ symmetry of **148$_1$** in solution. It can be assumed that the flipping of the envelop conformations of the five-membered ring formed between the Ar′ ligand and gallium is fast on the NMR timescale. The silicon-tin-bridged [1.1]FCPs showed *anti*-to-*anti* isomerization on the NMR timescale (see Chapter 4.2.2). If an *anti*-to-*anti* isomerization would occur for **148$_1$**, then the nitrogen-gallium donor bond would need to break, the ligand would need to rotate and the isomerization would need to occur at the same time. No *anti*-to-*anti* isomerization was observed for gallium- or aluminum-bridged [1.1]FCPs with larger ligands, while the indium-bridged [1.1]FCP **107** is known to undergo *anti*-to-*anti* isomerization.[14] Indium has a lower Lewis-acidity than aluminum and gallium, therefore, the nitrogen donor bond is weaker. As a result, the nitrogen-indium donor-bond can break more easily, and the *anti*-to-*anti* isomerization occurs fast

on the NMR timescale. VT-NMR spectroscopy was performed with **148$_1$** in order to investigate if elevated temperatures can increase the rate of this exchange. However, no fast *anti*-to-*anti* isomerization for **148$_1$** at the NMR timescale was observed at temperatures up to 80 °C.

Crystals suitable for single-crystal X-ray analysis of **148$_1$** were grown from toluene solutions. The X-ray analysis and the determination of the molecular structure were done by Dr. G. Schatte (SSSC). Species **148$_1$** crystallizes with two independent molecules in the unit cell. The ORTEP plot of one of the independent molecules of **148$_1$** is depicted in Figure 4-12.

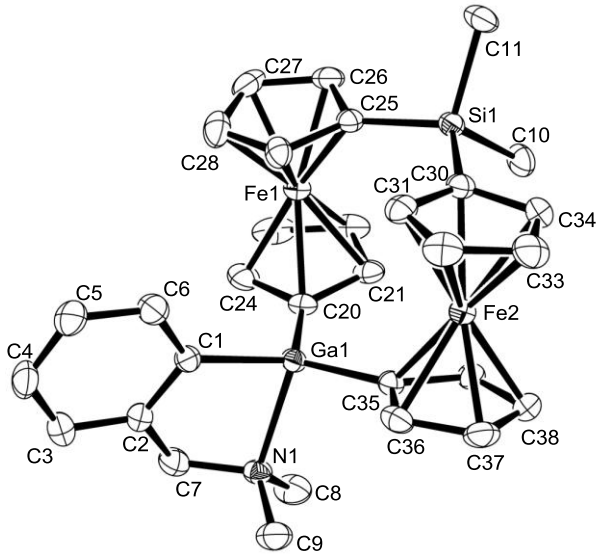


**Figure 4-12.** Molecular structure of **148$_1$** with thermal ellipsoids at the 50% probability level**.** Hydrogen atoms are omitted for clarity. Only one of two independent molecules is shown. Selected atom-atom distances [Å] (values for the second independent molecule shown in braces): Ga1–N1 2.1585(18) {2.158(2)}; Ga1–C1 1.983(2) {1.980(3)}; Ga1–C20 1.952(2) {1.962(2)}; Ga1–C35 1.962(2) {1.948(2)}; Fe1···Fe2 5.2777(5) {5.3281(4)}; C20···C35 3.362(3) {3.375(3)}, C25···C30 3.095(3) {3.115(3)}. Tilt angles between the least square planes of the C atoms of the Cp rings are 1.44(13)° {4.44(13)} (at Fe1) and 6.71(11)° {5.23(13)} (at Fe2). Reprinted with permission from Bagh, B.; Breit, N. C.; Gilroy, J. B.; Schatte, G.; Müller, J. *Chem. Comm.* **2012**, *48*, 7823-7825. Copyright 2012 The Royal Society of Chemistry.

The molecular structure in the solid state revealed **148$_1$** to exist in the expected *anti* conformation similar to its symmetrically bridged relatives **78** and **15**.[6d,13a] The distance between the *ipso*-Cp carbon atoms, which are connected by one bridging element, decreases when the size of the connecting bridging element decreases from gallium to silicon [in **148$_1$** the distance between the gallium-bound *ipso*-Cp carbon atoms C20···C35 are 3.362(3) Å {3.375(3)}, and the silicon-bound *ipso*-Cp carbon atoms C25···C30 are 3.095(3) Å {3.115(3)}]. The molecular structure of **149$_1$** showed the same structural parameters [the distance between the gallium-bound *ipso*-Cp carbon atoms C20···C35 is 3.347(3) Å, and the silicon bound *ipso*-Cp carbon atoms is C25···C30 3.120(3) Å]. It is likely that the different distances between the Cp groups influence the tilt angles α to be up to 6.71(11)° [tilt angles in **148$_1$**: 1.44(13), 4.44(13)° at Fe1 and 6.71(11), 5.23(13)° at Fe2 and tilt angles in **149$_1$**: 5.07(12)° at Fe1 and 4.35(12)º at Fe2] and that, therefore, the presence of two different bridging elements in [1.1]FCPs introduces this slight distortion. The Fe···Fe distances in **148$_1$** of 5.2777(5) and 5.3281(4) Å are very similar to the Fe···Fe distance in **149$_1$** with 5.3147(4) Å and in between the Fe···Fe distances of the dimethylsilyl-bridged [1.1]FCP (**15**) with 5.171(9) Å[13a] and the gallium-bridged [1.1]FCP equipped with the Ar′ ligand (**78**) with 5.462 Å.[6d] The coordination of the gallium atom in **148$_1$** is very similar to its relatives **149$_1$** and **78** [**148$_1$**: Ga–C1 = 1.983(2), 1.980(3) Å, Ga–N1 = 2.1585(18), 2.158(2) Å, N1-Ga-C1 = 83.96(8), 83.33(9)°; **149$_1$**: Ga–C1 = 1.973(2) Å, Ga–N1 = 2.1626(16) Å, N1-Ga-C1 = 84.51(7)°; **78**: Ga–C1 = 1.988(3) Å, Ga–N1 = 2.178(3) Å, N1-Ga-C1 = 84.51(7)°]

The mixture of ferrocenyl-based oligomers with silicon and gallium as alternating bridges (**148$_n$**) was isolated by precipitations of a toluene solution into hexane in a low

yield of 31%. $^1$H NMR spectrum of $\mathbf{148_n}$ revealed many broad peaks for the aromatic protons and multiple broad peaks for the Cp protons and the dimethylsilyl group. MALDI-TOF analysis of $\mathbf{148_n}$ revealed the presence of the cyclic oligomers $\mathbf{148_nc}$ and three kind of linear oligomers, $\mathbf{148_ml_1}$, $\mathbf{148_ml_2}$, and$\mathbf{148_ml_3}$ (Figure 4-13).

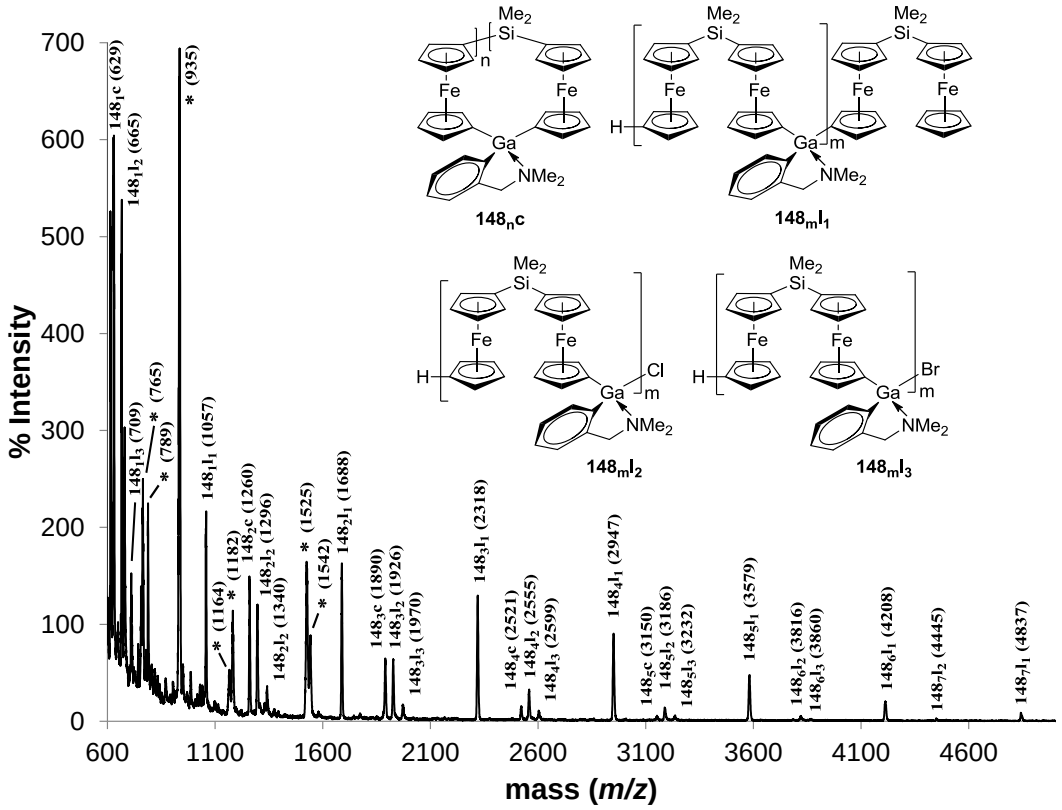


**Figure 4-13.** MALDI-TOF spectrum of $\mathbf{148_n}$ revealing the presence of $\mathbf{148_nc}$, $\mathbf{148_ml_1}$, $\mathbf{148_ml_2}$, and$\mathbf{148_ml_3}$ (* indicates unassigned peaks). Reprinted with permission from Bagh, B.; Breit, N. C.; Gilroy, J. B.; Schatte, G.; Müller, J. *Chem. Comm.* **2012**, *48*, 7823-7825. Copyright 2012 The Royal Society of Chemistry.

The linear oligomers can be distinguished by their end groups being either a dimethylsilyl-bound ferrocenyl moiety in $\mathbf{148_ml_1}$ or a gallium end group that is still equipped with the Ar′ ligand and chlorine or bromine $\mathbf{148_ml_2}$ and $\mathbf{148_ml_3}$ (Figure 4-13).

The linear oligomer **148$_m$l$_1$** showed the most intense peaks compared with the other species of similar repeating units. MALDI-TOF data suggests that the oligomers with bromine as an end group (**148$_m$l$_3$**) are underrepresented in the reaction mixture in comparison with the oligomers with chlorine as an end group (**148$_m$l$_2$**). The cyclic oligomers **148$_n$c** showed similar intensities by MALDI-TOF to **148$_m$l$_2$** for low numbers of repeating units up to n = 3. The intensity of the peaks in the MALDI-TOF spectrum for the cyclic species with n = 4 and n = 5 decreases significantly. Interestingly for the oligomers and polymers with alternating bridges of silicon and gallium equipped with the *p*-SiMe$_3$Ar´ ligand (**149$_n$c**, **149$_m$l$_1$**, **149$_m$l$_2$** and **149$_m$l$_3$**) a different intensity pattern was seen by MALDI-TOF analysis (Figure 4-14). In the MALDI-TOF spectrum of the silicon- and gallium-mixed-bridged polyferrocenes, equipped with the *p*-SiMe$_3$Ar´ ligand, the cyclic species **149$_n$c** can only be found in a very minor amount for n = 2 and not for any larger molecules, whereas the oligomers with the gallium chlorine or bromine end groups **149$_m$l$_2$** and **149$_m$l$_3$** show the highest intensities. The cause for the different compositions of **148$_n$** and **149$_n$** is not known. It would be surprising that a minor change of the ligand by incorporating a trimethylsilyl group in the *para* position would have such a large effect.

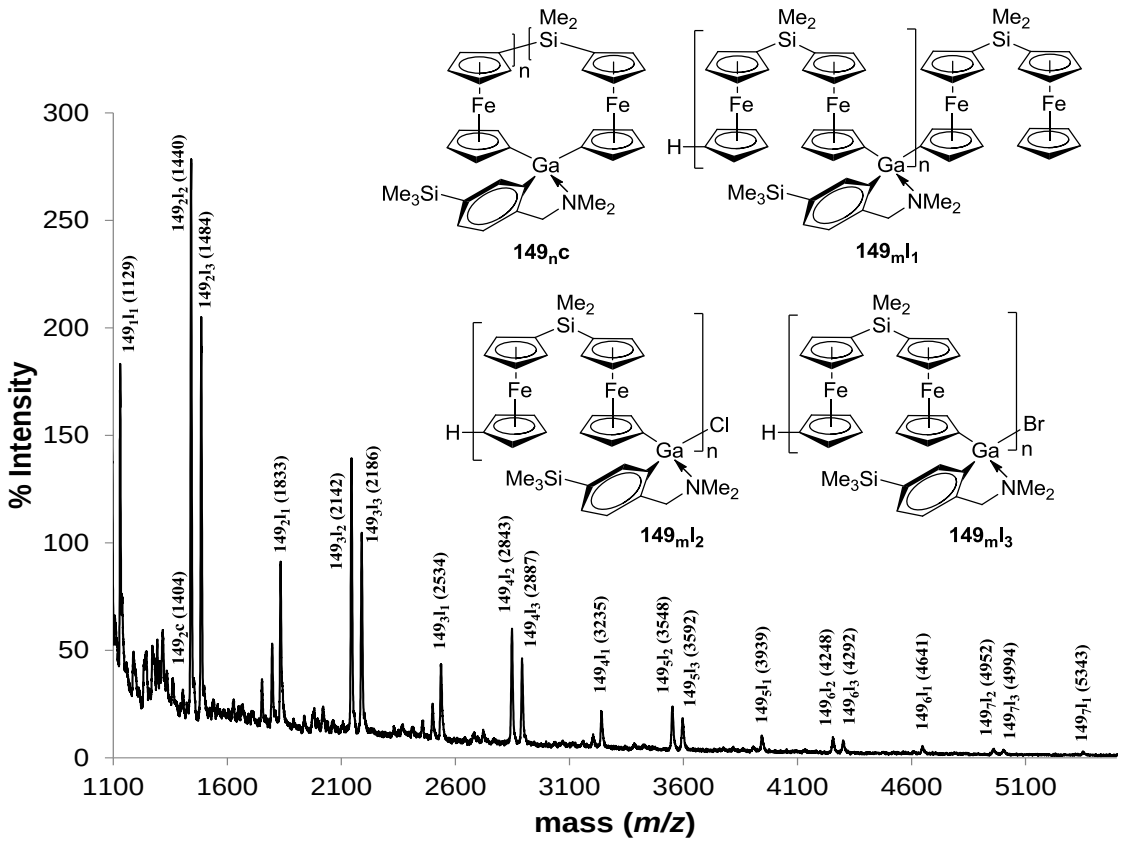


**Figure 4-14.** MALDI-TOF spectrum of $\mathbf{149_n}$ revealing the presence of $\mathbf{149_nc}$, $\mathbf{149_ml_1}$, $\mathbf{149_ml_2}$, and $\mathbf{149_ml_3}$. Reprinted with permission from Bagh, B.; Breit, N. C.; Gilroy, J. B.; Schatte, G.; Müller, J. *Chem. Comm.* **2012**, *48*, 7823-7825. Copyright 2012 The Royal Society of Chemistry.

It is remarkable that bromine was found as a part of the gallium end groups in $\mathbf{148_ml_3}$, though, of course, no gallium bromide containing species was used during the reactions. This leads to the conclusion that a bromine-chlorine exchange occurred. This exchange is likely due to reactions with LiBr similar to the reactions described in Chapter 2.2.4. The silicon-gallium-mixed-bridged oligomers $\mathbf{148_n}$ and $\mathbf{149_n}$ showed gallium-containing end groups, whereas the silicon-tin-bridged polyferrocenes $\mathbf{142_n}$, $\mathbf{143_n}$, $\mathbf{145_n}$, and $\mathbf{146_n}$ showed only ferrocenyl end groups. It is unknown, if the different end groups of the silicon-gallium-bridged oligomers and the silicon-tin-bridged polyferrocenes are a

consequence of the different bridging elements, the different reaction conditions, such as *n*BuLi instead of *t*BuLi and -78 °C instead of 0 °C, or the different workup conditions, like precipitations of a toluene solution into hexanes under inert gas conditions instead of repeated precipitations of a toluene solution into methanol in air. The reactions of **141** with a tin dichloride should have been repeated under the same reaction and workup conditions that were carried out during the synthesis of $\mathbf{148_n}$ and another MALDI-TOF measurement would have needed to be done, in order to conclude something about the origin of the different end groups in $\mathbf{142_n}$-$\mathbf{147_n}$ and $\mathbf{148_n}$-$\mathbf{149_n}$.

Oligomers $\mathbf{148_n}$ were investigated by DLS and GPC. The DLS data was evaluated similar to $\mathbf{129_n}$ (Chapter 3.2.1) and GPC analysis was carried out by Dr. J. B. Gilroy (University of Bristol, U.K.). The results obtained for DLS and GPC measurements were quite similar (Table 4-2). Both methods showed that the oligomers of $\mathbf{148_n}$ had an average molecular weight of only 3.0 kDa, which corresponds to 5 repeating units and 10 ferrocenyl moieties. Oligomers $\mathbf{149_n}$ had twice the size in terms of molecular weights with 10-11 repeating units. This could be another sign of the influence of the trimethylsilyl group in *meta* position to the gallium atom in the Ar´ ligand.

**Table 4-2.** DLS and GPC data for gallium-silicon-bridged ferrocenyl-based oligomers and polymers $\mathbf{148_n}$ and $\mathbf{149_n}$.

| | GPC | | | | DLS | |
|---|---|---|---|---|---|---|
| | $M_n$ [kDa] | $M_w$ [kDa] | PDI | $DP_w$ | $M_w$ [kDa] | $DP_w$ |
| $\mathbf{148_n}$ | 2.11 | 3.08 | 1.46 | 5 | 3.0 | 5 |
| $\mathbf{149_n}$ | 2.69 | 7.05 | 2.62 | 10 | 7.8 | 11 |

The results described in Chapter 4.2.3 were recently published as a short communication.[15]

### 4.2.4 Electrochemical Study of Mixed-bridged Ferrocenophanes

The redox behavior of the [1.1]FCPs **142$_1$** and **148$_1$** was studied with glassy carbon as a working electrode, a silver wire as the quasi reference electrode and a gold wire as the auxiliary electrode with $[Bu_4N][PF_6]$ as the supporting electrolyte and $CH_2Cl_2$ as the solvent. Two, well-separated redox waves were observed for both species, **142$_1$** and **148$_1$** (Figure 4-15 and Figure 4-16). Therefore, **142$_1$** and **148$_1$** are categorized as class II compounds according to Robin and Day.[16]

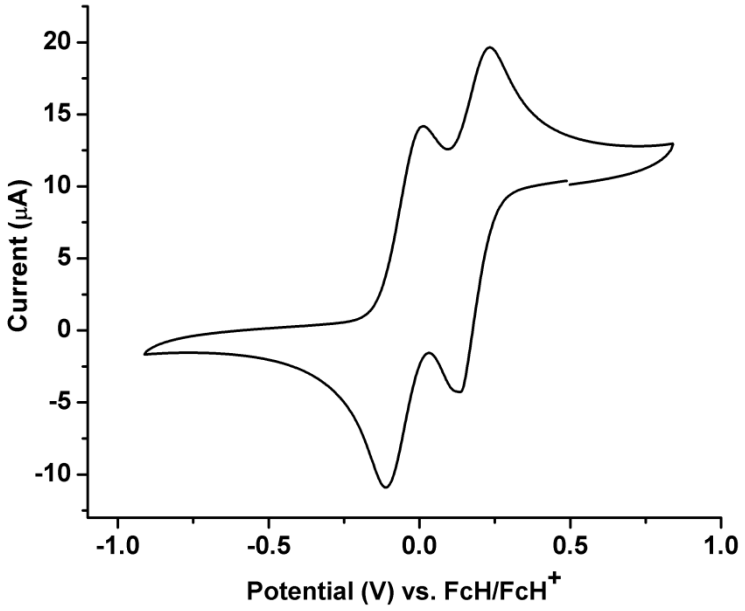


**Figure 4-15.** Cyclic voltammogram of silicon- and tin-bridged [1.1]FCP **142$_1$** referenced to $FcH/FcH^+$.

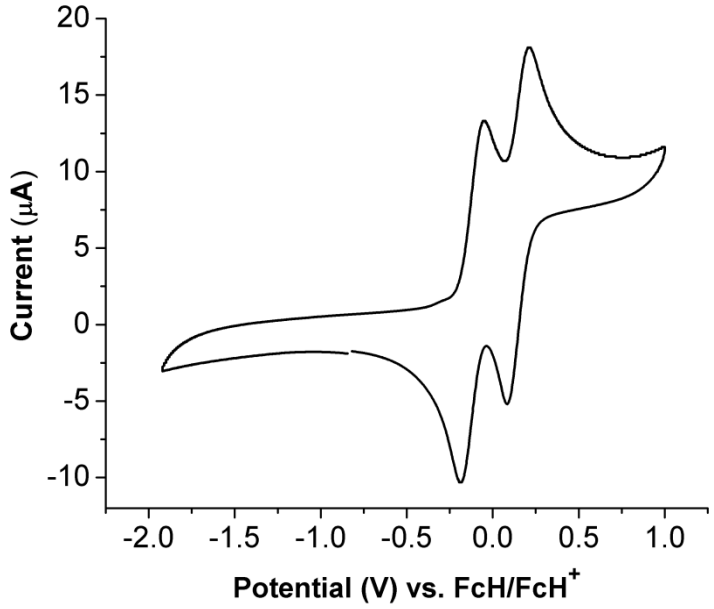


**Figure 4-16.** Cyclic voltammogram of the gallium- and silicon-bridged [1.1]FCP **$148_1$** referenced to $FcH/FcH^+$. Reprinted with permission from Bagh, B.; Breit, N. C.; Gilroy, J. B.; Schatte, G.; Müller, J. *Chem. Comm.* **2012**, *48*, 7823-7825. Copyright 2012 The Royal Society of Chemistry.

The $\Delta E_{1/2}$ values of **$142_1$** and **$148_1$** are in between the $\Delta E_{1/2}$ values that were reported for their symmetrically bridged relatives (Table 4-3). For **$149_1$** the same redox behavior was observed.[15]

**Table 4-3.** Halfwave potentials $E_{1/2}$ and $\Delta E_{1/2}$ for silicon, tin, gallium and mixed-bridged [1.1]FCPs referenced to the $FcH/FcH^+$ couple.

| | $SiMe_2$ $SiMe_2$ | $SnMe_2$ $SnMe_2$ | $SiEt_2$ $SnMe_2$ | (Ar′)Ga (Ar′)Ga | $SiMe_2$ | $(SiMe_3Ar')Ga$ $(SiMe_3Ar')Ga$ | $SiMe_2$ |
|---|---|---|---|---|---|---|---|
| **Nr** | **15** | | **$102_1$** | **78** | **$148_1$** | **80** | **$149_1$** |
| ref | 8 | 17 | | 6d | | 6k | 15 |
| $E_{1/2}$ [V] | -0.01 | -0.138 | -0.049 | 0.05 | -0.122 | -0.049 | -0.138 |
| $E_{1/2}$ [V] | 0.23 | 0.099 | 0.185 | 0.35 | 0.144 | 0.169 | 0.134 |
| $\Delta E_{1/2}$ [V] | 0.24 | 0.237 | 0.234 | 0.30 | 0.266 | 0.218 | 0.272 |

The redox behavior of the [1.1.1.1]FCP with alternating tin and silicon bridges (**$144_2$**) was measured under the same conditions. The cyclic voltammogram of **$144_2$**

displayed three well-separated redox waves of which the last redox wave had the highest intensity (Figure 4-17). The halfwave potentials $E_{1/2}$ of the three redox events are 0.002, 0.193 and 0.372 V. The redox waves are well separated with $\Delta E_{1/2}^{1-2}$ = 0.191 V and $\Delta E_{1/2}^{2-3}$ = 0.179 V.

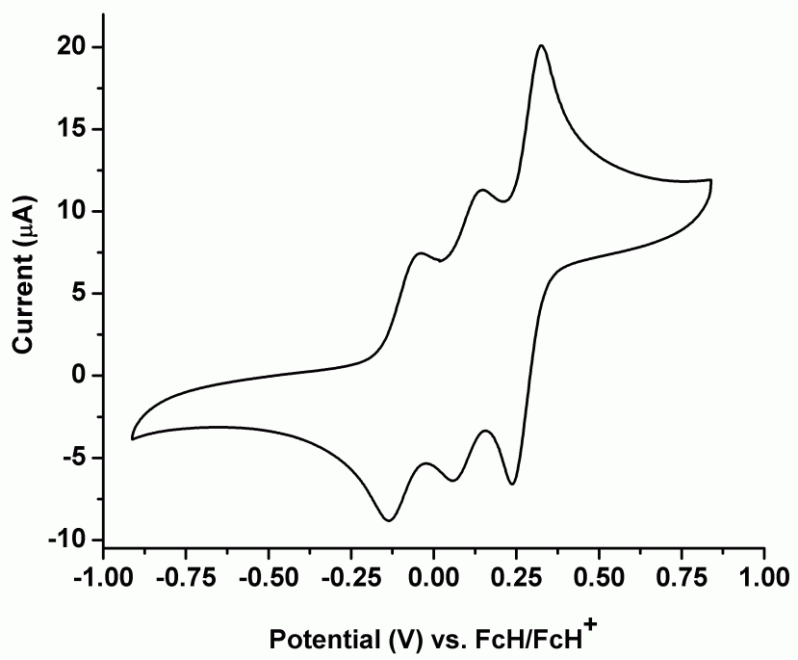


**Figure 4-17.** Cyclic voltammogram of the tin- and silicon-bridged [1.1.1.1]FCP **144$_2$**.

Four redox waves would be expected for **144$_2$**, since it contains four ferrocenediyl moieties. However, only three redox waves were observed and it was presumed that the oxidations / reductions of two ferrocenediyl moieties occurred at the same potential. The higher intensity of the last redox wave in the cyclic voltammogram of **144$_2$** indicated that this redox wave belongs to two electrons. However, the diffusion dependent cyclic voltammetry cannot give an accurate relationship between the current and the amount of oxidizing electrons. Therefore, a hydrodynamic method, using a rotating disk electrode, was chosen, in which the electrode moves and the steady state is attained rather quickly.[18]

Since this technique is diffusion independent, it is also time independent and the measured current at a certain potential is directly related to the amount of transferred electrons. The rotating disk electrode voltammogram of **144$_2$** depicted in Figure 4-18 clearly revealed that the first and second step corresponds to a current increase of approximately 0.000008 μA, whereas the third step showed a current increase of double the amount. Therefore, the last oxidation wave must be due to the oxidation of two ferrocenyl moieties in species **144$_2$**.

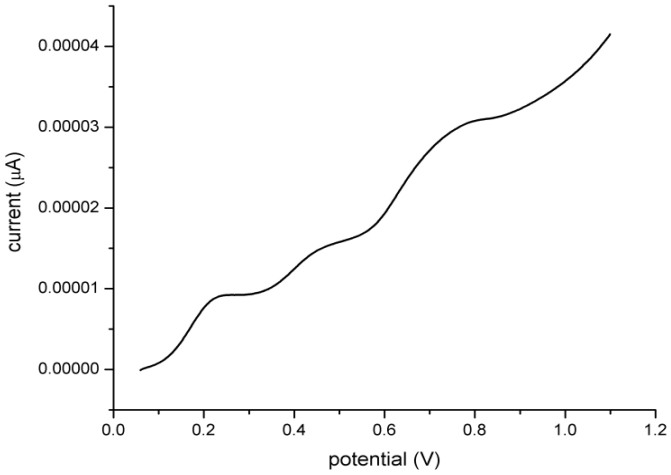


**Figure 4-18.** Rotating disk electrode voltammogram of the tin and silicon-bridged [1.1.1.1]FCP **144$_2$**.

Manners *et al.* studied the redox behavior of the dimethylsilyl-bridged [1.1.1.1]FCP (**34$_4$c**) for which four redox waves were observed.[8] The first two and the last two redox waves occurred at similar potentials, so that the first and third oxidation wave appeared like shoulders on the second and fourth oxidation wave. An explanation for the redox behavior of **34$_4$c** was suggested, in which first one iron center was oxidized with a subsequent oxidation of the opposite iron center (Scheme 4-7). This would be

followed by the oxidation of one more iron center and a last iron center at different potentials.

**Scheme 4-7.** Explanation for the redox-behavior of the dimethylsilyl-bridged [1.1.1.1]FCP **$34_4$c**.

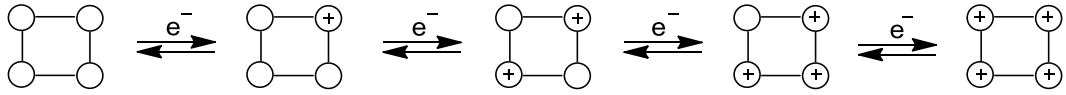


This explanation for the observed redox behavior fits well with the following assumptions: a) An oxidation occurring at a neighboring iron center to an oxidized iron center would require a higher energy than that of an iron center that is opposite to the oxidized iron center. This can be based on the higher distance of the iron centers to each other considering interactions through space as well as through bonds. b) Even though the iron center in the opposite position to the oxidized iron center is far away from the oxidized iron center, it still interacts weakly with the charge of the oxidized iron center. This can be seen by the fact that all oxidations occur at different potentials. However, the interaction is minor, based on the small difference in oxidation potentials for the ferrocenyl moieties in opposite position to each other.

For cyclic species with higher numbers of repeating units like **$34_5$c**, **$34_6$c**, and **$34_7$c**, no interaction was observed anymore between an oxidized iron center and not-neighboring iron centers.[8] This could be due to an increased Fe···Fe distance through space.

Three explanations are suggested to explain the observed redox behavior of **$144_2$** (Scheme 4-8).

**Scheme 4-8.** Possible pathways for the oxidation of **144$_2$** a), b), and c).

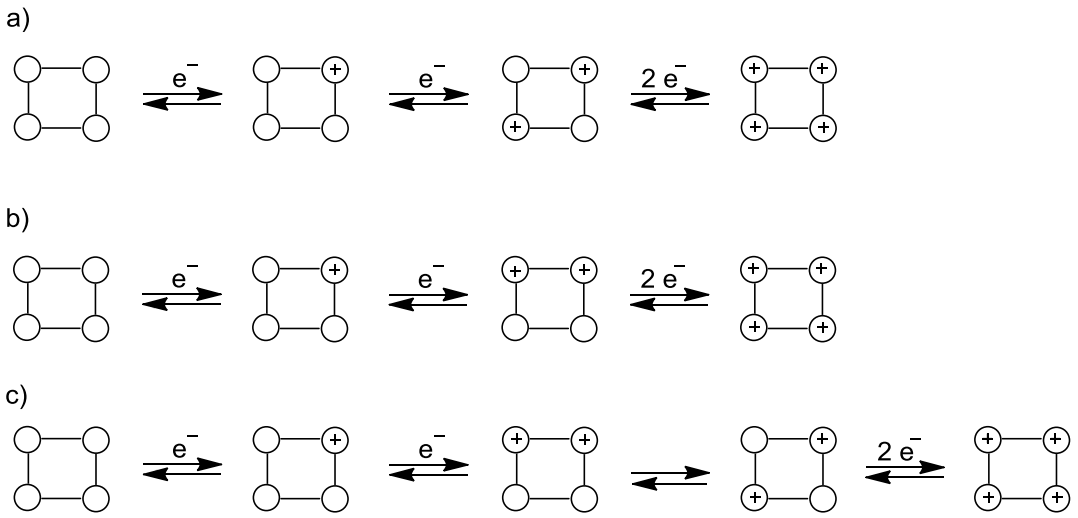


All pathways start with the oxidation of one random iron center. In pathway a), the oxidation of the first iron center is followed by the oxidation of the iron center that is the furthest away. The last step in pathway a) is the oxidation of the last two iron centers that are far away from each other at the same potential. Pathway b) has the second oxidation occurring at a neighboring iron atom to the first oxidized iron atom. The last two neighboring iron centers are oxidized at the same potential. Pathway c) is a combination of pathways a) and b). The second iron center to get oxidized is in a neighboring position to the first oxidized iron center. Then a rearrangement occurs and the charged iron centers are as far away from each other as possible. Afterwards, the oxidation of the two opposite iron centers occurs at the same potential. All three pathways, a), b), and c) have some drawbacks. Pathway a) has the weakness in the second oxidation step. The interaction between the first and the second iron center to be oxidized with $\Delta E_{1/2}$ = 0.191 V is rather similar to bis(ferrocenyl)dimethylsilane and diethylbis(ferrocenyl)silane with 0.215 and 0.204 V[6k] or the dimethylsilyl-bridged

[1.1]FCP (**15**) with 0.233 V.[8] However the bonding situation and the Fe···Fe distances in bis(ferrocenyl)silanes is similar to the neighboring ferrocenyl groups in **144$_2$** than to the opposite ferrocenyl groups in **144$_2$** ($Me_2SiFc_2$: 6.3150(4) Å, $Et_2SiFc_2$: 6.1409(6) Å, **144$_2$**: Fe1-Fe2 = 5.5979(5), Fe1-Fe4 = 5.9956(5), Fe2-Fe3 = 5.9813(5), Fe3-Fe4 = 5.5652(4), Fe1-Fe3 = 8.2023(5), Fe2-Fe4 = 8.1558(5) Å).[6k] Moreover, it would be unlikely that the presence of a distant oxidized iron center would show a rather strong interaction for the second oxidation, but no observable effect for the oxidation of the last iron center. The disadvantage of pathway b) lies in the oxidation of the third and fourth iron center. Based on the argument against pathway a), the second oxidation step fits well with the oxidation of a neighboring iron center. However, it would not make sense that the oxidation of the third iron center that is surrounded by one close and one distant oxidized iron center would require the same voltage to be oxidized as the last iron center that is additionally surrounded by another close, oxidized iron center. Pathway c) tries to accommodate the problems of pathway a) and b). It has the second oxidation occurring in neighboring position, which fits better with the observed $\Delta E_{1/2}$ values. The last two oxidations occur starting from the oxidized iron centers being opposite to each other and if the interaction of any oxidized iron center that is distant is negligible, it is well understandable that the third and fourth oxidation occur at the same potential. It can be expected that the oxidized charges are preferably as far away from each other as possible, which means in opposite positions for the doubly oxidized tetramer **144$_2$**. This would explain, if the charges can travel from one iron center to another iron center, how a shift from the oxidized iron centers being in neighboring position to the two oxidized iron centers being in opposite position could occur. However, it is unknown, why an oxidation of the iron centers in

opposite positions could not occur immediately. Another problem with pathway c) is that even if the oxidation in that order could be explained by the oxidation in opposite position being for unknown reasons not available, this argument does not make sense for the reduction that occurs with the same pattern, since then a shift from the favorable position of the charges on the iron centers to the less favorable position of the charges on iron centers in neighboring position would need to occur. The least likely pathway would be b), but pathway a) and c) also show significant problems.

Another option would be that pathway a) takes place, and the opposite iron centers are for an unknown reason in an unknown conformation significantly closer to each other than in the molecular structure in the solid state. The molecular structure would be different though after the third oxidation.

It might be considered, whether this unusual redox behavior could be explained by a different product than **144$_2$** that would have formed under these conditions, for example that an irreversible ring-opening occurred and a linear oligomer led to this redox behavior. Linear tetra(ferrocenyldimethylsilane) showed three redox events, but the first redox event included the oxidation of two iron centers, followed by two redox events for each one iron center (Scheme 4-9).[7c] Therefore, this possibility is excluded.

**Scheme 4-9.** Explanation for the redox-behavior of the linear dimethylsilyl-bridged ferrocenyl-based oligomer **34$_4$l**

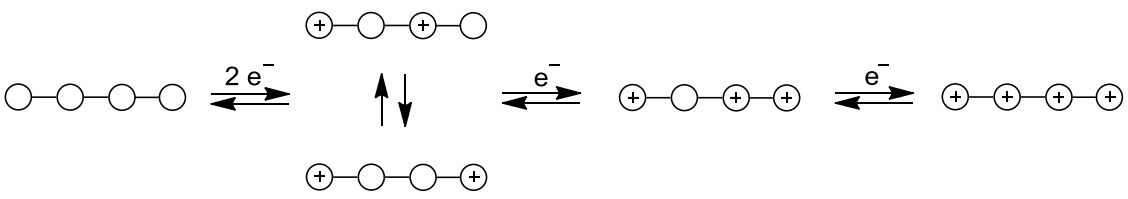

Interestingly, **$147_2$c** that showed a different conformation in the solid state than **$144_2$c**, exhibited the same redox behavior, whereas **$34_4$c** that displayed the same conformation in the solid state as **$144_2$c** exhibited a significantly different redox behavior. Therefore, it can be concluded that the presence of the two different bridging elements are the source for the unprecedented redox behavior of **$144_2$**.

The results of the redox behavior of **$148_1$** were published together with the synthesis and other characterizations of this species.[15] The results of the redox behavior of **$142_1$** and **$144_2$** are not published to date, however, a manuscript is in preparation and they might published in addition to results obtained by B. Bagh about the synthesis and characterization including electrochemical study of tin-bridged oligoferrocenes.[17]

## 4.3 Conclusion

[1.1]FCPs and polyferrocenes with alternating bridging elements with the combinations of silicon and tin and silicon and gallium were synthesized and characterized. The ratios of the different products, [1.1]FCPs, other cyclic oligomers, different kind of linear oligomers as well as the molecular weight of the oligomers depend on the bridging element as well as on the ligands on the bridging elements. Only when gallium dichlorides equipped with a slim ligand like Ar´ were utilized, [1.1]FCPs were formed as the major products. The formation of tin-bridged polyferrocenes is similar to the outcome of the reactions beween tin dichlorides equipped with small ligands and 1,1'-dilithioferrocene, which yielded mainly oligomers.[19] However, it is somewhat surprising that a significant amount of oligomers also formed in reactions with (Ar´)$GaCl_2$, because no formation of oligomers was described for reactions of (Ar´)$GaCl_2$ with 1,1'-dilithioferrocene.[6d] One possible explanation is the presence of silicon as the other bridging element changing the activation barriers of the ring-closing step or the condensation reaction.

Since [1.1]FCPs and polyferrocenes with alternating bridging elements are still in their infancy, many exciting possibilities for future research exist. It would be interesting to see, if in [1.1]FCPs with combinations of bridging elements that prefer *syn* or *anti* conformations, the *syn* or the *anti* conformation would be more dominant. One other interesting option for further research would be the synthesis and characterization of [1.1.1.1]FCPs and polyferrocenes with three alternating bridging elements. Scheme 4-10 displays the synthetic strategy for obtaining these species.

**Scheme 4-10.** Synthetic strategy to access [1.1.1.1]FCPs and polyferrocenes with three alternating bridging elements shown for silicon, tin, and gallium as bridging elements.

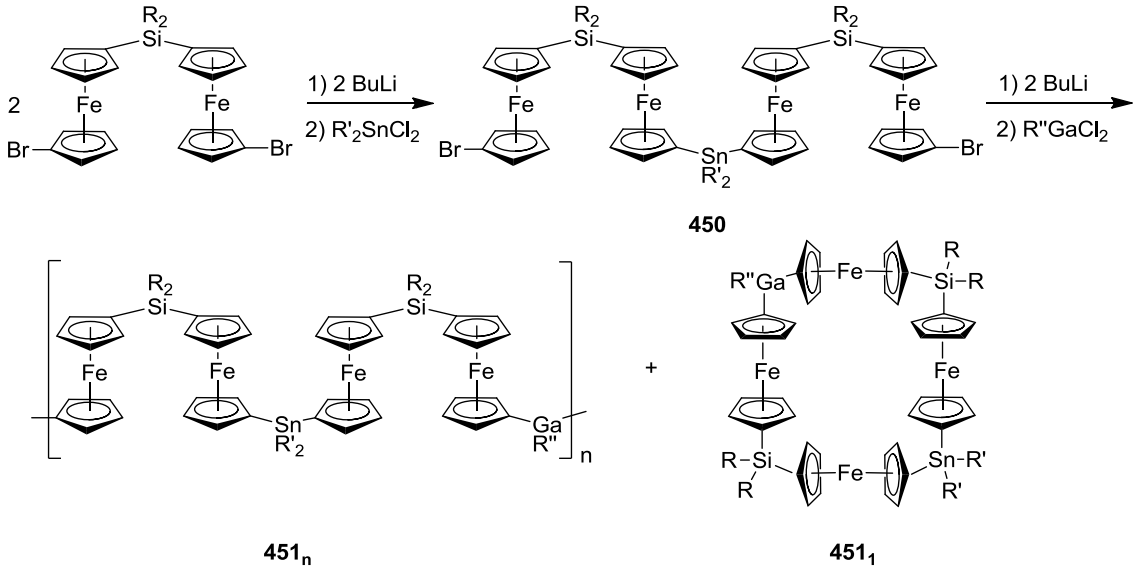


In a first step, a di(1'-bromoferrocenyl)silane would be reacted with one equivalent of a lithiation reagent and subsequent reaction with a tin dichloride would be expected to yield **450** as one of the major compounds. In the second step, **450** would be treated with a lithiation reagent and a gallium dichloride to give a mixture of $\mathbf{451_1}$ and $\mathbf{451_n}$. The study of the [1.1.1.1]FCP $\mathbf{451_1}$ as well as the polymers obtained with three different bridging elements in a well-defined ratio are also very interesting. It is likely that polymers of higher molecular weights could be obtained in this condensation reaction, because the starting material **450** already contains four ferrocenediyl moieties.

## 4.4 Experimental

**General information.** Syntheses were carried out partly using standard Schlenk technique and partly in atmosphere. Dry solvents were used for the reactions and ordinary solvents (as received from suppliers) were used for workup and purifications of air stable compounds. Solvents were dried using a MBraun Solvent Purification System and stored under nitrogen over 3 Å molecular sieves. All solvents for NMR spectroscopy were used as received from suppliers. Ferrocene, *n*BuLi, *t*BuLi, $n$Bu$_2$SnCl$_2$, and $t$Bu$_2$SnCl$_2$ were purchased from Sigma Aldrich, and $Me_2SiCl_2$, $Et_2SiCl_2$, and $Me_2SnCl_2$ were purchased from Alfa Aesar and were used as received. The compounds 1,1′-dibromoferrocene,[20] bis(ferrocenyl)diethylsilane,[5] bis(ferrocenyl)dimethyl-silane[5] (synthesized by Subhayan Dey), and (Ar′)GaCl$_2$[21] were synthesized as described in literature. $^1$H, $^{13}$C, $^{29}$Si and $^{119}$Sn NMR spectra were recorded on a Bruker 500 MHz Avance NMR spectrometer at 25 ºC in $C_6D_6$, $CDCl_3$ and toluene-$D_8$, respectively. $^1$H, $^{13}$C, $^{29}$Si NMR chemical shift values are relative to tetramethylsilane and $^{119}$Sn NMR values are relative to tributyl tin chloride (δ 152.0 in $CDCl_3$). $^1$H chemical shifts were referenced to the residual protons of the deuterated solvents (δ 7.15 for $C_6D_6$, 7.26 for $CDCl_3$ and 2.09, 6.98, 7.02 and 7.09 for toluene-$D_8$); $^{13}$C chemical shifts were referenced to the $C_6D_6$ signal at δ 128.00, the $CDCl_3$ signal at δ 77.00, and the toluene-$D_8$ signals at 20.40, 125.20, 128.00, 128.90 and 137.50. Mass spectra were measured on a VG 70SE and were reported in the form *m/z* (rel intens) [$M^+$] where '*m/z*' is the mass observed, 'rel intens' is the intensity of the peak relative to the most intense peak and '$M^+$' is the molecular ion or fragment; only characteristic mass peaks are reported. For isotopic patterns, only the mass peak of the isotopoloque or isotope with the highest natural abundance is listed.

**MALDI-TOF Mass Spectrometry.** MALDI-TOF mass spectra were collected on a 4700 Proteomics Analyzer (Applied Biosystems) equipped with a Nd:Yag laser, operating at 335 nm. Positive ion mass spectra were obtained in reflector mode over a range of 500 – 5000 *m/*z. Each spectrum was an accumulation of 12500 laser shots over 100 points on the sample (125 shots/point). Laser intensity was varied for each sample. Solutions of the analytes (1 mg $mL^{-1}$ thf solution) and dithranol (10 mg $mL^{-1}$ thf solution) were prepared and then mixed in a 1:10 ratio. The resulting solutions were drop-cast by micropipette into sample wells and allowed to evaporate for 1 h prior to sample analysis.

**Gel Permeation Chromatography (GPC).** Molecular weights of polymers and polydispersity indices (PDI = $M_w$ / $M_n$) of all samples were obtained using a Viscotek VE 2001 Gel Permeation Chromatograph equipped with automatic sampler, pump, injector, in-line degasser, column oven (30 °C), styrene/divinylbenzene columns with pore sizes of 500 to 100,000 Å, and VE 3580 refractometer. As the chromatography eluent, thf stabilized with 0.025% butylated hydroxytoluene (Fisher) was used, at a flow rate of 1.0 mL $min^{-1}$. Samples were dissolved in the eluent (2 mg $mL^{-1}$) and filtered (Acrodisc, PTFE membrane, 0.45 μm) before analysis. Calibration of the refractive index detector was performed using polystyrene standards purchased from Viscotek.

**DLS Analyses.** Dynamic light scattering experiments were performed using a nano series Malvern zetasizer instrument equipped with a 633 nm red laser. Samples were filtered through 0.2 μm syringe PTFE filters before they were analyzed in 1 cm glass cuvettes at concentrations of 5 mg $mL^{-1}$ and 2.5 mg $mL^{-1}$ in thf at 25 °C. The refractive index of the copolymers was assumed to be 1.5 (see Supporting Information for data).

**Electrochemistry.** A computer controlled system, consisting of a HEKA potentiostat PG590 (HEKA, Mahone Bay, NS, Canada) was used for the cyclic voltammetry experiments. CV data was collected using a multifunction DAQ card (BNC-2090 for **$102_1$** and **$104_2$** and PCI 6251 M Series, National Instruments Austin, Texas for **$108_1$**) and in-house software written in the LabVIEW environment. Rotating disk electrode data was measured with an Autolab PGSTAT302N, with an Autolab rotating disc electrode. Autolab control and data collection was done with the accompanying software, NOVA. For all cyclic voltammetry measurements, glassy carbon (BAS, 3 mm) was used as the working electrode, silver wire as the quasi-reference electrode, and a loop of gold wire as the auxiliary electrode. The rotating disc electrode data was obtained with platinum as a working electrode and gold as an auxiliary and quasi-reference electrode. The rotation speed was 300 rpm. All measurements were made against the quasi-reference electrode. The scan rate for the reported cyclic votammograms was 50 mV/s and 50 mV/s for the rotating disk electrode. The measurement of **$148_1$** was conducted inside a glovebox, whereas **$142_1$** and **$144_2$** were measured in air. All measurements were carried out at ambient temperature (22 °C). Before each measurement, 1 mM solutions of all species were freshly prepared in dry $CH_2Cl_2$ with 0.1 M $[Bu_4N][PF_6]$ as the supporting electrolyte. The electrolyte was dried overnight under high vacuum at 100 °C.

**General procedure for the syntheses of the three mixtures $142_n$, $143_n$, $144_n$.** *t*BuLi (1.7 M in pentane) was added dropwise to a cold solution of **141** in a mixture of dry thf/hexanes (1:9) under $N_2$-atmosphere. After the addition of *t*BuLi, the reaction mixture was stirred for 20 min at 0 °C, followed by the addition of a solution of $R'_2SnCl_2$ (R' = Me, *n*Bu, *t*Bu) in thf. The reaction mixture was warmed up to r.t. and stirred for

additional 2.5 h, resulting in a red solution. The following work-up was done in air, using ACS grade solvents as received. All volatiles were removed from the red solution, resulting in a red paste which was extracted with toluene. The toluene solution was concentrated to one third of its original volume and added dropwise to hexanes (3-4 times the volume of toluene solution) while stirring vigorously, resulting in a red solution with an off-white precipitate. The solid was filtered off and all volatiles were removed from the red solution, yielding a red paste which was redissolved in toluene. The toluene solution was added dropwise to MeOH (3-4 times the volume of the toluene solution) while stirring vigorously, resulting in a gummy red precipitate within an orange solution. The solid was filtered off, dried under high vacuum and dissolved in toluene. A second precipitation into MeOH resulted in a gummy red precipitate and a pale yellow solution. The solid was filtered off and dried under high vacuum at 65 °C for 16 h, yielding either red solid or gummy materials.

**Synthesis of $\mathbf{142_n}$.** As described in the general procedure, **141** (1.29 g, 2.10 mmol) in thf/hexanes (4 mL/36 mL), *t*BuLi (5.10 mL, 8.67 mmol), and $Me_2SnCl_2$ (0.463 g, 2.11 mmol) in thf (25 mL) resulted in $\mathbf{142_n}$ as a red solid (0.706 g, ~61%). $^1$H NMR ($C_6D_6$): δ 0.4 – 0.6 (br m, 6H, $SnMe_2$), 0.9 – 1.1 (br m, 4H, $CH_2$ of $SiEt_2$), 1.1 – 1.3 (br m, 6H, $CH_3$ of $SiEt_2$), 3.9 – 4.5 (br m, 16H, Cp). $^{13}$C NMR ($C_6D_6$): δ -8.5 ($SnMe_2$), 6.5 ($CH_2$ of $SiEt_2$), 8.6 ($CH_3$ of $SiEt_2$), 68.7 ($C_5H_5$), 74.0, 71.9, 70.1 (Si-bound $C_5H_4$), 74.7, 71.3, 69.3 (Sn-bound $C_5H_4$), 71.0. $^{29}$Si NMR: δ -2.9, -3.0 ($SiEt_2$). $^{119}$Sn NMR: δ -23.0, -15.8, -10.0, -7.5 ($SnMe_2$).

**Synthesis of $\mathbf{143_n}$.** As described in the general procedure, **141** (1.30 g, 2.11 mmol) in thf/hexanes (4mL/36mL), *t*BuLi (5.10 mL, 8.67 mmol), and *n*$Bu_2SnCl_2$ (0.649

g, 2.14 mmol) in thf (25 mL) resulted in **143$_n$** as a red solid (0.750 g, ~56 %). $^1$H NMR ($C_6D_6$): δ 0.9 – 1.1 (br m, 6H, $CH_3$ of Sn$^n$Bu$_2$), 1.1 – 1.2 (br m, 4H, $CH_2$ of $SiEt_2$), 1.2 – 1.3 (br m, 6H, $CH_3$ of $SiEt_2$), 1.3 – 1.4 ( br m, 4H, $CH_2$ of Sn*n*Bu$_2$), 1.4 – 1.6 (br m, 4H, $CH_2$ of Sn*n*Bu$_2$), 1.7 – 1.9 (br m, 4H, $CH_2$ of Sn$^n$Bu$_2$), 3.9 – 4.5 (br m, 16H, Cp). $^{13}$C NMR ($C_6D_6$): δ 6.5 ($CH_2$ of $SiEt_2$), 8.6 ($CH_3$ of $SiEt_2$), 11.9, 14.0, 27.9, 29.7 (Sn*n*Bu$_2$), 68.7 ($C_5H_5$), 74.0, 71.8, 70.0 (Si-bound $C_5H_4$), 74.9, 71.4, 69.2 (Sn-bound $C_5H_4$), 71.3. $^{29}$Si NMR: δ -3.0, -3.1 ($SiEt_2$). $^{119}$Sn NMR: δ -31.8, -30.4, -28.5, -26.6 (Sn$^n$Bu$_2$).

**Synthesis of 144$_n$.** As described in the general procedure, **141** (1.26 g, 2.05 mmol) in thf/hexanes (4mL/36mL), $^t$BuLi (5.00 mL, 8.50 mmol), and *t*Bu$_2$SnCl$_2$ (0.622 g, 2.05 mmol) in thf (25 mL) resulted in **144$_n$** as a red solid (0.848 g, ~66%). $^1$H NMR ($C_6D_6$): δ 0.9 – 1.1 (br m, 4H, $CH_2$ of $SiEt_2$), 1.1 – 1.3 (br m, 6H, $CH_3$ of $SiEt_2$), 1.3 – 1.5 (br m, 18H, Sn$^t$Bu$_2$), 3.9 – 4.5 (br m, 16H, Cp). $^{13}$C NMR ($C_6D_6$): δ 6.5 ($CH_2$ of $SiEt_2$), 8.6 ($CH_3$ of $SiEt_2$), 31.6 (C of Sn*t*Bu$_2$), 31.8 ($CH_3$ of Sn*t*Bu$_2$), 68.7 ($C_5H_5$), 74.0, 71.6, 69.9 (Si-bound $C_5H_4$), 74.9, 72.0, 70.7 (Sn-bound $C_5H_4$); plus additional unassigned peaks (see Figure S16). $^{29}$Si NMR: δ -2.9, -3.0 ($SiEt_2$). $^{119}$Sn NMR: δ -48.7, -43.1, -38.2, -34.4, (Sn*t*Bu$_2$), 75.2 (Sn*t*Bu$_2$Cl).

**Isolation and characterization of 142$_1$ and 144$_2$c.**

**142$_1$.** Isolated as orange crystals (0.041 g, 3%) from a solution of the mixture **142$_n$** in hexane at r.t. Crystals for attempted analysis of the molecular structure by single crystal X-ray analysis were isolated from the solutions in hexane at r.t., -22 °C and -78 °C, in acetone at -22 °C and in $Et_2O$ at -22 °C. $^1$H NMR ($C_6D_6$): δ 0.37 (s, 6H, $SnMe_2$), 0.88 – 0.92 (q, 4H, $CH_2$ of $SiEt_2$), 1.01 – 1.04 (t, 6H, $CH_3$ of $SiEt_2$), 4.25, 4.26, 4.29, 4.30 (pst, 16H, $C_5H_4$). $^{13}$C NMR ($C_6D_6$): δ -7.0 ($SnMe_2$), 8.1 ($CH_2$ of $SiEt_2$), 8.5 ($CH_3$ of

$SiEt_2$), 68.8 (*ipso*-C of Si-$C_5H_4$ or Sn-$C_5H_4$), 69.3 (*ipso*-C of Si-$C_5H_4$ or Sn-$C_5H_4$), 70.7, 74.3 (α and β-C of Si-$C_5H_4$), 70.8, 75.0 (α and β-C of Sn-$C_5H_4$). $^{29}$Si NMR: δ -2.3 ($SiEt_2$). $^{119}$Sn NMR: -23.0 ($Me_2Sn$). EIMS (70 eV): *m/z* (rel intens) 604 (100) [$M^+$], 589 (64) [$M^+$ Me], 440 (57) [$C_{23}H_{24}Fe_2Si^+$], 425 (37) [$C_{22}H_{21}Fe_2Si^+$], 411 (33) [$C_{21}H_{19}Fe_2Si^+$], 397 (20) [$C_{20}H_{17}Fe_2Si^+$], 333 (14) [$C_{15}H_{13}Fe_2Si^+$], 213 (15) [$C_{10}H_9FeSi^+$], 185 (12) [$C_{10}H_9Fe^+$], 93 (17) [$C_5H_5Si^+$]. HRMS (EI; m/z): calcd for $C_{26}H_{32}Fe_2SiSn$, 603.9994; found, 604.0016 (Δ(ppm) = 3.6).

**$144_2$c.** Isolated from the mixture **$144_n$** by column chromatography over silica gel (1:20 mixture of $CH_2Cl_2$/hexanes as eluent) as orange solid (0.045 g, 3%). The product **$144_2$c** was eluted as the fifth orange band. All the other four orange bands were mixture of compounds. Single crystals for X-ray analysis were obtained from hexane solution at r.t. $^1$H NMR ($C_6D_6$): δ 1.16 (q, 8H, $CH_2$ of $SiEt_2$), 1.25 (t, 12H, $CH_2$ of $SiEt_2$), 1.28 (s, 36H, *t*Bu), 4.11, 4.13, 4.28, 4.32 (pst, 32H, $C_5H_4$). $^{13}$C NMR (toluene-$D_8$): δ 6.6 ($CH_2$ of $SiEt_2$), 8.4 ($CH_3$ of $SiEt_2$), 28.6 (C of Sn*t*$Bu_2$), 31.4 ($CH_3$ of Sn*t*$Bu_2$), 70.0 (*ipso*-C of Si-$C_5H_4$ or Sn-$C_5H_4$), 70.5 (*ipso*-C of Si-$C_5H_4$ or Sn-$C_5H_4$), 71.7, 74.3 (α and β-C of Si-$C_5H_4$), 71.4, 75.0 (α and β-C of Sn-$C_5H_4$). EIMS (70 eV): *m/z* (rel intens) 1374 (23) [$M^+$], 1317 (5) [$M^+$ - *t*Bu], 985 (25) [$C_{41}H_{32}Fe_4Sn_2^+$], 838 (88) [$C_{43}H_{42}Fe_4Si_2^+$], 782 (100) [$C_{43}H_{42}Fe_3Si_2^+$]. HRMS (EI; m/z): calcd for $C_{64}H_{88}Fe_4Si_2Sn_2$, 1374.1866; found, 1374.1860 (Δ(ppm) = 0.4).

**Synthesis of $148_1$ and $148_n$.** *n*BuLi in hexanes (1.66 mL, 4.15 mmol) was added dropwise to a cold (-78 °C) solution of **140** (1.18 g, 2.01 mmol) in a mixture of dry thf (35 mL). After the addition of *n*BuLi, the reaction mixture was stirred for another 30 min at -78 °C, followed by the addition of a solution of (Ar′)$GaCl_2$ (0.533 g, 1.94 mmol) in

thf (30 mL). The reaction mixture was warmed up to r.t. and stirred for another 3 h, resulting in a red solution. All volatiles were removed from the red solution, resulting in a red paste which was extracted with toluene (35 mL). All volatiles were removed from the toluene solution, yielding a red paste. Hexane (50 mL) was added to the red paste and the mixture was stirred vigorously for 16 h, resulting in a red solution and red gummy material. The gummy material was filtered off and washed with hexanes (2 x 5 mL). The combined hexane phase was concentrated to approx. 20 mL and kept in a freezer (-78 °C) for 16 h and red crystals were isolated as pure **$148_1$** (0.355 g, 29%) and dried under high vacuum. The gummy material was dissolved in toluene (5 mL) and added dropwise to well stirred hexane (30 mL), resulting in a red solution with red gummy material sticking to the glass wall. The liquid was syringed off and the gummy material was dried under high vacuum, yielding a sticky red solid **$148_n$** (0.374 g, 31%).

$^1$H NMR of **$148_1$** ([$D_8$]toluene): δ 0.22 (s, 3H, $SiMe_2$), 0.72 (s, 3H, $SiMe_2$), 1.60 (s, 6H, $NMe_2$), 3.15 (s, 2H, $CH_2$), 3.80 (m, 2H, CH-β), 4.14 (m, 2H, CH-α), 4.21 (m, 2H, CH-α), 4.23 (m, 2H, CH-β), 4.25 (m, 2H, CH-β), 4.40 (m, 2H, CH-), 4.52 (m, 2H, CH-α), 4.82 (m, 2H, CH-α), 6.91 (d, 1H, Ar-3), 7.20 (t, 1H, Ar-4), 7.33 (t, 1H, Ar-5), 8.15 (d, 1H, Ar-6). $^{13}$C NMR of **$148_1$** (toluene-$D_8$): δ 0.45, 5.29 ($SiMe_2$), 45.37 ($NMe_2$), 66.25 ($CH_2$), 70.59, 70.72, 70.77, 71.20, 72.55, 72.79, 75.58, 76.85 (α- and β-C), 70.83, 71.03 (*ipso*-C of Cp rings), 127.28, 127.36, 136.71, 144.15, 149.88 ($C_6H_3$) [Note: one $C_6H_3$ peak is buried under the solvent peak]. EIMS (70 eV, $EI^+$): *m/z* (rel intens) 629 (100) [$M^+$], 428 (24) [$C_{22}H_{24}Fe_2Si^+$], 411 (12) [$C_{21}H_{19}Fe_2Si^+$]. HRMS (EI; *m/z*): calcd for $C_{31}H_{34}Fe_2GaNSi$, 629.0433; found, 629.0415 (Δ(ppm) = -2.8). Anal. Calcd. For $C_{31}H_{34}Fe_2GaNSi$: C, 59.09; H, 5.44; N, 2.22. Found: C, 59.07; H, 5.27; N, 2.12.

$^{1}$H NMR of **148$_{n}$** ($C_6D_6$): δ 0.47-0.77 (multiple peaks, 6H, $SiMe_2$), 1.70-1.85 (multiple peaks with one major broad peak at 1.78, 6H, $NMe_2$), 3.27 (broad peak, 2H, $CH_2$), 3.85-4.86 (multiple peaks, 16H, Cp), 6.72-7.11 (broad peaks, 1H, $C_6H_4$), 7.22-7.32 (broad peaks, 1H, $C_6H_4$), 7.33-7.44 (broad peaks, 1H, $C_6H_4$), 7.94-8.44 (broad peaks, 1H, $C_6H_4$). $^{13}$C NMR of **148$_{n}$** ($C_6D_6$): δ -0.45 (broad peak, $SiMe_2$), 45.93 (broad peak, $NMe_2$), 66.92 (broad peak, $CH_2$), 68.30-76.30 (multiple peaks, Cp), 124.50-151.00 (multiple peaks, $C_6H_4$).

## 4.5 References

(1) Nesmeyanov, A. N.; Kritskaya, I. I. *Bull. Acad. Sci. USSR Div. Chem. Sci (Engl. Transl.)* **1956**, 243-244.

(2) Sato, M.; Asai, M. *J. Organomet. Chem.* **1992**, *430*, 105-110.

(3) a) Watanabe, M.; Sato, M.; Nagasawa, A.; Motoyama, I.; Takayama, T. *Bull. Chem. Soc. Jpn.* **1998**, *71*, 2127-2136. b) Mueller-Westerhoff, U. T.; Nazzal, A.; Tanner, M. *J. Organomet. Chem.* **1982**, *236*, C41-C44.

(4) Bellas, V.; Rehahn, M. *Angew. Chem. Int. Ed.* **2007**, *46*, 5082-5104.

(5) Bagh, B.; Breit, N. C.; Dey, S.; Gilroy, J. B.; Schatte, G.; Harms, K.; Müller, J. *Chem. – Eur. J.* **2012**, *18*, 9722-9733.

(6) a) Schachner, J. A.; Lund, C. L.; Quail, J. W.; Müller, J. *Organometallics* **2005**, *24*, 785-787. b) Schachner, J. A.; Lund, C. L.; Quail, J. W.; Müller, J. *Organometallics* **2005**, *24*, 4483-4488. c) Lund, C. L.; Schachner, J. A.; Quail, J. W.; Müller, J. *Organometallics* **2006**, *25*, 5817-5823. d) Schachner, J. A.; Orlowski, G. A.; Quail, J. W.; Kraatz, H.-B.; Müller, J. *Inorg. Chem.* **2006**, *45*, 454-459. e) Schachner, J. A.; Tockner, S.; Lund, C. L., Quail, J. W.; Rehan, M.; Müller, J. *Organometallics* **2007**, *26*, 4658-4662. f) Lund, C. L.; Schachner, J. A.; Quail, J. W.; Müller, J. *J. Am. Chem. Soc.* **2007**, *129*, 9313-9320. g) Lund, C. L.; Schachner, J. A.; Burgess, I. J.; Quail, J. W.; Schatte, G.; Müller, J. *Inorg. Chem.* **2008**, *47*, 5992-6000. h) Bagh, B.; Gilroy, J. B.; Staubitz, A.; Müller, J. *J. Am. Chem. Soc.* **2010**, *132*, 1794-1795. i) Breit, N. C.; Ancelet, T.; Quail, J. W.; Schatte, G.; Müller, J. *Organometallics* **2011**, *30*, 6150-6158. j) Bagh, B.; Schatte, G.; Green, J. C. ; Müller, J. *J. Am. Chem. Soc.* **2012**, *134*, 7924-7936. k) Bagh, B.; Breit, N. C.; Harms, K.; Schatte, G.; Burgess, I.; Braunschweig, H.; Müller, J. *Inorg. Chem.* **2012**, *51*, 11155-11167.

(7) a) Foucher, D.A.; Ziembinski, R.; Tang, B. Z.; Macdonald, P. M.; Massey, J.; Jaeger, C. R.; Vancso, G. J.; Manners, I. *Macromolecules* **1993**, *26*, 2878 –2884. b) Osborne, A. G.; Whiteley, R. H.; Meads, R. E. *J. Organomet. Chem.* **1980**, *193*, 345 –357. c) Rulkens, R.; Lough, A. J.; Manners, I.; Lovelace, S. R.; Grant, C.; Geiger, W. E. *J. Am. Chem. Soc.* **1996**, *118*, 12683-12695. d) Jäkle, F.; Rulkens, R.; Zech, G.; Foucher, D. A.; Lough, A. J.; Manners, I. *Chem.–Eur. J.* **1998**, *4*, 2117-2128.

(8) Herbert, D. E.; Gilroy, J. B.; Chan, W. Y.; Chabanne, L.; Staubitz, A.; Lough, A. J.; Manners, I. *J. Am. Chem. Soc.* **2009**, *131*, 14958-14968.

(9) Setaka, W.; Sakamoto, K.; Kira, M.; Power, P. P. *Organometallics* **2001**, *20*, 4460-4462.

(10) Jutzi, P.; Kohl, F.; Hofmann, P.; Krüger, C.; Tsay, Y. H. *Chem. Ber.* **1980**, *113*, 757-769.

(11) Kumar, M.; Cervantes-Lee, F.; Pannell, K. H.; Shao, J. *Organometallics* **2008**, *27*, 4739-4748.

(12) Massey, J. A.; Kulbaba, K.; Winnik, M. A.; Manners, I. *J. Polym. Sci., Part B: Polym. Phys.* **2000**, *38*, 3032−3041.

(13) a) Zechel, D. L.; Foucher, D. A.; Pudelski, J. K.; Yap, G. P. A.; Rheingold, A. L.; Manners, I. *J. Chem. Soc. Dalton Trans.* **1995**, 1893-1899. b) Park, J.; Seo, Y.; Cho, S.; Whang, D.; Kim, K.; Chang, T. *J. Organomet. Chem.* **1995**, *489*, 23-25. c) Calleja, G.; Carré, F.; Cerveau, G. *Organometallics* **2001**, *20*, 4211-4215. d) Seyferth, D.; Withers, H. P. *Organometallics* **1982**, *1*, 1275-1282.

(14) Schachner, J. A.; Lund, C. L.; Burgess, I. J.; Quail, J. W.; Schatte, G.; Müller, J. *Organometallics*, **2008**, *27*, 4703-4710.

(15) Bagh, B.; Breit, N. C.; Gilroy, J. B.; Schatte, G.; Müller, J. *Chem. Comm.* **2012**, *48*, 7823-7825.

(16) Robin, M. B.; Day, P. *Adv. Inorg. Chem. Radiochem.* **1967**, *10*, 247-422.

(17) Bagh, B.; Müller, J. unpublished results.

(18) Bard, A. J.; Faulkner, L. R. *Electrochemical Methods*, 2nd ed.; John Wiley & Sons, Inc.: New York, 2001, Chap. 9.

(19) Seyferth, D.; Withers, H. P. *Organometallics* **1982**, *1*, 1275-1282.

(20) Shafir, A.; Power, M. P.; Whitener, G. D.; Arnold, J. *Organometallics*, **2000**, *19*, 3978-3982.

(21) Isom, H. S.; Cowley, A. H.; Decken, A.; Sissingh, F.; Corbelin, S.; Lagow, R. J. *Organometallics*, **1995**, *14*, 2400-2406.

CHAPTER 5
SYNTHESIS AND CHARACTERIZATION OF ALUMINUM- AND GALLIUM-BRIDGED [1.1]RUTHENOCENOPHANES

## 5.1 Introduction

[1.1]RCPs are scarcely studied species and only one heteroatom-bridged [1.1]RCP (**28**) was reported (Figure 5-1).[1] Moreover, the redox behavior and the solid-state structure was only studied for the methylene-bridged [1.1]RCP (**24**) (Figure 5-1).[2]

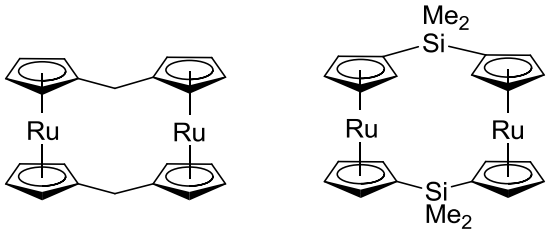


**24** **28**

**Figure 5-1.** The first carbon-bridged [1.1]RCP (**24**) and the silicon-bridged [1.1]RCP **28**.

The molecular structure of the [1.1]RCP **24** in *syn* conformation exhibited significant structural differences to the related [1.1]FCP **12**, which is most prominent in the degree of twist of the Cp rings (Figure 1-8; **24**: α' = 33-34° and **12**: α' = 13-14°).[2b] Species **24** displayed an unexpected redox behavior. One electrochemically reversible two-electron oxidation was observed for **24** instead of the expected two electrochemically irreversible oxidation waves in the presence of the traditional electrolyte anion $[BF_4]^-$ (Chapter 1.4.2).[2a] The solid-state structure of oxidized **24** (**47)** revealed a ruthenium-ruthenium bond that explains the unusual redox behavior of **24**.[3] Bis(ruthenocenium) dimers were similarly reported to form during the electrochemical treatment of ruthenocene and to be reversibly converted back to ruthenocene in the presence of weakly coordinating electrolyte anions.[4] However, the reactivity of **24** to form ruthenium-ruthenium bonds also with traditional electrolyte anions instead of the

suggested adducts with the coordinating electrolyte anions must be related to the proximity of ruthenium centers and possibly preformed non-bonding interaction between the ruthenium centers.[3] A more detailed description can be found in Chapters 1.2.3 and 1.4.2.

We wanted to extend the knowledge about [1.1]RCPs to aluminum- and gallium-bridged species and to investigate their molecular structure and redox properties. As shown in Chapter 1.5.2, our group successfully employed the Ar′ ligand for the synthesis of aluminum- and gallium-bridged [1.1]FCPs (**77** and **78**), which makes the Ar′ ligand the first ligand of choice for the synthesis of aluminum- and gallium-bridged [1.1]RCPs (Figure 5-2).[5] However, for the synthesis of aluminum- and gallium-bridged [1.1]metallarenophanes (**98**-**101**), the *p*-*t*BuAr′ ligand was utilized instead of the Ar′ ligand, in order to increase the solubility of the products and facilitated their characterization (Figure 5-2).[6] Both ligands were utilized for the synthesis of [1.1]RCPs, one bound to aluminum and the other to gallium.

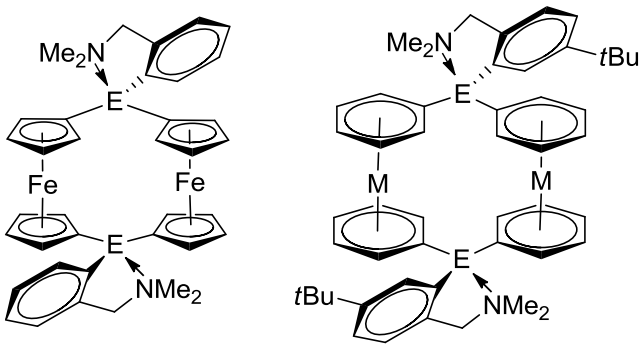


**Figure 5-2.** Aluminum- and gallium-bridged [1.1]FCPs equipped with the Ar′ ligand (**77** and **78**) and aluminum- and gallium-bridged [1.1]CAPs and [1.1]MAPs equipped with the *p*-*t*BuAr′ ligand (**98**-**101**).

## 5.2 Results and Discussion

(Ar′)$GaCl_2$ and (*p*-*t*BuAr′)$AlCl_2$ were reacted with the 1,1'-dilithioruthenocene tmeda adduct to afford the aluminum- and gallium-bridged [1.1]RCPs **152** and **153**, respectively, in a mixture with other species (Scheme 5-1). The other major species were oligomers $\mathbf{152_n}$ and $\mathbf{153_n}$. Moreover, the presence of hydrolyzed species like the protonated ligands was observed. The separation of these species was achieved by utilizing their different solubility. In a first step, the least soluble oligomers were precipitated out by adding a toluene solution to hexanes. The hydrolyzed species have the highest solubility and could be removed from the product by extensive washings with hexanes. However, the yield was highly diminished by this procedure so that the [1.1]RCPs **152** and **153** were only obtained in 15 and 17% yield, respectively.

**Scheme 5-1.** Synthesis of the first aluminum- and gallium-bridged [1.1]RCPs (**152** and **153**).

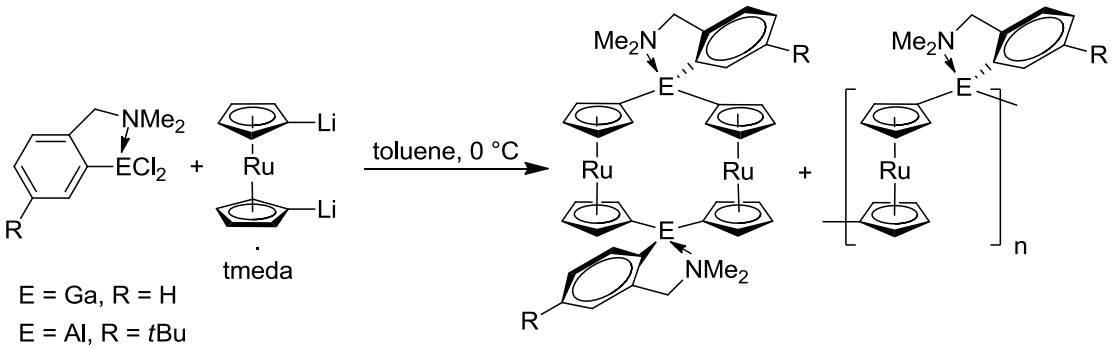


The $^1$H NMR spectrum of **152** exhibited two singlets in the aliphatic region for the dimethylamino and the methylene group and four multiplets in the aromatic region for aromatic protons on the ligand. The cyclopentadienyl protons in **152** showed the same pattern as in the respective [1.1]FCP **78** in which the signals for the α-protons were far

apart at δ 4.09 and 4.93 (δ 3.99 and 5.07 in **78**), whereas the signals for the β-protons were close to each other and nearly overlap at δ 4.55 and 4.59 (δ 4.37 and 4.48 in **78**).[5] The aluminum-bridged [1.1]RCP **153** showed essentially the same pattern as **152**, with the difference that one more singlet was observed in the aliphatic region for the *tert*-butyl group and only three signals for aromatic protons were present. The identity of **152** and **153** was confirmed by mass spectrometry.

Crystals suitable for single-crystal X-ray analysis were obtained for **152** from thf solutions by slow solvent evaporation. Dr. G. Schatte (SSSC) determined the molecular structure of **152** as shown in Figure 5-3.

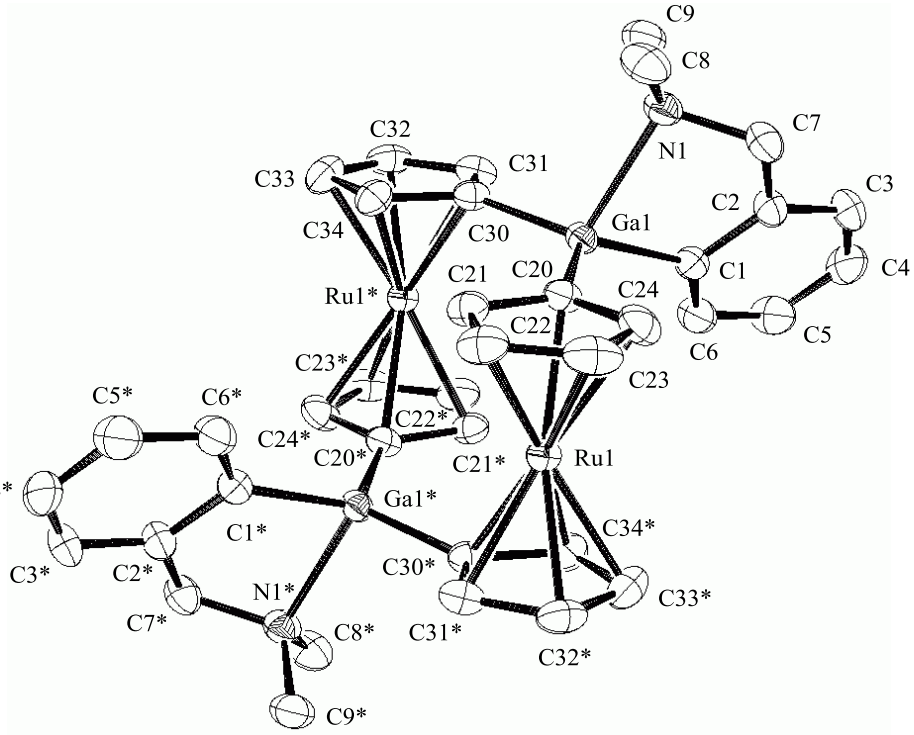


**Figure 5-3.** Molecular structure of the gallium-bridged [1.1]RCP **152** with thermal ellipsoids at the 50% probability level. Hydrogen atoms are omitted for clarity. Selected atom-atom distances [Å] and bond angles [°]: Ga1–C1, –C20, –C30 = 1.986(3), 1.954(3), 1.958(3); Ga1–N1 = 2.183(2); C1–Ga–N1 = 83.19(10); C2–C1–Ga1 = 112.2(2); C1–Ga1–C20, C1–Ga1–C30 = 115.46(11), 123.24(12).

The molecular structure revealed **152** to be in the expected *anti* conformation. The *ipso*-carbons occupy the *endo* and the nitrogen atoms occupy the *exo* positions. This mimics the structure of the respective [1.1]FCP **78**. Characteristic bond lengths, metal-metal distances and bond angles for **152** and **78** are presented in Table 5-1. No major difference was observed for the coordination environment of the gallium center and the metal···metal distance in **152** and **78**. The only major difference is the expected larger distance between two cyclopentadienyl rings with an average of 3.64 Å for **152** and 3.32 Å for **78**.[7] Conversely, species **152** showed none of the features of the carbon-bridged [1.1]RCP **24**. The high twist angle of the carbon-bridged species might therefore be only present in the *syn* conformers. Expectedly, the metal-metal distance is significantly longer in **152** than in **24** which is due to the increased size of the bridging element [Ru···Ru: 5.4614(4) Å (**152**), 4.70 Å (**24**)].[2b]

**Table 5-1.** Selected bond-length, metal-metal distances [Å] and bond angles [°] of (Ar´)$GaCl_2$, **78**, and **152**.

| | Ga1-C1 | Ga1-N1 | C1-Ga-N1 | Ga1-C20, Ga1-C30 | | M-M |
|---|---|---|---|---|---|---|
| (Ar´)$GaCl_2$[8] | 1.951(2) | 2.071(2) | 87.44(7) | --- | --- | --- |
| **78**[5] | 1.988(3) | 2.178(3) | 82.99 | 1.951(4) | 1.963(3) | 5.462 |
| **152** | 1.986(3) | 2.183(2) | 83.19(10) | 1.954(3) | 1.958(3) | 5.4614(4) |

The impure oligomers $\mathbf{152_n}$ and $\mathbf{153_n}$, obtained from precipitation of the toluene solution into hexanes, were investigated by $^1$H NMR spectroscopy and DLS analysis. The evaluation of the DLS data was carried out as described in Chapter 3.2.1. The $^1$H NMR spectra of $\mathbf{152_n}$ and $\mathbf{153_n}$ exhibited very broad signals similar to the low-molecular-weight polymers with the Pytsi$^{-SiMe_2}$ ligand ($\mathbf{80_n}$ and $\mathbf{81_n}$). The oligo(ruthenocenylalumane) $\mathbf{153_n}$ was found to have a molecular weight of 2.8(±0.4)

kDa, which translates into 6(±1) repeating units, while the respective gallane **152$_n$** exhibited higher molecular weights of 4.4(±0.5) kDa, corresponding to 10(±1) repeating units.

Interestingly, the salt-metathesis reactions of 1,1'-dilithioruthenocene with (Ar′)$GaCl_2$ or (*p*-*t*BuAr′)$AlCl_2$ led to the formation of oligomers **152$_n$** and **153$_n$** besides the expected [1.1]RCPs **152** and **153**, while for similar reactions with 1,1'-dilithioferrocene, 1,1'-dilithiochromarene, or 1,1'-dilithiomolybdarene no formation of oligomers was reported.[5,6] Based on the available data, no conclusion can be made, whether this different behavior is based on steric effects and the different distances (Cp···Cp: 3.64 Å for **152** and 3.32 Å for **78**)[7] or electronic effects in connection with the different electronegativity of the metals (Cr: 1.6; Mo: 1.8; Fe: 1.8; Ru: 2.2).[9] Salt-metathesis reactions of aluminum and gallium dichlorides equipped with the Mamx or Mx ligand also showed a different outcome depending on the metal being iron or ruthenium (Chapter 1.5.2 and Chapter 3.2.2).[10]

*Redox properties of the aluminum- and gallium-bridged [1.1]ruthenocenophanes*

One of the major interests was the study of the redox behavior of the aluminum- and gallium-bridged [1.1]RCPs **152** and **153** and to compare it to the redox behavior of the carbon-bridged [1.1]RCP **24** on the one hand and ruthenocene on the other hand. The redox behavior of **152** and **153** was studied with glassy carbon as a working electrode, a silver wire as the quasi reference electrode and a gold wire as the auxiliary electrode in dichloromethane as solvent. Two different supporting electrolytes, $[Bu_4N][PF_6]$ with a traditional electrolyte anion and $[Bu_4N][B\{C_6H_3(CF_3)_2\}_4]$ with a weakly coordinating electrolyte anion, were utilized during this study. In order to permit a direct comparison

of the aluminum- and gallium-bridged [1.1]RCPs with ruthenocene, cyclic voltammetry measurements were also carried out for ruthenocene (Figure 5-4 and Figure 5-5).

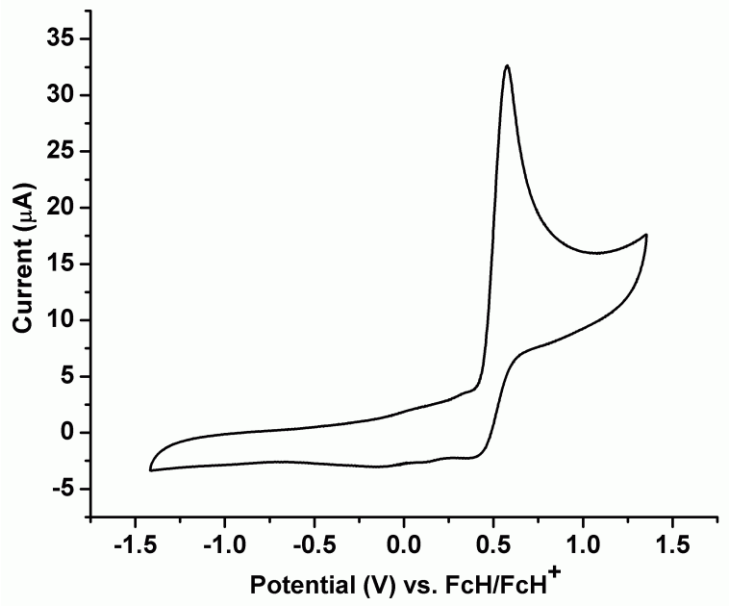


**Figure 5-4.** Cyclic voltammogram of ruthenocene in $CH_2Cl_2$ with $[Bu_4N][PF_6]$ as a supporting electrolyte referenced to the $FcH/FcH^+$ couple.

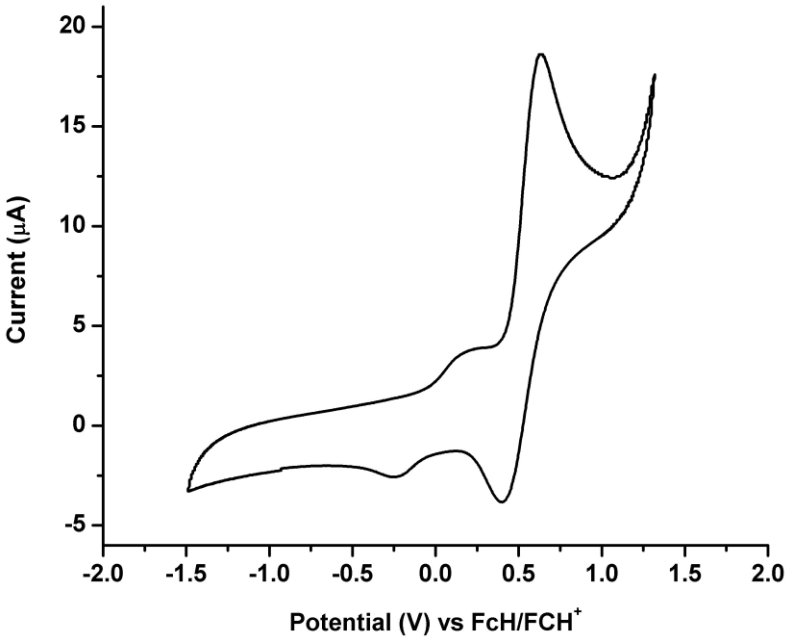


**Figure 5-5.** Cyclic voltammogram of ruthenocene in $CH_2Cl_2$ with $[Bu_4N][B\{C_6H_3(CF_3)_2\}_4]$ as supporting electrolyte referenced to the $FcH/FcH^+$ couple.

Ruthenocene showed the electrochemically irreversible oxidation wave, which is well-known to belong to a two-electron oxidation, when the traditional electrolyte anion $[PF_6]^-$ was employed. The oxidation wave of ruthenocene has its maximum at 0.58 V under these conditions. Significantly higher oxidation potentials than for ferrocene have been previously reported for example by Mueller-Westerhoff *et al.* with E = 420 V, when a $[Bu_4N][BF_4]$ was used as an electrolyte and benzonitrile was utilized as a solvent.[2a] In the presence of the weakly coordinating electrolyte anion $[B\{C_6H_3(CF_3)_2\}_4]^-$, the oxidation of ruthenocene is reversible and has its half wave potential at 0.52 V. Mann *et al.* and Geiger *et al.* reported an $E_{1/2}$ of 0.56 V for ruthenocene in the same solvent and supporting electrolyte, however with double the concentration of electrolyte.[4b,11] An additional redox wave can be seen at -0.035 V. The cyclic voltammogram of ruthenocene reported by Mann does not exhibit this redox wave.[11] However, the cyclic voltammogram reported by Geiger *et. al.* also exhibits an additional oxidation wave that they assigned to **42** (Figure 1-15).[4b]

The gallium-bridged [1.1]RCP **152** exhibited an electrochemically irreversible two oxidation waves at potentials of 0.34 and 0.62 V, when the supporting electrolyte $[Bu_4N][PF_6]$ was utilized (Figure 5-6). The separation $\Delta E^{ox}$ between these two maxima amounts to 0.28 V. The communication between the ruthenium centers is similar to other gallium-bridged [1.1]metallacyclophanes in the presence of traditional electrolyte anions ([1.1]FCP (**78**): $\Delta E_{1/2}$ = 0.30 V in $CH_2Cl_2$,[5] [1.1]FCP (**80**): $\Delta E_{1/2}$ = 0.309 V in $CH_2Cl_2$ and $\Delta E_{1/2}$ = 0.218 V in thf[12]; [1.1]CAP (**99**): $\Delta E_{1/2}$ = 0.215 V in thf;[6] [1.1]MAP (**101**): $\Delta E_{1/2}$ = 0.220 V in thf[6]). However, it ought to be noted that the separation of the oxidation waves in **152** is compared to the difference of the halfwave potentials of the

[1.1]metallacyclophanes. The first oxidation wave appears as a shoulder on the second oxidation wave. This limits the accuracy of the determination of the first oxidation potential and at the same time of the difference between the oxidation potentials. Based on the increased distance between the Cp rings in going from ferrocene to ruthenocene, the ruthenium center is more exposed and secondary reactions by nucleophilic attacks of solvent, electrolyte, or the substrate can occur. No reduction wave was observed in the cyclic voltammogram of **152** that would match the oxidation wave. Merely two very minor reduction waves were found at 0.00 and 0.51 V (Figure 5-6). These reduction waves could either belong to unreacted oxidized **152** or to one part of the reaction products that is reversible. For example, as a minor product a species with a ruthenium-ruthenium bond could have formed. Bis(ruthenocenium) **41** was shown to be able to undergo reduction to ruthenocene.[4b] Another option is that a part of the supposedly formed [**152**-$F_2$][$PF_6$]$_2$ can undergo reduction.

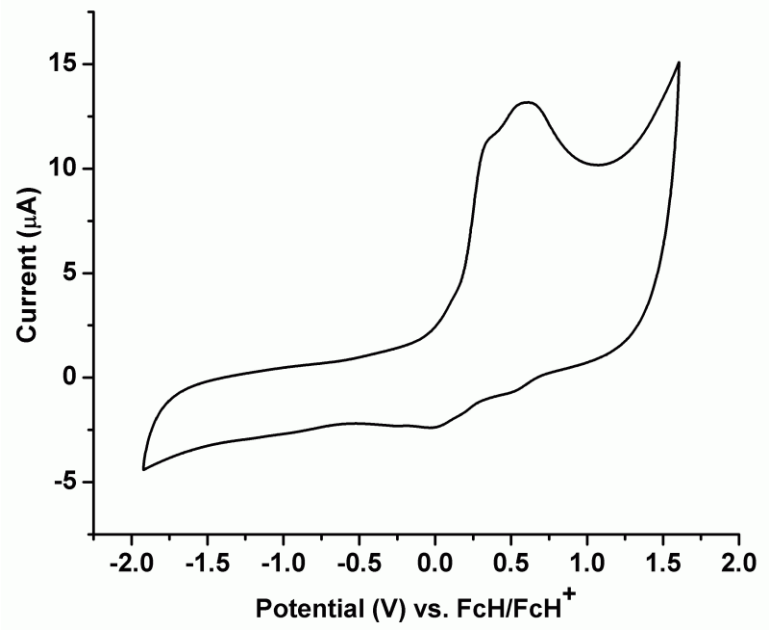


**Figure 5-6.** Cyclic voltammogram of the gallium-bridged [1.1]RCP **152** in $CH_2Cl_2$ with [$Bu_4N$][$PF_6$] as a supporting electrolyte referenced to $FcH/FcH^+$.

The cyclic voltammogram of **152** exhibited two reversible oxidation waves in the presence of the weakly coordinating electrolyte anion $[B\{C_6H_3(CF_3)_2\}_4]^-$ (Figure 5-7). The redox waves have half wave potentials of 0.13 and 0.79 V. The resulting $\Delta E_{1/2}$ value is with 0.66 V significantly higher than the $\Delta E$ value of 0.28 V obtained in the presence of the electrolyte $[Bu_4N][PF_6]$. Barrière and Geiger showed previously for the example of bis(fulvalene)dinickel that the $\Delta E_{1/2}$ value increases from 0.480 to 0.744 V when the electrolyte is changed from $[Bu_4N][PF_6]$ to $[Bu_4N][B\{C_6H_3(CF_3)_2\}_4]$ with $CH_2Cl_2$ as a solvent.[13] The authors attribute this change to the reduced ion pairing ability of larger electrolyte anions. The difference of these $\Delta E_{1/2}$ values is higher for **152** than bis(fulvalene)dinickel (for **152** $\Delta\Delta E_{1/2}$ = 0.38 V and for bis(fulvalene)dinickel $\Delta\Delta E_{1/2}$ = 0.26 V).[13] It ought to be noted that the difference between two oxidation waves $\Delta E$ is compared to the difference of two redox waves $\Delta E_{1/2}$. However, if the difference of only the oxidation waves of **152** in the presence of the electrolyte $[Bu_4N][B\{C_6H_3(CF_3)_2\}_4]$ are considered for a $\Delta E$ value, a similar value to $\Delta E_{1/2}$ is obtained ($\Delta E^{ox}$ = 0.65 V).

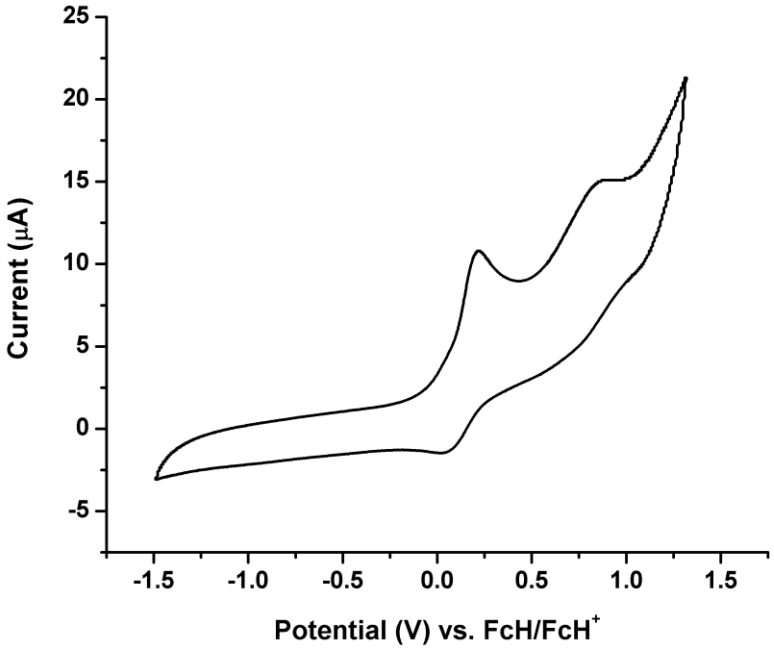


**Figure 5-7.** Cyclic voltammogram of the gallium-bridged [1.1]RCP **152** in $CH_2Cl_2$ with $[Bu_4N][B\{C_6H_3(CF_3)_2\}_4]$ as a supporting electrolyte referenced to $FcH/FcH^+$.

Geiger *et al.* performed an experiment in which $[Bu_4N][PF_6]$ was added to a solution of ruthenocene in the presence of a supporting electrolyte with a weakly coordinating anion ($[B(C_6F_5)_4]^-$ and $[B\{C_6H_3(CF_3)_2\}_4]^-$).[4b] Cyclic voltammetry measurements showed that with the addition of one equivalents of $[Bu_4N][PF_6]$ respective to ruthenocene the reversibility of the oxidation decreaces drastically. After the addition of 10 equivalents of $[Bu_4N][PF_6]$ the oxidation of ruthenocene was irreversible. We investigated the effect of the addition of $[Bu_4N][PF_6]$ to a solution of **152** in the presence of the supporting electrolyte $[Bu_4N][B\{C_6H_3(CF_3)_2\}_4]$. After the addition of 2 equivalents of $[Bu_4N][PF_6]$ respective to the [1.1]RCP a decrease in the reversibility was observed (Figure 5-8). In addition to the two major oxidation events at 0.24 and 0.73 V, another oxidation wave was observed at 0.50 V. The reduction waves appear at 0.51 and 0.04 V. This gives a $\Delta E^{ox}$ value of 0.50 V or a $\Delta E_{1/2}$ of 0.48 V, which is a decrease from

the respective values for **152** in pure $[Bu_4N][B\{C_6H_3(CF_3)_2\}_4]$. The source of the minor oxidation wave is unknown. However, it might be related to species with a ruthenium-fluorine bond.

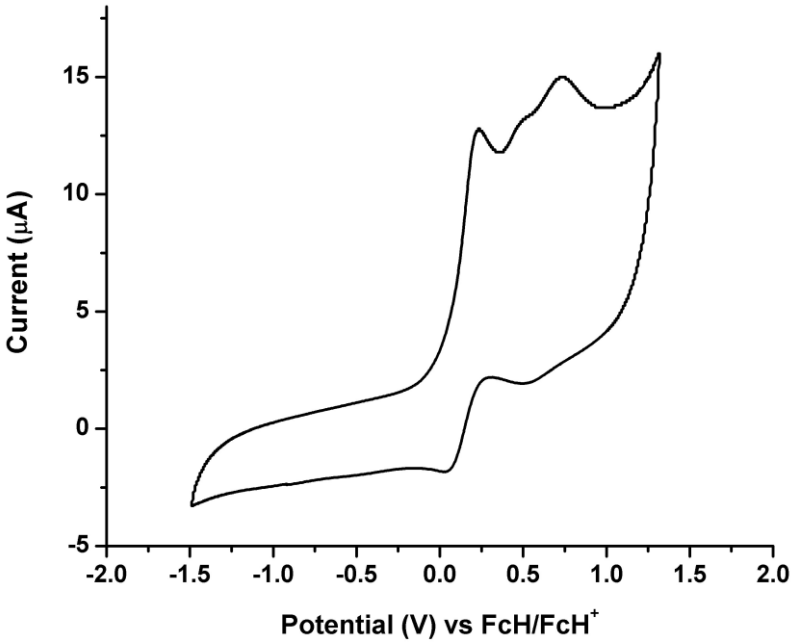


**Figure 5-8.** Cyclic voltammogram of the gallium-bridged [1.1]RCP **152** in $CH_2Cl_2$ with $[Bu_4N][B\{C_6H_3(CF_3)_2\}_4]$ as supporting electrolyte after the addition of 2 equivalents of $[Bu_4N][PF_6]$.

A further decrease of the $\Delta E^{ox}$ value to 0.38 V and of the electrochemical reversibility of the oxidation was observed after the addition of 20 equivalents of $[Bu_4N][PF_6]$ (Figure 5-9). The third oxidation wave observed after the addition of 2 equivalents of $[Bu_4N][PF_6]$ is not seen anymore, which might be due to a lower resolution of the cyclic voltammogram, an overlap with the second oxidation wave or a different redox behavior.

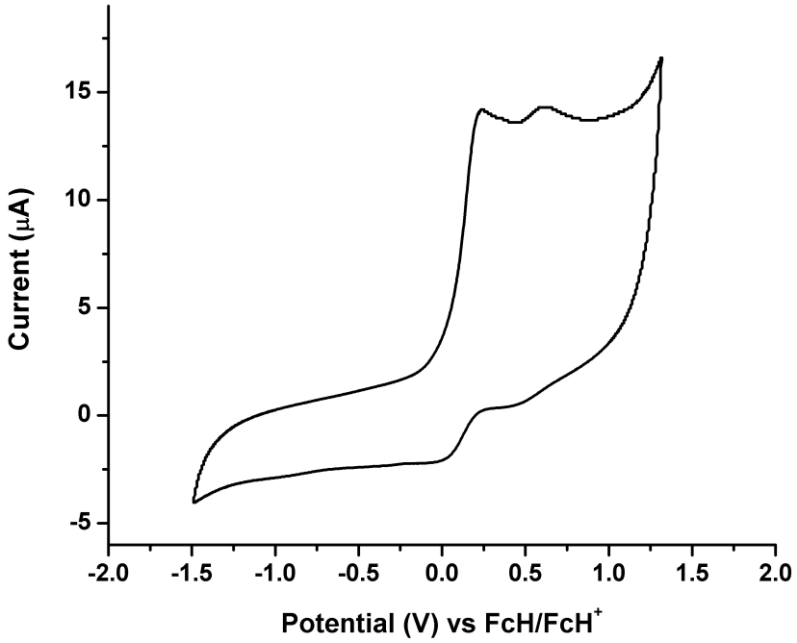


**Figure 5-9.** Cyclic voltammogram of the gallium-bridged [1.1]RCP **152** in $CH_2Cl_2$ with $[Bu_4N][B\{C_6H_3(CF_3)_2\}_4]$ as supporting electrolyte after the addition of 20 equivalents of $[Bu_4N][PF_6]$.

The cyclic voltammogram of the aluminum-bridged [1.1]RCP **153** with $[Bu_4N][PF_6]$ as the supporting electrolyte showed, similarly to **152**, two oxidation waves that were electrochemically not reversible (Figure 5-10). The oxidation waves of **153** at 0.31 and 0.72 V are with $\Delta E = 0.41$ V further separated from each other than in **152** ($\Delta E = 0.28$ V). A similar, but weaker trend was observed for the aluminum- and gallium-bridged [1.1]FCPs **79** and **80** (**80**: $\Delta E_{1/2} = 0.309$ V and **79**: $\Delta E_{1/2} = 0.332$ V).[12] Another similarity between **153** and **79** is the more intense second oxidation wave. As mentioned in Chapter 3.2.3, the source of this asymmetry and the increased splitting between the redox events is not understood, but it might be caused by the formation of additional, redox active products due to higher sensitivity and higher Lewis-acidity of the aluminum center in comparison with gallium. It can be excluded that the second oxidation peak with the high intensity at 0.72 V is purely ruthenocene, which has its oxidation potential at

0.58 V. Species **153** exhibited two very small reduction waves at 0.01 and 0.52 V, which are very similar to reduction waves in **152** at -0.00 and 0.51 V.

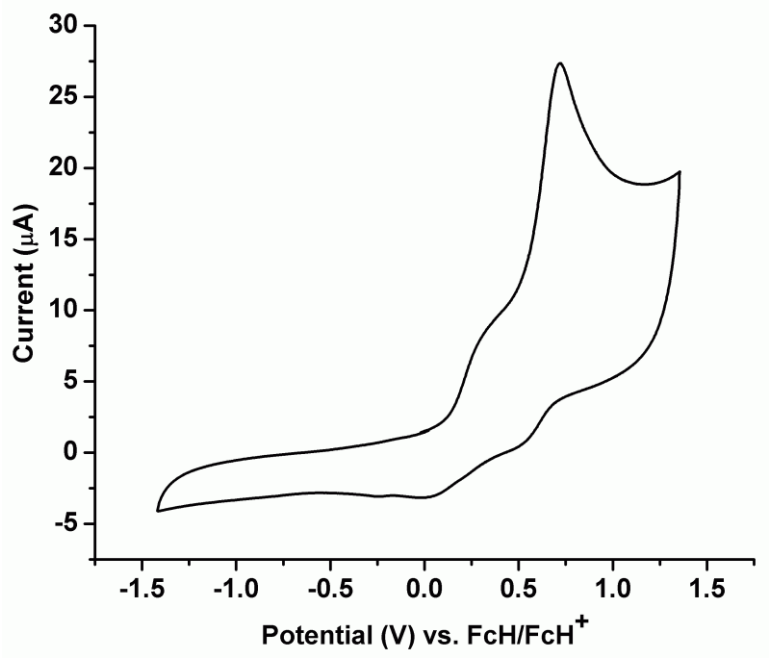


**Figure 5-10.** Cyclic voltammogram of the aluminum-bridged [1.1]RCP **153** in $CH_2Cl_2$ with $[Bu_4N][PF_6]$ as a supporting electrolyte referenced to $FcH/FcH^+$.

In contrast to the redox behavior of **152** with $[Bu_4N][B\{C_6H_3(CF_3)_2\}_4]$ as a supporting electrolyte, the cyclic voltammogram of **153** revealed irreversible oxidations (Figure 5-11). The oxidation waves have their maxima at 0.18 and 0.76 V with the second oxidation wave being more intense than the first one. The ΔE value with $[Bu_4N][B\{C_6H_3(CF_3)_2\}_4]$ as a supporting electrolyte is similarly to **152** significantly higher than that with $[Bu_4N][PF_6]$ (for **153**: with $[Bu_4N][B\{C_6H_3(CF_3)_2\}_4]$ ΔE = 0.58 V and with $[Bu_4N][PF_6]$ ΔE = 0.41). However, the ΔΔE value for **153** is lower than of **152** and also lower than for bis(fulvalene)dinickel (**153**: ΔΔE = 0.17 V, **152**: $\Delta\Delta E_{1/2}$ = 0.38 V, bis(fulvalene)dinickel: $\Delta\Delta E_{1/2}$ = 0.26 V). Two smaller reduction waves were observed at 0.51 and -0.05 V. Possibly the oxidation is partly reversible. It is intesting that the

conditions in this case the supporting electrolyte that lead to a reversible oxidation of ruthenocene and the gallium-bridged [1.1]RCP **152** still give an irreversible oxidation of the aluminum-bridged [1.1]RCP **153**. This suggests that the aluminum is playing a major part in the irreversibility of the electrochemical oxidation.

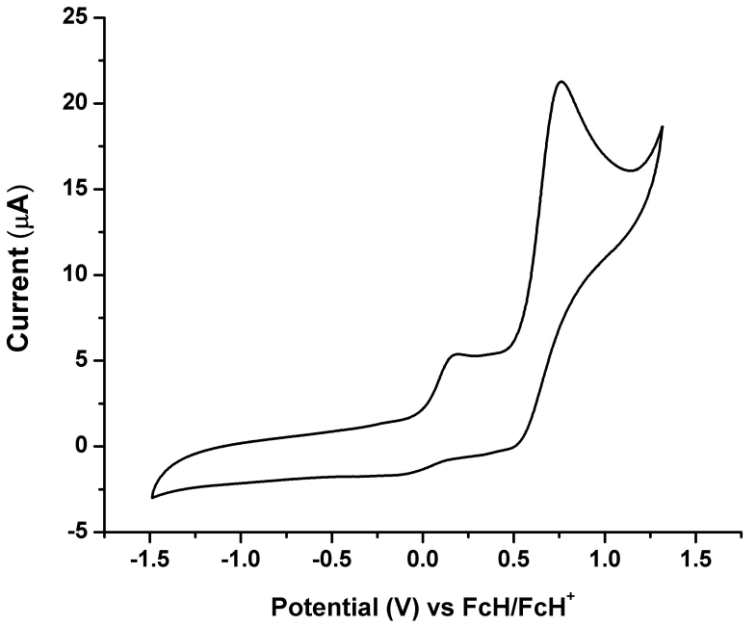


**Figure 5-11.** Cyclic voltammogram of the aluminum-bridged [1.1]RCP **153** in $CH_2Cl_2$ with $[Bu_4N][B\{C_6H_3(CF_3)_2\}_4]$ as a supporting electrolyte referenced to $FcH/FcH^+$.

It is worth mentioning that the first oxidation potential of **152** and **153** with the electrolytes $[Bu_4N][PF_6]$ and $[Bu_4N][B\{C_6H_3(CF_3)_2\}_4]$ always exhibits lower values than ruthenocene (Table 5-2). This difference is up to 0.46 V for **153** with the electrolyte $[Bu_4N][B\{C_6H_3(CF_3)_2\}_4]$. It was suggested for the methylene-bridged [1.1]RCP (**24**) that the oxidation of ruthenium and the formation of the ruthenium-ruthenium bond is promoted by a preformed non-bonding interaction of the two ruthenocene centeres.[3] This argument was based on the significantly lower oxidation potential of species **24** than ruthenocene by 0.50 V. However, the lower first oxidation potentials of species **152** and **153** suggest that there are other possible effects that could have lead to the reduced

oxidation potential of **24**. A non-bonding interaction between the two oxidation centers in **152** or **153** can be excluded based on the Ru···Ru distance in the solid state structure of **152** of 5.4614(4) Å. Moreover the inability of **152** and **153** to form an intramolecular ruthenium-ruthenium bond, which can be seen by their redox behavior excludes the formation of a non-bonding interaction of the ruthenium atoms.

**Table 5-2.** Data of the electrochemical study of ruthenocene, **152**, and **153** in the presence of the electrolytes $[Bu_4N][PF_6]$ and $[Bu_4N][B\{C_6H_3(CF_3)_2\}_4]$ ($[Bu_4N][BArF_{24}]$).

| | ruthenocene | | **152** | | | | **153** | |
|---|---|---|---|---|---|---|---|---|
| anion | $PF_6$ | $BArF_{24}$ | $PF_6$ | $BArF_{24}$ | 2 eq.[a] | 20 eq.[a] | $PF_6$ | $BArF_{24}$ |
| $E^{ox1}$ [V] | 0.58 | 0.64 | 0.34 | 0.22 | 0.24 | 0.24 | 0.31 | 0.18 |
| $E^{ox2}$ [V] | | 0.17 | 0.62 | 0.87 | 0.73 | 0.62 | 0.72 | 0.76 |
| $\Delta E^{ox}$ [V] | | | 0.28 | 0.65 | 0.49 | 0.38 | 0.41 | 0.58 |
| $E^{red1}$ [V] | | 0.40 | 0.51 | 0.72 | 0.51 | 0.47 | 0.52 | 0.51 |
| $E^{red2}$ [V] | | -0.24 | 0.00 | 0.05 | 0.04 | 0.00 | 0.01 | -0.05 |
| $\Delta E_{1/2}$ [V] | | | | 0.66 | 0.48 | | | |

a) Refers to equivalents of $[Bu_4N][PF_6]$ respective to **152** added to a solution of **152** with $[Bu_4N][BArF_{24}]$ as the main electrolyte.

## 5.3 Conclusion

The first aluminum- and gallium-bridged [1.1]RCPs **152** and **153** were synthesized and characterized. Species **152** and **153** are the first heteroatom-bridged [1.1]RCPs that were structurally and electrochemically characterized. The molecular structure in the solid state of **152** showed its *anti* conformation, whereas the methylene-bridged [1.1]RCP (**24**) exhibited a *syn* conformation in the solid state. This was expected based on the different size of the bridging elements. It can be attributed to the more rigid *anti* conformation that 152 shows nearly identical structural parameter to 78 in contrast to the **24**.

The redox behavior of both **152** and **153** is significantly different from **24**. In the presence of a traditional electrolyte anion **152** and **153** exhibited two irreversible oxidation waves, whereas **24** showed one reversible oxidation wave. This can be attributed to the different conformations and Ru···Ru distances of **152** and **24** [Ru···Ru: 5.4614(4) Å (**152**), 4.70 Å (**24**)]. In the presence of the weakly coordination electrolyte anion $[Bu_4N][B\{C_6H_3(CF_3)_2\}_4]$ the gallium-bridged [1.1]RCP (**152**) was reversibly oxidized similar to ruthenocene. However, oxidation of the aluminum-bridged [1.1]RCP (**153**) remained irreversible. This fact adds to previously reported difficulties concerning the redox behavior of aluminum-bridged [1.1]metallacyclophanes. It is likely that other [1.1]RCPs with larger bridging elements will display the same redox behavior as **152**.

A better understanding of the redox properties of [1.1]RCPs and ruthenocenyl-based polymers and the ability to assess possible applications could be gained by further investigations. The chemical fate of the electrochemically oxidized $\mathbf{152}^+$ could be studied by electrosynthesis or the chemical oxidation of **152** in the presence of traditional or electrolyte anions with the intention to isolate **154**, **155**, and **156** (Figure 5-12). Species

similar to **154** and **155** were postulated by Geiger *et al.*[4b] but their identification was not pursued, whereas **156** would be a new polymer. Moreover, the irreversibility of the oxidation of **152** and **153** in dependence of the scan rate could be investigated.

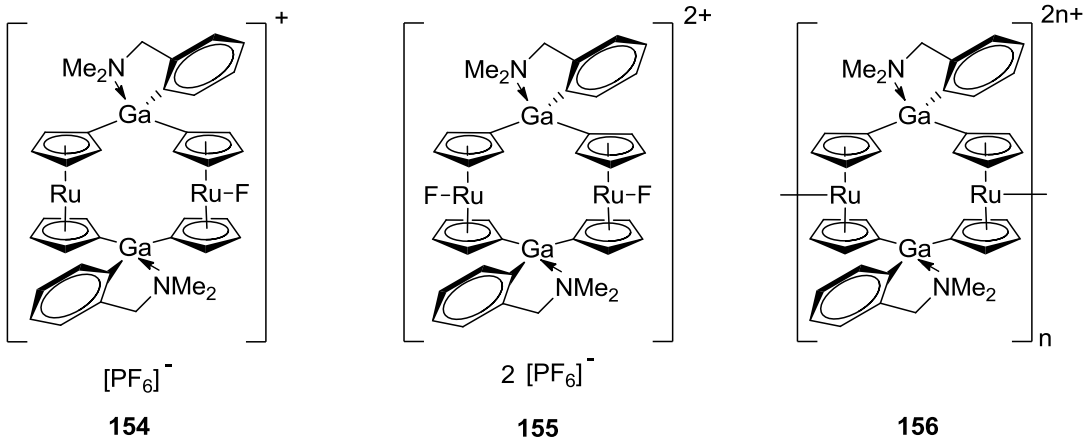


**Figure 5-12.** Possible oxidations products of **152** that could be obtained either by electrosynthesis or chemical oxidation, **154**, **155**, and **156**.

## 5.4 Experimental

**General information.** All syntheses were carried out using standard Schlenk and glovebox techniques. Solvents were dried using a MBraun Solvent Purification System and stored under nitrogen over 3 Å molecular sieves. 18.2 MΩ millipore water was obtained from a Milli-Q Millipore system. All solvents for NMR spectroscopy were degassed prior to use and stored under nitrogen over 3 Å molecular sieves. $RuCp_2$,[14] $(LiC_5H_4)_2Ru{\cdot}tmeda$,[15] (Ar′)$GaCl_2$,[8] (p-*t*BuAr)$AlCl_2$[6], and $Na[B\{C_6H_3(CF_3)_2\}_4]$[16] were synthesized as described in the literature. $^1H$ and $^{13}C$ NMR spectra were recorded on a Bruker 500 MHz Avance NMR spectrometer at 25 °C in $C_6D_6$ and $CDCl_3$, respectively. $^1H$ chemical shifts were referenced to the residual protons of the deuterated solvents (δ 7.15 for $C_6D_6$ and 7.26 for $CDCl_3$); $^{13}C$ chemical shifts were referenced to the $C_6D_6$ signal at δ 128.00, and the $CDCl_3$ signal at δ 77.00. C atoms directly bound to Al or Ga were not detected by $^{13}C$ NMR spectroscopy. Mass spectra were measured on a VG 70SE and were reported in the form m/z (rel intens) [$M^+$] where 'm/z' is the mass observed, 'rel intens' is the intensity of the peak relative to the most intense peak and '$M^+$' is the molecular ion or fragment; only characteristic mass peaks are reported. For isotopic patterns, only the mass peak of the isotopoloque or isotope with the highest natural abundance is listed.

**DLS Analysis.** Dynamic light scattering experiments were performed using a nano series Malvern zetasizer instrument equipped with a 633 nm red laser. Samples were filtered through 0.2 μm syringe PTFE filters before they were analyzed in 1 cm glass cuvettes at concentrations of 5 mg $mL^{-1}$ and 2.5 mg $mL^{-1}$ in thf at 25 °C. The refractive index of the oligomers was assumed to be 1.5.

**Electrochemical measurements.** A computer controlled system, consisting of a HEKA potentiostat PG590 (HEKA, Mahone Bay, NS, Canada) was used for the cyclic voltammetry experiments. Data was collected using a multifunction DAQ card (PCI 6251 M Series, National Instruments Austin, Texas) and in-house software written in the LabVIEW environment. Glassy carbon (BAS, 3 mm) was used as the working electrode. The quasi-reference electrode (QRE) was a silver wire and all measurements were made against the QRE. A loop of gold wire was used as the auxiliary electrode. Before each measurement, 1 mM solutions of **152** and **153** were freshly prepared in dry $CH_2Cl_2$. The concentration of the supporting electrolyte $[Bu_4N][PF_6]$ and $[Bu_4N][B\{C_6H_3(CF_3)_2\}_4]$ were 0.1 M and 0.05 M, respectively. Both electrolytes were dried overnight under high vacuum at 100 °C. The scan rate for the CVs reported was 50 mV/s. The measurements were conducted inside a glovebox and taken at ambient temperature (22 °C).

**Synthesis of $[(Ar')Ga(C_5H_4)_2Ru]_2$ (152).** A solution of $(Ar')GaCl_2$ (0.418 g, 1.52 mmol) in toluene (30 mL) was added slowly to a suspension of $(LiC_5H_4)_2Ru{\cdot}tmeda$ (0.547 g, 1.52 mmol) in toluene (30 mL) at 0 °C. After being stirred for 16 h at room temperature, the solid was filtered off. The amount of solvent was reduced under vacuum to approx. 4 mL, before the solution was added to stirred hexanes (40 mL). The oligomeric product was filtered off and washed with hexanes (3 x 4 mL). The solvent of the solution was removed under vacuum and the product was obtained after washings with hexanes (20 + 5 mL) (0.110 g, 17%). $^1$H NMR ($CDCl_3$): δ 2.32 (s, 12 H, $NMe_2$), 3.77 (s, 4 H, $CH_2$), 4.09 (pst, 4 H, α-Cp), 4.55 (pst, 4 H, ß-Cp), 4.59 (pst, 4 H, ß-Cp), 4.93 (pst, 4 H, α-Cp), 7.10 (d, 2 H, $C_6H_4$), 7.25 (m, 2 H, $C_6H_4$), 7.27 (m, 2 H, $C_6H_4$), 7.71 (d, 2 H, $C_6H_4$). $^{13}$C NMR ($CDCl_3$): δ 46.2 ($NMe_2$), 66.5 ($CH_2$), 71.1, 71.6, 75.4, 75.9 (Cp),

124.5, 126.6, 126.8, 136.7, 144.0, 150.0 ($C_6H_4$). EIMS (70 eV): *m/z* (rel intens) 868 (47) [$M^+$], 667 (32) [$(C_5H_5)Ru(C_5H_4)Ga(C_6H_4CH_2NMe_2)(C_5H_4)Ru(C_5H_5)^+$], 434 (100) [$Ga(C_6H_4CH_2NMe_2)(C_5H_4)Ru(C_5H_5)^+$], 431 (78) [$Ga(C_6H_4CH_2NMe)(C_5H_4)Ru(C_5H_5)^+$]. HRMS (EI; *m/z*): [$M^+$] calcd for $C_{38}H_{40}Ga_2N_2Ru_2$, 867.9801; found 867.9811 (Δppm = 1.2). Anal. Calcd for $C_{38}H_{40}Ga_2N_2Ru_2$ (866.32): C, 52.68; H, 4.65; N, 3.23. Found: C, 52.40; H, 4.85; N, 3.06. $^1$H NMR of $[(Ar')Ga(C_5H_4)_2Ru]_n$ (**152$_n$**) ($C_6D_6$): δ 1.7-2.5 (br, 6H, $NMe_2$), 2.9-3.8 (br, 2H, $CH_2$), 4.0-5.8 (br, 8H, Cp), 6.9-7.0 (br, 1H, Ar-H), 7.0-7.1 (br, 1H, Ar-H), 7.15-7.35 (br, 1H, Ar-H), 7.5-8.4 (br, 1H, Ar-H).

**Synthesis of [(*p*-*t*BuAr′)Al($C_5H_4$)$_2$Ru]$_2$ (153).** Following the same procedure as for **152**, (*p*-*t*BuAr′)$AlCl_2$ (0.436 g, 1.51 mmol) and ($LiC_5H_4$)$_2$Ru·tmeda (0.544 g, 1.51 mmol) were used to yield **153** (0.104 g, 15%) after hexane (30 mL) washings. $^1$H NMR ($CDCl_3$): δ 1.32 (s, 18 H, *t*Bu), 2.48 (s, 12 H, $NMe_2$), 3.91 (s, 4 H, $CH_2$), 4.07 (s, 4 H, α-Cp), 4.56 (s, 4 H, ß-Cp), 4.57 (s, 4 H, ß-Cp), 5.05 (s, 4 H, α-Cp), 7.01 (d, 2 H, 3-H), 7.27 (dd, 2H, 4-H), 7.91 (d, 2H, 6-H). $^{13}$C NMR ($CDCl_3$): 31.8 ($C(\underline{C}H_3)_3$), 34.6 ($\underline{C}(CH_3)_3$), 46.6 ($NMe_2$), 66.7 ($CH_2$), 71.3, 71.6, 76.3, 76.4 (Cp), 123.3, 124.0, 134.6, 141.7, 148.4 ($C_6H_3$). EIMS (70 eV): *m/z* (rel intens) 894 (66) [$M^+$], 680 (24) [$(C_5H_5)Ru(C_5H_4)Al(C_6H_3C(CH_3)_3CH_2NMe_2)(C_5H_4)Ru$-$(C_5H_5)H^+$], 432 (100) [$(C_5H_4)Al(C_6H_3C(CH_3)_3CH_2NMe)(C_5H_4)Ru^+$]. HRMS (EI; *m/z*): [$M^+$] calcd for $C_{46}H_{56}Al_2N_2Ru_2$, 894.2161; found 894.2179 (Δppm = 2.0). Anal. Calcd for $C_{46}H_{56}Al_2N_2Ru_2$ (893.05): C, 61.87; H, 6.32; N, 3.14. Found: C, 60.82; H, 6.21; N, 3.03.

**Synthesis of [$Bu_4N$][B{$C_6H_3(CF_3)_2$}$_4$].** A solution of *n*$Bu_4NBr$ (2.30 g, 7.14 mmol) in methanol (4.5 mL, HPCL grade) was added over 15 min to a solution of Na[B{$C_6H_3(CF_3)_2$}$_4$] (4.21 g, 6.05 mmol) in methanol (10 mL). Water (1.5 mL,

millipore) was added to the methanol solution. The stirring was stopped and the solution was first cooled to 0 °C for 30 min and then set to -25 °C over night. The solid was filtered off and washed with cold (-25 °C) methanol (5 mL). The electrolyte was purified by repeated crystallisations from mixtures of $CH_2Cl_2$ (8 mL) and hexane (6 ml). Drying in a desiccator over $P_2O_5$ yielded pure $[Bu_4N][B\{C_6H_3(CF_3)_2\}_4]$ (2.95g, 44%).

## 5.5 References

(1) Herberhold, M.; Bärtl, T. *Z. Naturforsch.* **1995**, *50b*, 1692-1698.

(2) a) Diaz, A. F.; Mueller-Westerhoff, U. T.; Nazzal, A.; Tanner, M. *J. Organomet. Chem.* **1982**, *236*, C45-C48. b) Rheingold, A. L.; Mueller-Westerhoff, U. T.; Swiegers, G. F.; Haas, T. J. *Organometallics* **1992**, *11*, 3411-3417.

(3) Mueller-Westerhoff, U. T.; Rheingold, A. L.; Swiegers, G. F. *Angew. Chem. Int. Ed. Engl.* **1992**, *31*, 1352-1354.

(4) a) Trupia, S.; Nafady, A.; Geiger, W. E. *Inorg. Chem.* **2003**, *42*, 5480-5482. b) Swarts, J. C.; Nafady, A.; Roudebush, J. H.; Trupia, S.; Geiger, W. E. *Inorg. Chem.* **2009**, *48*, 2156-2165.

(5) Schachner, J. A.; Orlowski, G. A.; Quail, J. W.; Kraatz, H.-B.; Müller, J. *Inorg. Chem.* **2006**, *45*, 454-459.

(6) Lund, C. L.; Schachner, J. A.; Burgess, I. J.; Quail, J. W.; Schatte, G.; Müller, J. *Inorg. Chem.* **2008**, *47*, 5992-6000.

(7) These values were calculated from the respective molecular structures.

(8) Isom, H. S.; Cowley, A. H.; Decken, A.; Sissingh, F.; Corbelin, S.; Lagow, R. J. *Organometallics* **1995**, *14*, 2400-2406.

(9) Greenwood, N. N.; Earnshaw, A. *Chemistry of the Elements*, 2nd ed.; Elsevier: Oxford, 2006; pp 1004 and 1074.

(10) a) Bagh, B.; Gilroy, J. B.; Staubitz, A.; Müller, J. *J. Am. Chem. Soc.* **2010**, *132*, 1794-1795. b) Bagh, B.; Schatte, G.; Green, J. C. ; Müller, J. *J. Am. Chem. Soc.* **2012**, *134*, 7924-7936. c) Chapter 3.2.2.

(11) Hill, M. G.; Lamanna, W. M.; Mann, K. R. *Inorg. Chem.* **1991**, *30*, 4687-4690.

(12) Bagh, B.; Breit, N. C.; Schatte, G.; Harms, K.; Burgess, I.; Braunschweig, H.; Müller, J. *Inorg. Chem*. **2012**, *51*, 11155-11167.

(13) Barrière, F.; Geiger, W. E. *J. Am. Chem. Soc.* **2006**, *128*, 3980-3989.

(14) Liu, D.; Xie, F.; Zhang, W. *J. Org. Chem.* **2007**, *72*, 6992-6997.

(15) Vogel, U.; Lough, A. J.; Manners, I. *Angew. Chem. Int. Ed.* **2004**, *43*, 3321-3325.

(16) Reger, D. L.; Wright, T. D.; Little, C. A.; Lamba, J. J. S.; Smith, M. D. *Inorg. Chem.* **2001**, *40*, 3810-3814.

# CHAPTER 6
# SUMMARY

Previous investigations into the synthesis of aluminum- and gallium-bridged [1]MCPs and their reactivity towards ROP found that the sterically bulky ligands attached to aluminum and gallium were hampering the ROP. However, salt-metathesis reactions between dilithioferrocene and aluminum or gallium dichlorides equipped with slim ligands yielded [1.1]FCPs. Therefore, the synthesis of new aluminum and gallium dihalides equipped with ligands of moderate steric bulk for subsequent reactions with lithiated metallocenes was pursued. The direct synthesis with aluminum or gallium trichlorides gave rise to the aluminum and gallium dihalides **113**, **121**, **122**, and **126**, whereas **112** and **124** were obtained from an indirect route via the respective dimethyl species (Figure 6-1).

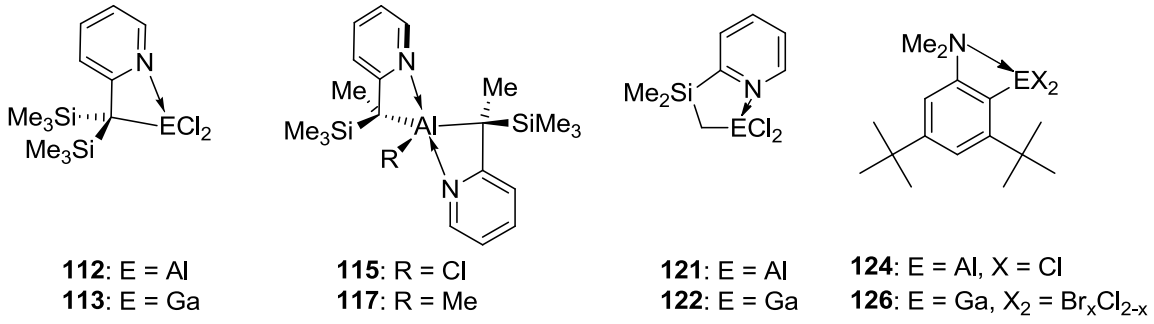


**112**: E = Al
**113**: E = Ga

**115**: R = Cl
**117**: R = Me

**121**: E = Al
**122**: E = Ga

**124**: E = Al, X = Cl
**126**: E = Ga, $X_2 = Br_xCl_{2-x}$

**Figure 6-1.** New aluminum and gallium dihalides equipped with ligands of moderate steric bulk and the aluminum bisligand species obtained during the course of this Ph.D. work.

Aluminum dihalides with the Pytsi$^{-2SiMe_2}$ ligand could not be obtained, since the direct and the indirect route lead to the formation of the bisligand species **115** and **117** (Figure 6-1). Interestingly, the stereoselective formation of *rac* isomers was observed. For **126** a chlorine-bromine exchange occurred during the reaction for which LiBr was found to be a possible source. The new aluminum and gallium compounds were fully

characterized and the molecular structure of either an aluminum or a gallium species was determined. The solid-state structures revealed the larger distances between the group-13-element center and bulky groups on the ligands in comparison with similar species decorated with the parent bulky ligands, Pytsi and Mamx.

Subsequent salt-metathesis reactions of the new aluminum and gallium dihalides with dilithioferrocene or dilithioruthenocene were consistent with the reduced steric bulk of the ligands by giving rise to a variety of products (Figure 6-2).

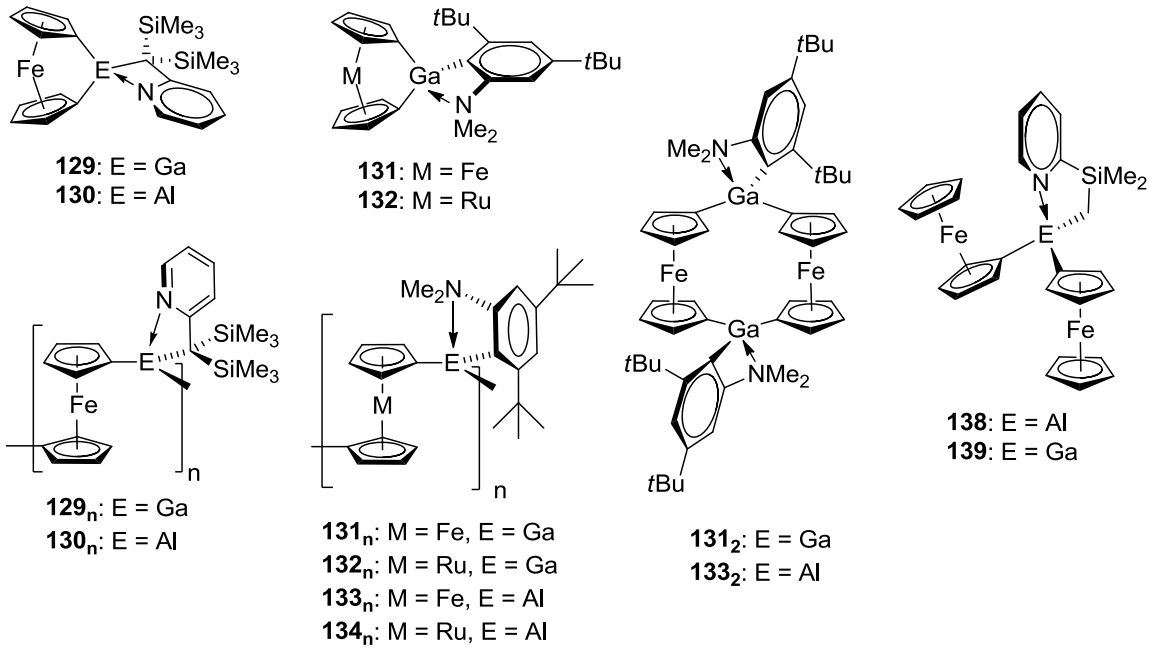


**Figure 6-2.** Aluminum- and gallium-bridged [1]FCPs, [1.1]FCPs, [1]RCPs, ferrocenyl-based or ruthenocenyl-based polymers or oligomers, and bis(ferrocenyl) compounds that were observed or isolated during this Ph.D. work.

When the Pytsi$^{-SiMe_2}$ ligand was employed, the salt-metathesis reaction gave rise to the aluminum- and gallium-bridged [1]FCPs **129** and **130** and ferrocenyl-based oligomers or low-molecular-weight polymers $\mathbf{129_n}$ and $\mathbf{130_n}$. The oligomers formed most likely from condensation reactions and the amount or length of the oligomers was subsequently increased by uncontrolled ROP of the respective [1]FCPs. The outcome of salt-metathesis

reactions with the Mx ligand showed an interesting dependence on the bridging element as well as on the sandwiched metal. In all cases, the respective polymers or oligomers (**131$_n$**-**134$_n$**) were obtained. However, the formation of [1]MCPs was only observed for gallium as a bridging element. These [1]MCPs **131** and **132** were not stable under the reaction conditions and underwent ROP. Based on the comparably high molecular weight of **133$_n$**, it can be assumed that also an aluminum-bridged [1]FCPs formed, but that it was significantly more reactive than **131**. The major influence of the different sandwiched metals is displayed by the formation of [1.1]FCPs (**131$_2$** and **133$_2$**), while no [1.1]RCPs as minor products were detected. Salt metathesis reactions of **121** and **122** with dilithioferrocene gave rise to [1.1]FCPs and oligomers that were not isolable.

Species **121** and **122** were then utilized for the synthesis of model compounds for ferrocenyl-based polymers, the bis(ferrocenyl) compounds **138** and **139** (Figure 6-2). Species **138** and **139** were fully characterized with the molecular structure of **138** exhibiting an attraction between the aluminum and the iron center. The redox behavior of **139** showed a smaller interaction between the two iron centers than in comparable [1.1]FCPs, whereas **138** showed a complex redox behavior similar to other aluminum-bridged [1.1]FCPs.

Future investigations in the area of aluminum- and gallium-bridged MCP and metallopolymers will have the research objective to obtain aluminum- and gallium-bridged [1]MCPs that can undergo ROP in a controlled fashion. Only then a control on the molecular weights of the polymers or even block-copolymers would be available. Since the ligands of moderate steric bulk investigated during this Ph.D. project rather

yielded oligomers and too reactive [1]MCPs, new avenues to pursue this research should be explored.

In a group project the first [1.1]FCPs with different bridging elements as well as the first polyferrocenes with alternating bridging elements were successfully synthesized (Scheme 6-1). Starting from a silicon-bridged bis(1'-bromoferrocenyl) compound the second bridging element was added as an element dichloride subsequent to the lithiation of **140** or **141**.

**Scheme 6-1.** Synthesis of [1.1]FCPs and polyferrocenes with alternating bridging elements that were carried out during this Ph.D. project.

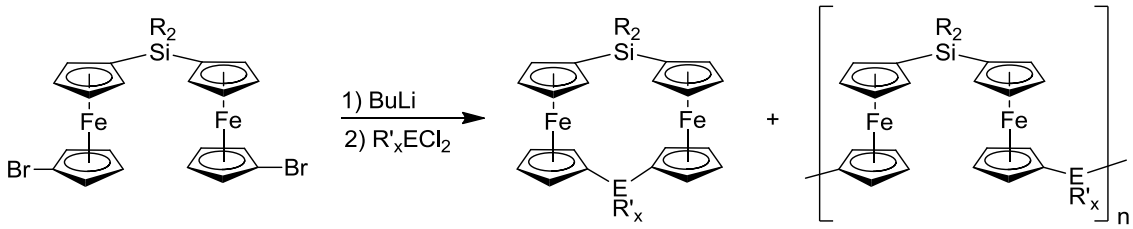


**140**: R = Me
**141**: R = Et

**$142_1$**: E = Sn, R = Et, R'$_x$ = $Me_2$
**$143_1$**: E = Sn, R = Et, R'$_x$ = *n*$Bu_2$
**$144_1$**: E = Sn, R = Et, R'$_x$ = *t*$Bu_2$
**$148_1$**: E = Ga, R = Me, R'$_x$ = Ar'

**$142_n$**: E = Sn, R = Et, R'$_x$ = $Me_2$
**$143_n$**: E = Sn, R = Et, R'$_x$ = *n*$Bu_2$
**$144_n$**: E = Sn, R = Et, R'$_x$ = *t*$Bu_2$
**$148_n$**: E = Ga, R = Me, R'$_x$ = Ar'

Reactions of **141** with dialkyldichlorostannes yielded mixtures of linear and cyclic polyferrocenes with alternating bridging elements as revealed by MALDI-TOF spectrometry. The silicon-tin-bridged [1.1]FCPs **$142_1$-$144_1$** were only formed as minor components and only **$142_1$** could be isolated. Macrocycles are scarcely studied species and we were able to contribute to this field by the study and isolation of the cyclic tetramer **$144_2$c** (Figure 6-3). The redox behavior of **$144_2$c** was particularly interesting since it is significantly different from the silicon-bridged [1.1.1.1]FCP **$34_4$c** and could not be fully explained to date. When (Ar´)$GaCl_2$ was utilized in the reaction with **140** and BuLi, the [1.1]FCP **$148_1$** was formed as a major product. The molecular structure and

redox behavior of **$148_1$** was found to be in between the properties of the two symmetrically bridged [1.1]FCPs **15** and **78**. In addition to **$148_1$**, a mixture of linear and cyclic polyferrocenes with alternating silicon and gallium as bridging elements was formed.

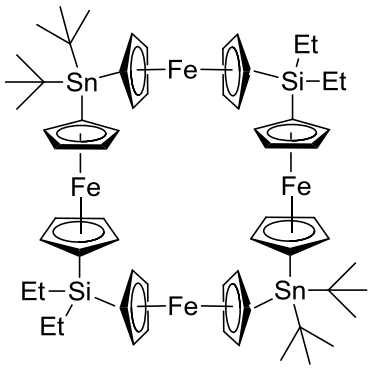


**$144_2$c**

**Figure 6-3.** The isolated and electrochemically studied [1.1.1.1]FCP **$144_2$c** with alternating tin and silicon bridging elements.

Future research in the field of [1.1]FCPs and polyferrocenes with alternating bridging elements will naturally consist of different combinations of bridging elements being used. However, the next synthetic challenge in this area might be the synthesis of [1.1.1.1]FCPs and polyferrocene with three different bridging elements in a defined order (Scheme 4-10).

The first aluminum- and gallium-bridged [1.1]RCPs (**152** and **153**) were obtained from salt-metathesis reactions of 1,1'-dilithioruthenocene with aluminum and gallium dichlorides with slim ligands (Figure 6-4).

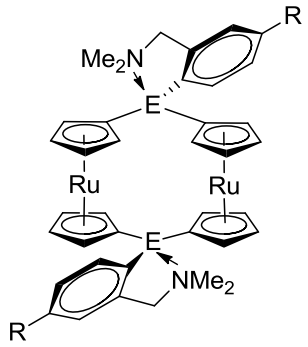


**152**: E = Ga, R = H
**153**: E = Al, R = *t*Bu

**Figure 6-4.** The first aluminum- and gallium-bridged [1.1]RCPs (**152** and **153**) synthesized during this Ph.D. project.

The only well-studied carbon-bridged [1.1]RCP (**24**) exhibited an increased twist of the Cp rings in the molecular structure in comparison with the respective [1.1]FCP (**13**). The proximity of the ruthenocenediyl moieties in **24** led to a ruthenium-ruthenium bond formation affording a reversible two-electron oxidation in the presence of a traditional electrolyte anion. The redox properties and structural features of **24** were contrasted by **152** and **153**. The molecular structure of **152** is - except for the expected larger Cp···Cp distances - congruent to its lighter homologue **78**. The redox behavior of **152** and **153** does not resemble the redox behavior of **24**. The expected two irreversible two-electron oxidations were observed for **152** and **153** in the presence of a traditional electrolyte anion. When a weakly coordinating electrolyte anion was utilized for the cyclic voltammetry measurement, a reversible oxidation was observed for the gallium-bridged [1.1]RCP (**152**), while the oxidation of the aluminum-bridged [1.1]RCP (**153**) remained irreversible.

The electrochemical results of **152** and **153** encourage further investigations. It would be interesting to investigate the chemical fate of the oxidized **152** with different electrolytes.

APPENDIX

CRYSTALLOGRAPHIC DATA

**(Pytsi$^{-SiMe_2}$)AlMe$_2$ (110)**: The crystallographic data of **110** was published in Breit, N. C.; Ancelet, T.; Quail, W.; Schatte, G.; Müller, J. *Organometallics* **2011**, *30*, 6150-6158. Crystallographic data has been deposited with the Cambridge Crystallographic Data Centre under CCDC 836327.

**Table A-1.** Crystal data and structure refinement for **110**.

| | |
|---|---|
| Empirical formula | $C_{14}H_{28}AlNSi_2$ |
| Formula weight | 293.53 |
| Temperature | 173(2) K |
| Wavelength | 0.71073 Å |
| Crystal system | Orthorhombic |
| Space group | P*bca* |
| Unit cell dimensions | a = 15.9215(2) Å $\alpha$= 90°.<br>b = 16.2335(2) Å $\beta$= 90°.<br>c = 28.9629(3) Å $\gamma$ = 90°. |
| Volume | 7485.80(15) Å$^3$ |
| Z | 16 |
| Density (calculated) | 1.042 mg/m$^3$ |
| Absorption coefficient | 0.224 mm$^{-1}$ |
| F(000) | 2560 |
| Crystal size | 0.20 x 0.15 x 0.05 mm$^3$ |
| Theta range for data collection | 1.92 to 25.35° |
| Index ranges | -19<=h<=17, -19<=k<=19, -34<=l<=34 |
| Reflections collected | 91938 |
| Independent reflections | 6844 |
| Completeness to theta = 25.68° | 99.9 % |
| Absorption correction | φ-scan |
| Max. and min. transmission | 0.9889 and 0.9566 |
| Refinement method | Full-matrix least-squares on F$^2$ |
| Data / restraints / parameters | 6844 / 0 / 342 |
| Goodness-of-fit on F$^2$ | 1.089 |
| Final R indices [I>2sigma(I)] | R1 = 0.0502 |
| R indices (all data) | wR2 = 0.1062 |
| Extinction coefficient | 0.00050(10) |
| Largest diff. peak and hole | 0.297 and -0.195 e.Å$^{-3}$ |

**(Pytsi$^{-SiMe_2}$)AlBr$_2$ (111)**: The crystallographic data of **111** was published in Breit, N. C.; Ancelet, T.; Quail, W.; Schatte, G.; Müller, J. *Organometallics* **2011**, *30*, 6150-6158. Crystallographic data has been deposited with the Cambridge Crystallographic Data Centre under CCDC 836328.

**Table A-2.** Crystal data and structure refinement for **111**.

| | | |
|---|---|---|
| Empirical formula | $C_{12}H_{22}AlBr_2NSi_2$ | |
| Formula weight | 423.29 | |
| Temperature | 173(2) | |
| Wavelength | 0.71073 Å | |
| Crystal system | Orthorhombic | |
| Space group | $P2_12_12_1$ | |
| Unit cell dimensions | a = 8.3242(6) Å | $\alpha$= 90°. |
| | b = 15.0855(9) Å | $\beta$= 90°. |
| | c = 15.2507(6) Å | $\gamma$ = 90°. |
| Volume | 1915.10(19) Å$^3$ | |
| Z | 4 | |
| Density (calculated) | 1.468 mg/m$^3$ | |
| Absorption coefficient | 4.390 mm$^{-1}$ | |
| F(000) | 848 | |
| Crystal size | 0.12 x 0.05 x 0.05 mm$^3$ | |
| Theta range for data collection | 2.79 to 25.668°. | |
| Index ranges | -10<=h<=10, -17<=k<=18, -18<=l<=18 | |
| Reflections collected | 29 183 | |
| Independent reflections | 3629 | |
| Completeness to theta = 25.68° | 99.8 % | |
| Absorption correction | multiscan | |
| Max. and min. transmission | 0.8103 and 0.6209 | |
| Refinement method | Full-matrix least-squares on F$^2$ | |
| Data / restraints / parameters | 3629 / 0 / 169 | |
| Goodness-of-fit on F$^2$ | 1.084 | |
| Final R indices [I>2sigma(I)] | R1 = 0.0441 | |
| R indices (all data) | wR2 = 0.0877 | |
| Absolute structure parameter | 0.031(12) | |
| Largest diff. peak and hole | 0.766 and -0.673 e.Å$^{-3}$ | |

**(Pytsi$^{-2SiMe_2}$)$_2$AlMe** (**117**): The crystallographic data of **117** was published in Breit, N. C.; Ancelet, T.; Quail, W.; Schatte, G.; Müller, J. *Organometallics* **2011**, *30*, 6150-6158. Crystallographic data has been deposited with the Cambridge Crystallographic Data Centre under CCDC 836329.

**Table A-3.** Crystal data and structure refinement for **117**.

| | | |
|---|---|---|
| Empirical formula | $C_{21}H_{35}AlN_2Si_2$ | |
| Formula weight | 398.67 | |
| Temperature | 173(2) K | |
| Wavelength | 1.54184 Å | |
| Crystal system | monoclinic | |
| Space group | C2/ *c* | |
| Unit cell dimensions | a = 16.387(5) Å | α= 90° |
| | b = 12.116(4) Å | β= 97.745(10)° |
| | c = 12.202(4) Å | γ = 90° |
| Volume | 2400.5(13) Å$^3$ | |
| Z | 4 | |
| Density (calculated) | 1.103 mg/m$^3$ | |
| Absorption coefficient | 1.736 mm$^{-1}$ | |
| F(000) | 864 | |
| Crystal size | 0.12 x 0.12 x 0.11 mm$^3$ | |
| Theta range for data collection | 4.55 to 69.61°. | |
| Index ranges | -18<=h<=19, -11<=k<=14, -14<=l<=14 | |
| Reflections collected | 6920 | |
| Independent reflections | 2161 [R(int) = 0.0861] | |
| Completeness to theta = 69.61° | 95.1 % | |
| Max. and min. transmission | 0.8387 and 0.8175 | |
| Refinement method | Full-matrix least-squares on F$^2$ | |
| Data / restraints / parameters | 2161 / 0 / 124 | |
| Goodness-of-fit on F$^2$ | 1.049 | |
| Final R indices [I>2sigma(I)] | R1 = 0.0582 | |
| R indices (all data) | wR2 = 0.1511 | |
| Extinction coefficient | 0.0013(5) | |
| Largest diff. peak and hole | 0.313 and -0.434 e.Å$^{-3}$ | |

**(Pytsi$^{-2SiMe_3}$)$GaCl_2$ (122)**: Published in Bagh, B.; Breit, N. C.; Harms, K.; Schatte, G.; Burgess, I.; Braunschweig, H.; Müller, J. *Inorg. Chem.* **2012**, *51*, 11155-11167. Crystallographic data has been deposited with the Cambridge Crystallographic Data Centre under CCDC 895302.

**Table A-4.** Crystal data and structure refinement for **122**.

| | | |
|---|---|---|
| Empirical formula | $C_8H_{12}Cl_2GaNSi$ | |
| Formula weight | 290.90 | |
| Temperature | 100(2) K | |
| Wavelength | 0.71073 Å | |
| Crystal system | Monoclinic | |
| Space group | C2/c | |
| Unit cell dimensions | a = 24.8987(15) Å | $\alpha$= 90° |
| | b = 8.4418(3) Å | $\beta$= 104.633(5)° |
| | c = 11.9599(7) Å | $\gamma$ = 90° |
| Volume | 2432.3(2) Å$^3$ | |
| Z | 8 | |
| Density (calculated) | 1.589 mg/m$^3$ | |
| Absorption coefficient | 2.758 mm$^{-1}$ | |
| F(000) | 1168 | |
| Crystal size | 0.31 x 0.20 x 0.08 mm$^3$ | |
| Theta range for data collection | 1.69 to 26.69° | |
| Index ranges | -31<=h<=31, -10<=k<=10, -13<=l<=15 | |
| Reflections collected | 15220 | |
| Independent reflections | 2577 [R(int) = 0.0526] | |
| Completeness to theta = 25.50° | 100.0 % | |
| Absorption correction | Semi-empirical from equivalents | |
| Max. and min. transmission | 0.8316 and 0.4669 | |
| Refinement | Full-matrix least-squares on F$^2$ | |
| Data / restraints / parameters | 2577 / 0 / 120 | |
| Goodness-of-fit on F$^2$ | 0.917 | |
| R index conventional [I>2sigma(I)] | R1 = 0.0218 | |
| R index (all data) | wR2 = 0.0501 | |
| Largest diff. peak and hole | 0.466 and -0.225 e.Å$^{-3}$ | |

**(Mx)GaBr$_x$Cl$_{2-x}$ (126)**: unpublished

**Table A-9.** Crystal data and structure refinement for **126**.

| | |
|---|---|
| Empirical formula | $C_{16}H_{26}Br_{0.59}Cl_{1.38}GN$ |
| Formula weight | 398.32 |
| Temperature | 100(2) K |
| Wavelength | 0.71073 Å |
| Crystal system | Orthorhombic |
| Space group | *Pnma* |
| Unit cell dimensions | a = 15.6156(8) Å α= 90° |
| | b = 9.9860(4) Å β= 90° |
| | c = 12.0928(5) Å γ= 90° |
| Volume | 1885.72(15) Å3 |
| Z | 4 |
| Density (calculated) | 1.403 mg/m$^3$ |
| Absorption coefficient | 2.903 mm-1 |
| F(000) | 817 |
| Crystal size | 0.34 x 0.14 x 0.11 mm$^3$ |
| Theta range for data collection | 2.13 to 26.77° |
| Index ranges | -19<=h<=19, -12<=k<=12, -15<=l<=14 |
| Reflections collected | 16428 |
| Independent reflections | 2116 [R(int) = 0.0642] |
| Completeness to theta = 25.25° | 100.0 % |
| Max. and min. transmission | 0.7451 and 0.4807 |
| Refinement method | Full-matrix least-squares on F2 |
| Data / restraints / parameters | 2116 / 8 / 128 |
| Goodness-of-fit on F$^2$ | 1.094 |
| Final R indices [I>2sigma(I)] | R1 = 0.0282 |
| R indices (all data) | wR2 = 0.0660 |
| Largest diff. peak and hole | 0.289 and -0.542 e.Å$^{-3}$ |

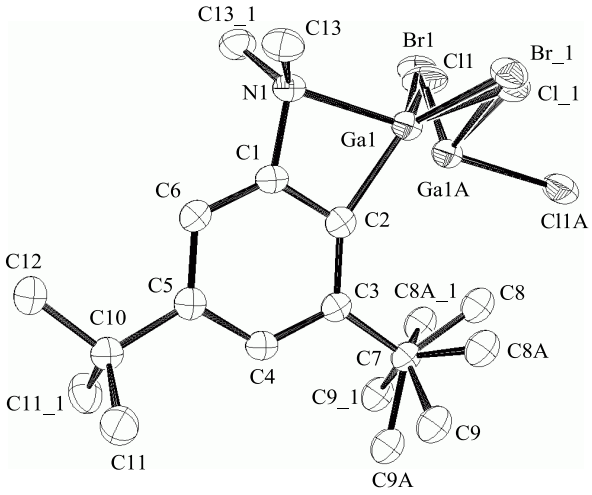


**Figure A-2.** Ortep plot of **126**, with thermal ellipsoids at the 50% probability level. Hydrogen atoms are omitted for clarity.

**Table A-10.** Atomic coordinates and equivalent isotropic displacement parameters ($Å^2$) for **126**. U(eq) is defined as one third of the trace of the orthogonalized $U^{ij}$ tensor.

| | x | y | z | U(eq) | Occupancy |
|---|---|---|---|---|---|
| C1 | 0.32808(14) | 0.2500 | -0.0267(2) | 0.0243(5) | 1 |
| C2 | 0.40118(15) | 0.2500 | 0.0382(2) | 0.0249(5) | 1 |
| C3 | 0.48128(14) | 0.2500 | -0.0129(2) | 0.0231(5) | 1 |
| C4 | 0.48200(15) | 0.2500 | -0.1285(2) | 0.0255(5) | 1 |
| C5 | 0.40798(16) | 0.2500 | -0.1942(2) | 0.0255(5) | 1 |
| C6 | 0.32838(15) | 0.2500 | -0.1411(2) | 0.0255(5) | 1 |
| C7 | 0.56576(15) | 0.2500 | 0.0515(2) | 0.0263(5) | 1 |
| C8 | 0.55145(19) | 0.2500 | 0.1761(3) | 0.0355(5) | 0.928(3) |
| C8A | 0.5676(15) | 0.121(2) | 0.122(2) | 0.0355(5) | 0.072(3) |
| C9 | 0.61716(13) | 0.1242(2) | 0.0211(2) | 0.0355(5) | 0.928(3) |
| C9A | 0.6456(16) | 0.2500 | -0.022(3) | 0.0355(5) | 0.072(3) |
| C10 | 0.41645(16) | 0.2500 | -0.3204(2) | 0.0283(6) | 1 |
| C11 | 0.46534(13) | 0.1239(2) | -0.35643(18) | 0.0389(5) | 1 |
| C12 | 0.32898(17) | 0.2500 | -0.3781(2) | 0.0342(6) | 1 |
| C13 | 0.19734(12) | 0.1285(2) | 0.02805(18) | 0.0338(4) | 1 |
| N1 | 0.25001(12) | 0.2500 | 0.04334(18) | 0.0254(5) | 1 |
| Cl1 | 0.3250(5) | 0.0745(7) | 0.2791(6) | 0.0423(12) | 0.676(3) |
| Cl1A | 0.4765(15) | 0.2500 | 0.355(2) | 0.043(6) | 0.03 |
| Ga1 | 0.33886(2) | 0.2500 | 0.17657(3) | 0.02695(12) | 0.97 |
| Ga1A | 0.3852(7) | 0.2500 | 0.2167(9) | 0.02695(12) | 0.03 |
| Br1 | 0.3106(5) | 0.0636(7) | 0.2778(5) | 0.0344(7) | 0.294(3) |

**Table A-11.** Selected bond lengths [Å] and angles [°] for **126**.

| | | | |
|---|---|---|---|
| C1-C6 | 1.383(4) | C10-C11#1 | 1.535(3) |
| C1-C2 | 1.386(3) | C10-C11 | 1.536(3) |
| C1-N1 | 1.484(3) | C2-Ga1 | 1.935(3) |
| C1-Ga1 | 2.464(3) | C2-Ga1A | 2.172(11) |
| C2-C3 | 1.395(3) | C3-C4 | 1.397(4) |
| C2-Ga1 | 1.935(3) | C3-C7 | 1.532(3) |
| C2-Ga1A | 2.172(11) | C4-C5 | 1.403(4) |
| C3-C4 | 1.397(4) | C13-N1 | 1.477(2) |
| C3-C7 | 1.532(3) | N1-C13#1 | 1.477(2) |
| C4-C5 | 1.403(4) | N1-Ga1 | 2.126(2) |
| C5-C6 | 1.399(3) | Cl1-Ga1A | 2.127(9) |
| C5-C10 | 1.532(4) | Cl1-Ga1 | 2.157(8) |
| C7-C8 | 1.522(4) | Cl1A-Ga1A | 2.20(3) |
| C7-C9A | 1.528(14) | Ga1-Cl1#1 | 2.157(8) |
| C7-C9#1 | 1.536(3) | Ga1-Br1 | 2.271(7) |
| C7-C9 | 1.536(3) | Ga1-Br1#1 | 2.271(7) |
| C7-C8A | 1.544(14) | Ga1A-Cl1#1 | 2.127(9) |
| C7-C8A#1 | 1.544(14) | Ga1A-Br1 | 2.317(9) |
| C10-C12 | 1.534(3) | | |
| | | | |
| C6-C1-C2 | 124.3(2) | C13#1-N1-C1 | 112.69(13) |
| C6-C1-N1 | 125.0(2) | C13-N1-C1 | 112.69(13) |
| C2-C1-N1 | 110.7(2) | C13#1-N1-Ga1 | 117.26(12) |
| C6-C1-Ga1 | 175.88(18) | C13-N1-Ga1 | 117.27(12) |
| C2-C1-Ga1 | 51.56(14) | C1-N1-Ga1 | 84.06(14) |
| N1-C1-Ga1 | 59.13(12) | Ga1A-Cl1-Ga1 | 23.5(3) |
| C1-C2-C3 | 119.1(2) | C2-Ga1-N1 | 70.93(9) |
| C1-C2-Ga1 | 94.33(16) | C2-Ga1-Cl1 | 123.18(18) |
| C3-C2-Ga1 | 146.5(2) | N1-Ga1-Cl1 | 111.7(2) |
| C2-C3-C4 | 116.8(2) | Cl1#1-Ga1-Cl1 | 108.6(4) |
| C2-C3-C7 | 123.1(2) | C2-Ga1-Br1 | 124.33(14) |
| C4-C3-C7 | 120.1(2) | N1-Ga1-Br1 | 106.36(19) |
| C3-C4-C5 | 124.1(2) | Cl1#1-Ga1-Br1 | 109.64(6) |
| C6-C5-C4 | 118.1(2) | C2-Ga1-Br1#1 | 124.33(14) |
| C6-C5-C10 | 122.3(2) | N1-Ga1-Br1#1 | 106.36(19) |
| C4-C5-C10 | 119.6(2) | Cl1#1-Ga1-Br1 | 109.64(6) |
| C1-C6-C5 | 117.5(2) | C2-Ga1-Br1#1 | 124.33(14) |
| C8-C7-C9A | 133.8(14) | N1-Ga1-Br1#1 | 106.36(19) |
| C8-C7-C3 | 112.1(2) | Cl1-Ga1-Br1#1 | 109.64(6) |
| C9A-C7-C3 | 114.1(14) | Br1-Ga1-Br1#1 | 110.0(3) |
| C8-C7-C9#1 | 108.29(15) | C2-Ga1-C1 | 34.11(9) |
| C3-C7-C9#1 | 109.15(14) | N1-Ga1-C1 | 36.81(7) |
| C8-C7-C9 | 108.29(15) | Cl1#1-Ga1-C1 | 124.50(19) |
| C3-C7-C9 | 109.15(14) | Cl1-Ga1-C1 | 124.50(19) |

| | | | |
|---|---|---|---|
| C9#1-C7-C9 | 109.8(2) | Br1-Ga1-C1 | 121.65(16) |
| C9A-C7-C8A | 107.6(10) | Br1#1-Ga1-C1 | 121.64(16) |
| C3-C7-C8A | 107.3(10) | Cl1-Ga1A-Cl1#1 | 110.9(6) |
| C9#1-C7-C8A | 143.6(10) | Cl1-Ga1A-C2 | 113.8(4) |
| C9A-C7-C8A#1 | 107.6(10) | Cl1#1-Ga1A-C2 | 113.8(4) |
| C3-C7-C8A#1 | 107.3(10) | Cl1-Ga1A-Cl1A | 91.0(5) |
| C9-C7-C8A#1 | 143.6(10) | Cl1#1-Ga1A-Cl1A | 91.0(5) |
| C8A-C7-C8A#1 | 113(2) | C2-Ga1A-Cl1A | 132.9(8) |
| C5-C10-C12 | 112.1(2) | Cl1#1-Ga1A-Br1 | 109.0(4) |
| C5-C10-C11#1 | 109.01(15) | C2-Ga1A-Br1 | 112.0(4) |
| C12-C10-C11#1 | 108.27(15) | Cl1A-Ga1A-Br1 | 94.8(5) |
| C5-C10-C11 | 109.01(15) | Cl1-Ga1A-Br1#1 | 109.0(4) |
| C12-C10-C11 | 108.27(15) | C2-Ga1A-Br1#1 | 112.0(4) |
| C11#1-C10-C11 | 110.1(2) | Cl1A-Ga1A-Br1#1 | 94.8(5) |
| C13#1-N1-C13 | 110.4(2) | Br1-Ga1A-Br1#1 | 106.9(5) |

Symmetry transformations used to generate equivalent atoms: #1 x,-y+1/2,z

**Table A-12.** Anisotropic displacement parameters (Å2) for **126**. The anisotropic displacement factor exponent takes the form: $-2\pi^2[ h^2a^{*2}U^{11} + ... + 2 h k a^* b^* U^{12} ]$.

| | $U^{11}$ | $U^{22}$ | $U^{33}$ | $U^{23}$ | $U^{13}$ | $U^{12}$ |
|---|---|---|---|---|---|---|
| C1 | 0.0225(11) | 0.0204(12) | 0.0301(13) | 0.000 | 0.0032(9) | 0.000 |
| C2 | 0.0269(11) | 0.0198(12) | 0.0279(13) | 0.000 | -0.0002(10) | 0.000 |
| C3 | 0.0234(11) | 0.0179(11) | 0.0281(13) | 0.000 | -0.0004(10) | 0.000 |
| C4 | 0.0243(11) | 0.0237(13) | 0.0287(13) | 0.000 | 0.0026(10) | 0.000 |
| C5 | 0.0284(12) | 0.0201(12) | 0.0280(14) | 0.000 | -0.0003(10) | 0.000 |
| C6 | 0.0238(11) | 0.0233(13) | 0.0294(13) | 0.000 | -0.0021(10) | 0.000 |
| C7 | 0.0228(11) | 0.0282(14) | 0.0280(13) | 0.000 | -0.0017(9) | 0.000 |
| C8 | 0.0291(8) | 0.0389(11) | 0.0386(10) | 0.000 | -0.0068(7) | 0.000 |
| C8A | 0.0291(8) | 0.0389(11) | 0.0386(10) | 0.000 | -0.0068(7) | 0.000 |
| C9 | 0.0291(8) | 0.0389(11) | 0.0386(10) | 0.000 | -0.0068(7) | 0.000 |
| C9A | 0.0291(8) | 0.0389(11) | 0.0386(10) | 0.000 | -0.0068(7) | 0.000 |
| C10 | 0.0279(12) | 0.0295(14) | 0.0275(13) | 0.000 | -0.0002(10) | 0.000 |
| C11 | 0.0424(11) | 0.0417(12) | 0.0326(11) | -0.0089 (10) | -0.0020(8) | 0.0099 (9) |
| C12 | 0.0336(13) | 0.0401(16) | 0.0290(14) | 0.000 | -0.0048(11) | 0.000 |
| C13 | 0.0296(9) | 0.0325(11) | 0.0393(11) | -0.0017 (9) | 0.0058(8) | -0.0075 (8) |
| N1 | 0.0220(9) | 0.0246(11) | 0.0295(11) | 0.000 | 0.0037(8) | 0.000 |
| Cl1 | 0.030(2) | 0.0489(19) | 0.0484(10) | 0.0235 (11) | 0.0096(10) | 0.0012 (13) |
| Cl1A | 0.034(11) | 0.071(18) | 0.026(11) | 0.000 | 0.007(9) | 0.000 |
| Ga1 | 0.02530(17) | 0.03009(18) | 0.02545(17) | 0.000 | 0.00241(12) | 0.000 |
| Ga1A | 0.02530(17) | 0.03009(18) | 0.02545(17) | 0.000 | 0.00241(12) | 0.000 |
| Br1 | 0.0293(19) | 0.0345(7) | 0.0395(7) | 0.0115 (6) | 0.0101(9) | -0.0025 (10) |

**Table A-13.** Hydrogen coordinates and isotropic displacement parameters (Å$^2$) for **126**.

| | x | y | z | U(eq) | Occupancy |
|---|---|---|---|---|---|
| H4 | 0.5360 | 0.2500 | -0.1647 | 0.031 | 1 |
| H6 | 0.2765 | 0.2500 | -0.1820 | 0.031 | 1 |
| H8A | 0.5149 | 0.3259 | 0.1964 | 0.053 | 0.464(2) |
| H8B | 0.6067 | 0.2578 | 0.2140 | 0.053 | 0.464(2) |
| H8C | 0.5235 | 0.1662 | 0.1980 | 0.053 | 0.464(2) |
| H8AA | 0.5779 | 0.0437 | 0.0738 | 0.053 | 0.072(3) |
| H8AB | 0.5126 | 0.1101 | 0.1597 | 0.053 | 0.072(3) |
| H8AC | 0.6136 | 0.1274 | 0.1768 | 0.053 | 0.072(3) |
| H9A | 0.5842 | 0.0442 | 0.0412 | 0.053 | 0.928(3) |
| H9B | 0.6716 | 0.1243 | 0.0614 | 0.053 | 0.928(3) |
| H9C | 0.6284 | 0.1237 | -0.0586 | 0.053 | 0.928(3) |
| H9AA | 0.6704 | 0.3402 | -0.0231 | 0.053 | 0.036(2) |
| H9AB | 0.6300 | 0.2230 | -0.0967 | 0.053 | 0.036(2) |
| H9AC | 0.6877 | 0.1869 | 0.0085 | 0.053 | 0.036(2) |
| H11A | 0.5229 | 0.1251 | -0.3241 | 0.058 | 1 |
| H11B | 0.4697 | 0.1221 | -0.4373 | 0.058 | 1 |
| H11C | 0.4346 | 0.0442 | -0.3309 | 0.058 | 1 |
| H12A | 0.3372 | 0.2422 | -0.4582 | 0.051 | 0.50 |
| H12B | 0.2989 | 0.3337 | -0.3615 | 0.051 | 0.50 |
| H12C | 0.2950 | 0.1741 | -0.3515 | 0.051 | 0.50 |
| H13A | 0.2334 | 0.0489 | 0.0364 | 0.051 | 1 |
| H13B | 0.1720 | 0.1292 | -0.0461 | 0.051 | 1 |
| H13C | 0.1517 | 0.1268 | 0.0836 | 0.051 | 1 |

**(Pytsi$^{-2SiMe_3}$)AlFc$_2$** (**138**): published in Bagh, B.; Breit, N. C.; Harms, K.; Schatte, G.; Burgess, I.; Braunschweig, H.; Müller, J. *Inorg. Chem.* **2012**, *51*, 11155-11167.

Crystallographic data has been deposited with the Cambridge Crystallographic Data Centre under CCDC 895303.

**Table A-14.** Crystal data and structural refinement for **138**.

| | |
|---|---|
| Empirical formula | $C_{28}H_{30}AlFe_2NSi$ |
| Formula weight | 547.30 |
| Temperature | 100 K |
| Wavelength | 0.71073 Å |
| Crystal system | Triclinic |
| Space group | $P\bar{1}$ |
| Unit cell dimensions | a = 10.6268 (9) Å $\alpha$= 88.174 (7)° |
| | b = 12.8724 (10) Å $\beta$= 82.917 (7)° |
| | c = 18.6478 (17) Å $\gamma$ = 87.039 (7)° |
| Volume | 2527.2 (4) Å$^3$ |
| Z | 4 |
| Density (calculated) | 1.438 mg/m$^3$ |
| Absorption coefficient | 1.25 mm$^{-1}$ |
| Crystal size | 0.21 × 0.21 × 0.01 mm$^3$ |
| Theta range for data collection | 1.6 to 25.0°. |
| Index ranges | -12<=h<=12, -15<=k<=15, -22<=l<=21 |
| Reflections collected | 13945 |
| Independent reflections | 6615 |
| Max. and min. transmission | 0.962 and 0.811 |
| Refinement method | Full-matrix least-squares on F$^2$ |
| Data / restraints / parameters | 6615 / 94 / 599 |
| Goodness-of-fit on F$^2$ | 0.581 |
| Final R indices [I>2sigma(I)] | R1 = 0.0421 |
| R indices (all data) | wR2 = 0.0886 |
| Largest diff. peak and hole | 0.28 and -0.23 e.Å$^{-3}$ |

**[SiEt$_2$fcSn*t*Bu$_2$fc]$_2$ (144$_2$)**: Published in Bagh, B.; Breit, N. C.; Dey, S.; Gilroy, J. B.; Schatte, G.; Harms, K.; Müller, J. *Chem. – Eur. J.* **2012**, *18*, 9722-9733. Crystallographic data has been deposited with the Cambridge Crystallographic Data Centre under CCDC 871838.

**Table A-19.** Crystal data and structure refinement for **144$_2$**.

| | | |
|---|---|---|
| Empirical formula | $C_{64}H_{88}Fe_4Si_2Sn_2$ | |
| Formula weight | 1374.30 | |
| Temperature | 173(2) K | |
| Wavelength | 0.71069 Å | |
| Crystal system | triclinic | |
| Space group | *P*1 | |
| | a = 14.6681(2) Å | α= 66.5243(8)° |
| | b = 14.7976(3) Å | β= 89.3170(10)° |
| | c = 16.0618(3) Å | γ = 77.2124(9)°. |
| Volume | 3107.03(10) Å$^3$ | |
| Z | 2 | |
| Density (calculated) | 1.469 Mg/m$^3$ | |
| Absorption coefficient | 1.776 mm$^{-1}$ | |
| F(000) | 1408 | |
| Crystal size | 0.25 x 0.20 x 0.18 mm$^3$ | |
| Theta range for data collection | 3.01 to 30.01°. | |
| Index ranges | -20<=h<=20, -20<=k<=20, -22<=l<=22 | |
| Reflections collected | 32741 | |
| Independent reflections | 14495 | |
| Completeness to theta = 30.01° | 98.8 % | |
| Max. and min. transmission | 0.7405 and 0.6651 | |
| Refinement method | Full-matrix least-squares on F$^2$ | |
| Data / restraints / parameters | 17952 / 0 / 665 | |
| Goodness-of-fit on F$^2$ | 1.047 | |
| Final R indices [I>2sigma(I)] | R1 = 0.0354 | |
| R indices (all data) | wR2 = 0.0794 | |
| Largest diff. peak and hole | 0.429 and -0.761 e.Å$^{-3}$ | |

**[SiMe$_2$fcGa(Ar´)fc]** (**148$_1$**): Published in Bagh, B.; Breit, N. C.; Gilroy, J. B.; Schatte, G.; Müller, J. *Chem. Comm.* **2012**, *48*, 7823-7825. Crystallographic data has been deposited with the Cambridge Crystallographic Data Centre under CCDC 878280.

**Table A-20.** Crystal data and structure refinement for **148$_1$**.

| | | |
|---|---|---|
| Empirical formula | $C_{31}H_{34}Fe_2GaNSi$ | |
| Formula weight | 630.10 | |
| Temperature | 173(2) K | |
| Wavelength | 0.71073 Å | |
| Crystal system | monoclinic | |
| Space group | $P2_1/c$ | |
| Unit cell dimensions | a = 27.7463(2) Å | $\alpha$= 90° |
| | b = 11.3739(2) Å | $\beta$= 96.8620(8)°. |
| | c = 17.6834(3) Å | $\gamma$ = 90°. |
| Volume | 5540.62(14) Å$^3$ | |
| Z | 8 | |
| Density (calculated) | 1.511 Mg/m$^3$ | |
| Absorption coefficient | 2.063 mm$^{-1}$ | |
| F(000) | 2592 | |
| Crystal size | 0.18 x 0.15 x 0.08 mm$^3$ | |
| Theta range for data collection | 1.48 to 29.57°. | |
| Index ranges | -38<=h<=38, -15<=k<=15, -24<=l<=24 | |
| Reflections collected | 28035 | |
| Independent reflections | 15486 [R(int) = 0.0370] | |
| Completeness to theta = 29.58° | 99.6 % | |
| Max. and min. transmission | 0.8523 and 0.7078 | |
| Refinement method | Full-matrix least-squares on F$^2$ | |
| Data / restraints / parameters | 15486 / 0 / 657 | |
| Goodness-of-fit on F$^2$ | 1.016 | |
| Final R indices [I>2sigma(I)] | R1 = 0.0377 | |
| R indices (all data) | wR2 = 0.0844 | |
| Largest diff. peak and hole | 0.560 and -0.536 e.Å$^{-3}$ | |

**[(Ar′)Gafc]$_2$ (152)**: unpublished.

**Table A-21.** Crystal data and structure refinement for **152**.

| | | |
|---|---|---|
| Empirical formula | $C_{38}H_{40}Ga_2N_2Ru_2$ | |
| Formula weight | 866.30 | |
| Temperature | 173(2) K | |
| Wavelength | 0.71073 Å | |
| Crystal system | monoclinic | |
| Space group | $P2_1/c$ | |
| Unit cell dimensions | a = 10.2097(3) Å | α= 90° |
| | b = 11.5783(3) Å | β= 103.4518(17)° |
| | c = 14.2527(4) Å | γ = 90° |
| Volume | 1638.60(8) Å$^3$ | |
| Z | 2 | |
| Density (calculated) | 1.756 mg/m$^3$ | |
| Absorption coefficient | 2.561 mm$^{-1}$ | |
| F(000) | 864 | |
| Crystal size | 0.18 x 0.13 x 0.08 mm$^3$ | |
| Theta range for data collection | 2.70 to 29.57° | |
| Index ranges | -14<=h<=14, -16<=k<=15, -19<=l<=19 | |
| Reflections collected | 8768 | |
| Independent reflections | 4591 [R(int) = 0.0298] | |
| Completeness to theta = 29.57° | 99.8 % | |
| Max. and min. transmission | 0.8214 and 0.6557 | |
| Refinement method | Full-matrix least-squares on F$^2$ | |
| Data / restraints / parameters | 4591 / 0 / 201 | |
| Goodness-of-fit on F$^2$ | 1.051 | |
| Final R indices [I>2sigma(I)] | R1 = 0.0342 | |
| R indices (all data) | wR2 = 0.0822 | |
| Largest diff. peak and hole | 1.101 and -0.776 e.Å$^{-3}$ | |

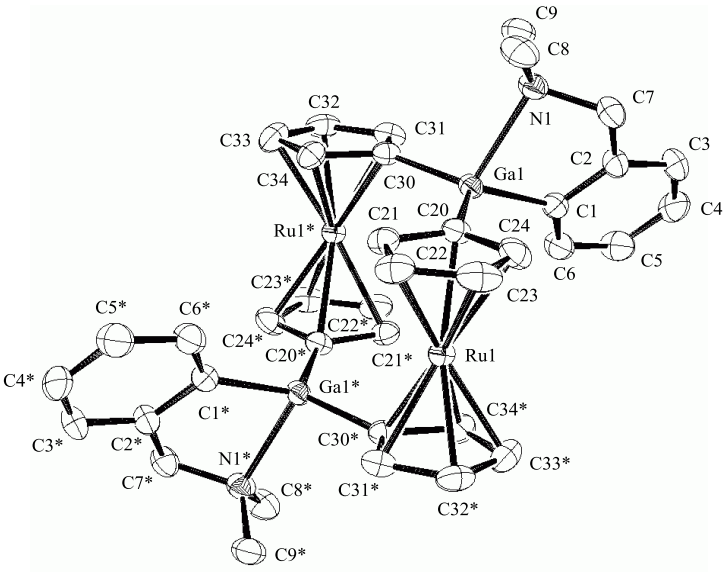


**Figure A-4.** Ortep plot of **152** with thermal ellipsoids at the 50% probability level. Hydrogen atoms are omitted for clarity.

**Table A-22.** Atomic coordinates ( x $10^4$) and equivalent isotropic displacement parameters ($Å^2$x $10^3$) for **152**. U(eq) is defined as one third of the trace of the orthogonalized $U^{ij}$ tensor.

| | x | y | z | U(eq) |
|---|---|---|---|---|
| Ru(1) | 11930(1) | 3745(1) | 4414(1) | 21(1) |
| Ga(1) | 8372(1) | 3672(1) | 3997(1) | 22(1) |
| N(1) | 6667(2) | 3041(2) | 2892(2) | 29(1) |
| C(1) | 8075(3) | 2227(2) | 4671(2) | 27(1) |
| C(2) | 6811(3) | 1734(3) | 4276(2) | 31(1) |
| C(3) | 6447(4) | 673(3) | 4591(2) | 40(1) |
| C(4) | 7354(4) | 77(3) | 5299(2) | 42(1) |
| C(5) | 8607(4) | 533(3) | 5690(2) | 41(1) |
| C(6) | 8955(3) | 1602(3) | 5373(2) | 34(1) |
| C(7) | 5869(3) | 2400(3) | 3474(2) | 33(1) |
| C(8) | 7169(3) | 2222(3) | 2259(2) | 36(1) |
| C(9) | 5841(3) | 3932(3) | 2310(2) | 39(1) |
| C(20) | 9926(3) | 3660(2) | 3415(2) | 25(1) |
| C(21) | 10694(3) | 4592(2) | 3152(2) | 28(1) |
| C(22) | 11880(3) | 4140(3) | 2910(2) | 34(1) |
| C(23) | 11870(3) | 2926(3) | 3028(2) | 34(1) |
| C(24) | 10684(3) | 2635(2) | 3333(2) | 30(1) |
| C(30) | 7662(3) | 5175(2) | 4267(2) | 26(1) |
| C(31) | 6447(3) | 5398(3) | 4574(2) | 34(1) |
| C(32) | 6201(3) | 6620(3) | 4551(2) | 38(1) |
| C(33) | 7271(3) | 7162(2) | 4238(2) | 34(1) |
| C(34) | 8158(3) | 6283(2) | 4064(2) | 28(1) |

**Table A-23.** Selected bond lengths [Å] and angles [°] for **152**.

| | | | |
|---|---|---|---|
| Ru(1)-C(32)#1 | 2.165(3) | C(2)-C(7) | 1.521(4) |
| Ru(1)-C(31)#1 | 2.168(3) | C(3)-C(4) | 1.385(5) |
| Ru(1)-C(33)#1 | 2.175(3) | C(4)-C(5) | 1.376(5) |
| Ru(1)-C(24) | 2.176(3) | C(5)-C(6) | 1.392(4) |
| Ru(1)-C(21) | 2.176(3) | C(20)-C(21) | 1.434(4) |
| Ru(1)-C(23) | 2.179(3) | C(20)-C(24) | 1.437(4) |
| Ru(1)-C(22) | 2.181(3) | C(21)-C(22) | 1.433(4) |
| Ru(1)-C(34)#1 | 2.192(3) | C(22)-C(23) | 1.416(4) |
| Ru(1)-C(20) | 2.206(3) | C(23)-C(24) | 1.420(5) |
| Ru(1)-C(30)#1 | 2.214(3) | C(30)-C(31) | 1.432(4) |
| Ga(1)-C(20) | 1.954(3) | C(30)-C(34) | 1.433(4) |
| Ga(1)-C(30) | 1.958(3) | C(30)-Ru(1)#1 | 2.214(3) |
| Ga(1)-C(1) | 1.986(3) | C(31)-C(32) | 1.436(4) |
| Ga(1)-N(1) | 2.183(2) | C(31)-Ru(1)#1 | 2.168(3) |
| N(1)-C(9) | 1.462(4) | C(32)-C(33) | 1.419(5) |
| N(1)-C(8) | 1.480(4) | C(32)-Ru(1)#1 | 2.165(3) |
| N(1)-C(7) | 1.489(4) | C(33)-C(34) | 1.422(4) |
| C(1)-C(6) | 1.384(4) | C(33)-Ru(1)#1 | 2.175(3) |
| C(1)-C(2) | 1.404(4) | C(34)-Ru(1)#1 | 2.192(3) |
| C(2)-C(3) | 1.388(4) | | |
| | | | |
| C(20)-Ga(1)-C(30) | 117.63(11) | C(4)-C(5)-C(6) | 119.6(3) |
| C(20)-Ga(1)-C(1) | 115.46(11) | C(1)-C(6)-C(5) | 121.9(3) |
| C(30)-Ga(1)-C(1) | 123.24(12) | N(1)-C(7)-C(2) | 109.8(2) |
| C(20)-Ga(1)-N(1) | 106.34(10) | C(21)-C(20)-C(24) | 105.3(3) |
| C(30)-Ga(1)-N(1) | 99.79(10) | C(21)-C(20)-Ga(1) | 130.8(2) |
| C(1)-Ga(1)-N(1) | 83.19(10) | C(24)-C(20)-Ga(1) | 123.1(2) |
| C(9)-N(1)-C(8) | 110.0(2) | C(22)-C(21)-C(20) | 109.4(2) |
| C(9)-N(1)-C(7) | 110.5(2) | C(23)-C(22)-C(21) | 107.7(3) |
| C(8)-N(1)-C(7) | 109.4(2) | C(22)-C(23)-C(24) | 107.6(3) |
| C(9)-N(1)-Ga(1) | 115.54(18) | C(23)-C(24)-C(20) | 110.0(3) |
| C(8)-N(1)-Ga(1) | 108.83(18) | C(23)-C(24)-Ru(1) | 71.10(16) |
| C(7)-N(1)-Ga(1) | 102.27(16) | C(20)-C(24)-Ru(1) | 72.03(15) |
| C(6)-C(1)-C(2) | 117.3(3) | C(31)-C(30)-C(34) | 105.8(2) |
| C(6)-C(1)-Ga(1) | 130.1(2) | C(31)-C(30)-Ga(1) | 127.4(2) |
| C(2)-C(1)-Ga(1) | 112.2(2) | C(34)-C(30)-Ga(1) | 126.3(2) |
| C(3)-C(2)-C(1) | 121.4(3) | C(30)-C(31)-C(32) | 109.2(3) |
| C(3)-C(2)-C(7) | 121.5(3) | C(33)-C(32)-C(31) | 107.4(3) |
| C(1)-C(2)-C(7) | 117.1(3) | C(32)-C(33)-C(34) | 107.9(3) |
| C(4)-C(3)-C(2) | 119.5(3) | C(33)-C(34)-C(30) | 109.6(3) |
| C(5)-C(4)-C(3) | 120.3(3) | | |

**Table A-24.** Anisotropic displacement parameters ($Å^2 x\ 10^3$)for **152**. The anisotropic displacement factor exponent takes the form: -2p2[ h2a*2U11 + ... + 2 h k a* b* U12 ]

| | $U^{11}$ | $U^{22}$ | $U^{33}$ | $U^{23}$ | $U^{13}$ | $U^{12}$ |
|---|---|---|---|---|---|---|
| Ru(1) | 19(1) | 22(1) | 21(1) | -1(1) | 4(1) | 2(1) |
| Ga(1) | 21(1) | 22(1) | 22(1) | -1(1) | 2(1) | -2(1) |
| N(1) | 27(1) | 31(1) | 25(1) | -1(1) | 0(1) | -2(1) |
| C(1) | 30(2) | 24(1) | 26(1) | -2(1) | 7(1) | -3(1) |
| C(2) | 33(2) | 28(1) | 34(2) | -4(1) | 10(1) | -8(1) |
| C(3) | 44(2) | 33(2) | 43(2) | -6(1) | 12(2) | -19(2) |
| C(4) | 66(2) | 26(1) | 36(2) | 3(1) | 18(2) | -10(2) |
| C(5) | 56(2) | 30(2) | 35(2) | 2(1) | 4(2) | 0(2) |
| C(6) | 39(2) | 30(1) | 31(2) | 1(1) | 2(1) | -4(1) |
| C(7) | 25(2) | 35(2) | 36(2) | -2(1) | 2(1) | -5(1) |
| C(8) | 38(2) | 39(2) | 29(2) | -9(1) | 4(1) | -4(1) |
| C(9) | 32(2) | 42(2) | 35(2) | 2(1) | -9(1) | 2(1) |
| C(20) | 24(1) | 29(1) | 20(1) | -1(1) | 1(1) | 2(1) |
| C(21) | 31(2) | 29(1) | 24(1) | 6(1) | 5(1) | 3(1) |
| C(22) | 32(2) | 46(2) | 28(1) | 6(1) | 11(1) | 4(1) |
| C(23) | 30(2) | 45(2) | 24(1) | -9(1) | 5(1) | 8(1) |
| C(24) | 30(2) | 31(1) | 27(1) | -7(1) | 1(1) | 3(1) |
| C(30) | 24(1) | 28(1) | 24(1) | -5(1) | 3(1) | -1(1) |
| C(31) | 22(1) | 41(2) | 38(2) | -12(1) | 5(1) | -4(1) |

**Table A-25.** Hydrogen coordinates ( x $10^4$) and isotropic displacement parameters ($Å^2$x $10^3$) for **152**.

| | x | y | z | U(eq) |
|---|---|---|---|---|
| H(3) | 5582 | 358 | 4323 | 48 |
| H(4) | 7110 | -650 | 5517 | 50 |
| H(5) | 9230 | 120 | 6172 | 49 |
| H(6) | 9821 | 912 | 5647 | 41 |
| H(7A) | 5247 | 1857 | 3054 | 40 |
| H(7B) | 5326 | 2950 | 3757 | 40 |
| H(8A) | 6404 | 1845 | 1824 | 54 |
| H(8B) | 7735 | 1637 | 2655 | 54 |
| H(8C) | 7700 | 2642 | 1879 | 54 |
| H(9A) | 6381 | 4347 | 1933 | 58 |
| H(9B) | 522 | 4476 | 2735 | 58 |
| H(9C) | 5067 | 3570 | 1872 | 58 |
| H(21) | 10454 | 5386 | 3140 | 34 |
| H(22) | 12552 | 4576 | 2706 | 41 |
| H(23) | 12537 | 2402 | 2922 | 40 |
| H(24) | 10428 | 1873 | 3464 | 36 |
| H(31) | 5891 | 4827 | 4763 | 41 |
| H(32) | 5459 | 6997 | 716 | 45 |
| H(33) | 7376 | 7968 | 4158 | 40 |
| H(34) | 8958 | 6410 | 3847 | 33 |